Nanostructured Aromatic Polymer Electrolytes for PEMFC : Structure-morphology-property interplay

Huu-Dat Nguyen

Communauté
UNIVERSITÉ Grenoble Alpes

THÈSE

Pour obtenir le grade de

DOCTEUR DE LA COMMUNAUTE UNIVERSITE GRENOBLE ALPES

Spécialité : **Matériaux, Mécanique, Génie Civil, Electrochimie**

Arrêté ministériel : 25 mai 2016

Présentée par

Huu-Dat NGUYEN

Thèse dirigée par **Cristina IOJOIU** (CNRS) et
codirigée par **Sandrine LYONNARD** (CEA)

préparée au sein du **Laboratoire d'Electrochimie et de Physico-chimie des Matériaux et des Interfaces (LEPMI)**
dans **l'École Doctorale Ingénierie – Matériaux, Mécanique, Environnement, Energétique, Procédés, Production (I-MEP2)**

Electrolytes polymères aromatiques nanostructurés pour PEMFC : Relation structure/morphologie/propriété

Thèse soutenue publiquement le **11 mai 2017**,
devant le jury composé de :

Monsieur Giuseppe PORTALE
Professeur assistant, Université de Groningen, Pays Bas, Examinateur
Madame Christel LABERTY-ROBERT
Professeur, Université Pierre et Marie Curie, Rapporteur
Madame Odile FICHET
Professeur des universités, Université de Cergy-Pontoise, Rapporteur
Madame Cristina IOJOIU
Chargé de recherche, CNRS, Directeur de thèse
Madame Sandrine LYONNARD
Chercheur CEA, CEA Grenoble, Co-Directeur de thèse
Monsieur Jean-Claude LEPRETRE
Professeur, Université Joseph Fourier, Président

Communauté
UNIVERSITÉ Grenoble Alpes

DISSERTATION

To obtain the degree of

DOCTOR FROM UNIVERSITY GRENOBLE ALPES

Specialty: **Materials, Mechanics, Civil Engineering, Electrochemistry**

Ministerial decree: 25 May 2016

Presented by

Huu-Dat NGUYEN

Dissertation directed by **Cristina IOJOIU** (CNRS) and
co-directed by **Sandrine LYONNARD** (CEA)

Prepared at **Laboratory of Electrochemistry and Physical Chemistry of Materials and Interfaces (LEPMI)**
At **Doctoral School Engineering – Materials, Mechanics, Environment, Energy, Procedures, Production (I-MEP2)**

Nanostructured Aromatic Polymer Electrolytes for PEMFC: Structure-Morphology-Property Interplay

Dissertation defended publicly on **11 May 2017**,
in front of the jury comprising of:

Mr. Giuseppe PORTALE
Assistant Professor, University of Groningen, Netherlands, Examiner
Ms Christel LABERTY-ROBERT
Professor, Pierre and Marie Curie University, Reviewer
Ms Odile FICHET
Professor, University of Cergy-Pontoise, Reviewer
Ms Cristina IOJOIU
Chargé de recherche, CNRS, Director
Ms Sandrine LYONNARD
CEA Researcher, CEA Grenoble, Co-director
Mr. Jean-Claude LEPRETRE
Professor, Joseph Fourier University, President

Preface

This thesis was realized from November 2013 to April 2017 at Laboratory of Electrochemistry and Physical Chemistry of Materials and Interfaces (LEPMI), UMR 5279 CNRS, in collaboration with Laboratory of Structure and Properties of Molecular Architecture (SPrAM), UMR 5819 CNRS, INAC/CEA Grenoble. The research is co-funded by French Government and Vietnamese Government via a Ph.D. fellowship.

The dissertation focuses on elucidating the structure-morphology-property relationship of aromatic ionomers for proton-exchange membrane fuel cells, and on developing new ionomers with designed molecular architecture. This work covers the whole cycle of proton-exchange membrane production ranging from synthesis of ionic functional moieties, block copolymer backbones, and ionomers, to film elaboration and essential characterizations at laboratory scale.

This thesis would not be terminated without the guidance of Dr. Cristina Iojoiu and Dr. Sandrine Lyonnard, to whom I would like to thank sincerely. I express my gratitude to Dr. Van-Man Tran and Dr. My-Loan-Phung Le at APC-Lab and Faculty of Chemistry, Vietnam National University at HoChiMinh City (VNU-HCM) for their sponsor. Thanks to Pr. Steven Holdcroft at Simon-Fraser University (Canada) for the collaboration in fuel cell tests and in catalyst-layer research. Thanks to Dr. Dominic Bresser at Karlsruhe Institute of Technology (Germany) for collaboration in studying single-ion aromatic polymer electrolyte based on the new aromatic ionomers for lithium-ion battery. Thanks to Dr. Patrick Judeinstein at CEA Saclay and Ms. Priscillia Soudant at LEPMI for measuring diffusion coefficient and result explanation. Thanks to Pr. Renaud Bouchet, Dr. Fannie Alloin, and Pr. Jean-Claude Leprêtre at LEPMI for productive discussions and advices. Thanks to Dr. Laure Cointeaux at LEPMI for experimental and technical helps. Thanks to Dr. Emilie Planes at LEPMI for DVS measurements and result analysis. Thanks to Dr. Lionel Porcar at Institut Laue-Langevin (ILL) and Dr. Jacques Jestin at Laboratoire Léon-Brillouin (LLB) for beamline alignment and helpful discussion during small-angle neutron scattering experiments. Thanks to Mr. Vincent Martin for SEC measurements and technical supports for TGA and DSC measurements. Thanks to Mr. Bernard Ferrari at LEPMI for preparing conductivity cells and electrodes. Thanks to all the colleagues and friends that I have had opportunity to work with and to share the moments of my stay in France. Thanks to my families for their unconditional support during the PhD period helping me to overcome all difficulties and to arrive to this final point. Finally, I would like to express my gratitude to the members of the evaluation committee for their time and corrections that help me to improve the manuscript.

Huu-Dat Nguyen

Abstract

Aromatic ionomers are currently considered as a promising alternative to Nafion® for proton-exchange membrane fuel cells thanks to their good oxidative stability, excellent thermal and mechanical properties, and low cost, etc. However, most sulfonated aromatic ionomers reported over the past decades show lower performance than that of Nafion. With similar ion-exchange capacity (IEC), on one hand, aromatic ionomers are much less conductive than Nafion, notably at low relative humidity. Aromatic ionomers with sufficient IEC to give equivalent conductivity to that of Nafion, on the other hand, exhibit excessively swelling behavior in water.

The shortcomings of sulfonated aromatic ionomers derive from (i) the random distribution of acidic groups on rigid polymer backbone leading to poor hydrophilic-hydrophobic separation, (ii) the proximity of proton-conducting moieties to the polymer main chain resulting in low structuration of ionic clusters, and (iii) the low acidity of aryl sulfonic acid. With the aim of overcoming these drawbacks, my PhD work focuses on developing new aromatic ionomer with improved morphology and properties via molecular architecture design, in combination with optimized membrane processing condition. Based on this objective, two series of aromatic ionomers based on partially-fluorinated multi-block copoly(arylene ether sulfone)s bearing pendant perfluorosulfonic acid (InX/Y series) or perfluorosulfonimide (SiX/Y series) side chains have been developed and characterized. Moreover, PEMs based on blend of Nafion and InX/Y ionomer have also been focused. Much attention has been paid to optimizing the membrane processing condition and elucidating the structure-morphology-property relation in these materials.

Keywords: proton-exchange membrane fuel cells (PEMFCs), aromatic ionomers, small-angle neutron scattering (SANS), structure-morphology-property interplay, perfluorosulfonic acid (PFSA), perfluorosulfonimide (PFSI), polymer electrolytes, membrane morphology, poly(arylene ether sulfone), multi-block copolymer, molecular architecture, proton conductivity.

Table of Content

Introduction

Power conversion from environmentally friendly and renewable resources such as solar energy, biomass, hydrogen, etc., and its storage are vital for our society in response to the needs of a modern life, the challenges of environmental pollution, climate change, and the finite nature of fossil fuels. With the ability to directly convert chemical energy stored in hydrogen into electrical energy with high fuel efficiency and low pollutant emission, proton-exchange membrane fuel cells (PEMFCs) are one of the most promising technologies for energy conversion of this century. The key component of a PEMFC is the proton-exchange membrane (PEM), which serves as conductors for hydrated protons and barriers for fuels, oxidants and electrons. Currently, the benchmark PEM materials for PEMFCs are perfluorosulfonic acid (PFSA) membranes such as Nafion, Gore, 3M, etc. Thanks to their chemical structure, i.e., a perfluorinated backbone bearing perfluorosulfonic acid side chains, PFSA-based PEMs exhibit highly hydrophilic-hydrophobic phase separation, along with high acidity of perfluorosulfonic acid functions, resulting in excellent thermal/oxidative stability and high fuel cell performances.

However, PFSA membranes are not referred to as successful PEM materials, and their drawbacks, i.e., (i) ionomer synthesis being not environmentally friendly, (ii) high production cost, (iii) high oxygen permeability that gives rise to peroxide formation leading to membrane-electrode-assembly (MEA) degradation, (iv) drop of conductivity and thermomechanical properties above 90 °C, limiting the operation of PEMFCs below this temperature, etc., have prevented PEMFCs from worldwide commercialization. Therefore, much effort has been dedicated to developing alternative PEM materials and more attention has been paid to aromatic ionomers owing to their excellent thermomechanical properties, high thermal/oxidative stabilities, ease of synthesis/modification, and low cost, etc. Unfortunately, most sulfonated aromatic ionomers cannot compete with Nafion in terms of PEM performance. For instance, sulfonated aromatic ionomers with higher ion-exchange capacity (IEC) show higher proton conductivity than that of Nafion® at high relative humidity (RH), but they drop their mechanical properties due to excessive swelling at high hydrated condition. On the other hand, aromatic ionomers with equivalent IEC to Nafion show lower proton conduction, especially at low RH.

With the aim of developing successful PEM materials for high-performance PEMFCs, this thesis is focused on not only new families of aromatic ionomers with designed chemical architecture, but also blend membranes based on aromatic ionomers and Nafion. Much effort has been paid to optimize the membrane elaborating condition and elucidate the morphology-property interplay.

The current manuscript is divided into four chapters:

Chapter 1 covers literature review on the current status of PEMFCs and the benchmark PEM material, e.g., Nafion®. Then, an overview on the structure-morphology-property relation of the state-of-the-art aromatic ionomers reported over the past decades, notably the impact of side chain structure and acidic moieties on morphologies and performances, is provided.

Chapter 2 focuses on partially-fluorinated multi-block copoly(arylene ether sulfone)s bearing perfluorosulfonic acids (namely InX/Y). A series of InX/Y ionomers with different block length and ion-exchange capacity were synthesized via modifying a protocol previously developed in our lab. Membrane preparation and characterization are divided into two parts. Chapter 2A focuses on the effects of block length and membrane processing condition on the morphology and properties of ionomer membranes.[1] Chapter 2B concentrates on controlling the microstructure-transport interplay of InX/Y ionomers via molecular architecture design.[2]

Chapter 3 deals with the study on blend membranes based on Nafion and InX/Y ionomers. A series of perfluorosulfonated multiblock copoly(arylene ether sulfone)/Nafion blend membranes with different content of Nafion were prepared by film-casting method and their morphologies as well as properties were characterized.[3]

Chapter 4 presents the syntheses and characterizations of partially-fluorinated multiblock co-poly(arylene ether sulfone)s bearing perfluorosulfonimide functions (named as SiX/Y). A range of SiX/Y ionomers with different block molar mass and IEC was obtained by Ullmann coupling reaction between brominated block copolymer backbone and perfluorosulfonyl imide functions. Their thermomechanical property, morphology, and transport property were systematically investigated towards PEM application.[4]

Finally, the thesis's overall conclusions and perspectives are announced.

References

(1) Assumma, L.; Nguyen, H.-D.; Iojoiu, C.; Lyonnard, S.; Mercier, R.; Espuche, E. *ACS Appl. Mater. Interfaces* **2015**, *7*, 13808−13820.

(2) Nguyen, H. D.; Assumma, L.; Judeinstein, P.; Mercier, R.; Porcar, L.; Jestin, J.; Iojoiu, C.; Lyonnard, S. *ACS Appl. Mater. Interfaces* **2017**, 9, 1671−1683.

(3) Nguyen, H.-D.; Jestin, J.; Porcar, L.; Lyonnard, S. Iojoiu, C. To be submitted to *Journal of Membrane Science*.

(4) Huu-Dat Nguyen, Emilie Planes, Priscillia Soudant, Lionel Porcar, Sandrine Lyonnard, Cristina Iojoiu. To be submitted to *Journal of Physical Chemistry.*

Chapter 1.

Literature Review

1. Fuel Cell and Its Current Status

1.1. Fuel Cells (FCs)

Fuel cell (FC) is an electrochemical device generating electricity through the oxidation of hydrogen at anode and the reduction of oxygen at cathode. The idea of fuel cells was invented by Sir William Grove in 1839.[1–4] Currently, fuel cells are employed in the following three areas: transportation, stationary and portable power generation.[5]

Fuel cells can be classified by electrolyte materials or by their operating temperature. Low temperature fuel cells (operating temperature < 200 °C) are alkaline fuel cells (AFCs), proton exchange membrane fuel cells (PEMFCs), direct methanol fuel cells (DMFCs), and phosphoric acid fuel cells (PAFCs). High temperature fuel cells which operate at 200–1000 °C are molten carbonate fuel cells (MCFCs) and solid oxide fuel cells (SOFCs).[1,2]

1.2. Proton Exchange Membrane Fuel Cells (PEMFCs)

In proton-exchange membrane fuel cells or polymer electrolyte membrane fuel cells (PEMFCs), proton-exchange membranes (PEMs) play the role of electrolytes. Typically, a single PEMFC consists of three main components: an anode, a cathode, and an electrolyte, i.e., a PEM, as depicted in **Figure 1.1**.[6–10]

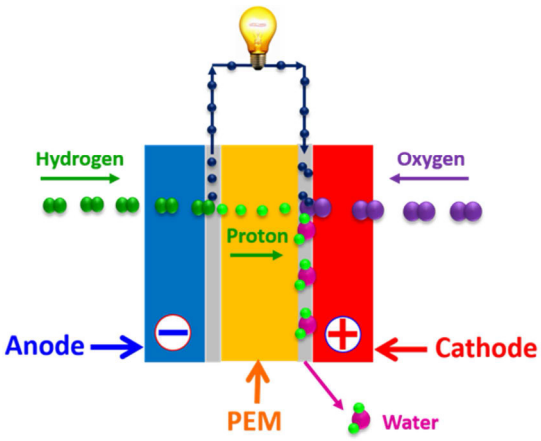

Figure 1.1. Schematic diagram of a single PEMFC.

PEMFCs are also classified into three categories depending on their operating temperatures: High-Temperature PEMFCs (HT-PEMFC) over 120 °C, Medium-Temperature PEMFCs (MT-PEMFC) from 70 °C to 120 °C, and Low-Temperature PEMFCs below 70 °C (LT-PEMFC).[11]

1.3. PEM Functions and Its Requirements

The PEM is referred to as the heart of a PEMFC. Its main role is to assure the migration of hydrated protons generated at anode to the cathode (where they recombine with reduced oxygen to form water) and prevent electron as well as fuel crossover. Due to the highly aggressive conditions inside fuel cells (i.e., high temperature, high pressure, the presence of oxygen and free radicals, etc.) successful PEMs must possess good thermomechanical properties in both dry and hydrated states, excellent chemical and electrochemical stabilities, high proton conductivity, but also low cost, etc.[12–14]

1.4. Commercializing Barriers of PEMFCs

Although PEMFCs have been commercially available for many years, technological advances have left three major challenges: cost, performance and lifetime, which are interrelated. Over the past decades, substantial effort has led to significant reduction of PEMFC cost. But, the cost reduction is mainly contributed by auxiliary facilities and catalyst, while the PEM cost is nearly unchanged due to widely employing PFSA membranes including Nafion®.[15] The lifetime of PEMFC could be improved if the membrane thickness is increased, but this also increases the cell cost by adding materials and lowering specific performance.[16]

2. Nafion® based PEMs

2.1. Introduction

Introduced by E. I. du Pont de Nemours and Company in the late 1960s, Nafion® is the representative of PFSA membranes comprising a PTFE backbone bearing different side chain architectures such as NeoseptaF™ (Tokuyama), Gore-Select™ (W.L. Gore and Associates, Inc.), Flemion™ (Asahi Glass Company), Asiplex™ (Asahi Chemical Industry), and Aquivion®, Hyflon® (Solvay Plastics), etc.[1,2,16–19] The application of Nafion® in PEMFCs in the early 1970s used to be considered as a major breakthrough of PEM technology.[1,20]

The high FC performances and the superior chemical/electrochemical stabilities of Nafion originate from (i) its chemical structure composed of an extremely hydrophobic flexible PTFE backbone coupled with a pendant perfluorosulfonic acid side chain (**Figure 2.1**) resulting in a neat nanophase separation between hydrophobic PTFE backbone and hydrophilic ionic domains, and (ii) the super-acidity of perfluorosulfonic acid groups as compared to other ionomers bearing aryl sulfonic acid functions.[16,17]

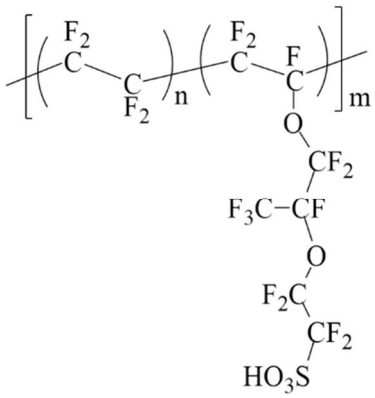

Figure 2.1. Chemical structure of Nafion.

2.2. Morphology of Nafion

A wealth of morphological models of Nafion has been reported in an attempt to precisely describe its morphology, the key contribution to the high performances.[17,21–24] Most of them were proposed based on small-angle scattering (SAS) profiles of Nafion in different physical states (dry and hydrated membranes, or solution). Both neutron (SANS) and X-rays (SAXS) scattering spectra of Nafion in hydrated state generally exhibit a number of hydration-dependent characteristic features related to a complex multi-scale organization directly impacted by water content. There are typically two correlation peaks, the so-called ionomer peak in the wave vector (Q) range of 0.1–0.2 $Å^{-1}$ and the so-called "matrix knee" observed at lower Q values (≈ 0.05–0.06 $Å^{-1}$). The presence of these peaks indicates a regular organization at two different length scales. Their position, shape and intensity are extremely sensitive to the hydration level, with systematic variations characteristic of the microscopic swelling behavior. While the ionomer peak is the fingerprint of all PFSA membranes and was attributed to the organization of ionic domains, the origin of the "matrix knee" is not completely elucidated. This feature was reported with a variety of shapes, positions and intensities depending on chemical architecture and membrane processing conditions.[17] In addition, another structural feature is a certain degree of crystallinity arising from ordering of PTFE backbone. It was shown that the crystallinity depends on the type of polymer and/or membrane processing condition.[25–27] Its influence on the quality of hydrophilic/hydrophobic separation and large-scale organization was observed but has not been elucidated. In particular, correlations between the degree of crystallinity and the matrix knee features were reported,[28–30] although they could not be rationalized in terms of long-range correlations of crystallites nor peculiarities of semi-crystalline versus amorphous regions.

To date, different structural models were proposed to account for the shape of the SAS spectra, particularly the origin of two scattering maxima and their variations along hydration level. In the following, a brief overview of the main models is presented.

In 1981, Gierke et al.[31–33] proposed the **cluster-network model** in which Nafion has inverted-micelle structure with spherical ionic clusters around 3–5 nm in diameter, and the clusters are interconnected by short channels about 1 nm in diameter (**Figure 2.2a**). At the same time, another model based on spherical ionic clusters, e.g., **modified core-shell model**, was proposed by Fujimura et al.[28,34] By analyzing SAXS and WAXD (wide-angle X-ray diffraction) of Nafion with different equivalent weight and counter cations, the authors concluded that the scattering behavior of Nafion has been best described by an intra-particle core-shell model (**Figure 2.2c**) similar to that proposed by MacKnight[35] and co-workers[36], rather than an inter-particle model (**Figure 2.2b**) as proposed by Cooper et al.[37] In the former, the ion-rich core is surrounded by the ion-poor shell composed mostly of perfluorocarbon chains, the core-shell particles being dispersed in a matrix of fluorocarbon chains and non-clustered ions.

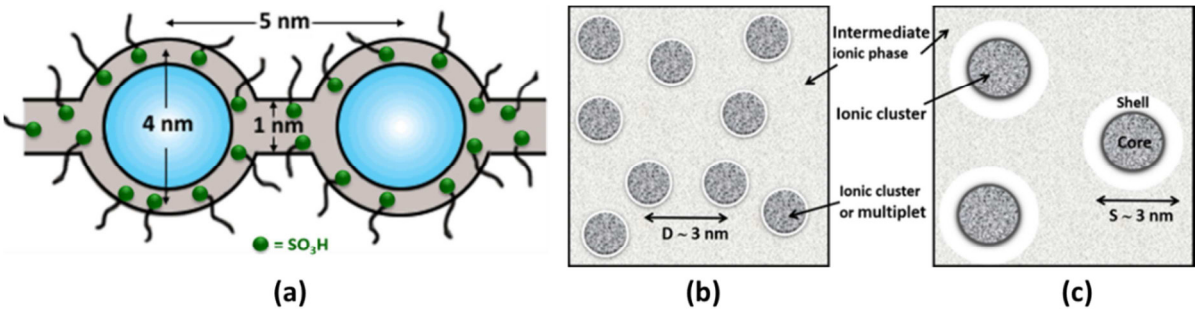

Figure 2.2. (a) Cluster-network, (b) inter-particle, and (c) intra-particle core-shell model for morphology of hydrated Nafion. Schemes adapted with permission from ref.[17] Copyright 2004 American Chemical Society.

The cluster-network model was widely accepted and considered as the most prevalent model in the literature until the late 90s as its accordance with available scattering results. However, new insights into morphological and dimensional evolution during swelling were gained later, due to progress in scattering techniques, capability to measure SAS spectra over extended Q-range. Additional investigations, and increasing information by numerical simulations[23,24,38] have gradually raised doubt about the spherical shape and spatial distribution of ionic clusters inside the semicrystalline matrix of Nafion.[17]

In 1997, Litt[39] proposed the so-called **simple lamellar model,** where ionic clusters of lamellar shape are introduced. In this model, the ionic domains are locally planar and parallel

to each other. As water is absorbed, the ionic domains swell and spread apart the nonpolar domains, leading to a parallel shift of the scattering maxima associated to lamellar ordering on non-polar domains correlations. The expansion is supposed to be impeded by the macromolecule tie that connect the conducting channels. This model has provided a more rational explanation for the reversible swelling behavior of Nafion, and the linear dependence of the ionomer peak with hydration degree (in contrast to the 1/3-power dependence for isotropic swelling of spherical structures). However, further work on swelling behavior reported by Gebel[40] and Young[41] revealed a dissimilar shift of the two maxima, incompatible with the lamellae-based structure proposed by Litt.[39] Therefore, a more sophisticated morphology was postulated. By studying the microstructure and the swelling behavior of Nafion membranes immersed in water–methanol under in-situ conditions, Haubold et al.[42] proposed a modified lamellar model, the **sandwich-like model**, which composes of a core region embedded by a shell, the former being either empty or filled by water-methanol (**Figure 2.3**). Although this model interestingly depicts details of a possible local structure, it does not provide an overall 3D pattern of hydrophilic/hydrophobic organization.

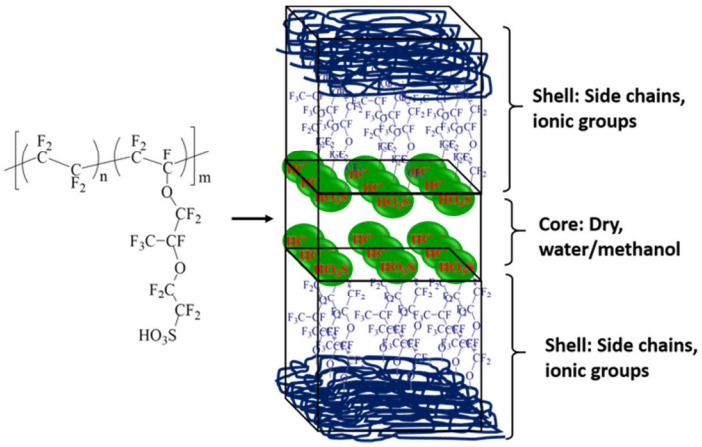

Figure 2.3. The sandwich-like model. Scheme adapted with permission from ref.[42] Copyright 2001 Elsevier.

More comprehensive models were developed after the years 2000, with the objective to unify the body of information accumulated on local, nanoscopic and mesoscopic structure. The focus was put on rationalizing under-looked details of SAS spectra, as asymptotic behaviors, form factors and hydration-dependent variations of peak positions, as well as elucidating the structure of ionomer solutions. The structure evolution of PFSA ionomers during swelling[40] as well as solution-cast process[43–45] was systematically studied by the group of Gebel using SAS technique.

■ In swollen membranes, a significant change in swelling behavior was found at polymer volume fraction (Φp) around 0.5.[46] This was attributed to a continuous transformation from water-in-polymer state to polymer-in-water state. Moreover, the high-Q asymptotic behavior in SAS spectra was scrutinized. A Porod's law (a Porod's slope of Q^{-4} revealing a sharp interface between two scattering objects),[47] was evidenced for all samples. This behavior typically indicates the presence of a sharp interface between two phases, e.g., polymer and ionic phases. The corresponding specific surface (σ) could be extracted using Guinier approximation[48,49] and was found to be 55 $Å^2$.

■ Evidence of rod-like elongated polymeric aggregates (Porod's slope of Q^{-1})[47,49] was reported in diluted ionomer solutions.[50] The local structure on the scale of a few nanometers is identical to that of swollen membrane (at equivalent Φp) implying the existence of a network of rod-like polymer particles in the latter.

Based on these key observations, Gebel proposed the so-called **elongated-aggregate model**.[46] In this model (see **Figure 2.4**), dry membranes contain separately spherical ionic clusters of ≈ 1.5 nm in diameter with center-to-center distance of ≈ 2.7 nm. During hydration, the clusters swell to form bulks of water surrounded by ionic groups at the interface to minimize interfacial energy. As water content (Φw) increases (between 0.3 and 0.5), structural reorganization occurs to retain specific surface area, forming water cylinders connecting the spherical clusters. At $\Phi p < 0.5$, a structure inversion occurs to form a connected network of rods. In over-swollen state, these rod-like structures are separated to yield a colloidal dispersion of isolated rods.

Despite proposing a more rational mechanism for the structure evolution from the isolated clusters to rod-like structures in solution, this model lacks a thermodynamic justification for the phase inversion process.[17] Therefore, it was further questioned, but it has already contained the primary ingredient of the nowadays widely accepted structural models, i.e., Nafion constituted of elongated polymer particles, and these reorganizing along hydration and dehydration sequences. The group of Gebel[51] later proposed the **ribbon-like model**, which originates from these ideas and was sustained by new sets of SAS data taken on i) extended range of Q-vectors, including the ultra-small angle region, and ii) using advanced contrast variation techniques available by SANS to evaluate the condensation of ions at the water-polymer interface. On analyzing these data, they proposed that Nafion is composed of flat elongated particles embedded in a continuous ionic medium, and organized in large scale bundles.

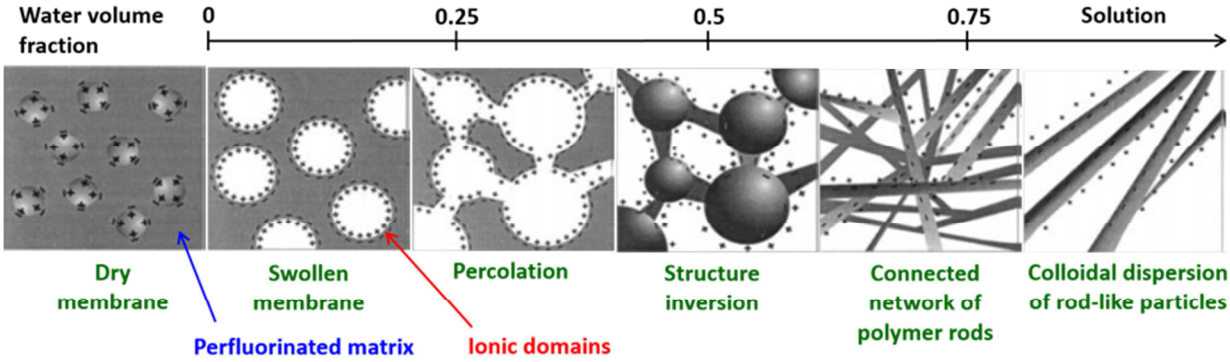

Figure 2.4. Schematic representation of the structural evolution as a function of water content. Schemes reprinted and adapted with permission from ref.[46] Copyright 2000 Elsevier.

In 2008, Schmidt-Rohr and Chen[52] proposed a **parallel cylinder model** (**Figure 2.5**) by simulating the SAS data of hydrated Nafion published by the Gebel's group (Rubatat et al.[50]). This model was supported by a NMR study.[53] The key feature of this microstructure is inverted micelle cylinders with large diameters even at low water content (e.g., 2.4 nm for a $\Phi w \approx 0.2$ corresponding to about 80% RH).

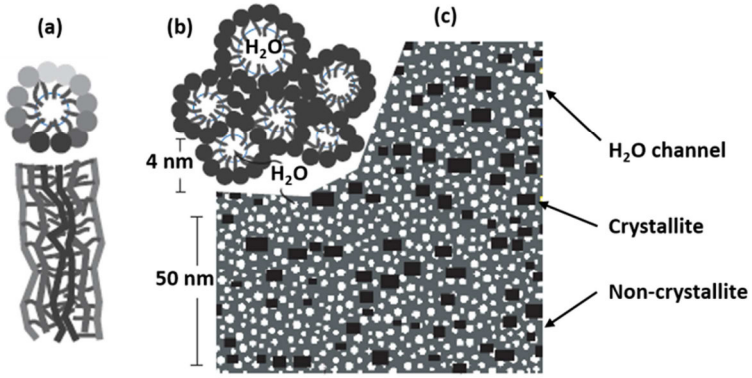

Figure 2.5. Schematic diagram of parallel cylinder model. (a) An inverted-micelle cylinder with the polymer backbones outside and the ionic side groups lining the water channel. (b) An approximately hexagonal packing of inverted-micelle cylinders. (c) Cross-sections through the cylindrical water channels (white) and the Nafion crystallites (black) in the non-crystalline Nafion matrix (dark grey). Schemes reprinted and adapted with permission from ref.[52] Copyright 2008 Nature Publishing Group.

However, Kreuer et Portale[54] raised doubts about this model since a constant number of cylinders requires significant structural reorganization to adjust changes of the water content, in contrast to extremely fast equilibration when water absorbs into the membrane.[55] Furthermore, the accumulation of equal charges is energetically unfavorable when they are not completely covered by water molecules. Therefore, they have sustained the locally flat

and narrow structures similar to lamellar model previously proposed by Litt.[39] or polymer ribbon morphology, as suggested by Rubatat et al.[51] as it allows protonic charge carriers to electrostatically interact with several sulfonic groups.

In conclusion, although details of the Nafion morphology are still debated and not fully elucidated, there is a consensus on the main features of Nafion's morphology.

■ Due to their amphiphilic character, hydrated PFSA membranes exhibit highly separated hydrophobic and ionic domains. The neat separation between polar and non-polar regions yields the formation of a well-defined scattering maximum, the ionomer peak. The interfacial region is sharp, leading to a typical Porod's behavior in the high-Q region of the scattering spectra.

■ Increasing the water content results in more extended and better connected ionic domains. The size and shape of ionic domains is rather irregular, with indications of a preferred locally flat topology (in particular at low hydration).

■ The domain expansion is accompanied by modifications of the topology of the interface between the ionic domains and the polymer matrix. Recently, the morphology and swelling of PFSAs have been shown to resemble that of ionic surfactants,[56–58] highlighting the predominant effect of side-chains and acidic functions in controlling the size, shape and organization of ionic domains.

2.3. Alternative Ionomers to PFSA

Despite excellent proton conductivity, and unsurpassed longevity in a fuel cell environment, Nafion® and other PFSA ionomer membranes suffer from certain drawbacks such as high cost, production process including strongly toxic and environment-unfriendly intermediates,[13] low conductivity at low relative humidity, drop of conductivity at temperatures above 80–90 ^{0}C, and low mechanical properties at high temperatures.[12,59] Other shortcomings of the perfluorinated ionomers are related to their high methanol permeability allowing methanol crossover from the anode to the cathode in DMFCs,[13] high osmotic drag, which makes water management at high current densities difficult. As a consequence, considerable effort has been dedicated to developing alternative PEM systems for PEMFCs.[11,12,15,20,60,61]

3. Aromatic Ionomers – A Promising Alternative to Nafion®

Among numerous alternative to PFSA, investigated over the past decades, aromatic ionomers are more promising for the next-generation PEM materials due to their availability, processability, wide variety of chemical compositions, and stability in the fuel cell environment. On the view of chemical structure, aromatic ionomers compose of an aromatic polymer backbone bearing ion-conducting groups, mostly aryl sulfonic acid. Based on the distribution of ionic groups along the polymeric backbone, aromatic ionomers can be classified into random ionomers with statistical distribution of the ionic functions, or block ionomers with segmented distribution of ionic functions. For each type, the ionic functions can be directly attached onto the polymer backbone or separated by a spacer. These molecular features play an important role in final morphologies and PEM performances. As concerning the structure backbone a large variety of ionomers have been studied, i.e., polysulfone (PES), poly(arylene ether) (PAE), and poly(ether ketone) (PEK), polyimide, polybenzimidazole, etc. The aim of this part is to review the state of the arts on prevalent aromatic ionomers to outline the advantages and drawbacks of each material as well as to establish their structure-morphology-property relation. The study has been focused mainly on aromatic ionomers based on PES, PAE, and PEK.

3.1. Ionomers with Sulfonic Acid Directly Attached to Polymer Backbone

3.1.1. SO_3H Attached to 'Ortho-to-Ether' Positions

3.1.1.1. Post-Sulfonation

The simplest way to attach active proton-exchange sites onto polymer backbones is electrophilic substitution in the presence of sulfonation agents such as chlorosulfonic acid ($ClSO_3H$), oleum, trimethylsilyl chlorosulfonate (TMSClS, $(CH_3)_3SiSO_3Cl$), etc. In this approach, the sulfonic groups are located at ortho-position to electron-donating groups, i.e., ether groups. Depending on chemical structure of original polymer backbone, a random or block ionomer will be obtained. A comparative study on effects of sulfonation agents on the sulfonation of bisphenol A-based poly(ether sulfone)s[62] indicated the formation of more inhomogeneous sulfonated ionomer and more side reaction yielding to chain cleavages in presence of a strong sulfonating agent, i.e., $ClSO_3H$ as compared to TMSClS. The advantage of the latter is that the reaction takes place in homogeneous media, due to the protection of acidic function by trimethylsilyl, that allows both a more homogeneous sulfonation and a significant decrease of side reactions. Nerveless, it is well known post-sulfonation of polymer suffers from several drawbacks such as the lack of control of sulfonation degree and of the

number of ionic function per structural units, the presence of side reactions which leads to chain breaking, etc.[60,63]

3.1.1.2. Bottom-up Copolymerization

The shortcomings of post-sulfonation method have led researchers to come up with a more effective way to control ionomer's structure and degree of sulfonation (DS) – the direct polymerization of disulfonated comonomers. A wide range of statistic ionomers, derived from disodium 3,3'-disulfonate-4,4'-dichlorodiphenylsulfone (SDCDPS) (**Figure 3.1a**), was synthesized and reported by the McGrath's group. Among the random aromatic ionomers bearing aryl sulfonic acid functions (as-), as-PES35 (**Figure 3.1b**) with IEC ~ 1.5 meq/g, synthesized by direct copolymerization of SDCDPS, DCDPS (4,4'-dichlorodiphenylsulfone) and BP (bisphenol), showed highest performance and has been used as a reference to evaluate other ionomers.[59,64] By varying the SDCDPS/DCDPS molar ratio, a series of random ionomer with different DS and IEC, namely as-PESx, where x is the DS, is obtained.[65] Other statistic ionomers were obtained by varying BP by its derivatives in the synthesis procedure.[64]

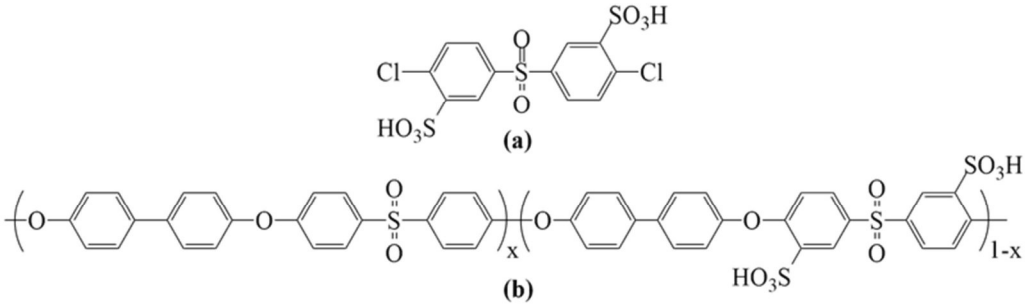

Figure 3.1. Chemical structures of (a) SDCDPS and (b) random ionomer as-PESx.

The conductivity of these statistic ionomers is lower than that of Nafion despite higher water uptake and IEC. This behavior is originated from the polymer's chemical architecture, i.e., (i) the random attachment of ionic functions, in combination with the stiffness of aromatic polymer backbone, resulting in poor hydrophobic/hydrophilic phase separation (**Figure 3.2a**), (ii) the proximity of ionic function to the backbone leading to the poor structuration of ionic domains, and (iii) the lower acidity of aryl sulfonic acid as compared to perfluorosulfonic acid in Nafion. Thus, SAXS profiles of as-PES random ionomer was essentially featureless, implying low phase separation and poor structuration of ionic domains.[66] In addition, the location of sulfonic acid on polymer main chain, the ortho-to-ether position, is considered as the origin of the low thermal and oxidative stability of sulfonated aromatic ionomers, especially at high sulfonation degree.[67]

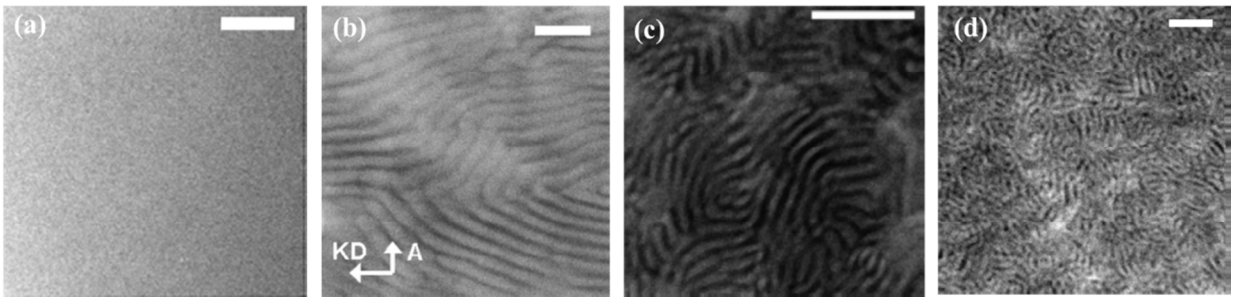

Figure 3.2. TEM images of (a) as-PES35,[66] (b) as-PES/PES 10/10 DFBP,[68] (c) as-PES/6FPES 15/15,[69] (d) as-PES/6FPEEK 14/14.[70] Scale bar = 100 nm. Reprinted and adapted with permission from (a) ref.[66] Copyright 2009 Elsevier. (b) ref.[68] Copyright 2009 Elsevier. (c) ref.[69] Copyright 2013 Wiley Periodicals, Inc. (d) ref.[70] Copyright 2011 Elsevier.

The puzzle concerning membrane morphology, i.e., the hydrophilic/hydrophobic phase separation, has been successfully overcome with multi-block copolymers. To obtain such ionomers, fully sulfonated oligomers such as as-PES100, synthesized from SDCDPS and BP, were performed as hydrophilic block, while the chemical structure of hydrophobic blocks as well as linkage groups between the blocks were varied to generate a wide range of block copolymers (**Figure 3.3**). The IEC of obtained ionomers was controlled by the feed ratio and the length of two oligomers submitted to the coupling reaction.

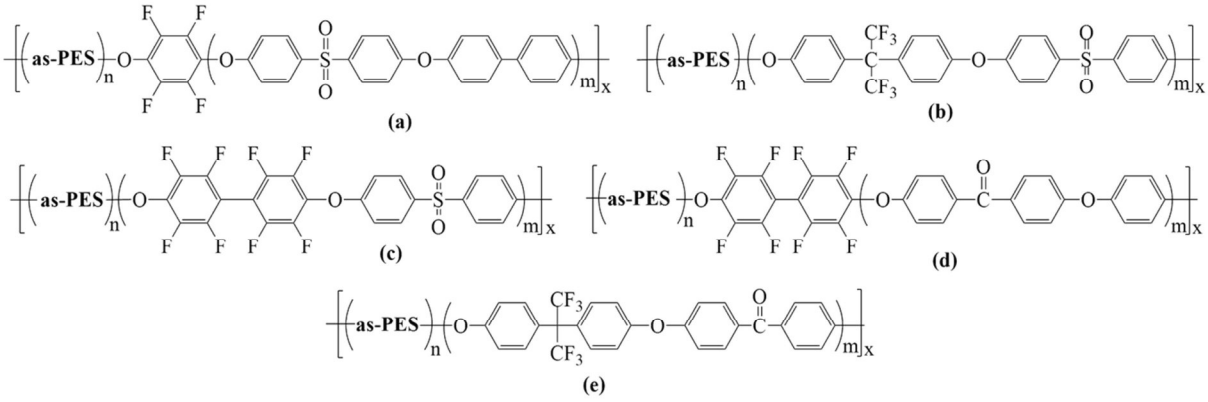

Figure 3.3. Chemical structures of block copolymers: a) as-PES/PES, b) as-PES/6FPES, c) as-PES/FPES, d) as-PES/PEEK, e) as-PES/6FPEEK.

In fact, ionomers with multi-block structure exhibit characteristic features, i.e., a lamellar morphology (**Figure 3.2b–d**) and an anisotropic swelling behavior in water (swelling through plane higher than swelling in-plane).[69,71] SAS profiles of as-PES/PES membranes in Cs^+-salt form showed two maxima at two different length scales: (i) a well-defined peak at lower Q range of 0.013–0.02 $Å^{-1}$ (at a typical length scales of ~30–50 nm), and (ii) a poor-defined ionomer peak and at higher Q range of ~0.03 $Å^{-1}$ (at a typical length scales of ~20 nm).[66]

Together with TEM images, it seems that the larger length scale (at lower Q) corresponds to the distance between hydrophobic domains, while the smaller length scale (at higher Q) is responsible for that between hydrophilic domains. From microscopic and SAS results, one may conclude that sulfonated multi-block copolymers possess highly hydrophobic-hydrophilic separation.

Owing to the well-developed hydrophilic/hydrophobic separation, most block ionomers showed higher proton conduction both in water (**Table 3.1**) and at reduced RH (**Figure 3.4**) in comparison to that of their statistic analogs with similar IEC.

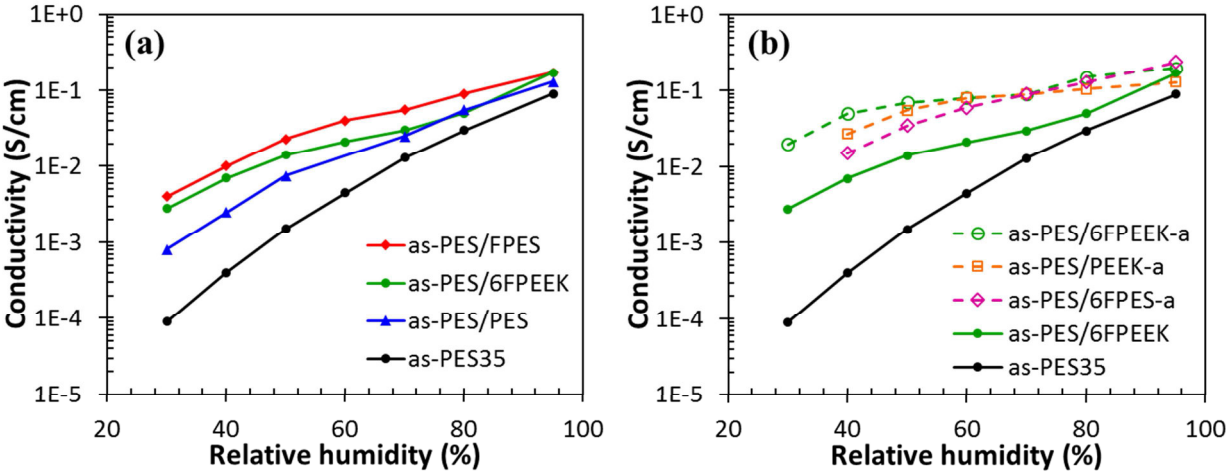

Figure 3.4. Proton conductivity vs reduced humidity at 80 °C of (a) not annealed and (b) annealed (marked with suffix -a) SDCDPS-based ionomer membranes. 1) as-PES35,[72] 2) as-PES/PES 10/10 with HFB linked group,[68,73] 3) as-PES/FPES 15/15,[72,74] 4) as-PES/6FPES 15/15,[69] 5) as-PES/PEEK 17/17,[71] 6) as-PES/6FPEEK 14/14.[70]

For instance, as-PES/PES block copolymer (**Figure 3.3a**) showed slightly higher conductivity than that of as-PES35 in full humidification (**Table 3.1**) but much higher conductivity at reduced RH due to better connectivity of the proton-conducting channels (**Figure 3.4a**). As concerning the mechanical properties the membranes based on multi-block copolymers show lower tensile strength but higher elongation to failure, as compared to random ones.[69] Moreover, the properties of multi-block ionomers are tailored by IEC, block size, chemical composition of both blocks, linkage moieties between the blocks, as well as membrane manufacturing conditions.

Table 3.1. Film Elaborating Condition and Properties of SDCDPS-based Ionomers

Ionomers X/Y (kg/mol)	IEC (meq/g)	WU (%)[a]	σ (S/cm)	Drying method[b]
Nafion® 212[70]	1.0	22	0.12	
as-PES35[70,72]	1.30-1.52	50	0.07	1
as-PES/PES 5/5 DFPB[68]	1.39	33	0.088	1
as-PES/PES 10/10 DFPB	1.28	60	0.095	1
as-PES/PES 5/5 HFB	1.30	35	0.08	1
as-PES/PES 10/10 HFB	1.38	68	0.10	1
as-PES/PES 15/15 HFB	1.40	79	0.11	1
as-PES/FPES 5/5[72,74]	1.30	31	0.09	1
as-PES/FPES 8/10	1.30	52	0.12	1
as-PES/FPES 15/15	1.40-1.50	78	0.14	1
as-PES/6FPES 6/6[69]	1.53	48	0.17	2
as-PES/6FPES 10/10	1.55	55	0.18	2
as-PES/6FPES 15/15	1.56	60	0.2	2
as-PES/PEEK 5/5[71]	1.60	47	0.11	2
as-PES/PEEK 9/9	1.65	50	0.12	2
as-PES/PEEK 17/17	1.70	85	0.13	2
as-PES/6FPEEK 5/5[70]	1.50	60	0.11	2
as-PES/6FPEEK 9/9	1.55	55	0.15	2
as-PES/6FPEEK 14/14	1.50	55	0.17	2

[a]At 30 °C in water. [b]Drying with method 1 (under UV lamp at 40-45 °C, then under vacuum at 110 °C) or method 2 (under UV lamp at 40-45 °C, then annealed under vacuum at 195-250 °C depending on Tg of the hydrophobic block). The number next to the name is molar mass of hydrophilic/hydrophobic block in kg/mol.

Effect of IEC and block size. It was reported that the size of hydrophobic/hydrophilic domains and the degree of phase separation increases with block length. Increasing IEC leads to higher water uptake and proton conductivity, but lower mechanical properties and thermal-oxidative stability.[67,72] It was demonstrated the ionomers with equivalent molecular weight for both blocks show better structuration and the longer the blocks, the better the connectivity of hydrophilic domains, leading to higher water uptake and proton conduction (**Table 3.1**).[69]

Effect of block's chemical structure and linkage groups. The presence of fluorine in hydrophobic block increases its hydrophobicity and, thus, increases the hydrophobic/hydrophilic phase separation, which results in better structuration of ionomer membranes. Thus, the block-copolymers as-PES/6FPES (**Figure 3.3b**)[69] and as-PES/FPES (**Figure 3.3c**)[72,74] having partially fluorinated hydrophobic blocks showed higher conductivities than that of as-PES/PES in the whole range of humidity, and the highest conductivity of membranes was obtained with as-PES/FPES membrane (**Figure 3.4a**). It was also reported the linkage group between two blocks influences both degree of phase separation and proton conductivity. Thus, as-PES/PES having DFBP (decafluorobiphenyl) linkage group showed better hydrophilic/hydrophobic separation along with slightly higher proton conductivity than that of as-PES/PES with HFB (hexafluorobenzene) linkage group in both full hydration condition and at reduced RH.[68]

Effect of membrane manufacturing conditions. In addition to chemical structure, thermal annealing was found to have prominent effects on morphology and properties of ionomer membranes. In the annealing process, the "as-cast" membranes, initially dried at ~ 45 °C to remove free solvent, were submitted to thermal treatment at 150–250 °C depending on Tg of hydrophobic blocks. The annealed membranes showed higher performance, i.e., mechanical properties and proton conductivity at reduced humidity, with lower water uptake than those of "as-cast" membranes (**Figure 3.4b**). The effect of annealing was observed for both random[75] and block copolymer.[70,76] Interestingly, annealed as-PES/PEEK[71] with non-fluorinated hydrophobic block show comparable conductivity with that of other block copolymers having partially fluorinated hydrophobic block. This behavior was explained by the semi-crystalline structure of diphenylketone moiety which results in more distinct nanophase separation between semi-crystalline hydrophobic PEEK domains and disulfonated hydrophilic as-PES domains. Moreover, the combination of diphenylketone and 4,4'-hexafluoroisopropylidenediphenol (6F-BPA) to form partially fluorinated PEEK as hydrophobic block (6FPEEK) slightly increase membrane performance at reduced RH.

In addition to thermal annealing, casting solvent[77] and acidification method, etc., also have considerable effects on morphology and properties of ionomer membranes. By simply using selective solvent, further enhancement in morphology of ionomers was achieved.[66] In terms of acidification, membranes acidified at 100 °C showed higher water absorption and proton conductivity than those of membranes acidified at 30 °C.[78]

3.1.2. SO_3H Attached to Positions other than 'Ortho-to-Ether'

All aromatic ionomers discussed above possess sulfonic acid groups attached to ortho-to-ether position which was attributed to the desulfonation in harsh condition.[79] Moreover, it was reported that SO_3H group grafted onto ortho-to-ether position lowers electron density of the neighboring ether groups and facilitate the nucleophilic attack, resulting in the hydrolysis of ether linkages.[67] In contrast, the SO_3H in meta-to-ether position showed stabilizing effect[80] and its acidity could be improved by the presence of an electro-withdrawing group in proximity.[81] Therefore, several groups have developed aromatic ionomers possessing sulfonic acid groups attached to (i) ortho-position to the electro-withdrawing sulfone group or (ii) meta-position to the ether group.

Ortho-to-sulfone position. This approach was firstly proposed by Kreuer et al.[82] by reporting as-PPS100, a sulfonated poly(phenylene sulfone) containing merely sulfone connecting units between phenyl rings (**Figure 3.5a**). With full degree of sulfonation, as-PPS100 shows extremely high IEC (4.5 meq/g) with one sulfonic acid group on each aromatic ring. However, as-PPS100 cannot be applied as a free-standing PEM due to its water solubility and brittleness. Therefore, random ionomer with reduced IEC ~1.3–2.3 meq/g (as-PPSx where x is DS, **Figure 3.5b**),[83] or multi-block copolymers bearing as-PPS100 hydrophilic block (as-PPS/PES and as-PPS/6FPES, **Figure 3.5c**)[84] (IEC ~ 1.2–1.7 meq/g) were developed. SAXS profiles and microscopic images of the block copolymers showed lamellar morphology with distinct correlation lengths around 15 nm and well continuous hydrophilic phases. At low relative humidity (16–50 %) and high temperatures 120–160 °C, the conductivity of the random copolymer (IEC ~ 1.3 meq/g) is in the range of $3 \times 10^{-4} - 3 \times 10^{-3}$ S/cm, while that of the block copolymer (IEC ~ 1.6 meq H^+/g) is $1.5 - 7 \times 10^{-2}$ S/cm. With extremely electron-deficient aromatic rings, PPS-based ionomers exhibited high thermal and hydrolytic stability, as well as low swelling in water at high temperature. Thus, in Fenton's reagent (3 ppm Fe^{2+} in 30% H_2O_2 solution) at 25 °C, optimized as-PPSx membrane started to disintegrate after 80h and disappeared after 135h while the sulfonated poly(phenylene sulfide sulfone) started to decompose after 35h, and completely dissolved

after 53h.[83] Moreover, the decomposition temperature of SO_3H groups was also increased to 300 °C,[83] as compared to ~270 °C when attached to ortho-to-ether position.[72]

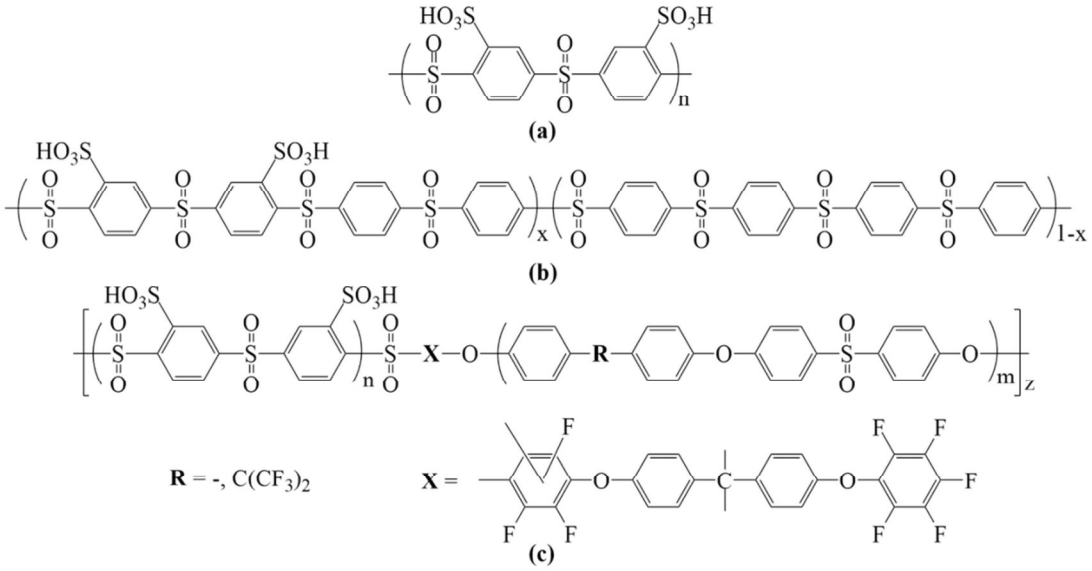

Figure 3.5. Chemical structure of (a) homopolymer as-PPS100, (b) random ionomer as-PPSx, (c) block copolymer as-PPS/PES (R = -) and as-PPS/6FPES (R = $C(CF_3)_2$).

The higher thermal stability of sulfonic acid groups when attached to ortho-to-sulfone position was also reported by Jannasch et al.[85] on random poly(arylene sulfone)-based ionomers bearing aryl sulfonic acid groups (as-PASx, x is DS). The ionomers were obtained by direct polymerization of unsulfonated thiol monomers with a tetra-sulfonated thiol comonomer, followed by selective oxidation to convert thioether to sulfone. Similar to as-PPSx, as-PASx contains exclusively electron-withdrawing sulfone bridges between the aromatic units inducing a high thermal and hydrolytic stability. In fully hydrated condition, as-PAS50 (IEC ~2.2 meq/g) showed higher proton conductivity than that of Nafion NRE212 in all temperature range (from −20 to 120 °C), notably at subzero temperature. At 30% RH and 80 °C, as-PAS50 membrane reached equivalent conductivity to that of Nafion NRE212 membrane (0.01 S/cm).

Jannasch et al.[86] also developed a block copolymer bearing as-PAS100 hydrophilic block (IEC ~3.7 meq/g) and non-sulfonated PES block (as-PAS/PES1, **Figure 3.6a**). AFM images of block copolymer surfaces showed a clear phase separation on the ~30 nm scale with well-connected hydrophilic domains. As expected, the water uptake and proton conductivity increased with increasing block size at a given IEC. All block copolymer membranes also showed an anisotropic swelling. The influence of the bond position on aromatic rings of hydrophilic block, i.e., either meta- or para-linked sequence (**Figure 3.6a**) was also studied. It

was reported that ionomer with meta-connection of IEC 1.3 meq/g performs as one with para-bridges of IEC 1.8 meq/g. This behavior was explained by higher mobility of the polymers with meta-bond, evidenced by lower Tg and higher water uptake.

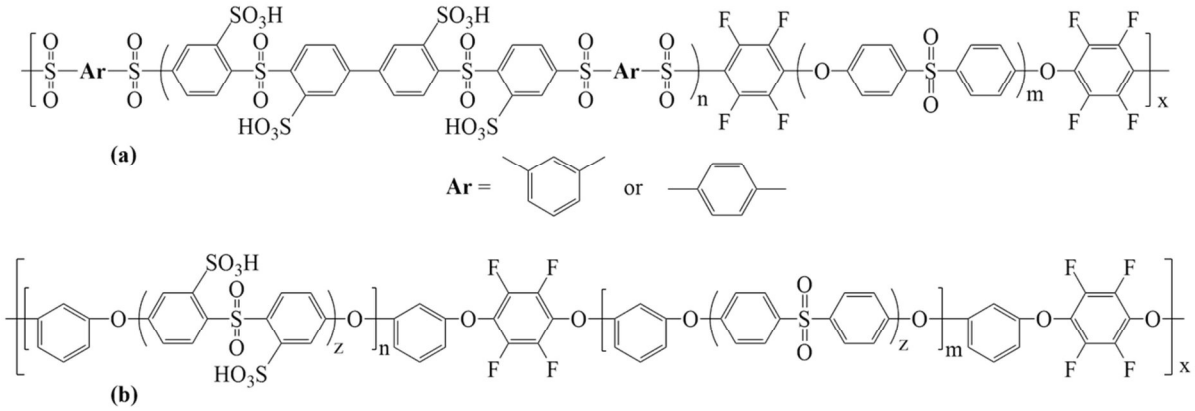

Figure 3.6. Chemical structure of block copolymers (a) as-PAS/PES1 with meta- or para-connection, (b) as-PAS/PES2 (z = 1) and as-PAS/PES3 (z = 2).

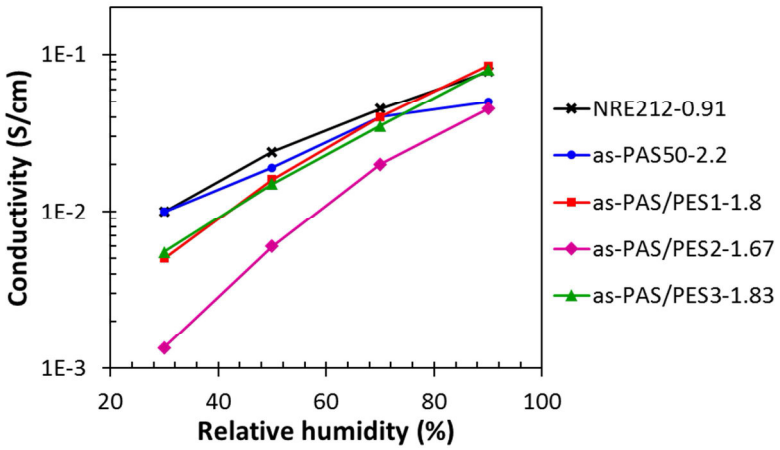

Figure 3.7. Conductivity vs RH at 80 °C of random and block copolymers proposed by Jannasch et al.[85–87] The number next to the sample name is IEC.

In 100% humidity, as-PAS/PES1 with IEC > 1.3 meq/g for meta-connection and IEC > 1.8 meq/g for para- connection showed higher proton conductivity than that of Nafion NRE212. By varying the comonomer structure, furthermore, two other block copolymers with similar structure were synthesized (as-PAS/PES2 and as-PAS/PES3, **Figure 3.6b**).[87] At 100% RH, both block copolymers with IEC > 1.4 meq/g showed higher proton conductivity than that of Nafion NRE212. The as-PAS/PES3 bearing four sulfonic acid groups per repeating unit showed much higher proton conductivity than that of as-PAS/PES2 with two sulfonic acids per repeating unit. Unfortunately, below 70% RH these ionomers with segmented

structure showed lower proton conductivity than that of its random analog as-PAS50 (maybe due to lower IEC) and Nafion NRE212 (**Figure 3.7**).

Meta-to-ether position. Kerres et al.[88] investigated effects of SO_3H group located in different positions of the arylene ring and found that sulfonic acid at the meta-position to ether or sulfone groups showed higher thermal and chemical stability than that at the ortho-position to ether and sulfone. Based on that idea, two series of random sulfonated poly(arylene ether) bearing aryl sulfonic acid in meta-to-ether position were reported by Guiver et al.[81,89] One has a partially fluorinated backbone (as-FPAE, **Figure 3.8a**), and the other possesses highly polar nitrile groups in the main chain (as-PAEN, **Figure 3.8b**).

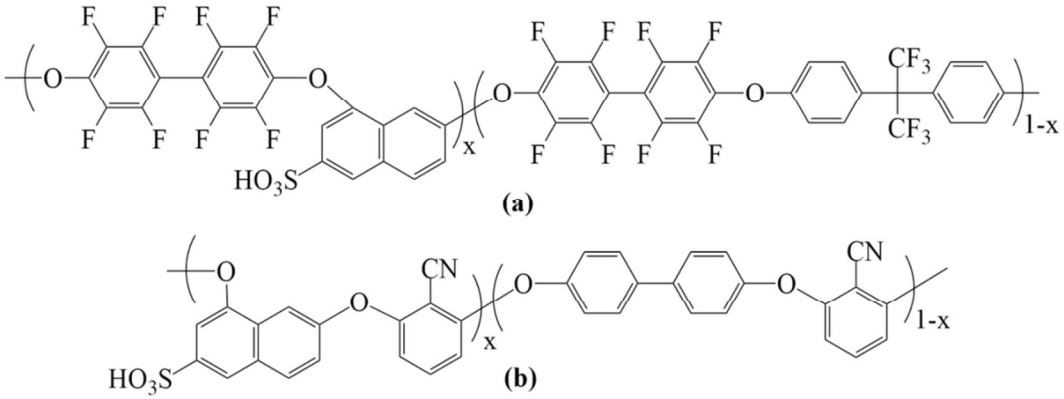

Figure 3.8. Chemical structure of a) as-FPAE and b) as-PAEN.

Both ionomers showed high conductivity at fully hydrated conditions: 2.7×10^{-2} – 1.02×10^{-1} S/cm at 90 °C for as-FPAE with IEC 0.84 – 1.4 meq H^+/g and 6.4×10^{-2} – 1.4×10^{-1} measured at 80 °C for as-PAEN with IEC 1.6 – 1.9 meq H^+/g. However, as-PAEN ionomers having nitrile groups on polymer backbone showed much lower water uptake than that of as-FPAE ionomers bearing partially fluorinated moieties due to the interaction between sulfonic acid and nitrile groups. Consequently, as-PAEN with much higher IEC did not show increased conductivity as compared to that of as-FPAE.

3.1.3. Conclusions

To be considered as successful PEM materials alternative to Nafion, much effort has been done to improve chemical structure, morphologies, and properties, etc., of sulfonated aromatic ionomers. By bottom-up polymerization, sulfonated aromatic ionomers with controlled chemical structure and sulfonation degree can be synthetized. The poor phase separation of random ionomers was significantly enhanced by the development of multi-block ionomers. The position of sulfonic function on the aromatic ring influences the thermal stability of ionomers, the meta position was reported to be the most stable. In addition, most block

copolymers exhibit lamellar morphologies with well-developed hydrophilic-hydrophobic separation and interconnected hydrophilic domains on the scale of 10–30 nm, that seems to be the origin of higher proton conductivity as compared to the random analogs. However, the morphologies and performances of block copolymers rely on chemical architecture of both blocks, as well as membrane processing conditions, i.e., solvent selectivity, thermal annealing and acidification.

Unfortunately, these ionomers show a poor phase separation between the ionic function and the polymer backbone and the acidity of ionic function is lower than that of Nafion. The improvement of these characteristics should lead to ionomer with better performances. Rational approaches focused on these features will be widely discussed in the next sections.

3.2. Ionomers with Sulfonic Acid Attached to Fluorenyl Groups

Many researches were focused on the aromatic ionomers bearing sulfonated fluorenyl moieties due to their advantages such as (i) easier sulfonation, (ii) higher stability of sulfonic acid on the pendant phenylene groups, and (iii) improved water affinity at high temperature leading to higher proton conductivity.

3.2.1. Homopolymers and Random Copolymers

Two series of poly(arylene sulfone) containing sulfofluorenyl groups, i.e., homopolymer SFES1 and random copolymer SFES2 (**Figure 3.9**), were reported by Watanabe et al.[90,91] The ionomers were obtained by post-sulfonation which takes place only at 2,7-position on fluorenyl moieties and the degree of sulfonation (expressed as y in **Figure 3.9**) is controlled by simply adjusting the amount of chlorosulfonic acid in the reaction. Due to the rigidity of polymer backbone, SFES1 with IEC ~1.48 meg/g showed lower water uptake than that of Nafion 112. For instance, when equilibrated at 85 °C and 93% RH, the water uptake of the SFES1 membrane was ~17.5 wt% (λ ~6.6), as compared to ~15 wt% (λ ~9.2) of Nafion 112. At 100 °C and 100% RH, SFES1 (y ~0.35, IEC ~1.14 meq/g) and SFES2 (IEC ~1.35 meq/g) showed comparable conductivity to that of Nafion 112 (~0.2 S/cm). At reduced RH, SFES1 and SFES2 (with IEC ~1.5 meq/g) showed similar performance, but much lower than that of Nafion 112 in all humidity range (**Figure 3.10**). In Fenton's reagent (3% H_2O_2 containing 2 ppm $FeSO_4$) at 80 °C, the dissolution of SFES membranes started after 40 minutes and the molecular weight is lowered to 1/3 of the original after 1h. The oxidative stability decreases with IEC. The thermal degradation of SFES1 started above 250 °C in nitrogen atmosphere.

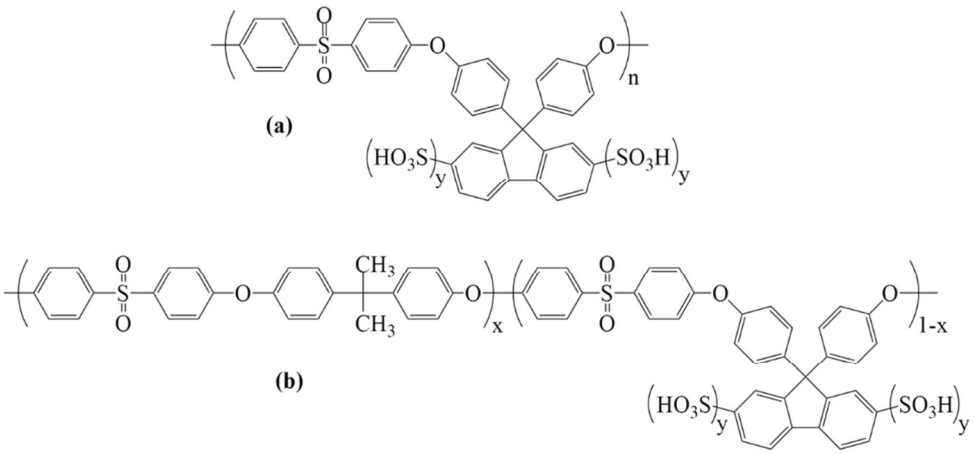

Figure 3.9. SFES-based (a) homopolymer SFES1 and (b) random copolymer SFES2.

Then, a study on influence of chemical structure of the backbone on membrane performance was conducted. In this aim, (i) the backbone structure was modified by copolymerizing the dihydroxyfluorene with other monomers such as monoaromatic monomer, i.e., nitrile benzene or hydrophobic monomer, i.e., decafluorobiphenyl (**Figure 3.11**),[92] (ii) fluorenyl moiety was substituted with methyl (**Figure 3.12a**),[93] (iii) the dihydropxyfluorene were copolymerized with sulfonated monomer (**Figure 3.12b**).[93]

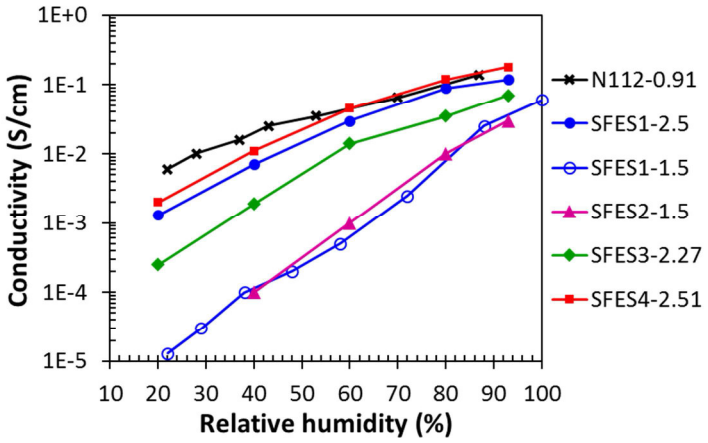

Figure 3.10. Proton conductivity vs RH at 80 °C of various random SFES ionomer. The number next to the sample name is IEC.

In the first approach, studied by Shimura at al.,[92] all the ionomers with IEC ranging from 1.6 to 2.7 meq/g, showed much lower performance than those of Nafion 112 and SFES1 (y ~ 0.9, IEC 2.5 meq/g) in all humidity range. The lower conductivity in the case of ionomer based on nitrile benzene segments can be explain by interactions between CN and SO_3H while in the case of partially fluorinated ionomers (**Figure 3.11e**) this is surprising. The polymer containing nitrile group on meta-position (**Figure 3.11c**) showed highest oxidative stability in Fenton's reagent due to no displaceable hydrogen atoms meta to the nitrile groups.

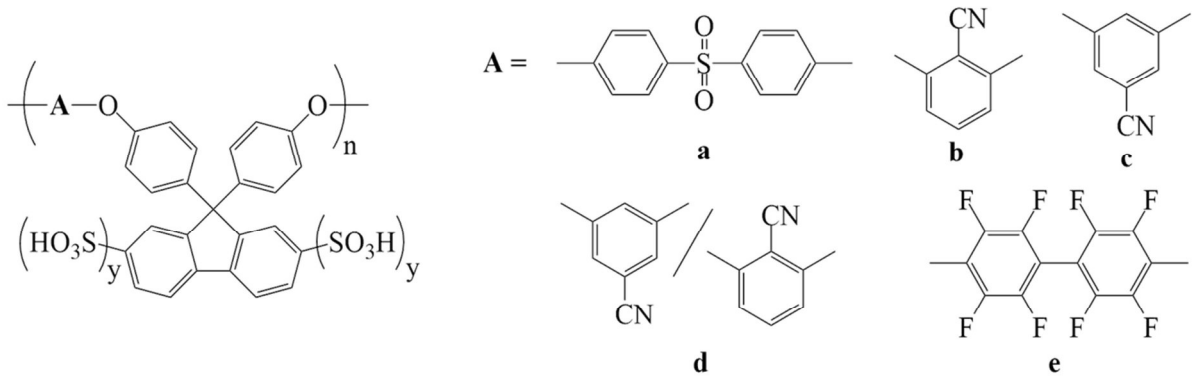

Figure 3.11. SFES-based copolymers obtained from different comonomers. (a) DFDPS, (b) 2,6-DFB, (c) 3,5-DFB, (d) 2,6-DFB/3,5-DFB, (e) DFBP.

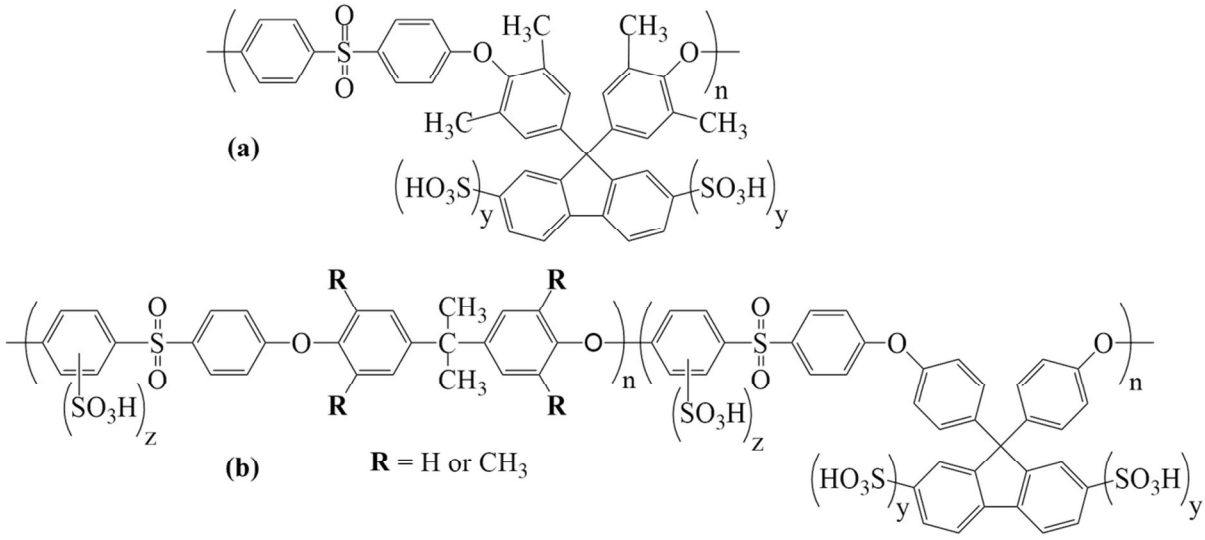

Figure 3.12. Methylated SFES-based ionomer: (a) SFES3, (b) SFES4.

In the series of ionomers containing methyl groups on fluorenyl moiety (SFES3) or on backbone (SFES4) (**Figure 3.12**)[93] it was reported that dimensional stability was significantly improved for the methylated ionomer membranes in comparison with that of the non-methylated ones (SFES1 and SFES2). Isopropylidene tetramethylbiphenylene moieties seems to be more effective than the methyl-substituted fluorenyl groups in improving ionomer morphologies and performances. Thus, STEM analyses revealed that the connectivity of ionic clusters of SFES4 membrane was significantly improved as compared to that of SFES1 and was similar to that of Nafion® 112. As a result, while SFES3 showed lower conductivity in all humidity range as compared with SFES1, SFES4 resulted in much higher conductivity than its analog SFES2 (**Figure 3.10**). Moreover, the presence of methyl groups on adjacent phenylene rings also improve membrane's oxidative stability.

3.2.2. Multi-Block Copolymers

A series of multi-block copolymers containing highly sulfonated SFES1 hydrophilic blocks with different hydrophobic blocks were developed. Depending on chemical composition of the hydrophobic block, the sulfonation could be performed before[94] or after[95–98] the coupling process. Thus in the case of SFES/PES and SFES/PNES (**Figure 3.13** on the left), the sulfonation of block copolymer backbone have to be performed before the coupling because both blocks are susceptible to be sulfonated. In the case of SFES/mPES and SFES/PEKS, due to the electron withdrawing effect of SO_2 and CO groups, and/or to the substitution ether-to-ortho position with CH_3 groups, the sulfonation will be selective, will take place only on SFES block.

As compared to the random copolymer SFES1 most block copolymers exhibit lamellar morphology with distinct and well-connected hydrophilic domains of 10–11 nm, increasing with IEC and block length, but the latter is more influential. Moreover, block copolymer membranes showed an anisotropic swelling behavior in hydrated state and the water uptake increased with IEC and block length due to larger and better-interconnected hydrophilic domains, leading to higher proton conductivity. For the majority of block copolymers it was reported much higher proton conductivity at reduced RH (**Figure 3.13** on the right) than SFES1 ionomer. However, it is not the case for ionomer with methylated hydrophobic block. Thus, SFES/mPES showed lowest conductivities, ~ 9×10^{-4} S/cm at 20% RH. Rigid structure of a tetra-methylated BPA species might restrict the packing of hydrophilic blocks and/or mobility of their ionic sites, which leads to poor performance of the ionomer. SFES/PES and SFES/PNES exhibited similar performance in all humidified condition. Ionomer SFES/PEKS reaches highest conductivities among the block copolymers and higher than that of Nafion above 70% RH. This behavior was explained by the chain flexibility, ketone-bridge are more flexible as compared to naphthalene or covalent junction in SFES/PNES and SFES/PES structures, respectively. It can be also supposed the semi-crystalline nature of diphenylketone moiety should result in higher phase separation between semi-crystalline hydrophobic domains and hydrophilic domains, as in the case of as-PES/PEEK ionomer. In terms of oxidative stability, the Fenton's reagent (3% H_2O_2 containing 2 ppm $FeSO_4$) at 80 °C completely dissolved most block copolymer membranes with IEC > 2 after 1h and the residual weight increased with decreasing IEC.

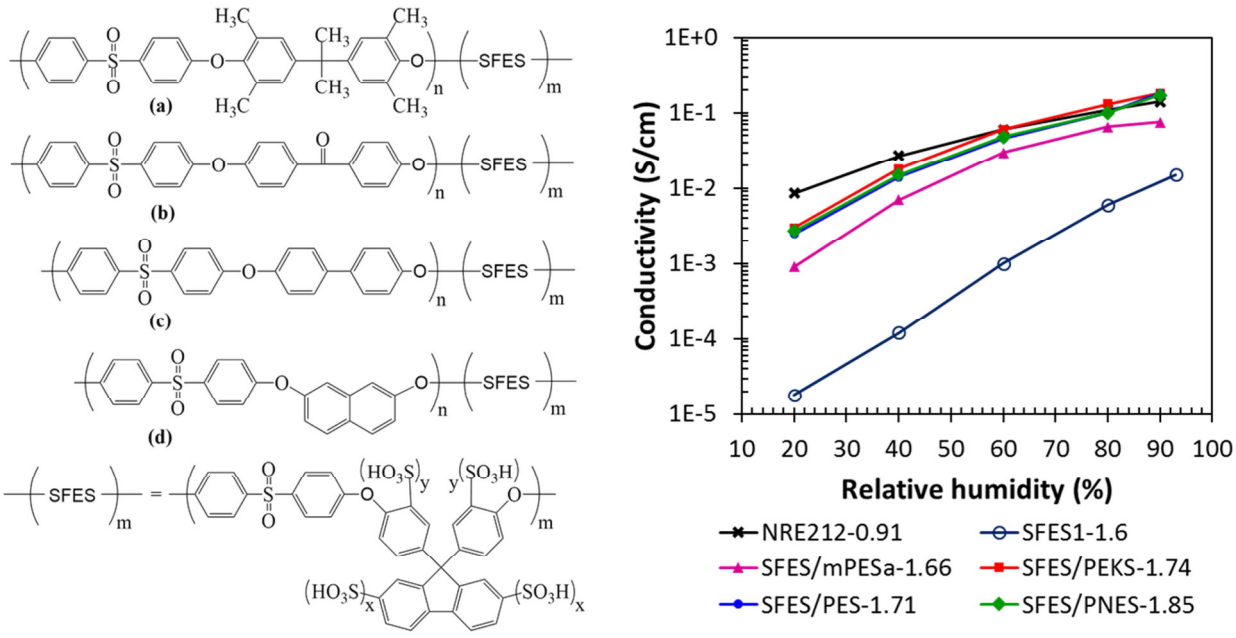

Figure 3.13. Chemical structure of SFES-based block copolymers with different hydrophobic blocks (left) and their conductivity measured at 80 °C (right) with similar IEC in comparison to random SFES and Nafion® 112 membrane. (a) SFES/mPESa,[96] (b) SFES/PEKS,[95,97,98] (c) SFES/PES,[94] (d) SFES/PNES.[94] The number next to the sample name is IEC.

3.2.3. Conclusions

Due to the high rigidity of polymer backbone, random SFES ionomers bearing sulfofluorenyl groups with different main chain structure didn't showed improved performance as compared to random poly(ether sulfone)-based aromatic ionomer with sulfonic acids directly attached to the main chain (as-PES35) possessing similar IEC (~1.5 meq/g). However, SFES1 with higher IEC (~2.5 meq/g) showed better connectivity of ionic domains and much improved performance. Morphologies and properties of random SFES-based ionomers has been improved by tuning their molecular architecture and the most effective approach was developing ionomers with segmented structure with improved hydrophilic/hydrophobic phase separation. As compared to their random analogs, most multi-block copolymers give better structuration with well-connected hydrophilic domains and higher conductivities. Although sulfonic acid groups on the fluorenyl groups are known more stable to both hydrolysis and oxidation, all sulfonated fluorenyl-based ionomers did not show superior oxidative stability in comparison with as-PES-based ionomer and their oxidative stability drastically decreased with IEC.

3.3. Ionomers with Sulfonic Functions Spaced from Backbone

A plausible approach to improve the structuration of ionic domains and the performance of aromatic ionomers is to space the ionic functions from polymer backbones via a spacer. The spacer can be (i) an arylene ring or polyarylene chain, (ii) an alkyl chain, (iii) a perfluoroalkyl chain. The flexibility of the spacer and its electron-withdrawing capacity are expected to have strong impacts on the structuration of ionic domains and the acidity of the acidic groups attached.

3.3.1. Ionic Functions Spaced by a Phenylene Spacer

3.3.1.1. Spacer Directly Connected to Main Chain

A wide range of random aromatic ionomers based on poly(ether ketone) (PEK),[99,100] and poly(ether sulfone) (PES)[101,102] backbone bearing sulfo-phenylene side chain (containing one or two arylene rings, marked as ph- or dph-, respectively) was reported by the group of Guiver (**Figure 3.14**). These ionomers can be obtained by bottom-up method or by post-sulfonation. The post-sulfonation predominately occurs at the strongly active para-position of pendent phenyl rings without evidence of chain degradation.[102] Unfortunately, this structure leads to poor morphology due to a high rigidity of main chains and side chain, and the low mobility of ionic functions. Thus, TEM image of ph-PEK bearing sulfo-phenylene side chain showed no obvious phase separation.[99] As a result, to obtain equivalent proton conductivity to that of Nafion at 100% RH, an IEC at least 1.8 meq/g is needed for most of the ionomers.

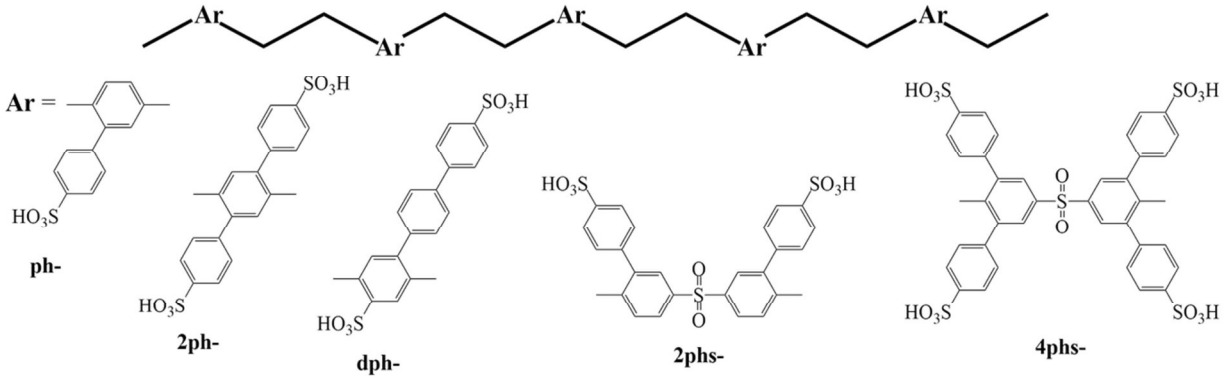

Figure 3.14. Representatives of aromatic ionomers bearing various phenylene side chains.

In Fenton's reagent (3% H_2O_2 containing 2 ppm $FeSO_4$) at 80 °C, however, these ionomers exhibited an excellent oxidative resistance. For instance, 2ph-PES40 (IEC ~1.50 meq/g) maintained film integrity after 4h.[101] To overcome the drawbacks of the random ionomers, a series of poly(ether sulfone)-based block copolymers bearing short phenylene side chains (ph-PES/FPES) was developed (**Figure 3.15**).[103] The block copolymer showed a

lamellar morphology with interconnected hydrophilic domains of 5–10 nm in width and an anisotropic swelling behavior. This result also revealed the contribution of partially fluorinated hydrophobic block (FPES). To obtain equivalent proton conductivity to that of Nafion 112 in water, an IEC at least 1.4 meq/g is sufficient and with the same IEC ionomers possessing larger block exhibited higher performance. The most conductive block copolymer (IEC ~ 1.82 meg/g) showed higher proton conductivity than that of Nafion 112 above 60% RH.

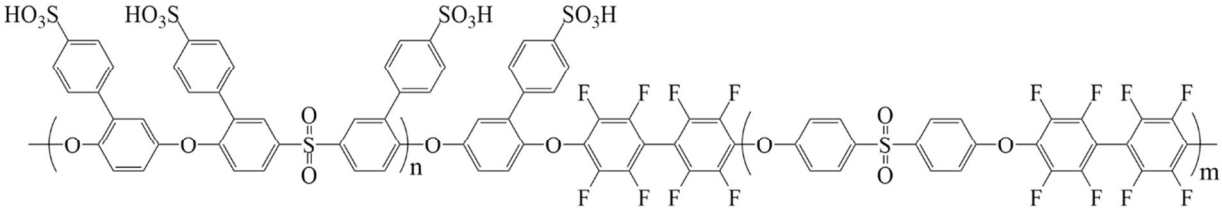

Figure 3.15. Aromatic block copolymer ph-PES/FPES.

3.3.1.2. Spacer Connected via Ketone Bridge

Ionomers bearing sulfobenzoyl (sbz-) side chains were firstly reported by Jannasch et al.[104,105] The ionomers were obtained by lithiation of polymer backbone using BuLi as a metalation agent, followed by the reaction of the lithiated sites with 2-sulfobenzoic acid cyclic anhydride. When attached to different aromatic backbones, i.e., poly(arylene ether)s, poly(arylene ether sulfide)s, and poly(arylene sulfide)s, it was reported that Tg of the backbones influence the size of ionic clusters.[106] In fact, SAXS spectra showed that the ionic clustering was promoted by ionomers with more flexible backbones and lower Tg, resulting in higher proton conductivity. However, ionomers with higher Tg possessed a higher thermal stability. In contrast, when grafted on two different poly(ether sulfone) backbones, i.e., 4,4'-biphenol-based and bisphenol A-based poly(sulfone) (sbz-PES and sbz-PESa, respectively, **Figure 3.16**), sbz-PES with higher rigidity of polymer main chain showed almost twice the conductivity (at 60 °C) than that of sbz-PESa (64 vs 34 mS/cm, respectively) with the same IEC (~1.5 meq/g) and water content (~30 wt%).[104] However, all the samples had similar activation energies, which indicated that the proton conduction occurred through the same mechanism.

Then, on the PESa backbone the sulfonic acid groups are attached onto benzoyl-based side chains with different structure and their impacts on the ionic clustering and properties of PEMs were investigated (**Fig. 3.17**).[107,108]

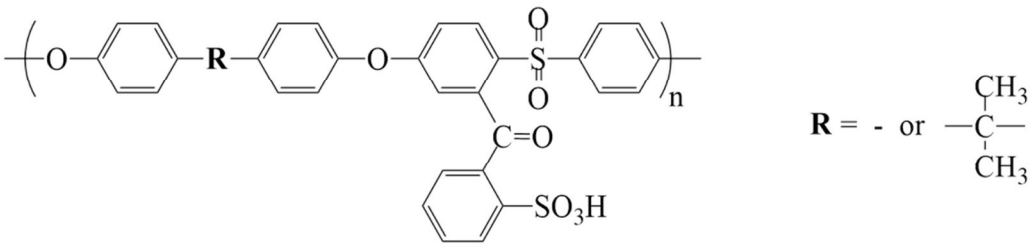

Figure 3.16. Chemical structure of sbz-PES (R = −) and sbz-PESa (R = −C(CH$_3$)$_2$−).

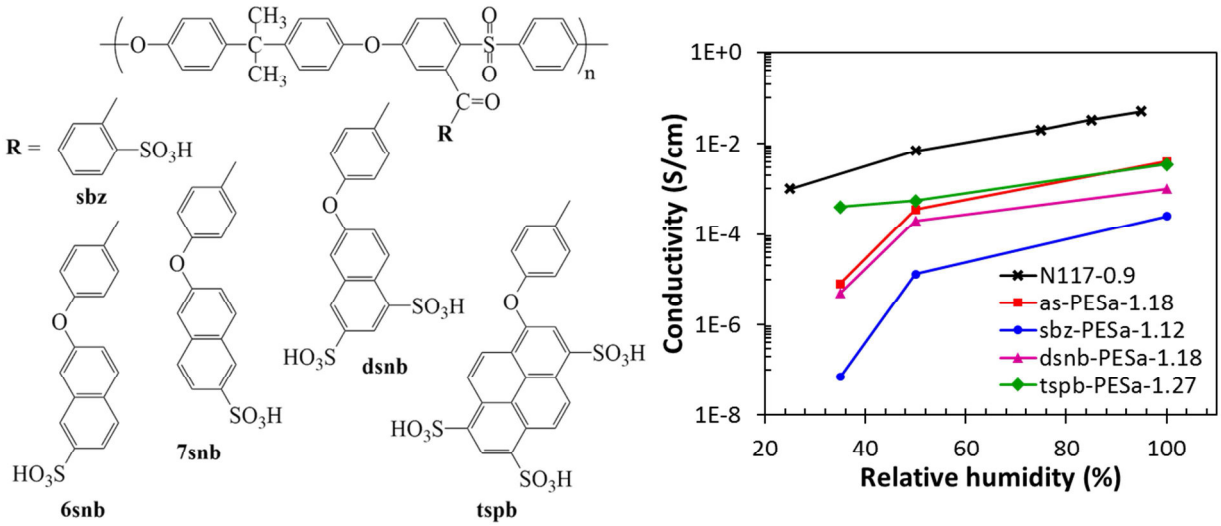

Figure 3.17. Chemical structure of PESa bearing different side chains (left) and their proton conductivity vs RH at 25 °C (right). The number next to the sample name is IEC.

SAXS profile of sbz-PESa appears with an unclear ionomer peak, indicating a poor clustering of the ionic sites, while a well-defined ionomer peak was observed in the case of extended side chains (**Table 3.2**). The short spacer between main chain and sulfonic acid group present in sbz-PESa was not sufficient to promote an efficient clustering. The peak intensity increases and its position shifts toward lower q with the side chain length, indicating a larger ionic domain. As a result, the ionomer bearing extended side chain (6snb-PSU) with IEC 0.77 meq/g showed equivalent conductivity versus temperature to that of sbz-PESa with IEC 1.12 meq/g. The position of the sulfonic group on the side chain, seems to play an important role in transport property, i.e., when the sulfonic function is in sixth position (6snb-PSU) the conductivity was higher than that in seventh position (7snb-PSU).[108] Ionomers with two or three sulfonic acid groups per naphthalene ring (dsnb-PESa and tspb-PESa, respectively, **Figure 3.17**) showed improved performance and both show comparable conductivities at the same IEC.[107] Unfortunately, all aromatic ionomers in this work showed lower conductivity than that of Nafion at reduced RH range and did not exhibit improved

performance as compared to post-sulfonated as-PESa.[108] To obtain higher proton conductivity than that of Nafion, an IEC > 1.4 meq/g is required for all ionomers.

Table 3.2. Properties of Sulfobenzoyl-based Aromatic Ionomers

Ionomers	IEC (meg/g)	WU[a] (%)	λ^a	$D_{ionic}{}^b$ (nm)
as-PESa	1.15-1.83	22-77	11-23	2.4-2.5
sbz-PESa	0.74-1.12	20-21	10-15	2.2-2.7
6snb-PESa	0.39-0.77	12-13	9-17	3.7
7snb-PESa	0.8	15	11	3.5
dsnb-PESa	1.18-1.71	27-55	12-18	4.0-4.4
tspb-PESa	0.6-2.11	17-104	16-27	4.4-7.1

[a]In water at room temperature. [b]Measured from SAXS profiles.

3.3.1.3. Conclusions

Both the main chain and side chain structure have strong impact on morphology and transport properties of ionomer membranes. In comparison to sulfobenzoyl-based side chains, generally, the phenylene rings directly attached to the main chain showed less phase separation due to the more rigid pendant chain, which results in lower proton conductivity. Moreover, random ionomers bearing extended benzoyl-based spacer with higher mobility and larger size resulted in much improved structuration of ionic domain. As expected, the block copolymer bearing phenylene side chains showed a lamellar morphology with interconnected hydrophilic domains of 5–10 nm in width and an anisotropy swelling behavior. An IEC ~1.82 meg/g is needed to obtain higher proton conductivity than that of Nafion 112 above 60% RH. Equivalent proton conductivity with lower IEC should be expected for block copolymer bearing extended benzoyl-based spacer. However, such a block ionomer is still missing in literature.

3.3.2. Ionic Functions Spaced by an Alkyl Spacer

It is widely accepted that alkyl groups are highly susceptible to degradation in the harsh condition during fuel cell operation due to the low dissociation energy of C–H (350 kJ/mol), as compared to 485 kJ/mol of C–F.[109] Moreover, by bonding the sulfonic function to alkyl spacer the acidity is decrease as compared to that of aryl sulfonic acid. Thus, the order of the acidities of the pendant sulfonic acid groups is $-CF_2CF_2SO_3H$ (estimated pKa from −12 to −14)[110–112] > $-C_6H_4SO_3H$ (estimated pKa ~ −2.5)[113] > $-(CH_2)_3SO_3H$ (estimated pKa ~ −0.6).[111] Recent work, however, revealed that the introduction of alkyl groups into polyimide-based ionomers have positive effects on their hydrolytic stability without sacrificing proton conductivity, oxidative and mechanical properties.[114–116] This behavior was explained by both steric and electron-donating effect of alkyl groups. The latter raises the electron density of imide nitrogen atoms, alleviating the nucleophilic attack of water. Recently, much attention has been paid to elucidating the influence of flexible alkyl spacers on the organization of ionic domains and the performance of aromatic ionomers.

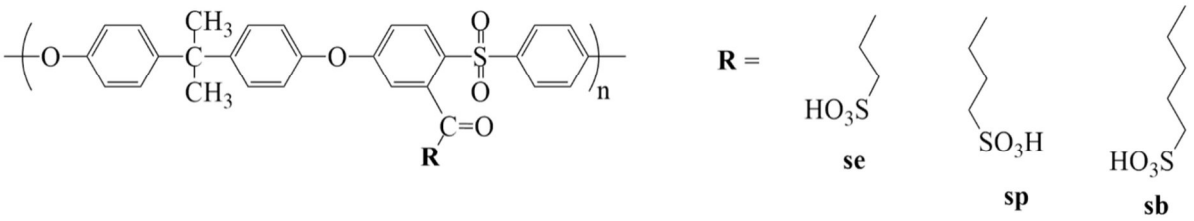

Figure 3.18. PESa bearing different sulfoalkyl side chains.

Jannasch et al.[117] reported a series of bisphenol A-based polysulfones (PESa) bearing different sulfoalkyl side chains, e.g., sulfoethyl (se-PESa), sulfopropyl (sp-PESa), sulfobutyl (sb-PESa) (**Figure 3.18**). The ionomers were obtained by lithiation-sulfination method, followed by the reaction with corresponding bromoalkanesulfonate. The thermal decomposition of all three ionomers occurred slightly above 300 °C, implying similar thermal stability to that of directly sulfonated as-PESa and sulfophenylated ph-PESa ionomers. The authors observed an improved water uptake of these ionomers as compared to that of as-PESa which was explained by the hydrophilic/hydrophobic phase separation. Particularly, as-PESa with DS ~0.8 dissolved in water at room temperature[118] while the sulfoalkylated polymers (DS ~0.6–0.9) maintained their dimensional stability when equilibrated in water up to critical swelling temperatures (T_{crit}) between 70 and 100 °C where the membranes excessively absorbed water. Consequently, the proton conductivity dramatically increased above T_{crit}. In

comparison to se-PESa and sb-PESa, sp-PESa showed higher water uptake, along with higher proton conductivity in all measured condition.

A series of partially fluorinated poly(ether sulfone) (6FPES) bearing two or four sulfobutoxyphenyl side chain (2sbp-6FPES or 4sbp-6FPES, respectively, **Figure 3.19a**) was reported by Guiver et al.[119] The ionomers ware obtained by sequential bromination, followed by Suzuki coupling of functional side chains. In comparison to Nafion 117, 2sbp-6FPES and 4sbp-6FPES (both with IEC ~1.6 meq/g) showed lower relative water uptake, methanol permeability, higher proton conductivity in fully hydrated condition. Moreover, 4sbp-6FPES showed slightly higher conductivity than that of 2sbp-6FPES. Surprisingly, all membranes with IEC < 1.6 meq/g showed lower water uptake than that of Nafion 117 membrane. Unfortunately, no data was reported at reduced humidity. In comparison with their analogues 6FPES containing stiff pendant sulfophenyl groups, 2sbp-6FPES and 4sbp-6FPES with similar IEC displayed higher proton conductivity and much lower water uptake.

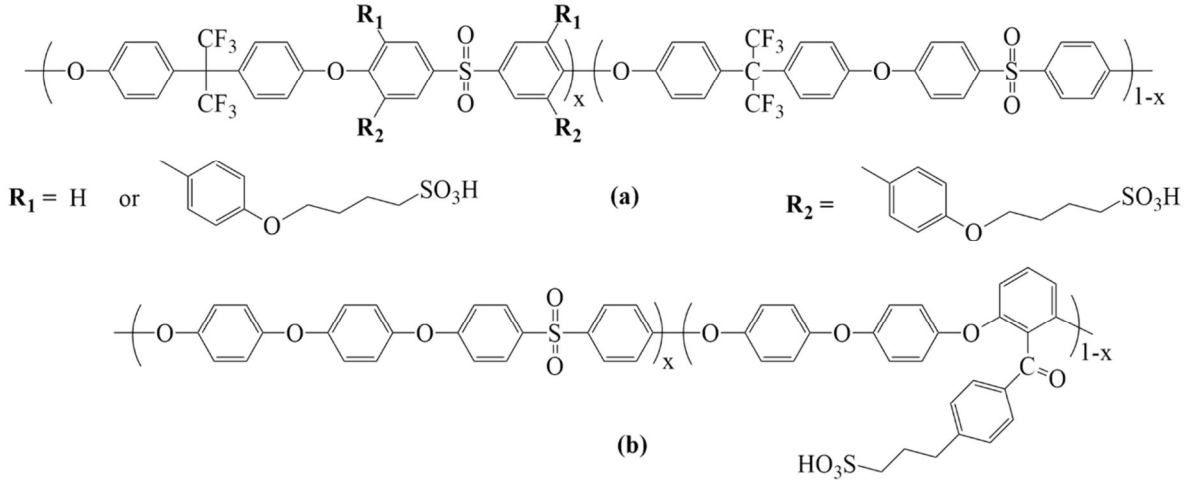

Figure 3.19. Chemical structure of (a) 2sbp-6FPES and 4sbp-6FPES, (b) spb-PES.

Similar results were reported by Jiang et al.[120] on random poly(ether sulfone)s bearing 4-sulfopropylbenzoyl pendant groups (spb-PES, **Figure 3.19b**) prepared by bottom-up method. Particularly, sp-PES exhibited good thermal and oxidative stability with T_d > 225 °C (acid-form) while 96 wt % membrane weight was retained after treated in Fenton's reagent at 80 °C for 1h. Moreover, within 4h treatment the membranes did not dissolved, suggesting good oxidative stability. The membranes exhibited high proton conductivities with less temperature dependence due to the phase separation between the hydrophilic sulfonic acid groups and the hydrophobic polymer main chain. TEM images showed that the average size of hydrophilic domains increased with DS and reached the value of around 40 nm in spb-PES70.

Conclusions. With similar main chain structure, ionomers bearing flexible sulfoalkylated side chain showed higher phase separation than that of those containing rigid phenylene side chains and lower water uptake than that of directly sulfonated ionomers. However, mostly of the reports concern random aromatic ionomers bearing flexible sulfoalkyl side chain while their analogs with multi block structure are missing in literature. In terms of side chain length, ionomers bearing sulfopropyl groups showed higher performance than that of sulfoethyl and sulfobutyl. Ionomers bearing four side chain per repeating unit showed higher performance than that with two side chain per repeating unit. However, due to the reduced acidity and the low C–H dissociation energy, the incorporation of sulfoalkylated side chain neither succeed to ionomers with improved proton conductivity nor improved thermal/oxidative stability.

3.3.3. Ionic Functions Spaced by an Perfluoroalkyl Spacer

A large work has recently focused on aromatic ionomers bearing perfluoroalkyl sulfonic acid (PFSA) pendant chains, as that of Nafion despite the cost and environmental issue. Due to high flexibility and hydrophobicity of side chains, super acidity of perfluorosulfonic acids, membranes with improved structuration and percolation of ionic domains and enhanced conductivities are expected from these kind of ionomers.[121] Moreover, the presence of fluorine on side chains can also reduce the water swelling and promote adhesion and electrochemical compatibility with Nafion-based electrodes.[67]

3.3.3.1. Influence of Main Chain Structure

Watanabe et al.[113,122] reported a series of poly(arylene ether)s containing pendant superacid groups on fluorenyl moieties (ps-PAE, **Figure 3.20**). The perfluoroalkyl sulfonic acid groups (ps-) were tethered to brominated PAE backbone by Ullmann's coupling reaction with copper. By varying the difluoro-comonomer, a series of ionomers with different main chain structure was obtained.

TEM images of ps-PAE membranes (IEC ~1.4–1.52 meq/g) exhibited a characteristic hydrophilic/hydrophobic separation with small interconnected ionic clusters (d_{ionic} ~2-3 nm), while larger clusters, but separated from each other, were observed in the post-sulfonated analog membrane bearing aryl sulfonic acid functions (SFES1, IEC ~1.59 meq/g). It is likely that the aggregation of pendant perfluorosulfonic acid groups is the formation of percolated ionic domains is more favorable than that of aryl sulfonic acid groups because of their higher polarity and flexibility. Therefore, ps-PAE membranes absorbed more water than SFES1 one (**Table 3.3**). Moreover, in reduced humidified condition, the ps-PAE membranes showed much higher proton conductivities, which was explained by both (i) higher dissociation of

perfluorosulfonic acid than that of aryl sulfonic at low RH, and (ii) better percolation of ionic domains.

Table 3.3. Properties of Aromatic Ionomers Bearing Perfluorosulfonic Acid Groups

Ionomers	IEC (meg/g)	σ^a (S/cm)	λ^b	d_{ionic} (nm)
NRE212	0.91	0.14	7.1	5 – 6
SFES1	1.59	0.014	4.5	
ps-PAE	0.87	0.035	5.7	
ps-PAE	1.4	0.12	5.3	2 – 3
ps-PSK	1.32	0.05	6.0	
as-PES	1.33	0.021	92	
as-PES	1.51	0.035	185	
ps-PES	1.34	0.077	88	3.7
ps-PES	1.58	0.12	172	
ps-FPAE1	1.40	//		4.3 – 6
ps-PEK/PES	1.29	0.13	8.3	10

[a]measured at 80 °C, ~90% RH. [b]membranes were equilibrated at 80% RH, 80 °C for 3h.

On the other hand, the interconnected ionic clusters of ps-PAE is smaller in diameter than that of Nafion (~5–6 nm) despite possessing similar side chain structure. The rigid main chain of ps-PAE seems to prevent the aggregation of the ionic side chains. It may be the reason why the conductivity of ps-PAE membranes is still lower than that of Nafion in all humidity range.

With similar IEC, the ionomer ps-PAE1 (**Figure 3.20a**) with partially fluorinated backbone showed lower water uptake and higher proton conductivity (humidity dependence at 80 °C) than that of ps-PAE2 (**Figure 3.20b**), as expected. Surprisingly, TGA measurements showed that the thermal decomposition of ps-PAE started at 180 °C even under argon flow.

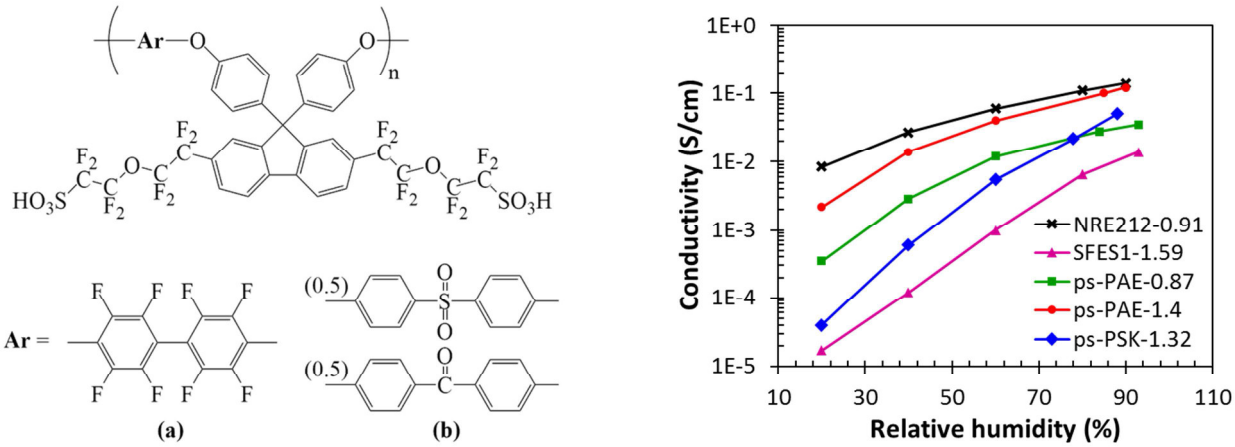

Figure 3.20. Chemical structure of (a) ps-PAE, (b) ps-PSK (left) and their proton conductivity vs RH at 80 °C (right).

Yoshimura et al.[123] reported the same behaviors with a series of random poly(ether sulfone) bearing the same pendant perfluoroalkyl sulfonic acid side chain (ps-PES, **Figure 3.21a**). The perfluorosulfonated side chains (ps-) were also attached to PES backbone by Ullmann's coupling reaction. The SAXS measurement showed that the ionic cluster size of ps-PES (IEC ~1.4 meg/g) is ~3.7 nm, smaller than that of Nafion (d_{ionic} ~4.2 nm) despite higher water content (38 wt% vs 23 wt%), which indicated the rigid main chain influence the aggregation of the side chain in ps-PES ionomers. However, the d_{ionic} of ps-PES is larger in comparison with that of ps-PAE mentioned above. Although the two cluster sizes were determined by two different methods with different water content, the comparison can be possible by exploiting d_{ionic} of Nafion as a standard. Particularly, in the same measuring condition with not much difference in λ, the ratio d_{ionic} of ps-PES /d_{ionic} of Nafion is ~0.88, while that number in the case of ps-PAE is 0.4–0.5. This observation reinforces the assumption on the effect of the main chain rigidity on the aggregation of ionic side chains. The PAE backbone bearing fluorenyl groups is more rigid than the PES one leading to smaller ionic domains. In comparison to directly sulfonated analogue (as-PES) with similar IEC, ps-PES showed slightly higher water uptake, but much improved conductivity at reduced humidity (50-90%).

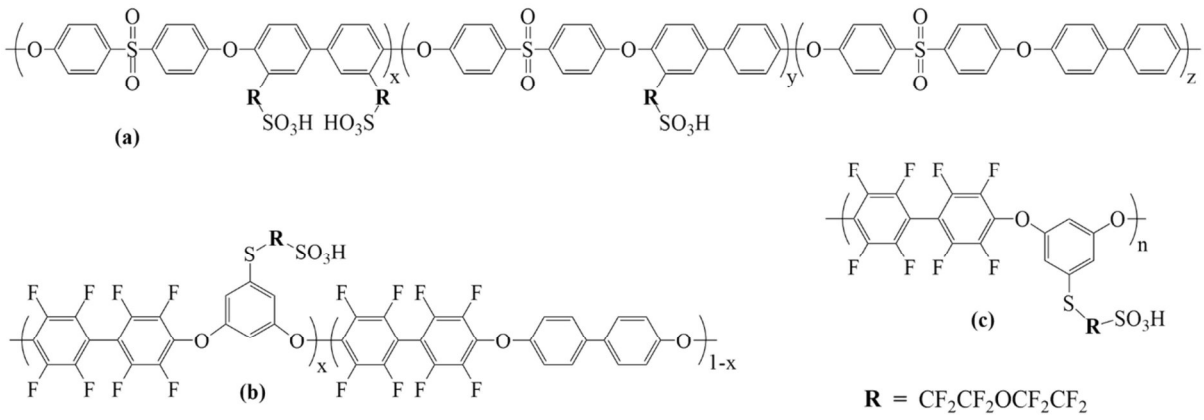

Figure 3.21. Chemical structure of (a) ps-PES, (b) random ps-FPAE, (c) homo ps-FPAE.

Recently, Iojoiu et al.[124,125] report a series of partially fluorinated poly(arylene ether)s (FPAE) bearing perfluorosulfonated side chain (ps-) by bottom-up method (**Figure 3.21b, c**). Due to high molecular weight of structural unit, the homo-polymer ps-FPAE1 showed a IEC of only 1.4 meq/g (**Figure 3.21c**). D_{ionic} of ps-FPAE1 (the acid form obtained from Li-salt form), analyzed from SANS spectra, ranges from 4.3 to 6.0 nm (with λ from 15 to 48). As compared to ps-PAE and ps-PES, the ionic domain size of ps-FPAE is largest and most similar to that of Nafion, implying the most effective aggregation of ionic side chains. This behavior is promoted by (i) the highly flexible main chain with meta-connection and (ii) the presence of fluorine on the polymer backbone which improves the hydrophilic/hydrophobic phase separation. The proposed materials show superior proton conductivity than Nafion, especially at low relative humidity.

The impact of main chain structure on morphology and properties of the random ionomers led researcher to develop block copolymers bearing perfluorosulfonic acid side chain with the aim of further improving the morphology and performance. The idea was firstly exploited by Watanabe et al.[126] by developing a series of block copoly(ether ketone)s containing the same pendant superacid groups (ps-PEK/PES, **Figure 3.22**). The ionomers were synthesized by coupling two oligomers, followed by Ullmann coupling reaction with the perfluorinated ionic compound. As expected, STEM images of the block copolymer exhibited well interconnected spherical and elliptic hydrophilic domains of about 10 nm in diameter which were much larger than that of their random analogs (ps-PSK). Therefore, with similar IEC (~1.3 meg/g) block copolymer showed higher water uptake and proton conductivity than that of their random analogs (0.13 vs 0.05 S/cm, at 80 °C and 90 % RH).

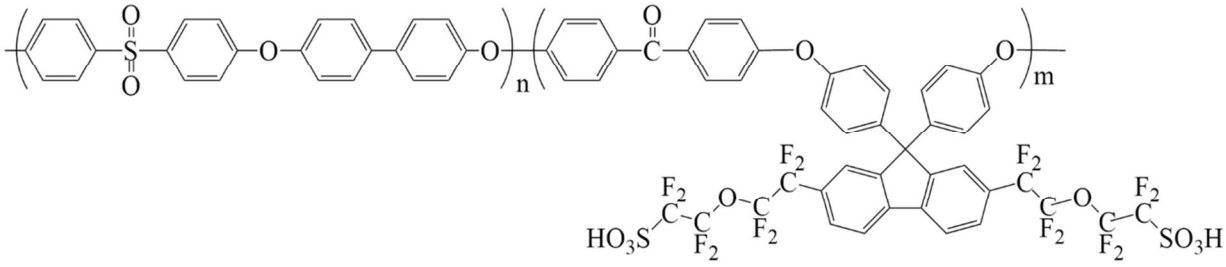

Figure 3.22. Chemical structure of multi-block copolymer ps-PEK/PES.

3.3.3.2. Influence of Side Chain Structure

The impact of perfluoroalkyl side chains as well as their structure were systematically investigated by Hickner et al.[127–129] which was carried out on a series of ionomers with the same bisphenol A-based poly(ether sulfone) backbone (PESa) bearing different side chain structure (**Figure 3.23**). The ionomers were obtained via borylation of aromatic C–H bonds and Suzuki coupling with sulfonated phenyl bromides. Firstly, the impact of perfluoroalkyl spacer (ps1-), as compared to phenyl (ph-) and alkyl (sp-) spacer, was reported. The second part of the work focused on the impact of perfluoroalkyl spacer with difference in length and structure.

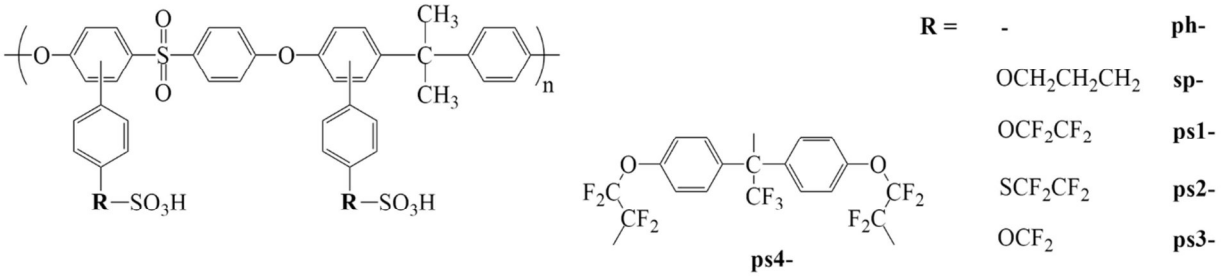

Figure 3.23. PESa bearing different pendant acidic moieties.

In the first part,[127] it is reported that the ionic inter-domain of PESa-based ionomers increased with the side chain length (**Table 3.4**). However, TEM images showed that the ionic domain of these aromatic ionomers is similar and much smaller than that of Nafion 112. As discussed above, this behavior comes from the rigidity of the polymer backbone, along with the shorter side chain of the aromatic ionomers. Despite a minor effect on morphology of these materials, perfluoroalkyl spacer have a large impact on water uptake and proton conductivity particularly at low RH. At full degree of sulfonation, particularly, ps1-PESa absorbed significantly less water than ph-PESa and sp-PESa (e.g., 39 vs 66 and 140 wt%, respectively). For the membranes with similar IEC (~ 2 meg/g), ps1-PESa was found to absorb slightly more water than sp-PESa due to better connectivity of ionic domains. In spite of lower IEC and WU, moreover, ps1-PESa showed significantly higher proton conductivity

under low RH conditions compared to that of the sulfonated aryl and alky analogs (ph-PESa and sp-PESa, respectively). Therefore, one may conclude that the stronger acidity of ionomers bearing perfluorosulfonic acids has a major contribution on the conductivity. It is surprising that the ionomer bearing perfluoroalkyl spacer showed lowest thermal stability (~ 170 °C) in comparison to that of the ones with phenyl and alkyl spacer (220 and 250, respectively). However, the thermal stability of perfluorosulfonic acid in this work is in accordance with that reported by Watanabe et al.[113] By comparing with the thermal stability of Nafion (~ 280 °C), it seems that when attached to aromatic polymer backbones, perfluorosulfonic acid moieties become less stable than when attached to a perfluorinated one.

Table 3.4. Properties of PESa Bearing Different Acidic Functions

Ionomers	DS (%)	IEC_{exp} (meg/g)	WU (wt%) (λ)[a]	d_{ionic}[b] (nm)
N112	-	0.86	19 (12)	3-5
ph-PESa	67.5	2.0	47 (13)	-
ph-PESa	100	2.57	140 (30)	2.0
sp-PESa	80.0	1.96	32 (9)	-
sp-PESa	100	2.29	66 (16)	2.8
ps1-PESa	100	1.94	39 (11)	2.7

[a]*In liquid water at RT.* [b]*Determined from SAXS profile of dry membranes.*

The size and the structure of perfluoroalkyl spacer were found to have influences on the morphology and properties of aromatic ionomers.[128] In fact, TEM images of aromatic ionomers bearing different perfluoroalkyl side chains (see **Figure 3.23**) showed that the size of ionic domains increases with the length of side chains. The largest ionic domain was reported for the ionomer with branched side chain (ps4-PESa). The size of these ionic domains (ranging from 1 to 3 nm) is still much smaller than that of Nafion 112. However, SAXS analysis of both experimental and simulated data showed a minor effect of side chain structure on morphology of the aromatic ionomers (**Table 3.5**).

With similar IEC, the membrane containing the shortest $-OCF_2SO_3H$ pendant (ps3-PESa) showed lowest proton conductivity. The polymer membrane with $-SCF_2CF_2SO_3H$ pendant chains (ps2-PESa) absorbed more water and showed enhanced proton conductivity compared to ps1-PESa, possibly owing to higher polarizability of sulfur than oxygen. Among them, the ionomer with a branched side chain structure (ps4-PESa) exhibited larger ionic domain, more

distinct phase separation, and higher proton conductivity compared to the one with linear side chain structure. These results suggest that not only the super-acidity of perfluoroalkyl sulfonic acid but also the topology of sulfonated groups can play a significant role in proton conduction in a PEM membrane.

Table 3.5. Properties of PESa Bearing Different Perfluoroalkyl Spacers

Ionomers	IEC_{exp} (meg/g)	WU (wt%) (λ)[a]	d_{ionic}[b] (nm)	d_{ionic}[c] (nm)
ps1-PESa	1.97	24 (6.8)	2.61	2.4
ps2-PESa	1.91	29 (8.5)	2.61	2.5
ps3-PESa	2.19	29 (7.3)	2.61	2.3
ps4-PESa	2.13	37 (9.6)	2.80	3.5

[a]At 30 °C and 98% RH. [b]Determined from SAXS profile of dry membranes. [c]Simulated values.

3.3.3.3. Influence of Counter Cation

In addition to polymer backbone and side chain structure, Iojoiu et al.[124] reported that counter cations also have influence on both morphology and performance of aromatic ionomers. The work was conducted on a series of ps-FPAE membranes (see **Figure 3.21b, c**) cast from the solutions of ionomers in their Li^+ and K^+ forms. The ionic domains of the membranes obtained from Li-salt form are more homogeneous and better percolated, while those obtained from K-salt form are composed of two types of the ionic clusters: one with very high organization and another with worse organization. Such morphology dictates the higher proton conductivity of the ps-FPAE membranes cast initially in Li-salt form, compared to those obtained from ionomers in K-salt form. Despite a huge different in morphology, similar swelling behavior of the two ionomers was reported.

3.3.3.4. Conclusions

In comparison to aromatic polymer bearing aryl sulfonic acid functions, ionomers bearing perfluorosulfonic acid side chain exhibited higher nanostructured and percolated ionic domains. This morphological feature, along with higher dissociation ability, led to higher proton conductivity, notably at reduced RH. The morphology and properties of perfluorosulfonated ionomers were determined by both main chain and side chain structure as well as the counter cation. The more rigid is the main chain, the smaller and disconnected is the ionic domain which results in lower performance. The presence of fluorine on the main chain results in lower water uptake, but higher proton conductivity. The presence of fluorine

on alkyl side chain leads to higher water uptake and much improved proton conductivity due to (i) higher acidity of acidic functions and (ii) higher hydrophilic/hydrophobic phase separation. With regards to the impact of side chain structure, ionomers possessing longer and branched side chains result in better interconnected ionic domains than those of ionomers bearing shorter and linear side chain, respectively. In comparison to random ionomers bearing the same side chain, the block copolymer expressed much higher performance owing to higher hydrophilic/hydrophobic phase separation, along with larger ionic domains. With similar side chain length, however, the ionic domains of most perfluorosulfonated aromatic ionomer are smaller than those of Nafion and the rigidity of aromatic polymer backbone is believed to be the origin of this behavior.

3.4. Ionomers with Sulfonimide-based Acidic Moieties

The charge on perfluorosulfonyl imide anion is highly delocalized on the adjacent sulfoxides due to the electron-withdrawing and fluorinated alkyls.[130] Moreover, they showed improved thermal stability as compared to perfluorosulfonic acid moiety.[131] However, in comparison to sulfonic acid, ionomers bearing sulfonimide (Si) and perfluorosulfonimide (PFSI) functions received much less attention for PEM application, while their salt, bis(trifluoromethane)sulfonimide (TFSI), were widely studied as highly dissociated salt for polymer electrolyte in lithium-ion batteries.

A wide range of monomers and ionomers bearing perfluorosulfonimide function (psi-) was developed by DesMarteau et al.[132–137] Moreover, a comparison of fuel cell performance carried out on Nafion® 117 and its perfluorosulfonimide counterpart (psi-PTFE, **Figure 3.24a**) reported by Savett et al.[138] showed a similar dependency of conductivity on humidity and temperature on both ionomers, suggesting a similar conduction mechanism.

The first aromatic ionomer based on poly(ether sulfone)s bearing sulfonimide function (si-PES, **Figure 3.24b**) synthesized by bottom-up copolymerization of a trifluoromethanesulfonamide-containing comonomer was reported by Cho et al.[139] The authors reported a conductivity close to that of the sulfonated counter one (as-PES). With IEC < 1.4 meq/g, si-PES showed similar water uptake to that of its sulfonated counterpart (as-PES), but with higher IEC, si-PES showed much higher water uptake than that of as-PES. Compared with as-PES30, si-PES showed weaker temperature dependence, showing less activation energy than the sulfonic acid containing copolymers. In TGA measurement under nitrogen flow, si-PES was stable up to 250 °C, not higher than that of its sulfonated counterpart (as-PES).

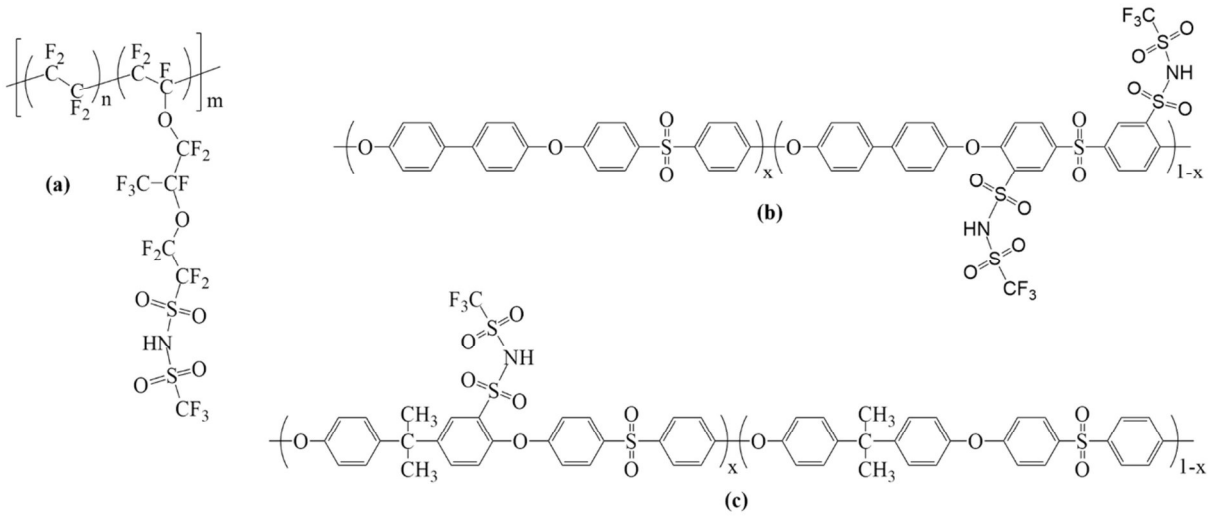

Figure 3.24. Chemical structure of (a) psi-PTFE, (b) si-PES, and (c) si-PESa ionomers.

Recently, Assumma et al.[140] reported a series of Bisphenol A-based poly(ether sulfone) containing sulfonimide groups (si-PESa, **Figure 3.24c**) developed by chemical modification of their sulfonated counterparts (as-PESa). The si-PESa membranes exhibited higher water uptake and conductivity than those of as-PESa. For example, with similar ionic exchange capacity (IEC), i.e., 1.8 meg/cm^3 at 60 °C and 95% RH, the conductivity of si-PESa is 10 mS/cm while that of as-PESa is 3.5 mS/cm.

Conclusions. Few publications on aromatic ionomers bearing sulfonimide function were reported. With the same IEC, aromatic ionomers bearing sulfonimide perfluorosulfonimide function showed higher proton conductivity at high RH, in combination with a higher water uptake in full hydrated condition than those of sulfonated analogs with similar main chain structure. These behaviors could be explained by the higher dissociation, the larger volume and the longer length of sulfonimide functions. Considering these interesting results, an aromatic ionomer bearing perfluorosulfonimide functions, possessing higher gas-phase acidity and hydrophobicity than that of perfluorosulfonic acid and sulfonimide, should give higher performance. However, considering the excessive water uptake of these ionomers, it should be advantageous either to cross-link the membrane or to tailor block copolymers, hence nanostructured sulfonimide ionomers.

3.5. Overall Conclusions and Thesis Objectives

This chapter covers a literature review on the principle and the current status of PEMFCs, as well as the challenges they must overcome to meet the market's requirements. The primary puzzle preventing PMEFCs from widespread commercialization is allied with widely exploiting of PFSA membranes as PEMs. This chapter also includes a scientific revision to the current status of the benchmark PEM material, the Nafion®, and of its promising alternative for the next generation of high performance PEM materials − the aromatic ionomers. Much attention, therefore, has been paid to elucidating the structure-morphology-property interplay of aromatic ionomers to highlight the role of ionomer components, notably the impact of side chain structure and acidic moiety, on membrane morphology and functional properties with the aim of providing a guidance for developing new aromatic ionomers with designed molecular architecture.

Despite advantages such as the availability, the processability, and the wide variety of chemical compositions, etc., the first generation of aromatic ionomers, e.g., the post-sulfonated ones, exhibited many shortcomings. Therefore, many other alternative approaches for ionomer synthesis have been proposed. As an example, the bottom-up method was used to prepare sulfonated aromatic ionomers with controlled chemical architecture and sulfonation degree, as well as with low side reactions. The poor phase separation of random ionomers was solved with the development of multi-block ionomers, while their thermal/oxidative stability could be improved by relocating acidic functions to deactivated position on arylene ring or by modifying the backbone structure. Most block copolymers exhibited lamellar morphologies with high hydrophilic/hydrophobic separation and interconnected hydrophilic domains on the scale of 10–30 nm. Their final morphologies and performances were shown to be determined by chemical architecture of both blocks, as well as membrane processing conditions, i.e., solvent selectivity and thermal annealing, etc.

However, the sulfonated aromatic ionomers were still presenting several drawbacks, mostly associated with (i) the poor structuration of ionic domains due to the proximity of ionic groups to the polymer main chain and (ii) the low acidity of aryl sulfonic acid function, which also need to be decoded to further improve the polymer performances. Therefore, considerable efforts have been focused to that aim by locating sulfonic acid groups on fluorenyl moieties, by introducing a spacer between ionic function and polymer main chain, or by exploiting other acidic moieties with higher acidity.

Unfortunately, ionomers having sulfonic acid groups on fluorenyl moieties did not exhibit improved thermal/oxidative stability. Moreover, due to the high rigidity of polymer backbone, higher IEC was needed to acquire equivalent performance to Nafion, as compared to other aromatic ionomers. It has to be pointed out that most fluorenyl-based multi-block copolymers give highly phase separation with well-connected hydrophilic domains on the scale of 10–11 nm leading to higher proton conductivity than that of corresponding random ionomers at reduced RH.

Random ionomers bearing rigid arylene side chains (ph-PES) did not show improved phase separation and proton conductivity. In contrast, multi-block copolymer (ph-PES/FPES) with fluorinated hydrophobic blocks exhibited a lamellar morphology with well-defined hydrophilic/hydrophobic phase separation, and interconnected hydrophilic domains of 5–10 nm in width. In comparison to rigid phenylene side chain, the extended benzoyl-based ones with higher mobility and larger size resulted in much improved structuration of ionic domain.

Random ionomers bearing flexible alkyl spacer show improved water uptake, along with better organization of ionic domains. Despite improved morphology, sulfoalkylated ionomers showed low proton conductivity due to the low acidity of alkyl sulfonic acid. The drawback of sulfoalkylated ionomers was solved by developing ionomers bearing perfluorosulfonic, sulfonimide, and perfluorosulfonimide side chains. At this point, random ionomers bearing perfluorosulfonic functions (ps-PES) showed higher conductivity in the whole range of humidity and temperature as compared to random sulfonated ionomers (e.g., as-PES, ph-PES, sp-PES, etc.). Aromatic ionomers bearing sulfonimide functions shows higher proton conduction, but the conductivity was performed only in water and at high relative humidity.

From the above observations, aromatic ionomers with multi-block main chain structure bearing a flexible perfluoroalkyl side chain terminated by a perfluorosulfonic superacid function appear to be the most promising candidate for the next generation of PEM materials. The route to synthesize this kind of ionomers was explored and established in our lab by Luca Assumma[141] and Olesia Danyliv[124,125,142] during their PhD. The main objectives of the present dissertation are (i) to optimize the film-elaborating conditions, i.e., solvent selectivity and thermal annealing, and (ii) to elucidate structure-morphology-property interplay in the new ionomers. This work was extended to perfluorosulfonated multi-block copoly(arylene ether sulfone)/Nafion blend membranes for improved morphology and performance. Finally, multi-block aromatic ionomers bearing perfluorosulfonimide functions were synthesized and characterized in consideration for PEM application.

REFERENCES

(1) Carrette, L.; Friedrich, K. A.; Stimming, U. *ChemPhysChem* **2000**, *1*, 162–193.

(2) Wang, Y.; Chen, K. S.; Mishler, J.; Cho, S. C.; Adroher, X. C. *Appl. Energy* **2011**, *88*, 981–1007.

(3) Carrette, L.; Friedrich, K. A.; Stimming, U. *Fuel Cells* **2001**, *1*, 5–39.

(4) Steele, B. C. H.; Heinzel, A. *Nature* **2001**, *414*, 345–352.

(5) Peighambardoust, S. J.; Rowshanzamir, S.; Amjadi, M. *Int. J. Hydrogen Energy* **2010**, *35*, 9349–9384.

(6) Hermann, A.; Chaudhuri, T.; Spagnol, P. *Int. J. Hydrogen Energy* **2005**, *30*, 1297–1302.

(7) Jiao, K.; Li, X. *Prog. Energy Combust. Sci.* **2011**, *37*, 221–291.

(8) Mehta, V.; Cooper, J. S. *J. Power Sources* **2003**, *114*, 32–53.

(9) Holdcroft, S. *Chem. Mater.* **2014**, *26*, 381–393.

(10) de Bruijn, F. A.; Dam, V. A. T.; Janssen, G. J. M. *Fuel Cells* **2008**, *8*, 3–22.

(11) Park, C. H.; Lee, C. H.; Guiver, M. D.; Lee, Y. M. *Prog. Polym. Sci.* **2011**, *36*, 1443–1498.

(12) Hickner, M. A.; Ghassemi, H.; Kim, Y. S.; Einsla, B. R.; McGrath, J. E. *Chem. Rev.* **2004**, *104*, 4587–4612.

(13) Kerres, J. A. *J. Memb. Sci.* **2001**, *185*, 3–27.

(14) Bose, S.; Kuila, T.; Nguyen, T. X. H.; Kim, N. H.; Lau, K.; Lee, J. H. *Prog. Polym. Sci.* **2011**, *36*, 813–843.

(15) Zhang, H.; Shen, P. K. *Chem. Soc. Rev.* **2012**, *41*, 2382–2394.

(16) Borup, R.; Meyers, J.; Pivovar, B.; Kim, Y. S.; Mukundan, R.; Garland, N.; Myers, D.; Wilson, M.; Garzon, F.; Wood, D.; Zelenay, P.; More, K.; Stroh, K.; Zawodzinski, T.; Boncella, J.; McGrath, J. E.; Inaba, M.; Miyatake, K.; Hori, M.; Ota, K.; Ogumi, Z.; Miyata, S.; Nishikata, A.; Siroma, Z.; Uchimoto, Y.; Yasuda, K.; Kimijima, K.-I.; Iwashita, N. *Chem. Rev.* **2007**, *107*, 3904–3951.

(17) Mauritz, K. A.; Moore, R. B. *Chem. Rev.* **2004**, *104*, 4535–4585.

(18) Schmittinger, W.; Vahidi, A. *J. Power Sources* **2008**, *180*, 1–14.

(19) Peron, J.; Mani, A.; Zhao, X.; Edwards, D.; Adachi, M.; Soboleva, T.; Shi, Z.; Xie, Z.; Navessin, T.; Holdcroft, S. *J. Memb. Sci.* **2010**, *356*, 44–51.

(20) Kreuer, K.-D. *Chem. Mater.* **2014**, *26*, 361–380.

(21) Kusoglu, A.; Weber, A. Z. *Chem. Rev.* **2017**, *117*, 987–1104.

(22) Yakovlev, S.; Balsara, N. P.; Downing, K. H. *Membranes (Basel).* **2013**, *3*, 424–439.

(23) Paddison, S. J.; Paul, R. *Phys. Chem. Chem. Phys.* **2002**, *4*, 1158–1163.

(24) Paddison, S. *Solid State Ionics* **1998**, *113–115*, 333–340.

(25) Kusoglu, A.; Kushner, D.; Paul, D. K.; Karan, K.; Hickner, M. A.; Weber, A. Z. *Adv. Funct. Mater.* **2014**, *24*, 4763–4774.

(26) Page, K. A.; Landis, F. A.; Phillips, A. K.; Moore, R. B. *Macromolecules* **2006**, *39*, 3939–3946.

(27) Fernandes, A. C.; Ticianelli, E. A. *J. Power Sources* **2009**, *193*, 547–554.

(28) Fujimura, M.; Hashimoto, T.; Kawai, H. *Macromolecules* **1981**, *14*, 1309–1315.

(29) Saccà, A.; Carbone, A.; Pedicini, R.; Portale, G.; D'Ilario, L.; Longo, A.; Martorana, A.; Passalacqua, E. *J. Memb. Sci.* **2006**, *278*, 105–113.

(30) Lin, H. L.; Yu, T. L.; Huang, C. H.; Lin, T. L. *J. Polym. Sci. Part B Polym. Phys.* **2005**, *43*, 3044–3057.

(31) Gierke, T. D.; Munn, G. E.; Wilson, F. C. *J. Polym. Sci. Polym. Phys. Ed.* **1981**, *19*, 1687–1704.

(32) Hsu, W. Y.; Gierke, T. D. *Macromolecules* **1982**, *15*, 101–105.

(33) Hsu, W. Y.; Gierke, T. D. *J. Memb. Sci.* **1983**, *13*, 307–326.

(34) Fujimura, M.; Hashimoto, T.; Kawai, H. *Macromolecules* **1982**, *15*, 136–144.

(35) MacKnight, W. J.; Taggart, W. P.; Stein, R. S. *J. Polym. Sci. Symp.* **1974**, *45*, 113–128.

(36) Roche, E. J.; Stein, R. S.; Russell, T. P.; MacKnight, W. J. *J. Polym. Sci. Polym. Phys. Ed.* **1980**, *18*, 1497–1512.

(37) Marx, C. L.; Caulfield, D. F.; Cooper, S. L. *Macromolecules* **1973**, *6*, 344–353.

(38) Eikerling, M.; Kornyshev, A. A.; Kuznetsov, A. M.; Ulstrup, J.; Walbran, S. *J. Phys. Chem. B* **2001**, *105*, 3646–3662.

(39) Litt, M. H. Reevaluation of Nafion Morphology. *American Chemical Society, Polymer Preprints, Division of Polymer Chemistry*, 1997, *38*, 80–81.

(40) Gebel, G.; Moore, R. B. *Macromolecules* **2000**, *33*, 4850–4855.

(41) Young, S. K.; Trevino, S. F.; Tan, N. C. B. *J. Polym. Sci. Part B Polym. Phys.* **2002**, *40*, 387–400.

(42) Haubold, H.-G.; Vad, T.; Jungbluth, H.; Hiller, P. *Electrochim. Acta* **2001**, *46*, 1559–1563.

(43) Loppinet, B.; Gebel, G. *J. Phys. Chem.* **1997**, *101*, 1884.

(44) Loppinet, B.; Gebel, G. *Langmuir* **1998**, *14*, 1977–1983.

(45) Gebel, G.; Loppinet, B. *J. Mol. Struct.* **1996**, *383*, 43–49.

(46) Gebel, G. *Polymer (Guildf).* **2000**, *41*, 5829–5838.

(47) Beaucage, G. *J. Appl. Crystallogr.* **1995**, *28*, 717–728.

(48) Roche, E. J.; Stein, R. S.; MacKnight, W. J. *J. Polym. Sci. Polym. Phys. Ed.* **1980**, *18*, 1035–1045.

(49) Windsor, C. G. *J. Appl. Crystallogr.* **1988**, *21*, 582–588.

(50) Rubatat, L.; Rollet, A. L.; Gebel, G.; Diat, O. *Macromolecules* **2002**, *35*, 4050–4055.

(51) Rubatat, L.; Gebel, G.; Diat, O. *Macromolecules* **2004**, *37*, 7772–7783.

(52) Schmidt-Rohr, K.; Chen, Q. *Nat. Mater.* **2008**, *7*, 75–83.

(53) Li, J.; Park, J. K.; Moore, R. B.; Madsen, L. A. *Nat. Mater.* **2011**, *10*, 507–511.

(54) Kreuer, K.-D.; Portale, G. *Adv. Funct. Mater.* **2013**, *23*, 5390–5397.

(55) Kusoglu, A.; Modestino, M. A.; Hexemer, A.; Segalman, R. A.; Weber, A. Z. *ACS Macro Lett.* **2012**, *1*, 33–36.

(56) Berrod, Q.; Lyonnard, S.; Guillermo, A.; Ollivier, J.; Frick, B.; Manseri, A.; Améduri, B.; Gebel, G. *Macromolecules* **2015**, *48*, 6166–6176.

(57) Hanot, S.; Lyonnard, S.; Mossa, S. *Nanoscale* **2016**, *8*, 3314–3325.

(58) Hanot, S.; Lyonnard, S.; Mossa, S. *Soft Matter* **2015**, *11*, 2469–2478.

(59) Wang, F.; Hickner, M.; Kim, Y. S.; Zawodzinski, T. A.; McGrath, J. E. *J. Memb. Sci.* **2002**, *197*, 231–242.

(60) Rozière, J.; Jones, D. J. *Annu. Rev. Mater. Res.* **2003**, *33*, 503–555.

(61) Kraytsberg, A.; Ein-Eli, Y. *Energy & Fuels* **2014**, *28*, 7303–7330.

(62) Genova-Dimitrova, P.; Baradie, B.; Foscallo, D.; Poinsignon, C.; Sanchez, J. . *J. Memb. Sci.* **2001**, *185*, 59–71.

(63) Alberti, G.; Casciola, M.; Massinelli, L.; Bauer, B. *J. Memb. Sci.* **2001**, *185*, 73–81.

(64) Harrison, W. L.; Wang, F.; Mecham, J. B.; Bhanu, V. A.; Hill, M.; Kim, Y. S.; McGrath, J. E. *J. Polym. Sci. Part A Polym. Chem.* **2003**, *41*, 2264–2276.

(65) Wang, F.; Hickner, M.; Ji, Q.; Harrison, W.; Mecham, J.; Zawodzinski, T. A.; McGrath, J. E. *Macromol. Symp.* **2001**, *175*, 387–395.

(66) Lee, M.; Park, J. K.; Lee, H. S.; Lane, O.; Moore, R. B.; McGrath, J. E.; Baird, D. G. *Polymer (Guildf).* **2009**, *50*, 6129–6138.

(67) Hou, H.; Di Vona, M. L.; Knauth, P. *ChemSusChem* **2011**, *4*, 1526–1536.

(68) Badami, A. S.; Lane, O.; Lee, H. S.; Roy, A.; McGrath, J. E. *J. Memb. Sci.* **2009**, *333*, 1–11.

(69) Chen, Y.; Rowlett, J. R.; Lee, C. H.; Lane, O. R.; VanHouten, D. J.; Zhang, M.; Moore, R. B.; McGrath, J. E. *J. Polym. Sci. Part A Polym. Chem.* **2013**, *51*, 2301–2310.

(70) Chen, Y.; Guo, R.; Lee, C. H.; Lee, M.; McGrath, J. E. *Int. J. Hydrogen Energy* **2012**, *37*, 6132–6139.

(71) Chen, Y.; Lee, C. H.; Rowlett, J. R.; McGrath, J. E. *Polymer (Guildf).* **2012**, *53*, 3143–3153.

(72) Yu, X.; Roy, A.; Dunn, S.; Badami, A. S.; Yang, J.; Good, A. S.; Mcgrath, J. E. *J. Polym. Sci. Part A Polym. Chem.* **2009**, *47*, 1038–1051.

(73) Lee, H.-S.; Roy, A.; Lane, O.; Dunn, S.; McGrath, J. E. *Polymer (Guildf).* **2008**, *49*, 715–723.

(74) Roy, A.; Yu, X.; Dunn, S.; McGrath, J. E. *J. Memb. Sci.* **2009**, *327*, 118–124.

(75) Lee, C. H.; Lee, K.-S.; Lane, O.; McGrath, J. E.; Chen, Y.; Wi, S.; Lee, S. Y.; Lee, Y. M. *RSC Adv.* **2012**, *2*, 1025.

(76) Guo, R.; Lane, O.; Vanhouten, D.; Mcgrath, J. E. *Ind. Eng. Chem. Res.* **2010**, *49*, 12125–12134.

(77) Jun, M.-S.; Choi, Y.-W.; Kim, J.-D. *J. Memb. Sci.* **2012**, *396*, 32–37.

(78) Kim, Y. S.; Wang, F.; Hickner, M.; Mccartney, S.; Hong, Y. T.; Harrison, W.; Zawodzinski, T. A.; Mcgrath, J. E. *J. Polym. Sci. Part B Polym. Phys.* **2003**, *41*, 2816–2828.

(79) Jannasch, P. *Fuel Cells* **2005**, *5*, 248–260.

(80) Taeger, A.; Vogel, C.; Lehmann, D.; Lenk, W.; Schlenstedt, K.; Meier-Haack, J.

Macromol. Symp. **2004**, *210*, 175–184.

(81) Gao, Y.; Robertson, G. P.; Guiver, M. D.; Mikhailenko, S. D.; Li, X.; Kaliaguine, S. *Polymer (Guildf).* **2006**, *47*, 808–816.

(82) Schuster, M.; de Araujo, C. C.; Atanasov, V.; Andersen, H. T.; Kreuer, K.-D.; Maier, J. *Macromolecules* **2009**, *42*, 3129–3137.

(83) Schuster, M.; Kreuer, K.-D.; Andersen, H. T.; Maier, J. *Macromolecules* **2007**, *40*, 598–607.

(84) Titvinidze, G.; Kreuer, K.-D.; Schuster, M.; de Araujo, C. C.; Melchior, J. P.; Meyer, W. H. *Adv. Funct. Mater.* **2012**, *22*, 4456–4470.

(85) Weiber, E. A.; Takamuku, S.; Jannasch, P. *Macromolecules* **2013**, *46*, 3476–3485.

(86) Takamuku, S.; Jannasch, P. *Macromolecules* **2012**, *45*, 6538–6546.

(87) Takamuku, S.; Jannasch, P. *Adv. Energy Mater.* **2012**, *2*, 129–140.

(88) Xing, D.; Kerres, J. *Polym. Adv. Technol.* **2006**, *17*, 591–597.

(89) Kim, D. S.; Robertson, G. P.; Guiver, M. D.; Lee, Y. M. *J. Memb. Sci.* **2006**, *281*, 111–120.

(90) Miyatake, K.; Chikashige, Y.; Watanabe, M. *Macromolecules* **2003**, *36*, 9691–9693.

(91) Chikashige, Y.; Chikyu, Y.; Miyatake, K.; Watanabe, M. *Macromolecules* **2005**, *38*, 7121–7126.

(92) Shimura, T.; Miyatake, K.; Watanabe, M. *Eur. Polym. J.* **2008**, *44*, 4054–4062.

(93) Miyatake, K.; Chikashige, Y.; Higuchi, E.; Watanabe, M. *J. Am. Chem. Soc.* **2007**, *129*, 3879–3887.

(94) Bae, B.; Hoshi, T.; Miyatake, K.; Watanabe, M. *Macromolecules* **2011**, 3884–3892.

(95) Bae, B.; Miyatake, K.; Uchida, M.; Uchida, H.; Sakiyama, Y.; Okanishi, T.; Watanabe, M. *ACS Appl. Mater. Interfaces* **2011**, *3*, 2786–2793.

(96) Bae, B.; Miyatake, K.; Watanabe, M. *ACS Appl. Mater. Interfaces* **2009**, *1*, 1279–1286.

(97) Bae, B.; Miyatake, K.; Watanabe, M. *Macromolecules* **2010**, *43*, 2684–2691.

(98) Bae, B.; Yoda, T.; Miyatake, K.; Uchida, H.; Watanabe, M. *Angew. Chem. Int. Ed. Engl.* **2010**, *49*, 317–320.

(99) Liu, B.; Robertson, G. P.; Kim, D.; Guiver, M. D.; Hu, W.; Jiang, Z. *Macromolecules* **2007**, *40*, 1934–1944.

(100) Liu, B.; Hu, W.; Kim, Y. S.; Zou, H.; Robertson, G. P.; Jiang, Z.; Guiver, M. D. *Electrochim. Acta* **2010**, *55*, 3817–3823.

(101) Liu, B.; Robertson, G. P.; Kim, D. S.; Sun, X.; Jiang, Z.; Guiver, M. D. *Polymer (Guildf).* **2010**, *51*, 403–413.

(102) Li, N.; Shin, D. W.; Hwang, D. S.; Lee, Y. M.; Guiver, M. D. *Macromolecules* **2010**, *43*, 9810–9820.

(103) Li, N.; Hwang, D. S.; Lee, S. Y.; Liu, Y. L.; Lee, Y. M.; Guiver, M. D. *Macromolecules* **2011**, *44*, 4901–4910.

(104) Karlsson, L. E.; Jannasch, P. *Electrochim. Acta* **2005**, *50*, 1939–1946.

(105) Lafitte, B.; Karlsson, L. E.; Jannasch, P. *Macromol. Rapid Commun.* **2002**, *23*, 896–

900.

(106) Jutemar, E. P.; Jannasch, P. *ACS Appl. Mater. Interfaces* **2010**, *2*, 3718–3725.

(107) Lafitte, B.; Jannasch, P. *Adv. Funct. Mater.* **2007**, *17*, 2823–2834.

(108) Jutemar, E. P.; Jannasch, P. *J. Memb. Sci.* **2010**, *351*, 87–95.

(109) Li, Q.; He, R.; Jensen, J. O.; Bjerrum, N. J. *Chem. Mater.* **2003**, *15*, 4896–4915.

(110) Kim, Y. S.; Pivovar, B. S. *Annu. Rev. Chem. Biomol. Eng.* **2010**, *1*, 123–148.

(111) Bordwell, F. G. *Acc. Chem. Res* **1988**, *21*, 456–463.

(112) Raamat, E.; Kaupmees, K.; Ovsjannikov, G.; Trummal, A.; Kütt, A.; Saame, J.; Koppel, I.; Kaljurand, I.; Lipping, L.; Rodima, T.; Pihl, V.; Koppel, I. A.; Leito, I. *J. Phys. Org. Chem.* **2013**, *26*, 162–170.

(113) Mikami, T.; Miyatake, K.; Watanabe, M. *ACS Appl. Mater. Interfaces* **2010**, *2*, 1714–1721.

(114) Asano, N.; Aoki, M.; Suzuki, S.; Miyatake, K.; Uchida, H.; Watanabe, M. *J. Am. Chem. Soc.* **2006**, *128*, 1762–1769.

(115) Asano, N.; Miyatake, K.; Watanabe, M. *Chem. Mater.* **2004**, *16*, 2841–2843.

(116) Yasuda, T.; Miyatake, K.; Hirai, M.; Nanasawa, M.; Watanabe, M. *J. Polym. Sci. Part A Polym. Chem.* **2005**, *43*, 4439–4445.

(117) Karlsson, L. E.; Jannasch, P. *J. Memb. Sci.* **2004**, *230*, 61–70.

(118) Nolte, R.; Ledjeff, K.; Bauer, M.; Mulhaupt, R. *J. Memb. Sci.* **1993**, *83*, 211–220.

(119) Wang, C.; Shin, D. W.; Lee, S. Y.; Kang, N. R.; Lee, Y. M.; Guiver, M. D. *J. Memb. Sci.* **2012**, *405–406*, 68–78.

(120) Pang, J.; Zhang, H.; Li, X.; Wang, L.; Liu, B.; Jiang, Z. *J. Memb. Sci.* **2008**, *318*, 271–279.

(121) Chang, Y.; Brunello, G. F.; Fuller, J.; Hawley, M.; Kim, Y. S.; Disabb-Miller, M.; Hickner, M. A.; Jang, S. S.; Bae, C. *Macromolecules* **2011**, *44*, 8458–8469.

(122) Miyatake, K.; Shimura, T.; Mikami, T.; Watanabe, M. *Chem. Commun. (Camb).* **2009**, 6403–6405.

(123) Yoshimura, K.; Iwasaki, K. *Macromolecules* **2009**, *42*, 9302–9306.

(124) Danyliv, O.; Iojoiu, C.; Lyonnard, S.; Sergent, N.; Planes, E.; Sanchez, J.-Y. *Macromolecules* **2016**, *49*, 4164–4177.

(125) Danyliv, O.; Gueneau, C.; Iojoiu, C.; Cointeaux, L.; Thiam, A.; Lyonnard, S.; Sanchez, J.-Y. *Electrochim. Acta* **2016**, *214*, 182–191.

(126) Mikami, T.; Miyatake, K.; Watanabe, M. *J. Polym. Sci. Part A Polym. Chem.* **2011**, *49*, 452–464.

(127) Chang, Y.; Brunello, G. F.; Fuller, J.; Disabb-Miller, M. L.; Hawley, M. E.; Kim, Y. S.; Hickner, M. A.; Jang, S. S.; Bae, C. *Polym. Chem.* **2013**, *4*, 272–281.

(128) Chang, Y.; Mohanty, A. D.; Smedley, S. B.; Abu-Hakmeh, K.; Lee, Y. H.; Morgan, J. E.; Hickner, M. A.; Jang, S. S.; Ryu, C. Y.; Bae, C. *Macromolecules* **2015**, *48*, 7117–7126.

(129) Xu, K.; Oh, H.; Hickner, M. A.; Wang, Q. *Macromolecules* **2011**, *44*, 4605–4609.

(130) Koppel, I. A.; Taft, R. W.; Anvia, F.; Zhu, S.-Z.; Hu, L.-Q.; Sung, K.-S.; DesMarteau, D. D.; Yagupolskii, L. M.; Yagupolskii, Y. L.; Ignat'ev, N. V.; Kondratenko, N. V.; Volkonskii, A. Y.; Vlasov, V. M.; Notario, R.; Maria, P.-C. *J. Am. Chem. Soc.* **1994**, *116*, 3047–3057.

(131) Thomas, B. H.; Shafer, G.; Ma, J. J.; Tu, M.-H.; DesMarteau, D. D. *J. Fluor. Chem.* **2004**, *125*, 1231–1240.

(132) Desmarteau, D.; Hunter, L. *J. Fluor. Chem.* **1991**, *52*, 7–12.

(133) Zhu, S.-Z.; Jin, G.-F.; DesMarteau, D. D. *Chinese J. Chem.* **2002**, *20*, 1268–1273.

(134) Creager, S. E.; Sumner, J. J.; Bailey, R. D.; Ma, J. J.; Pennington, W. T.; Desmarteau, D. D. *Electrochem. Solid-State Lett.* **1999**, *2*, 434–436.

(135) Zhang, J.; Desmarteau, D. D.; Zuberi, S.; Ma, J.; Xue, L.; Gillette, S. M.; Blau, H.; Gerhardt, R. *J. Fluor. Chem.* **2002**, *116*, 45–48.

(136) Atkins, J. R.; Sides, C. R.; Creager, S. E.; Harris, J. L.; Pennington, W. T.; Thomas, B. H.; Desmarteau, D. D. *J. New Mater. Electrochem. Syst.* **2003**, *6*, 9–15.

(137) Ford, L. A.; DesMarteau, D. D.; Smith, D. W. *J. Fluor. Chem.* **2005**, *126*, 651–658.

(138) Savett, S. C.; Atkins, J. R.; Sides, C. R.; Harris, J. L.; Thomas, B. H.; Creager, S. E.; Pennington, W. T.; Desmarteau, D. D. *J. Electrochem. Soc.* **2002**, *149*, A1527–A1532.

(139) Cho, C. G.; Kim, Y. S.; Yu, X.; Hill, M.; McGrath, J. E. *J. Polym. Sci. Part A Polym. Chem.* **2006**, *44*, 6007–6014.

(140) Assumma, L.; Iojoiu, C.; Albayrak Ari, G.; Cointeaux, L.; Sanchez, J.-Y. *Int. J. Hydrogen Energy* **2014**, *39*, 2740–2750.

(141) Assumma, L.; Iojoiu, C.; Mercier, R.; Lyonnard, S.; Nguyen, H. D.; Planes, E. *J. Polym. Sci. Part A Polym. Chem.* **2015**, *53*, 1941–1956.

(142) Danyliv, O.; Iojoiu, C.; Barbier, V.; Martin, V.; Sanchez, J.-Y. *J. Fluor. Chem.* **2016**, *189*, 43–50.

Chapter 2.

Partially-Fluorinated Multiblock Copoly(Arylene Ether Sulfone)s Bearing Perfluorosulfonic Acid Functions

Preamble

In this chapter, we present the synthesis and characterization of partially-fluorinated multi-block copoly(ether sulfone)s bearing perfluorosulfonic acid functions (InX/Y ionomer), a new aromatic ionomer with designed molecular architecture. A series of InX/Y ionomers with different block size and ion-exchange capacity (IEC) was synthesized by bromination of partially-fluorinated multiblock copoly(arylene ether sulfone), followed by perfluoro-sulfonation via Ullmann reaction. The partially fluorinated multiblock copoly(ether sulfone)s (namely PES-FPES) was synthesized by "one-pot-two-step synthesis". The synthesis procedure was slightly modified from a protocol previously developed in our lab.[1] Due to the low solubility of the hydrophobic FPES block in DMSO, especially at high molecular weight, the PES-FPES multi-block copolymers in this work were synthesized in DMAc instead of DMSO. The chemical structure of the intermediates and the final products was followed by ^{1}H and ^{19}F NMR spectroscopy. The thermal and thermomechanical properties of the ionomers were characterized by DSC, TGA, and DMA. The synthesis procedure and ionomer characterization are briefly presented in **Annexe 1**.

The main objective of this chapter is to establish the relation between molecular architecture, membrane processing condition and functional properties, with the aim of producing the highest performance PEM materials for a viable use in PEMFCs. During the project, we have synthesized around 100 samples with the following parameters

IEC	from 0.96 to 1.56 meq/g
block length	from 5000 to 15000 g/mol
casting solvents	DMSO and DMAc
thermal annealing	150 °C

and investigate their sorption, morphology, thermomechanical and transport properties. Our findings were published in *ACS Applied Materials & Interfaces*.[2,3]

References

(1) Assumma, L.; Iojoiu, C.; Mercier, R.; Lyonnard, S.; Nguyen, H. D.; Planes, E. *J. Polym. Sci. Part A Polym. Chem.* **2015**, *53*, 1941–1956.

(2) Assumma, L.; Nguyen, H.-D.; Iojoiu, C.; Lyonnard, S.; Mercier, R.; Espuche, E. *ACS Appl. Mater. Interfaces* **2015**, *7*, 13808–13820.

(3) Nguyen, H. D.; Assumma, L.; Judeinstein, P.; Mercier, R.; Porcar, L.; Jestin, J.; Iojoiu, C.; Lyonnard, S. *ACS Appl. Mater. Interfaces* **2017**, *9*, 1671–1683.

Chapter 2A.

Effects of Block Length and Membrane Processing Conditions on the Morphology and Properties of Perfluorosulfonated Poly(arylene ether sulfone) Multiblock Copolymer Membranes for PEMFC

Assumma, L.; **Nguyen, H.-D.**; Iojoiu, C.; Lyonnard, S.; Mercier, R.; Espuche, E. *ACS Appl. Mater. Interfaces* **2015**, *7*, 13808−13820. DOI: 10.1021/acsami.5b01835

Effects of Block Length and Membrane Processing Conditions on the Morphology and Properties of Perfluorosulfonated Poly(arylene ether sulfone) Multiblock Copolymer Membranes for PEMFC

Luca Assumma,[†,‡] Huu-Dat Nguyen,[†,‡] Cristina Iojoiu,[†,‡] Sandrine Lyonnard,[⊥] Régis Mercier,[§] and Eliane Espuche[§]*

[†]Univ. Grenoble Alpes, LEPMI, F-38000 Grenoble, France

‡CNRS, LEPMI, F-38000 Grenoble, France

[⊥]CEA-Grenoble, INAC/SPrAM, Groupe Polymères Conducteurs Ioniques, UMR-5819, CEA-CNRS-UJF, 17 Rue de Martyrs 38054 Grenoble, CEDEX 9 France

[§]Ingénierie des Matériaux Polymères, UMR-5223, IMP@LYON1, Université de Lyon, Université Lyon 1, 15 Bd. A Latarjet, 69622, Villeurbanne CEDEX France

ABSTRACT: Perfluorosulfonated poly(arylene ether sulfone) multiblock copolymers have been shown to be promising as proton exchange membranes. The commonly used approach for preparation of the membrane is solvent casting; the properties of the resulting membranes are very dependent on the membrane processing conditions. In this paper, we study the effects of block length, selectivity of the solvent, and thermal treatment on the membrane properties such as morphology, water uptake, and ionic conductivity. DiMethylSulfOxide (DMSO), and DiMethylAcetamide (DMAc) were selected as casting solvents based on the Flory–Huggins parameter calculated by inversion gas chromatography (IGC). It was found that the solvent selectivity has a mild impact on the mean size of the ionic domains and the expansion upon swelling, while it dramatically affects the supramolecular ordering of the blocks. The membranes cast from DMSO exhibit more interconnected ionic clusters yielding higher conductivities and water uptake as compared to membranes cast from DMAc. A 10-fold increase in proton conductivity was achieved after thermal annealing of membranes at 150 °C, and the ionomers with longer block lengths show conductivities similar to Nafion at 80 °C and low relative humidity (30%).

KEYWORDS: perfluorosulfonated aromatic ionomers, block copolymer, polymer electrolyte membrane, PEMFC, solvent selectivity, membrane annealing

1. Introduction

Proton exchange membrane fuel cells (PEMFC) are one of the most promising technologies to produce renewable energy. Among the components of PEMFC, the proton conducting membrane (PEM) plays a deciding role in system performances such as power density, durability, electricity cost, etc.[1] The membranes are, generally, based on ionomers. Among them, the most studied are the perfluorosulfonic acid ionomers (PFSA) such as Nafion or Aquivion because of their microstructure and high proton conductivity as well as superior chemical and electrochemical stabilities.[2–6] However, due to their high cost, low conductivities, poor mechanical strength, and high fuel permeability above 80 °C and at low relative humidity (RH), an alternative solution to Nafion and other PFSA membranes have to be found.[7–9] Therefore, a challenging issue lies in developing alternative PEMs toward low-cost and high-performance proton-conducting polymers with good mechanical properties and high conductivity at low RH.[10–12] The key success of advanced PEM is to design membranes with long-range continuity of both the conducting and the mechanically robust hydrophobic domains.[12–17] Therefore, ionomers able to self-organize attract a lot of attention for PEMFC application. Among them, the sulfonated aromatic multiblock copolymers were largely studied as PEM.[18–23]

As a result of the thermodynamic incompatibility among building blocks, the copolymers spontaneously self-organize, leading to phase separation and ordered nanostructures and hence providing materials with synergy of properties. Lee et al.[24] investigated the properties of PEMs consisting of disulfonated and unsulfonated poly(arylene ether sulfone), and showed that the longer the blocks are, the higher the proton conductivity becomes. This effect was attributed to more continuously distributed hydrophilic domains.

Recently, another approach based on increasing the acidity of ionic functions was explored to enhance the proton conductivities of alternative PEMs. Aromatic ionomers bearing aryl sulfonimide acid[25,26] or alkyl perfluoro alkyl sulfonic acid side chains,[27–35] instead of aryl sulfonic acid, were considered. The poly(arylene ether)s bearing perfluorosulfonic acid side groups showed higher proton conductivity than poly(arylene ether)s functionalized with aryl sulfonic acid. In the spirit of sulfonated ionomers, further improvements of the proton-conducting properties were gained by designing block copolymer structures. Mikami et al.[35] and Assumma et al.[36,37] recently reported on perfluoroalkyl sulfonic acid-modified poly(arylene ether) and found that the bloc structure improves the proton-conductivities as compared to random ionomers with the same ion exchange capacity (IEC). Moreover,

Assumma et al.[36,37] found that the partially fluorinated poly(arylene ether sulfone) multiblock copolymers bearing perfluorosulfonic functions lead to highly nanostructured membranes with morphology and conductivity close to those of Nafion.

In addition to the chemical structure and composition of ionomers, some pioneering works pointed out that the membrane preparing conditions are another critical factor to be considered for advanced PEM design.[38,39] Membranes are usually prepared by the casting method, i.e., dilute polymer solutions are cast onto a petri dish. The processing conditions drastically influence the microstructure[40] and the final properties of PEMs. In the case of block copolymers, the final morphologies of PEMs obtained by casting are strongly controlled by the interaction parameters between the casting solvent and each of the two blocks (A and B) (χ_{solv-A} and χ_{solv-B}), as well as the interaction between blocks A and B (χ_{A-B}).[41]

To evidence and understand the impact of processing conditions on PEM properties, some works were focused on the effects of casting solvent[24,42−47] and thermal annealing.[48−51] Recently, Lee et al.[24] reported on the high dependency between the proton conductivity of a block copolymer, the casting solvent nature, and the drying conditions.

The above considerations highlight that the design of new high performance ionomers requires to select molecular architectures capable of producing well-connected and efficient proton conduction pathways, on the one hand, and that significant optimizations can be reached, on the other hand, after adequately tuning the elaboration process conditions. In this work, we have investigated PEMs based on new poly(arylene ether sulfone) multiblock copolymers bearing perfluorosulfonic functions. We explored the potential of this class of ionomers by tuning the parameters, namely average block lengths and membrane processing conditions. The selected multiblock copolymers consist of fully perfluorosulfonated (ps-PES) and partially perfluorinated (FPES) polysulfones with three different lengths (for chemical structures, see **Figure 1** and **Table 1**). A statistically random copolymer ps-PES with an ionic exchange capacity of 1.3 meq. H^+/g was also considered as a control reference. We investigated the impact of casting solvent selectivity, block length, and annealing at 150 °C on the properties of interest, i.e., conductivity and water uptake. At the microscopic scale, the complex chemistry−selectivity interplay was scrutinized by measuring the phase-separated structural organization using small-angle neutron scattering. The conductivities of these ionomers are close to those of Nafion, while the mechanical properties are much better.[36] Moreover, these ionomers led, by casting in DMSO, to highly nanostructured membranes.[37]

The detailed analysis of the structure-to-property relationship provided in this work can serve as guidelines for block copolymer optimization toward enhanced performances in fuel cells.

2. Experimental Section

2.1. Materials

Partially fluorinated poly(arylene ether sulfone) multiblock copolymers bearing perfluorosulfonic functions (**Figure 1**) were synthesized by regioselective bromination of partially fluorinated poly(arylene ether sulfone) multiblock copolymers (PES-FPES), followed by Ullman coupling reaction with lithium 1,1,2,2-tetra-fluoro-2-(1,1,2,2-tetrafluoro-2-iodoethoxy)ethanesulfonate, as described previously.[36] The nomenclature for these copolymers is ionomer, InX/Y, where X and Y are the length of hydrophilic (ps-PES) and hydrophobic (FPES) blocks. For instance, In10/10 refers to an ionomer with the length of segment ps-PES = 10 000 g/mol and of FPES = 10 000 g/mol. The ion-exchange capacity (IEC) has been determined by NMR and acid−base titration in organic solution and the protocols were described previously (**Table 1**).[36]

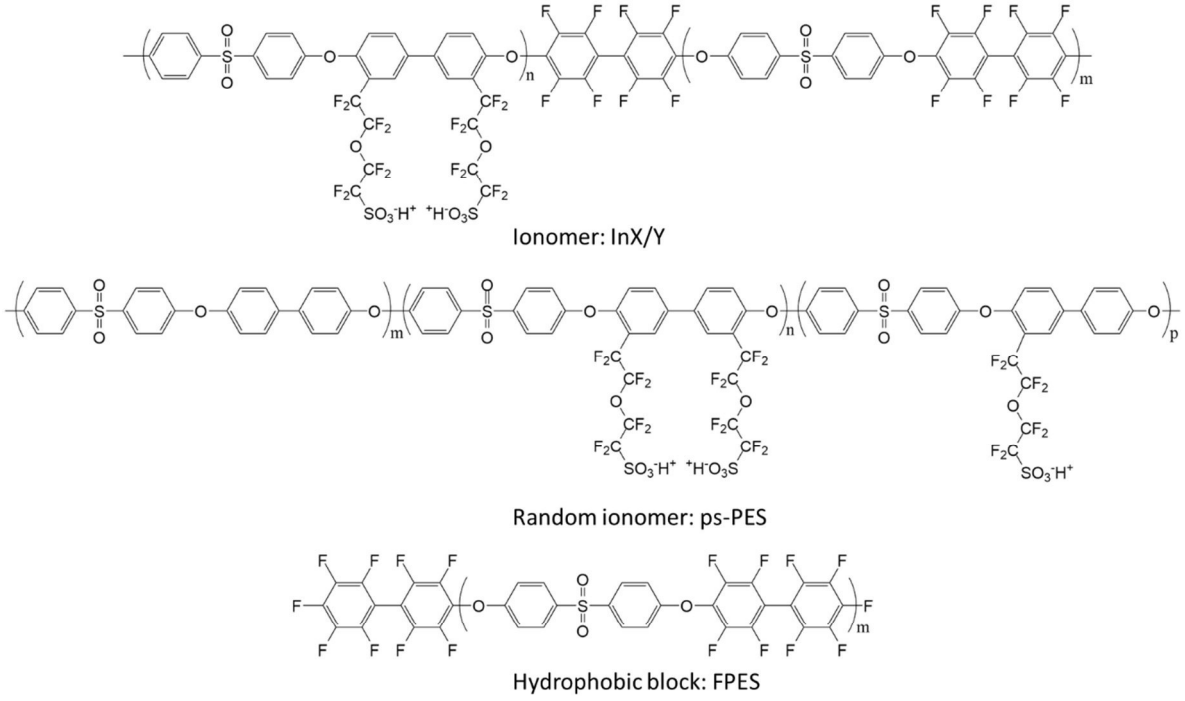

Figure 1. Chemical structure of ionomers and hydrophobic block (FPES).

The random ionomer, ps-PES, with an IEC of 1.3 meq H^+/g was obtained by bromination of commercial polysulfone (Radel), followed by Ullman coupling reaction with lithium 1,1,2,2-tetrafluoro-2-(1,1,2,2-tetrafluoro-2-iodoethoxy)ethanesulfonate, as described previously (**Figure 1**).[36]

The FPES oligomer was synthesized by polycondensation of 4,4′-dihydroxydiphenylsulfone (DHDPS) with Decafluorobiphenyl (DFBP) purchased from Alfa Aesar, as described previously (**Figure 1**).[36]

Table 1. Average Blocks Molar Mass and IEC of Studied Block Copolymers and Random Ionomer

ionomers	ps-PES (g/mol)	FPES (g/mol)	IEC (meq H^+/g)
In5/5	5000	5000	1.30 ± 0.10
In10/10	10000	10000	1.35 ± 0.10
In15/15	15000	15000	1.32 ± 0.10
ps-PES	-	-	1.30 ± 0.10

2.2. Column Preparation and IGC Setup

In order to select the solvent for membrane casting, the interaction between the solvent and polymers were measured by inversion gas chromatography (IGC). The IGC experiments were performed using a PerkinElmer Clarus 480 gas chromatograph, equipped with a flame ionization detector (FID). The data acquisition was made with the AZUR software. High purity helium and methane were used as the carrier gas and marker, respectively. The flow rate of helium was measured with a soap bubble flowmeter connected at the end of the column, at room temperature. The experiments were performed at infinite dilution, by manually injecting 0.1 μL of each probe with a 1 μL Hamilton syringe. At least three injections of each probe were made, and the retention time was taken as the average of the three measurements. The retention times of the probes were determined by following the protocol described elsewhere.[52]

The following four solvents of the highest available purity (purchased from Aldrich), able to dissolve the InX/Y copolymers, were used as probes: dimethylformamide (DMF), dimethylsulfoxide (DMSO), dimethylacetamide (DMAc), and diethyleneglycoledime-tyhylether (DGDE) (**Table 2**). The stationary phase was prepared by coating the solid support, Chromosorb W HP (100/120) mesh (purchased by Antelia, France), with the polymer (ps-PES or FPES) by following the method proposed by Al-Saigh and Munkwas.[53] Acetone was used to prepare the polymer solutions of FPES and ps-PES in the lithium salt-form for coating. The

process followed for the preparation of the column was described in detail elsewhere.[54,55] The IGC experimental conditions and the column characteristics are presented in **Table 3**.

Table 2. Physical Characteristics of Used Solvents for IGC

solvent	dipolar moment (μ)	dielectric constant (ε)	T_b (°C)
DMSO	3.9	47.3	189
DMAc	3.7	37.2	166
DMF	3.9	38.3	153
DGDE	-	7.3	140

Table 3. Chromatographic Conditions and Column Specification

injector temperature (^oC)	200
detector temperature (^oC)	200
column temperatures (^oC)	Ps-PES: 260, 265, 270, 275 FPES: 220, 230, 240, 250
column type of material	SS 316 ASTM A-269
column length (cm)	70
lumn O.D (inch)	1/8
loading (%)	20.7
flow rate (ml/min)	10

2.3. Preparation of ps-PES and InX/Y Membranes

The ionomers in the lithium salt form were dissolved in the two solvents that were chosen after calculation of the Flory–Huggins parameter from IGC analysis, i.e., DMSO and DMAc, respectively. The solution containing 7 wt % of InX/Y in lithium salt form was stirred for 24h at 60 °C. After that, the solution was centrifuged for 30 min at 5000 rpm to remove solid impurities. Then, the solution was degassed under vacuum for 30 min to remove the air bubbles. The degassed solution was cast onto a glass plate using a casting knife (Elcometer 4340 Automatic Film Applicator), and the solvent was evaporated in an oven at 60 °C.

In this work, we investigated the properties of "as-cast membranes" and "annealed membranes". The "as-cast membranes" were obtained by following the protocol described by Assumma et al.[36] Then the membranes were rinsed many times in distilled water over 24h to remove acid traces. The free solvent membrane was verified by ^{1}H NMR. The resulting block copolymer ionomer membranes in acidic form are named: InX/Y-A6 (cast from DMAc) or InX/Y-S6 (cast from DMSO). The annealed membranes are obtained from the "as-cast membranes". The "as-cast membranes" were submitted to an additional thermal treatment, after drying at 60 °C, they were annealed in a vacuum chamber at 150 °C for 24h. The annealed membranes with a thickness ranging between 120 and 150 µm were then acidified following the same method than that use for the "as-cast membranes". The free solvent membrane was verified by ^{1}H NMR. The resulting block copolymer ionomer membranes in acidic form are named as InX/Y-A15 or InX/Y-S15 (for membrane cast from solvent DMAc or DMSO, respectively).

Nafion 117 membranes. Nafion 117 membrane (thickness 176 µm) was reactivated before using.[36]

2.4. Water Uptake

The membranes InX/Y or ps-PES in acidic form were vacuum-dried at 60 °C for 48h, weighed, and immersed in deionized water at different temperatures ranging from 30 to 80 °C (the temperature was increased 10 °C each 24h). The water uptakes (WU, %) of membranes are reported in weight percent according to **Equation 1**:

$$WU = \frac{W_{wet} - W_{dry}}{W_{dry}} \times 100 \qquad (\mathbf{1})$$

where W_{wet} and W_{dry} are the weights of the wet and dry membranes, respectively.

The hydration number (λ), which is defined as the number of water molecules absorbed per sulfonic acid unit, was determined from the water uptake and the ion-exchange capacity (IEC) of the dry membrane, according to **Equation 2**.

$$\lambda = \frac{WU \times 10}{IEC \times MW_{water}} \qquad (\mathbf{2})$$

where MW_{water} is the molecular weight of water (18.01 g/mol).

2.5. Proton Conductivity

Proton conductivities of membranes at different temperatures and relative humidity (RH) were determined by measuring their resistances by impedance spectroscopy. The analysis is

performed with impedance analyzer Material Mates M2 7260 in the frequency range from 1 Hz to 10 MHz. The measurement of the membrane resistance is conducted through-plane with the help of the two in-lab made cells. The membrane is placed in-between the lower and the upper electrode (stainless steel), the pressure is applied by the spring on the upper electrode. In order to control the RH and the temperature, the measurements were carried out in a climatic chamber VC 4018 of Vötsch Industrietechnik. The measurements were performed at constant RH, i.e., 95% in the range of temperature from 30 to 90 °C or at constant temperature, i.e., 80 °C and 30–95% RH. The temperature (or RH) was increased with a step of 10 °C (or 10% RH), the measurements were performed after a stabilization time of 8h.

2.6. Differential Scanning Calorimetry (DSC)

The DSC measurements were performed using a DSC 1 STARe System from Mettler Toledo. The measurements were carried out under argon atmosphere with a heating scan of 20 °C per minute. The glass transition temperatures of "as-cast" and "annealed membrane" were determined from the first heating scan performed from 25 to 300 °C.

2.7. Small Angle Neutron Scattering (SANS)

SANS measurements were performed on the D22 spectrometer at the Institut Laue Langevin, Grenoble, France. The measurement protocol, briefly presented here, is similar to that we described in ref 36. Thus, two configurations were used to cover an extended Q-range from 8.5×10^{-3} to 0.6 $Å^{-1}$, Q being the scattering vector defined as $Q = (4\pi/\lambda)\sin(\theta/2)$ where λ is the wavelength of the incident neutron beam, and θ is the total scattering angle. The isotropic 2D patterns recorded in the two configurations were radially averaged to obtain the 1D scattered intensities I(Q), and further corrected using standard procedures (detector efficiency, background, and empty cell subtraction). As data taken in the two configurations were perfectly overlapping in the intermediate Q-region, the I(Q) were merged to obtain a single spectrum for each sample. Prior to the SANS experiment, the membranes were inserted in quartz Helma cells, closed quickly, and maintained at room temperature.

2.8. NMR Spectroscopy

Residual Solvent Analysis. ^{1}H NMR spectroscopy was conducted on a Bruker Avance 400 spectrometer. For membranes prepared from DMAc, a 0.07-g portion of membranes was dissolved 0.7 mL in DMSO.d6 and NMR spectra was obtained after 64 scans. For membranes cast from DMSO, the membrane was dissolved DMF.d7.

Chemical shift of membranes cast from DMAc: ^{1}H NMR: (DMSO.d6): The peaks at δ (ppm) 7.90–8.20 (m), 7.48 (d), 7.34–7.18 (m) were attributed to the aromatic protons of ionomer InX/Y and the peaks at δ (ppm) 2.946 (s), 2.787 (s), 1.961 (s) for DMAc.

Chemical shift of membranes cast from DMSO: 1H NMR: (DMF.d7): The peaks at δ (ppm) 8.45–8.25 (m), 7.8 (d), 7.65–7.45 (m) were attributed to the aromatic protons of ionomer InX/Y and the peaks at δ (ppm) 2.478 (s) for DMSO.

The amount of DMAc residual solvents (wt %) or solvent contain (SU) and the solvation number (λ_{sol}), which can be defined as the number of solvent molecules absorbed per ionic function, in the ionomer films for the "as-cast membranes" and "as-annealed membranes" was calculated with **Equation 3** and **Equation. 4**:

$$\lambda_{sol} = \frac{[solvent]}{[SO_3H]} = \left[\frac{I_{sol}}{N_{sol}}\right] \Big/ \left[N_{ion} \times \frac{I_{pol}}{N_{pol}}\right] \quad (\mathbf{3})$$

$$SU = \frac{\lambda_{sol} \times IEC \times MW_{sol}}{10} \quad (\mathbf{4})$$

where I_{sol} is the integral of solvent peak, I_{pol} is the integral of ionomer peak region (from 7.1 to 8.3 ppm for DMSO.d6 and from 7.3 to 8.5 ppm for DMF.d7), N_{sol} is the number of hydrogen corresponding to each solvent peak (N_{sol} = 3 for DMAc and 6 for DMSO), N_{ion} is the number of ionic unit per polymer repeating unit (N_{ion} = 2), N_{pol} is the number of hydrogen per polymer repeating unit corresponding to polymer peak (N_{pol} = 27.32), IEC is the ionic-exchange capacity (meq. H^+/g), and $MW_{solvent}$ is the molecular weight of the solvent (DMAc 87.12 g/mol and DMSO 78.13 g/mol).

2.9. Gas Permeability

The permeation experiments were performed under an anhydrous state for hydrogen and oxygen. The membrane was placed between the two compartments of the permeation cell. The effective membrane area was 3 cm^2. The cell was thermostated at 20 ± 1 °C. A preliminary high vacuum desorption was realized to ensure that the static vacuum pressure changes in the downstream compartment were smaller than the pressure changes due to the gas diffusion. A 3.0×10^5 Pa gas pressure was introduced in the upstream. The evolution of the pressure in the downstream compartment was followed with a datametrics pressure sensor. A steady-state line was obtained after a transitory state by plotting the measured pressure versus time. The permeability coefficient, P, expressed in barrer unit (1 barrer = 10^{-10} cm^3_{STP} cm cm^{-2} s^{-1} cm_{Hg}^{-1} = 7.5×10^{-18} $Nm^3 \cdot m \cdot m^{-2} \cdot s^{-1} \cdot Pa^{-1}$ = 3.348×10^{-16} $mol \cdot m \cdot m^{-2} \cdot s^{-1} \cdot Pa^{-1}$), was calculated from the slope of the steady-state line.

2.10. Dynamic Mechanical Analysis (DMA)

DMA was performed with DMA Q800 device of TA Instruments in the temperature range from 20 to 350 °C using a temperature ramp of 2 °C·min^{-1}. Data treatment was performed with TA Universal Analysis software. The dried membranes, in lithium form, of average dimensions 15 × 6 mm^2 and thickness of 120−160 μm are introduced in the clamp of film tension. The following settings are chosen: multifrequency-strain mode, frequency 1.0 Hz, preload force 0.1 N, force track 150%, and strain deformation was fixed at 0.05%.

3. Results and Discussion

3.1. Solvent Selectivity

The degrees of solvent selectivity of casting solvents for the component blocks were determined by measuring the Flory−Huggins parameter of ps-PES and FPES by IGC. The Flory−Huggins theory allows the calculation of the polymer−solvent interaction parameter (χ_{P-S}^{∞}). This parameter is considered as a crucial criterion to select a suitable solvent for an industrial process and also to predict solubility, degree of swelling, or polymer−solvent compatibility. By IGC technique, the material under study (ps-PES and FPES) is packed into the column into which carefully selected probes, i.e., solvents (**Tables 2** and **4**) were injected at infinite dilution concentration in order to make sure that the retention is governed by the stationary phase (ps-PES, FPES) and probe (solvent) interactions as well as the probe−probe interactions are avoided.[55] The key measurement in IGC experiments is the net retention volume of the probes, V_N that it is expressed as the volume of the carrier gas necessary to elute the solute from the column and allows one to calculate the Flory−Huggins interaction parameter χ_{P-S}^{∞}[56] (see **Supporting Information**, **SI**, and **Table 4**). According to the Flory−Huggins theory, values of the interaction parameter smaller than 0.5 are indicative of good solvents for the material under study, whereas values greater than 0.5 represent unfavorable polymer−solvent interactions.[55] On the basis of this statement from **Table 4**, it can be concluded that only DMAc is a good solvent out of the four employed solvents for FPES segment. Concerning the interaction parameters for the segment ps-PES, all the $\chi_{ps-PES-S}^{\infty}$ values are negative, and the lowest values are obtained with DMSO followed by DMAc. However, the measurements of V_N for the ps-PES were performed at a temperature lower than its Tg in order to avoid the degradation of ps-PES (Tg and Td are very close, 290 and 298, respectively).[36] Thus, the χ_{P-S}^{∞} calculated in this case is more representative of the interactions between the solvent and the surface of ps-PES coated silica. However, the calculated values of χ generally decrease with an increase in the temperature. This is attributed

to enhanced segmental motions of polymer chains at higher temperatures, thus creating an extra free volume with which the probe can interact.[56] Therefore, if the measurements were performed at higher temperature, then even lower values could be obtained. However, in order to confirm that DMSO and DMAc are good solvents, we also performed a solubility test for ps-PES. We observed that more than 50 wt % of ps-PES was dissolved in both solvents at room temperature. These results fully corroborate the observation that DMSO and DMAc are good solvents for ps-PES.

On the basis of these results, we selected to work with (i) DMAc as the casting solvent which is able to dissolve both blocks of ionomers InX/Y and (ii) DMSO as a selective solvent able to dissolve the ionomers InX/Y but being a good solvent only for ps-PES block.

Table 4. Values of Floy−Huggins Interaction Parameters Calculated from Net Retention Volume of the Probes Measured by IGC

T[a] (°C)	$\chi^{\infty}_{FPES-DMAc}$	$\chi^{\infty}_{FPES-DMF}$	$\chi^{\infty}_{FPES-DGDE}$	$\chi^{\infty}_{FPES-DMSO}$
220	0.34	0.58	0.65	0.66
230	0.34	0.55	0.63	0.65
240	0.34	0.50	0.73	0.64
250	0.31	0.47	0.77	0.60
T[b] (°C)	$\chi^{\infty}_{ps-PES-DMAc}$	$\chi^{\infty}_{ps-PES-DMF}$	$\chi^{\infty}_{ps-PES-DGDE}$	$\chi^{\infty}_{ps-PES-DMSO}$
260	-3.38	-2.26	-1.72	-3.2
265	-3.19	-2.18	-1.66	-3.14
270	-2.99	-2.14	-1.63	-3.04
275	-2.91	-2.10	-1.60	-2.93

[a] Tg_{FPES} = 220 °C, Td_{PES} = 530 °C; [b] $Tg_{ps\text{-}PES}$ =290 °C, and $Td_{ps\text{-}PES}$ = 298 °C.

3.2. Morphology of PEMs

A morphological study was conducted using SANS to investigate the effect of solvent selectivity on the resulting microstructure of multiblock copolymers films. In **Figure 2**, we display the SANS profiles of hydrated ps-PES and block copolymers cast at 60 °C in DMSO and DMAc, prepared at intermediate hydration numbers (λ in the range 25−29).

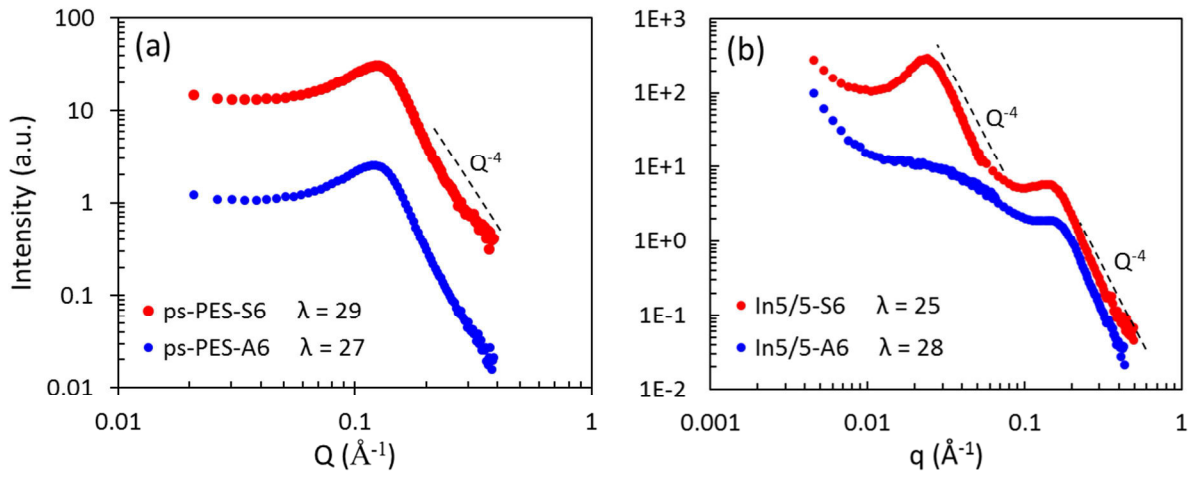

Figure 2. SANS profiles of (a) ps-PES and (b) In5/5. The spectra have been shifted vertically for clarity. The ionomer peak at Q ≈ 0.1–0.2 $Å^{-1}$ is the signature of nanophase separation between ionic domains and polymer backbone. An additional low-Q peak is found in block copolymer membranes, as due to the self-organization of hydrophilic/hydrophobic blocks. The dashed lines represent the Q^{-4} Porod behavior, indicating the presence of a sharp interface at the nanoscale.

For ps-PES (**Figure 2a**), we observe a well-defined and intense scattering maximum in the Q-range, where the ionomer peak is usually observed in PFSA materials (Q ≈ 0.13 $Å^{-1}$). The ionomer peak is the signature of hydrophilic/hydrophobic phase separation at the nanoscale. The ps-PES polymers therefore exhibit nanoscale organization with mean separation distances between ionic domains, $d_{ionic} = 2\pi/Q_0$, where Q_0 is the position of the ionomer peak, equal to 5 nm at hydrations λ ≈ 27–29. As the shape and position of the ionomer peaks for ps-PES cast in DMSO and DMAc are similar at the same local hydration, we can conclude that the casting solvent does not significantly impact the ionic nanodomain organization in ps-PES ionomers. The SANS profiles of the cast block copolymer In5/5 (**Figure 2b**) were measured on a more extended Q-range and are compared in **Figure 2b**. The block copolymer membrane SANS spectra exhibit two prominent features: an ionomer peak located typically at Q ≈ 0.15–0.2 $Å^{-1}$, as in the ps-PES, and an additional low-angle scattering intensity at Q ≈ 0.02–0.03 $Å^{-1}$, which can be ascribed to structural correlations between hydrophobic block domains.

The presence of two scattering maxima indicates a complex multiphase polymer organization at typical length scales of few nanometers and few tens of nanometers. These characteristic features are impacted by the choice of the casting solvent. The well-defined high-Q ionomer peak is found in the same Q-range for In5/5-S6, In5/5-A6, and ps-PES ionomers. We observe some broadening of the peak in the DMAc-cast membrane, which can

indicate a more disordered distribution of ionic domains than in DMSO-cast and ps-PES membranes. Yet, in these materials, the formation of ionic domains appears to be rather insensitive to the block architecture and the casting solvent. Therefore, it is predominantly triggered by the common presence of perfluorinated pendent chains bearing acidic functions. In contrast, the low-Q correlation feature appears to be drastically affected by the nature of the solvent. The peak is very intense and sharp in DMSO-cast block copolymers, while a large and ill-defined correlation bump is observed in DMAc-cast membranes. Note that such a low-Q feature does not exist in ps-PES polymers, as the low-angle scattering is flat although not measured at the same low Q values as In5/5. Hence, we can conclude that the film cast in DMSO presents a remarkable structural organization due to the self-assembly of blocks units forming large-scale ordered domains,[37] while block segregation is not favored when using DMAc as a solvent, such that a more random distribution of hydrophobic and hydrophilic segments leads to poor long-range order. This behavior can be consistently rationalized in terms of solvent affinity with the blocks. The DMSO film casting process produces enhanced long-range order due to the selectivity of DMSO (as described in section 3.1) relatively to DMAc. FPES chain segregation is favored by (i) the low solubility of FPES in DMSO solvent and (ii) the immiscibility between ps-PES and FPES blocks. These effects contribute to the formation of well-structured FPES domains at high ionomer dilution. Contrarily, DMAc being a good solvent for both blocks, it plays the role of compatibilizer. Because of their intrinsic chemical incompatibility, the two blocks tend to separate at high polymer concentration, and a drastic decrease in copolymer chain mobility yields to the formation of more disordered hydrophobic domains.

These findings suggest that the casting solvent significantly affects the large-scale blocks organization, with a limited effect on nanoscale phase separation between ion-containing domains and polymer backbone. The choice of a casting solvent able to compatibilize the blocks introduces structural disorder into the multiscale morphology. Further insights into the ionic domain organization can be gained by inspecting the swelling behavior of the cast membranes. Ionomer films were prepared over an extended range of hydration numbers, from λ = 0 to 46 mol water/mol SO_3H, to evaluate in detail the membrane structure at the nanoscale. In **Figure 3**, we display the incoherent background-subtracted SANS spectra of swollen membranes cast in DMAc (a) and DMSO (b) for In5/5.

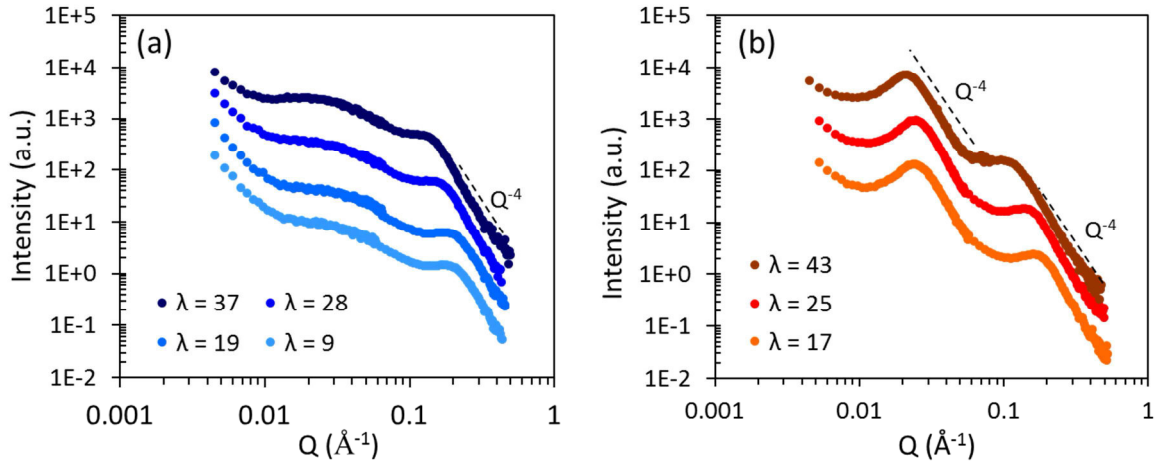

Figure 3. Evolution of SANS spectra of the aromatic ionomers upon water content. (a) In5/5-A6 and (b) In5/5-S6. The spectra are shifted vertically for clarity. The dashed lines represent the Q^{-4} Porod behavior, indicating the presence of a sharp interface at the nanoscale.

The ionomer peak present in both films increases in intensity and shifts toward smaller Q values as the hydration is increased, evidencing the continuous increase of d_{ionic} correlation distances due to nanoscale swelling. The incorporation of water molecules within the hydrophilic phase significantly increases the volume of the hydrophilic domains (therefore raising the correlation distance) while enhancing the SANS contrast. The same behavior characterizes also the low-Q peak (hydrophobic peak), showing that the block domains are moved apart along hydration. Interestingly, we note that the low-Q peak of DMAc-cast membranes remains larger and less pronounced as compared with that of DMSO cast films over the whole hydration range. The The nanoscale swelling can be quantitatively analyzed by extracting the characteristic correlation distances d_{ionic} from the ionomer peak positions and plotting the dilution law $d_{ionic} = f(\lambda)$. As seen in **Figure 4a**, d_{ionic} expands from 3 to 6 nm typically, with similar variations for both films (DMSO and DMAc) as a function of λ. Furthermore, the expansion of ionic domains $\Delta d_{ionic} = d_{ionic} - d_0$ can be extracted, d_0 being the $\lambda = 0$ interpolation of the swelling law (**Figure 4b**). The obtained linear behavior with a slope close to 1 is comparable to that of Nafion membrane. Such behavior can be ascribed to the dilution of a locally two-dimensional structure and was interpreted for PFSA materials in the framework of a semi-lamellar local morphology[57,58] or ribbon-like hydrophobic aggregates.[59]

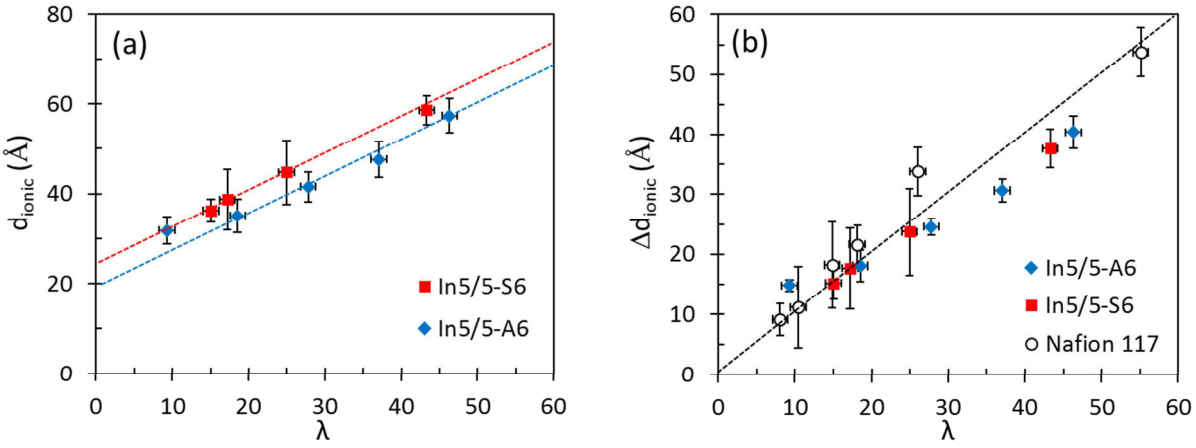

Figure 4. (a) Swelling law, i.e., mean separation distances between ionic domains, d_{ionic}, as a function of the hydration number λ. (b) Ionic domains mean size, Δd_{ionic}, as a function of the hydration number. The d_0 values are extrapolated from the swelling law at $\lambda = 0$.

Clearly, the nanoscale swelling of ionic domains in DMSO and DMAc cast membranes is due to the selective incorporation of water in the highly hydrophilic sulfonate- containing regions. This is mostly driven by the nature of local interactions between charged species and the low water wettability of hydrophobic pendant chain, independently from the chemical architecture of ps-PES and FPES main chains and their self-assembling behavior.

Complementary information on the hydrophobic/hydrophilic phase separation can be gained by extracting the area of polymer–water interface per polar head (specific surface) from the asymptotic behavior of the scattering curves at large Q-values (**Figure 5**).

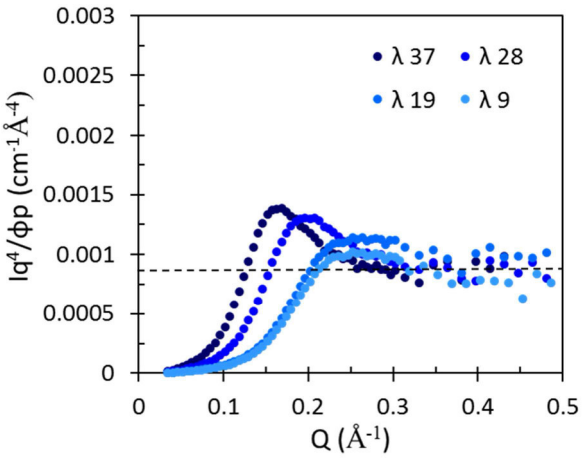

Figure 5. Porod representation of SANS spectra for In5/5-A6. The dashed line represents the high-Q asymptotic plateau showing the presence of a sharp interface.

In the presence of a sharp polymer–water interface, the intensity has to scale as Q^{-4} according to the Porod's law. The specific surface σ can be extracted from **Equation 5**:

$$Lim_{q\to\infty}\frac{Iq^4}{\Phi_p} = 2\pi\Delta\rho^2\Phi_p\frac{\sigma}{\nu_0} \quad (5)$$

where Δρ is the scattering length density difference between the hydrophobic block and the hydrophilic block, while ν_0 is the average volume of polymer per repeat unit of hydrophobic block. As we need to compare the same polymer cast with different solvents, the impact of solvent can be evaluated by considering the ratio of the high-Q intensities for the film cast in DMAc/DMSO (**Equation 6**).

$$\frac{\left(\frac{IQ4}{\phi_p}\right)DMAc}{\left(\frac{IQ4}{\phi_p}\right)DMSO} = \frac{\sigma_{DMAc}}{\sigma_{DMSO}} \quad (6)$$

Then, the experimental value of the ratio directly informs on the nature of the interface. A value of 1.3 is found that corresponds to an increase of specific surface in DMAc-cast films by 30% as compared to that obtained in DMSO. The higher specific surface for the DMAc-cast membrane is consistent with the ill-defined large-scale organization due to unfavored block segregation, as previously discussed. A more randomly distributed ill-defined block structure indeed implies that the hydrophilic domains are likely to be more isolated and less connected as compared to the film cast in DMSO. This observation points out that the membrane morphology is determined by the local topology of ionic domains, which similarly expands upon hydration in DMSO or DMAc cast membranes, as well as the ionic network connectivity (better in DMSO-cast membranes). Both properties are likely to impact the performance in terms of water uptake and conductivity, as will be investigated in detail in the following sections.

3.3. Thermomechanical Properties

The impact of casting solvent on the thermo-mechanical properties of membranes In5/5 were investigated by measuring the temperature dependent storage modulus and tan δ spectra (**Figure 6a–c**) by DMA. The measurements were performed on membranes based on ionomers in lithiated form in order to avoid the ionomer degradation at temperatures higher than 200 °C.[36] The thermo-mechanical response of the membranes is shown to significantly differ depending on the elaboration solvent. Indeed, the storage modulus of the membrane cast in DMSO shows two relaxation temperatures that correspond to a two-step decrease of storage modulus. In contrast, for the membrane cast from DMAc, only one relaxation

temperature is observed. For the DMSO-cast membranes, the first relaxation (at 220 °C) might correspond to motions of the chain of the hydrophobic domains,[36] while the second relaxation can be associated with the creeping of the whole chain, as due to the breaking of ionic interactions between the lithiated sulfonic side chains.

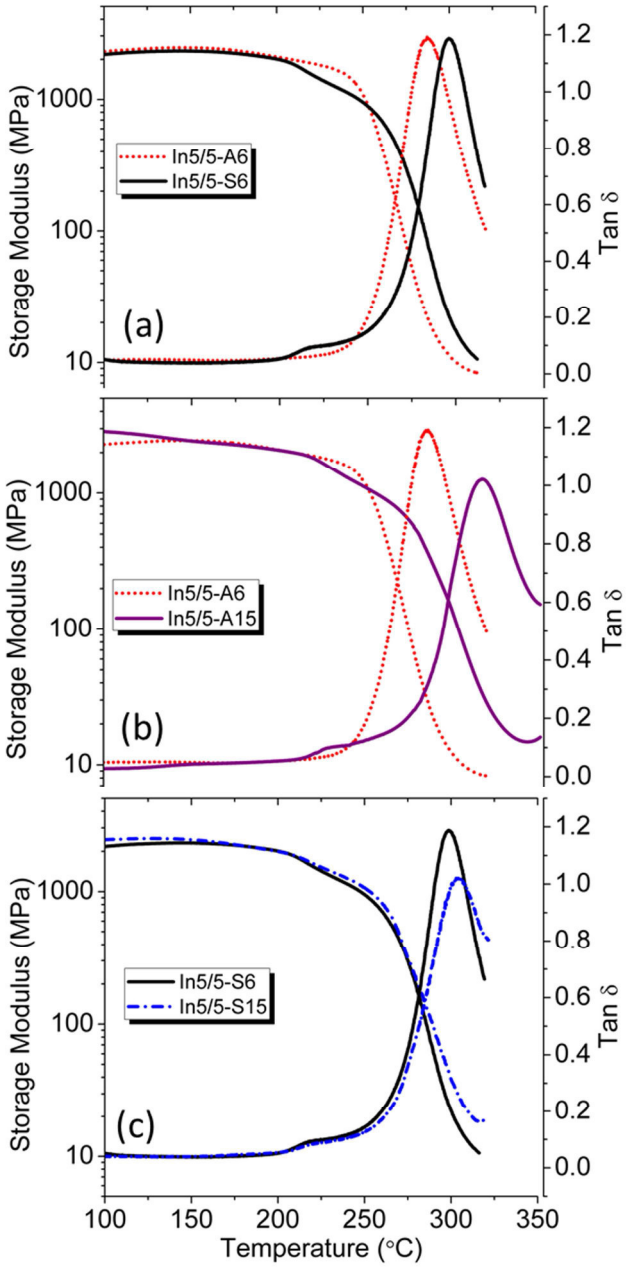

Figure 6. DMA profiles of In5/5 membranes in lithium-salt form: Storage modulus and tan δ vs temperature. (a) Membranes cast from DMAc and DMSO at 60 °C. (b) Membranes cast from DMAc at 60 °C and annealed at 150 °C (c) Membranes cast from DMSO at 60 °C and annealed at 150 °C. The membranes were washed in water and well dried before to perform DMA.

It is interesting to point out that the relaxation temperature of the DMAc-cast membrane has a value between those of DMSO-cast membranes. In addition, the relaxation peak is much larger. These findings suggest that the hydrophobic domains are well separated and percolated for the membrane cast from DMSO, while the separation is much less effective in the case of the membrane cast from DMAc. The DMA results therefore corroborate the conclusions of the SANS study on the effect of solvent selection on the quality of phase separation.

With the aim of improving the membrane performances, the study was extended to a series of InX/Y membranes of different block lengths obtained directly after casting at 60 °C ("as- casting membranes"), and further annealed at 150 °C ("annealed membranes"). The thermo-mechanical behavior of annealed membranes was also investigated using DMA on the In5/5 annealed membranes, and again, we find different behaviors in DMAc and DMSO membranes. A huge effect is noticed on the DMAc membranes (**Figure 6b**). A small peak appears on the tan δ plot, and the decrease of the storage modulus evolves toward two- slope behavior. As a consequence, the annealing process seems to significantly improve the phase separation between hydrophobic and hydrophilic chains. Interestingly, the annealed DMAc-cast membranes present similar thermomechanical responses as the non-annealed DMSO-cast membranes. This suggests that the annealing procedure transforms a rather poorly separated block material into a well-ordered block structure. Regarding the DMSO-cast membranes (**Figure 6c**), the annealing treatment has a very limited effect on the thermomechanical properties, with only a small shift of the main relaxation peak. As this peak is due to chain creeping because of the breaking of ionic bonds, the observed shift could be related to stronger interactions between ionic functions, which can be presumably related to a better local organization of ionic moieties within ionic domains.

3.4. Water Uptake and Conductivity

Following the study of In5/5 and ps-FES morphology and thermomechanical properties, we explored the effects of solvent selectivity and annealing through the water uptake and conductivities.

3.4.1. "As-Casting Membranes"

3.4.1.1. Water Uptake

The capacity of the different membranes, i.e., ps-PES and InX/Y, to uptake water was evaluated at different temperatures. The results expressed in λ (mol H_2O/mol SO_3H) are represented in **Figure 7a** and compared to Nafion® 117 as a reference. We notice that the aromatic membranes exhibit higher water uptake as compared to Nafion 117. From **Figure**

7a, significant effects of block structure, block length, and solvent selectivity on the water uptake of the ionomer membranes were observed. First, it is noteworthy to point out that despite having close IEC values with respect to block copolymer materials, the water uptake of the ps-PES based membrane drastically increases after 60 °C. Above 80 °C, it is completely soluble in water. In contrast, the membranes of block copolymers, InX/Y, absorb a moderate amount of water and keep their integrity. This result clearly proves the advantage of block structure. However, with increasing block length of the InX/Y, the water uptake increases significantly. Similar behavior was reported for the sulfonated multiblock copolymers and was explained by a better percolation of hydrophilic domains with increasing sulfonated block length.[27]

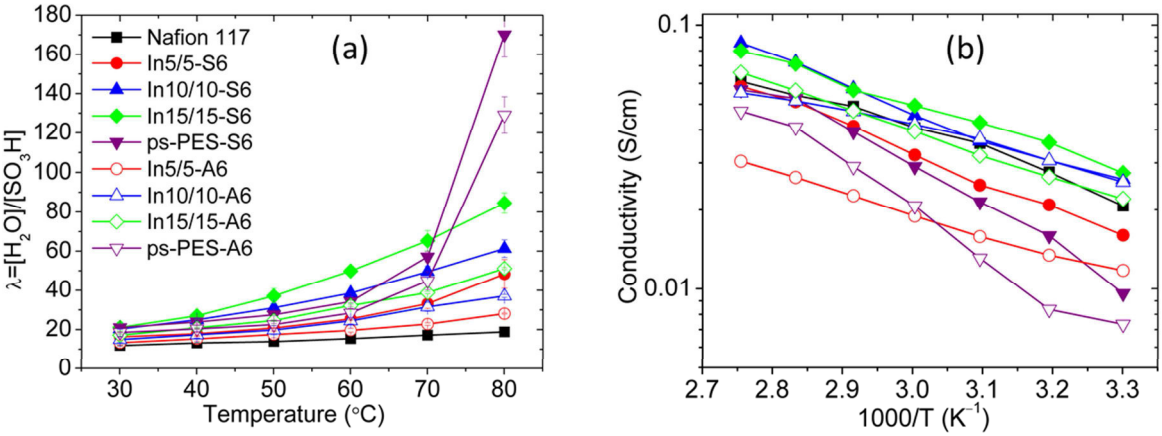

Figure 7. (a) Evolution of hydration number (λ) with the water immersing temperature (b) Evolution of proton conductivity with 1000/T at 95% RH. (Errors limits for conductivities are ±14%.)

A general finding is that the utilization of DMSO as a casting solvent increases the water uptake of resulting membranes as compared with those obtained from DMAc cast membranes. Such a difference seems to be more pronounced in the case of InX/Y as compared to ps-PES. The reduced water uptake of films cast from DMAc could be explained by (i) the presence of isolated and less connected hydrophilic domains, as evidenced from the SANS analysis in the case of InX/Y membranes and/or (ii) the amount of the residual casting solvent trapped in the membrane before its acidification. The latter hypothesis was checked by quantitatively analyzing the membrane composition by ^{1}H NMR after the drying process (on the membrane in lithium salt form). We observed that the amount of residual solvent, calculated from ^{1}H NMR (see **Experimental Section**), strongly depends on the solvent nature. In the case of DMSO cast membranes, about 10 wt % of residual solvent was found while only 2 wt % in the case of DMAc cast membrane. At this stage, we can suppose that the

solvent can be retained within the membranes by strong interactions with the lithium perfluorosulfonate, or trapped in hydrophobic or hydrophilic domains with high Tg (220 and 150 °C respectively).[36] In order to gain further insight, the membranes were also analyzed after their immersion in acidic water followed by washing with deionized water. Any presence of residual solvent was detected in the NMR spectra. Taking into account the high Tg of these polymers,[36] more specifically that of the hydrophobic block in InX/Y materials (which cannot be plasticized by water molecules), we can hypothesize that (i) the residual solvent was mostly present in hydrophilic domains and therefore totally exchanged by water along the hydration process, yielding solvent free membranes at the end, (ii) more free volumes could be formed in the hydrophilic domains of dried membranes cast from DMSO as compared to those cast from DMAc due to the different amounts of residual solvent exchanged by the water. The presence of solvent-induced free volumes left after the casting process should affect the final gas permeability of the membranes. Therefore, we investigated the oxygen and hydrogen permeability properties in In5/5 membranes prepared from DMSO and DMAc solutions and determined the respective permeation coefficients. The gas permeability of hydrophobic polymer, FPES membrane, was also measured. All data are summarized in **Table 5**.

Table 5. Gas Permeability Coefficients of the In5/5 Copolymers Prepared from DMAc and DMSO Solvent and of the FPES Homopolymer

membrane	PH_2 (barrer)	PO_2 (barrer)
In5/5-S6	7.83	0.48
In5/5-A6	8.80	0.51
FPES-A6	42.96	6.33

We observe that the copolymers In5/5 exhibit similar oxygen permeability coefficients independent of the casting solvent. Such a finding underlines that the difference in free volumes within the hydrophilic phase, as possibly due to higher residual solvent amount in DMSO-cast membranes, is not significant enough to play a predominant role in the gas transport mechanism in the anhydrous state. Moreover, the copolymer permeability coefficients are significantly lower than those measured on the FPES membrane. Such an important decrease of gas permeability, observed when ps-PES segments are bonded to FPES segments into In5/5, supports the arrangement of sulfonated domains into a very low

permeable phase under anhydrous conditions. This result is in agreement with similar trends already observed on sulfonated copolyimides.[60] Additionally, it is interesting to note that slightly higher hydrogen permeability values are obtained for In5/5-A6 in comparison to In5/5-S6. This effect could be assigned to a slightly higher extent of hydrophobic/hydrophilic interfacial regions in the first membrane. The permeation measurements hence nicely corroborate the morphological picture proposed after the SANS study, which evidenced the presence of isolated and less connected hydrophilic domains in DMAc-cast materials and the substantial increase of specific surface with respect to DMSO- cast membranes. According to the permeability results, these interfacial areas could contribute to gas diffusion only for molecules with small kinetic diameters.

To summarize these results, we conclude that the presence of variable quantities of residual solvents in the DMSO/DMAc cast membranes (before their acidification) do not have a substantial impact on gas permeability. Hence, the presence of limited/extended free volumes within the two types of membranes cannot primarily cause the observed water uptake variations. Accordingly, the water uptake behavior rather originates from the solvent-dependent morphologies induced by solvent-block specific interactions, as described in the SANS section. Increasing the degree of structural order (DMSO-cast materials) favors the incorporation of water molecules into the 3D interconnected network of regular ionic domains distributed within ordered blocky domains.

3.4.1.2. Conductivity

The effects of solvent selectivity as well as the block length of the multiblock copolymers were studied by measuring the proton conductivity (σ). **Figure 7b** presents the evolution of conductivities with 1000/T, at 95% RH for membranes ps-PES and InX/Y multiblock copolymers, prepared in both solvents (DMAc, DMSO) as well as Nafion 117 as reference for comparison. A general property regarding the impact of solvent selectivity on proton conductivities emerges from a direct inspection of Figure 6b. Indeed, it is seen that all membranes prepared from DMSO solution are more conductive than those obtained from DMAc. This situation could simply originate from the higher ability of DMSO-cast membranes to uptake water, as previously evidenced in **Figure 7a**. However, if we examine the results of **Figure 7b** more deeply, we can add several interesting comments on the effect of solvent selectivity. First, it can be underlined that the solvent selectivity seems to impact much more significantly In5/5 as compared to ps-PES. We found a $\sigma_{DMSO/DMAc}$ ratio of almost 2 for In5/5, while only a value of 1.3 for the ps-PES membranes. In addition, the proton

conductivities of the multiblock copolymer membranes are shown to increase significantly with increasing block length, In15/15 > In10/10 > In5/5. This effect is systematically observed for both DMSO and DMAc cast-membranes, but not to the same extent. Indeed, the $\sigma_{DMSO/DMAc}$ ratio diminishes when the block length increases, i.e., it decreases from 2 in the case of In5/5 membranes to 1.5 and 1.4 for In10/10 and In15/15 membranes, respectively. Therefore, the shorter the blocks, the more the nature of the casting solvent impacts the overall membrane performance. We can tentatively ascribe such behavior to morphological peculiarities. Short blocks architectures could indeed be more sensitive to the introduction of structural disorder produced by the use of DMAc. In turn, on increasing the FPES segment size, the compatibilizing effect of DMAc is likely to be reduced; therefore more block-separated local units might possibly form.

It seems that increasing the block length does not lead to a proportional increase in proton conductivities. In10/10-S6 membranes conduct twice as well as In5/5-S6 membranes, but only limited improvement is gained with In15/15-S6 membranes at low temperatures. At temperatures higher than 70 °C, the conductivities of DMAC-cast In10/10 and In15/15 are even comparable. This could indicate that there is an optimum for producing ordered-enough morphologies already reached with the block size of 10 000 g/mol. We also note that the conductivities of ionomers In10/10 and In15/15 are close to those of Nafion 117 up to 60 °C, and higher at higher temperatures, showing the interesting potential of the as-cast block copolymer materials in view of fuel cell applications.

Table 6. Thermal Transitions of As-Cast and Annealed Membranes

membrane	Tg (°C)	
	as-casting	annealed
$In5/5_{DMSO}$	88 ± 2	104 ± 2
$In10/10_{DMSO}$	78 ± 2	112 ± 2
$In15/15_{DMSO}$	80 ± 2	108 ± 2
$In05/05_{DMAc}$	83 ± 2	105 ± 2
$In10/10_{DMAc}$	78 ± 2	110 ± 2
$In15/15_{DMAc}$	82 ± 2	102 ± 2

3.4.2. Annealed Membranes

The "as-cast membranes" in lithium salt form were annealed at 150 °C to probe the beneficial effect of thermal annealing on conductivities and water uptakes. The temperature of 150 °C was chosen in relation to the Tg of the "as-casting membrane" and the "annealed membrane". As can be seen from **Figure 8** and **Table 6**, the Tg of "as-casting membranes" ranges from 80 to 90 °C (**Table 6**) while after annealing, the Tg of the membranes increase by at least 20 °C, yet reaching maximum values around 110 °C. These values are much lower than those of ionomers in acidic or lithium form, as previously reported (Tg ionic domain ≈ 150 °C, Tg hydrophobic domains ≈ 220 °C).[36] This could be explained by the presence of residual solvent molecules which interact preferentially with ionic functions, leading to an important decrease of the Tg associated with the ionic domains. Thus, annealing under the present conditions (150 °C in the presence of residual solvent located predominately in ionic domains) is expected to favor the reorganization of ionic domains. After the thermal treatment, the amount of residual solvent in the annealed membrane, calculated by ^{1}H NMR analysis, decreases from 10 wt % to almost 8 wt % in the case of membranes cast from DMSO, and from 2% to almost 1% in the case of membrane cast from DMAc.

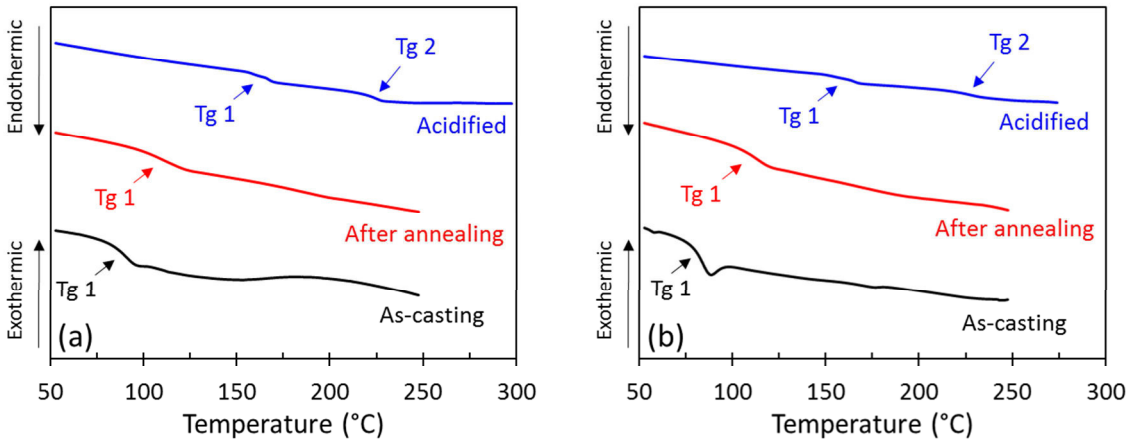

Figure 8. DSC diagrams of "as-cast" and "annealed" In15/15 membranes cast from (a) DMAc and (b) DMSO.

3.4.2.1. Conductivities and Water Uptakes

Thermal annealing of the copolymer membranes at 150 °C lead to lower water uptake and much improved conductivities as compared to those of membranes dried at 60 °C (**Figure 9**). For example, at 80 °C and 95% RH, the proton conductivity of In5/5-S15 is 2 times higher than that of In5/5-S6, and 1.3 higher than Nafion 117, while the water uptake is decreased by 20%. All the membranes (except for In5/5-A15) show higher conductivities than Nafion 117

in the investigated range of temperatures (**Figure 10**). This spectacular increase of conductivities is observed for the membranes cast from both solvents, with a gain almost of the same order of magnitude with respect to non-annealed materials. The striking difference in the conducting behavior between annealed and non-annealed samples, along with the greatly reduced water uptake upon annealing, suggests that the annealing treatment permits a more efficient proton transport within the phase-separated material. This could be due to a beneficial impact of annealing on the co-continuous nanophase separated morphology, the local arrangement of neighboring side chains and/or improved connectivity of ionic channels, and favorable organization of conductive domains at higher scales. The hypothesis of structural reorganization is supported by our DMA analysis.

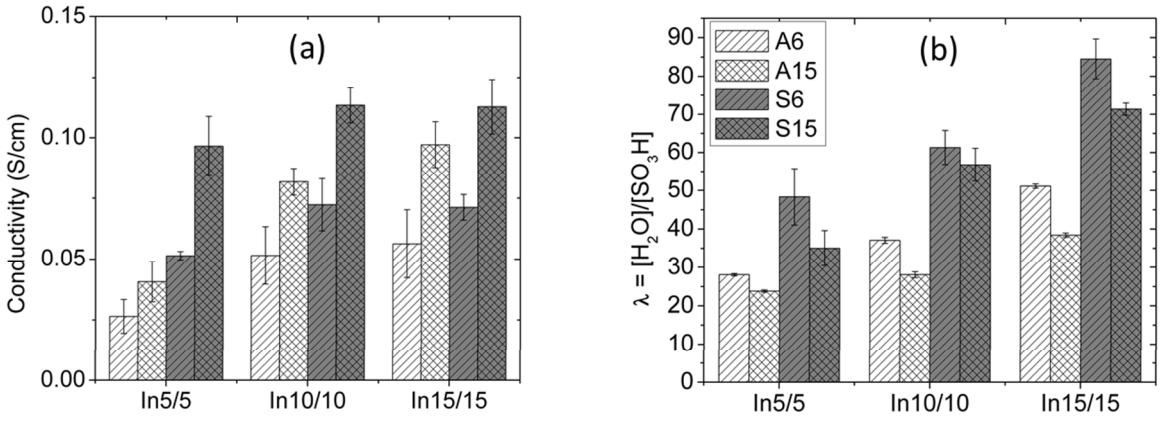

Figure 9. (a) Conductivities at 95% RH and (b) water uptake (the hydration number) at 80 °C of annealed and non-annealed membranes.

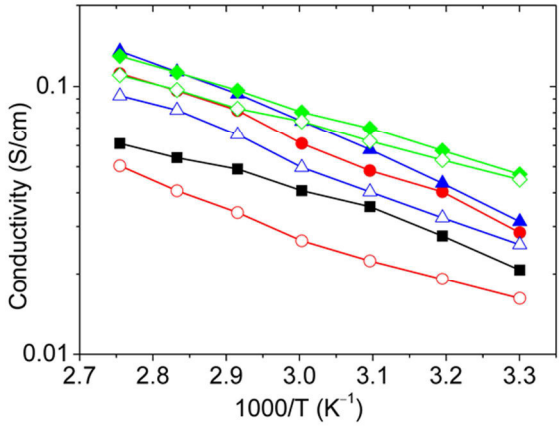

Figure 10. Evolution of proton conductivity with 1000/T at 95% of RH of InX/Y annealed membranes: In5/5-S15 (red ●), In10/10-S15 (blue ▲), In15/15-S15 (green ◆), In5/5-A15 (red ○), In10/10-A15 (blue △), In15/15-A15 (green ◇), Nafion 117 (black ■). (Errors limits for conductivities are ±14%).

Regarding the impact of casting solvent selectivity on the membrane conductivities, it is interesting to point out that the gaps in conductivity of InX/Y membranes cast in DMSO and DMAc remain on the same order of magnitude as those of membranes cast at 60 °C. The $\sigma_{DMSO/DMAc}$ ratio is about 2 in annealed In5/5, whereas for In10/10 and In15/15, we found values of 1.3 and 1.2, respectively (**Figure 9**). Accordingly, the local topology of ionic domains as well as the ionic network connectivity must be substantially improved by the thermal treatment for membranes obtained from both solvents. As the annealing temperature is lower than the Tg of the hydrophobic blocks, it can be hypothesized that the thermal treatment mostly induces reorganization of ionic domains due to pendant chain relaxations and enhanced mobility.

The impact of RH on proton conductivity has been studied for these multiblock copolymers membranes cast from DMSO. **Figure 11** shows the proton conductivity at 80 °C as a function of RH for annealed and non-annealed membranes. Again, it is not surprising to observe the huge impact of annealing on the conductivity, especially at low RH. At 30% RH, the conductivities of annealed membranes are 10 times higher than those of non-annealed ones. Moreover, we obtain conductivity values for In15/15-S15 similar to those of Nafion 117. Another important result is the lower dependence of the proton conductivity of the annealed membrane on the humidity levels. Combined with the aforesaid beneficial effects of annealing in reducing water uptake and improving phase separation between the hydrophilic and hydrophobic domains, this observation further confirms the importance of membrane elaboration in developing PEM with excellent performances.

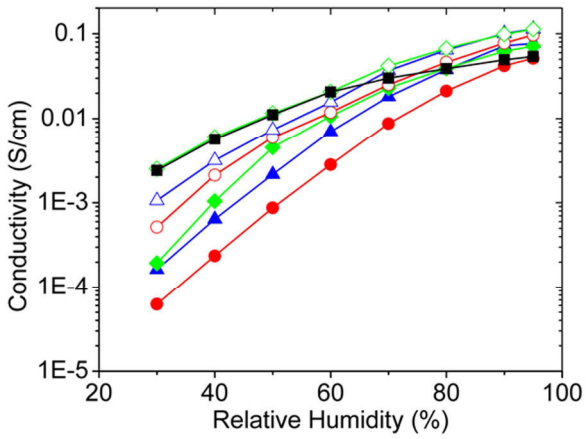

Figure 11. Proton conductivity at 80 °C of Nafion 117 (black ■), In5/5-S6 (red ●), In10/10-S6 (blue ▲), In15/15-S6 (green ◆), In5/5-S15 (red ○), In10/10-S15 (blue △), In15/15-S15 (green ◇). (Errors limits for conductivities are ±14%).

4. Conclusions

The overall goal of the present work was to study how the solvent selectivity, block length, and thermal annealing affect the functional properties (conductivity and water uptake) of new promising ionomers, i.e., perfluorosulfonated poly(arylene ether sulfone) multiblock copolymers. To determine the degree of selectivity of the solvent, the Flory–Hugins parameters between selected solvents and ps-PES and FPES blocks, respectively, were calculated by an original method, i.e., IGC. DMSO and DMAc were selected as casting solvents for the study, as DMSO was identified to be a selective solvent, while DMAc is able to dissolve both segments of the copolymers. The selectivity of the solvents was shown to have no significant impact on the expansion of ionic domains upon swelling, while it dramatically affects the supramolecular ordering of the blocks. This finding highlights the complex interplay between solvent-modulated local interactions, peculiar block-induced morphologies, and hydration-dependent hydrophilic domains topology. We show that PEM performance is determined by a subtle balance between these effects, which was noticeably optimized by thermal treatment. The combination of block length-casting solvent selectivity-membrane processing conditions was shown to result in a very significant increase in performance, with conductivities higher than state-of-the-art PFSA membranes. This study provides a detailed understanding of how block copolymer properties are affected by block length averages and the elaboration method, providing essential clues for a more rational design of efficient block copolymer membranes for fuel cells.

ASSOCIATED CONTENT

Supporting Information

A short description on calculation of the Flory–Huggins parameters are presented. The Supporting Information is available free of charge on the ACS Publications website at DOI: 10.1021/acsami.5b01835.

AUTHOR INFORMATION

Corresponding Author *Phone: +33 (0)476 82 65 61. Fax: +33 (0) 476 82 67 77. E- mail: Cristina.Iojoiu@lepmi.grenoble-inp.fr (C.I.).

Author Contributions

The manuscript was written through contributions of all authors.

ACKNOWLEDGMENTS

The authors would like to thank the FEDER-FUI France for providing financial support to this research work in the framework of the project "Nano-structurated High Performance Polymer". The Institut Laue Langevin is acknowledged for providing access to beam time, and we are grateful to L. Porcar for beamline alignment and his kind help during the experiments. We thank S. Papadopoulou for his help with the ICG column preparation. This work was performed within the framework of the Centre of Excellence of Multifunctional Architectured Materials "CEMAM" no. AN-10-LABX-44−01.

REFERENCES

(1) Zhang, H.; Shen, P. K. Advances in the High Performance Polymer Electrolyte Membranes for Fuel Cells. *Chem. Soc. Rev.* **2012**, *41*, 2382−2394.

(2) Mauritz, K. A.; Moore, R. B. State of Understanding of Nafion. *Chem. Rev.* **2004**, *104*, 4535−4585.

(3) Paddison, S. J.; Paul, R. The Nature of Proton Transport in Fully Hydrated Nafion. *Phys. Chem. Chem. Phys.* **2002**, *4*, 1158−1163.

(4) Peron, J.; Mani, A.; Zhao, X.; Edwards, D.; Adachi, M.; Soboleva, T.; Shi, Z.; Xie, Z.; Navessin, T.; Holdcroft, S. Properties of Nafion NR-211 membranes for PEMFCs. *J. Membr. Sci.* **2010**, *356*, 44−51.

(5) Haubold, H.-G.; Vad, T.; Jungbluth, H.; Hiller, P. Nanostructure of Nafion: A SAXS study. *Electrochim. Acta* **2001**, *46*, 1559−1563.

(6) Duan, Q.; Wang, H.; Benziger, J. Transport of Liquid Water Through Nafion Membranes. *J. Membr. Sci.* **2012**, *392−393*,88−94.

(7) Kerres, J. A. Development of Ionomer Membranes for Fuel Cells. *J. Membr. Sci.* **2001**, *185*,3−27.

(8) Hickner, M. A.; Ghassemi, H.; Kim, Y. S.; Einsla, B. R.; McGrath, J. E. Alternative Polymer Systems for Proton Exchange Membranes (PEMs). *Chem. Rev.* **2004**, *104*, 4587−4612.

(9) Kreuer, K.-D. Ion Conducting Membranes for Fuel Cells and other Electrochemical Devices. *Chem. Mater.* **2014**, *26*, 361−380.

(10) Collette, F. M.; Lorentz, C.; Gebel, G.; Thominette, F. Hygrothermal Aging of Nafion. *J. Membr. Sci.* **2009**, *330*,21−29.

(11) Rozière, J.; Jones, D. J. Non-Fluorinated Polymer Materials for Proton Exchange Membrane Fuel Cells. *Annu. Rev. Mater. Res.* **2003**, *33*, 503−555.

(12) Choi, J.-H.; Ye, Y.; Elabd, Y. A.; Winey, K. I. Network Structure and Strong Microphase Separation for High Ion Conductivity in Polymerized Ionic Liquid Block Copolymers. *Macromolecules* **2013**, *46*, 5290−5300.

(13) Hoarfrost, M. L.; Segalman, R. A. Ionic Conductivity of Nanostructured Block Copolymer. *Macromolecules* **2011**, *44*, 5281− 5288.

(14) Young, W.-S.; Epps, T. H. Ionic Conductivities of Block Copolymer Electrolytes, with various Conducting Pathways: Sample Preparation and Processing Considerations. *Macromolecules* **2012**, *45*, 4689−4697.

(15) Weber, R. L.; Ye, Y.; Schmitt, A. L.; Banik, S. M.; Elabd, Y. A.; Mahanthappa, M. K. Effect of Nanoscale Morphology on the Conductivity of Polymerized Ionic Liquid Block Copolymers. *Macromolecules* **2011**, *44*, 5727−5735.

(16) Virgili, J. M.; Hoarfrost, M. L.; Segalman, R. A. Effect of an Ionic Liquid Solvent on the Phase Behavior of Block Copolymers. *Macromolecules* **2010**, *43*, 5417−5423.

(17) Torquato, S. Optimal Design of Heterogeneus Materials. *Annu. Rev. Mater. Res.* **2010**, *40*, 101−129.

(18) Bates, F. S.; Fredricjson, G. H. Block Copolymers?Designer Soft Materials. *Phys. Today* **1999**, *52*,32−38.

(19) Lee, H. S.; Roy, A.; Lane, O.; Dunn, S.; McGrath, J. E. Hydrophilic−hydrophobic Multiblock Copolymers Based on Poly- (arylene ether sulfone) via Low-Temperature Coupling Reactions for Proton Exchange Membrane Fuel Cells. *Polymer* **2008**, *49*, 715−723.

(20) Lee, H. S.; Roy, A.; Lane, O.; McGrath, J. E. Synthesis and Characterization of Poly(arylene ether sulfone)-b-Polybenzimidazole Copolymers for High Temperature Low Humidity Proton Exchange Membrane Fuel Cells. *Polymer* **2008**, *49*, 5387−5396.

(21) Lee, H. S.; Badami, A.; Roy, A.; McGrath, J. E. Segmented Sulfonated Poly(Arylene Ether Sulfone)-b-Polyimide Copolymers for Proton Exchange Membrane Fuel Cells. Copolymer Synthesis and Fundamental Properties. *J. Polym. Sci., Part A: Polym. Chem.* **2007**, *45*, 4879−4890.

(22) Zhao, C.; Lin, H.; Shao, K.; Le, X.; Ni, H.; Wang, Z.; Na, H. Block Sulfonated Poly(ether ether ketone)s (SPEEK) Ionomers with High Ion-Exchange Capacities for Proton Exchange Membranes. *J. Power Sources* **2006**, *162*, 1003−1009.

(23) Wang, H.; Badami, A.; Roy, A.; McGrath, J. E. Multiblock Copolymers of Poly(2,5-benzophenone) and Disulfonated Poly- (arylene ether sulfone) for Proton-Exchange Membranes. I. Synthesis and Characterization. *J. Polym. Sci., Part A: Polym. Chem.* **2007**, *45*, 284−294.

(24) Lee, M.; Park, J. K.; Lee, H.-S.; Lane, O.; Moore, R. B.; McGrath, J. E.; Baird, D. G. Effects of Block Length and Solution- Casting Conditions on the Final Morphology and Properties of Disulfonated Poly(arylene ether sulfone) Multiblock Copolymer Films for Proton Exchange Membranes. *Polymer* **2009**, *50*, 6129−6138.

(25) Assumma, L.; Iojoiu, C.; Albayrakari, G.; Cointeaux, L.; Sanchez, J.-Y. Polysulfone Containing Sulfonamide Groups as Proton Exchange Membrane for Fuel Cells. *Int. J. Hydrogen Energy* **2014**, *39*, 2740− 2750.

(26) Cho, C. G.; Kim, Y. S.; Yu, X.; Hill, M.; McGrath, J. E. Synthesis and Characterization of Poly(arylene ether sulfone) Copolymers with Sulfonimide Side Groups for a Proton-Exchange Membrane. *J. Polym. Sci, Part A: Polym. Chem.* **2006**, *44*, 6007−6014.

(27) Yoshimura, K.; Iwasaki, K. Aromatic Polymer with Pendant Perfluoro Alkyl Sulfonic Acid for Fuel Cell Applications. *Macromolecules* **2009**, *42*, 9302−9306.

(28) Li, H.; Jackson, A. B.; Kirk, N. J.; Mauritz, K. A.; Storey, R. F. Poly(arylene ether sulfone), Statistical Copolymers Bearing Perfluoroalkylsulfonic Acid Moieties. *Macromolecules* **2011**, *44*, 694−702.

(29) Nakabayashi, K.; Higashihara, T.; Ueda, M. Polymer Electrolyte Membranes Based on Poly(Phenylene ether)s with Pendant Perfluoro Alkyl Sulfonic Acids. *Macromolecules* **2011**, *44*, 1603−1609.

(30) Xu, K.; Oh, H.; Hickner, M. A.; Wang, Q. Highly Conductive Aromatic Ionomers with Perfluorosulfonic Acid Side Chains for Elevated Temperature Fuel Cells. *Macromolecules* **2011**, *44*, 4605− 4609.

(31) Miyatake, K.; Shimura, T.; Mikami, T.; Watanabe, M. Aromatic Ionomers with Superacids Groups. *Chem. Commun.* **2009**, *42*, 6403− 6405.

(32) Mikami, T.; Miyatake, K.; Watanabe, M. Poly(arylene ether)s Containing Super Acid Groups as Proton Exchange Membranes. *ACS Appl. Mater. Interfaces* **2010**, *2*, 1714−1721.

(33) Chang, Y.; Brunello, G. F.; Fuller, J.; Disabb-Miller, M. L.; Hawley, M. E.; Kim, Y. S.; Hickner, M. A.; Jang, S. S.; Bae, C. Polymer Electrolyte Membranes Based on Poly(arylene ether sulfone) with Pendant Perfluorosulfonic Acid. *Polym. Chem.* **2013**, *4*, 272−281.

(34) Chang, Y.; Brunello, G. F.; Fuller, J.; Hawley, M.; Kim, Y. S.; Disabb-Miller, M.; Hickner, M. A.; Jang, S. S.; Bae, C. Aromatic Ionomers with Highly Acidic Sulfonate Groups: Acidity, Hydration, and Proton Conductivity. *Macromolecules* **2011**, *44*, 8458−8469.

(35) Mikami, T.; Miyatake, K.; Watanabe, M. Synthesis and Properties of Multiblock Copoly(arylene ether)s Containing Superacid Groups for Fuel Cell Membranes. *J. Polym. Sci., Part A: Polym. Chem.* **2011**, *49*, 452−464.

(36) Assumma, L.; Iojoiu, C.; Mercier, R.; Lyonnard, S.; Nguyen, H. D.; Planes, E Synthesis of Partially Fluorinated Poly(arylene ether sulfone) Multiblock Copolymers Bearing Perfluorosulfonic Functions. *J. Polym. Sci., Part A: Polym. Chem.* **2015**, *53*, 1941–1956.

(37) Nguyen, H. D.; Assumma, L.; Judeinstein, P.; Mercier, R.; Porcar, L.; Jestin, J.; Iojoiu, C.; Lyonnard, S. Controlling Microstructure-Transport Interplay in Highly Phase-Separated Perfluorosulfonated Aromatic Multiblock Ionomers via Molecular Architecture Design. *ACS Appl. Mater. Interfaces* **2017**, DOI: 10.1021/acsami.6b12764.

(38) Park, C. H.; Lee, C. H.; Guiver, M. D.; Lee, Y. M. Sulfonated Hydrocarbon Membranes for Medium-Temperature and Low- Humidity Proton Exchange Membrane Fuel Cells (PEMFCs). *Prog. Polym. Sci.* **2011**, *36*, 1443−1498.

(39) Robertson, G. P.; Mikhailenko, S. D.; Wang, K.; Xing, P.; Guiver, M. D.; Kaliaguine, S. Casting Solvent Interactions with Sulfonated Poly(ether ether ketone) During Proton Exchange Membrane Fabrication. *J. Membr. Sci.* **2003**, *219*, 113−121.

(40) Noda, A.; Susan, M. A. B. H.; Kudo, K.; Mitsushima, S.; Hayamizu, K.; Watanabe, M. Brønsted Acid−Base Ionic Liquids as Proton Conducting Nonacqueus Electrolyte. *J. Phys. Chem. B* **2003**, *107*, 4024−4033.

(41) Hamley, I. W. *Introduction to Block Copolymers, Developments in Block Copolymer Science and Technology*; John Wiley & Sons, Ltd: New York, 2004, Vol. *1*, pp 1−29.

(42) Adams, F. V.; Nxumalo, E. N.; Krause, R. W. M.; Hoek, E. M. V; Mamba, B. B. The Influence of Solvent Properties on the Performances of Polysulfone/β-Cyclodextrin Polyurethane Mixed Matrix Membranes. *J. Appl. Polym. Sci.* **2013**, *130*, 2005−2014.

(43) Mineart, K. P.; Jiang, X.; Jinnai, H.; Takahara, A.; Spontak, R. J. Morphological Investigation of MidBlock Sulfonated Block Ionomers Prepared from Solvents Differing in Polarity. *Macromol. Rapid Commun.* **2015**, *36 (5)*, 432−438.

(44) Zhang, F.; Zhang, H.; Qu, C. Influence of Solvent on Polymer Prequaternization toward Anion-Conductive Membrane Fabrication for All-Vanadium Flow Battery. *J. Phys. Chem. B* **2012**, *116*, 9016– 9022.

(45) Li, W.; Zhang, F.; Yi, S.; Huang, C.; Zhang, H.; Pan, M. Effects of Casting Solvent on Microstructrue and Ionic Conductivity of Anhydrous Sulfonated Poly(ether ether ketone)-inoic Liquid Composite Membranes. *Int. J. Hydrogen Energy* **2012**, *37*, 748−754.

(46) Jun, M.-S.; Choi, Y.-W.; Kim, J.-D. Solvent Casting Effects of Sulfonated Poly(ether ether ketone) for Polymer Electrolyte Membrane Fuel Cell. *J. Membr. Sci.* **2012**, *396*,32−37.

(47) Cho, K.-Y.; Park, J.-K.; Jung, H.-Y. The Effect of Solvent Casting Condition on the Electrochemical Properties of Nafion/Polyvinylidene Fluoride Copolymer Blends for Direct Methanol Fuel Cell. *Chem. Eng. Commun.* **2015**, *202*, 593−599.

(48) Ding, X.; Didari, S.; Fuller, T. F.; Harris, T. A. L. Effects of Annealing Conditions on the Performances of Solution Cast Nafion Membranes in Fuel Cells. *J. Electrochem. Soc.* **2013**, *160*, F793−F797.

(49) Alberti, G.; Narducci, R.; Di Vona, M. L.; Giancola, S. Annealing of Nafion 1100 in the Presence of an Annealing Agent: A Powerful Method for Increasing Ionomer Working Temperature in PEMFCs. *Fuel Cells* **2013**, *13*, 42−47.

(50) Wang, J.; Yang, M.; Dou, P.; Wang, X.; Zhang, H. Influences of Annealing on the Perfluorosulfonated Ion-Exchange Membranes Prepared by Melt Extrusion. *Ind. Eng. Chem. Res.* **2014**, *53*, 14175−14182.

(51) Yang, L.; Tang, J.; Li, L.; Ai, F.; Chen, X.; Yuan, W. Z.; Zhang, Y. Properties of Precursor Solution Cast PFSI Membranes with Various Ion Exchange Capacities and Annealing Temperatures. *RSC Adv.* **2013**, *3*, 7289−7295.

(52) Conder, J. R.; Young, C. L. *Physicochemical Measurement by Gas Chromatography*; Wiley: New York, **1979**.

(53) Al-Saigh, Z. Y.; Munk, P. Study of Polymer−Polymer Interaction Coefficients in Polymer Blends Using Inverse Gas Chromatography. *Macromolecules (Washington, DC, U. S.)* **1984**, *17*, 803−809.

(54) Papadopoulou, S. K.; Dritsas, G.; Karapanagiotis, I.; Zuburtikudis, I.; Panayiotou, C. Surface Characterization of Poly-(2,2,3,3,3-pentafluoropropyl methacrylate) by Inverse Gas Chromatography and Contact Angle Measurements. *Eur. Polym. J.* **2010**, *46*, 202−208.

(55) Papadopoulou, S. K.; Panayiotou, C. Thermodynamic Characterization of Poly(1,1,1,3,3,3-hexafluoroisopropyl methacrylate) by Inverse Gas Chromatography. *J. Chromatogr. A* **2012**, *1229*, 230−236.

(56) Naik, H. G.; Aminabhavinaik, T. M. Gas−Liquid Chromato- graphic Study of Polystyrene−n-Alkane Interactions. *J. Appl. Polym. Sci.* **2001**, *80*, 1291−1298.

(57) Kreuer, K. D.; Portale, G. A. A Critical Revision of the Nano-Morphology of Proton Conducting Ionomers and Polyelectrolytes for Fuel Cell Applications. *Adv. Funct. Mater.* **2013**, *23*, 5390−5397.

(58) Litt, M. H. A Reevaluation of Nafion Morphology. *Polym. Prepr.* **1997**, *38*, 80−81.

(59) Rubatat, L.; Gebel, G.; Diat, O. Evidence of Elongated Polymer Aggregates in Nafion. *Macromolecules* **2004**, *37*, 7772−7783.

(60) Piroux, F.; Espuche, E.; Mercier, R.; Pinéri, M.; Gebel, G. Gas Transport Mechanism in Sulfonated Polyimides Consequences on Gas Selectivity. *J. Membr. Sci*. **2002**, *209*, 241−253.

Supporting Information

Effects of Block Length and Membrane Processing Conditions on the Morphology and Properties of Perfluorosulfonated Poly(arylene ether sulfone) Multiblock Copolymer Membranes for PEMFC

Luca Assumma,[†,‡] Huu-Dat Nguyen,[†,‡] Cristina Iojoiu,[†,‡] Sandrine Lyonnard,[⊥] Régis Mercier,[§] and Eliane Espuche[§]*

[†]Univ. Grenoble Alpes, LEPMI, F-38000 Grenoble, France

‡CNRS, LEPMI, F-38000 Grenoble, France

[⊥]CEA-Grenoble, INAC/SPrAM, Groupe Polymères Conducteurs Ioniques, UMR-5819, CEA-CNRS-UJF, 17 Rue de Martyrs 38054 Grenoble, CEDEX 9 France

[§]Ingénierie des Matériaux Polymères, UMR-5223, IMP@LYON1, Université de Lyon, Université Lyon 1, 15 Bd. A Latarjet, 69622, Villeurbanne CEDEX France

Corresponding Author's email address: Cristina.Iojoiu@lepmi.grenoble-inp.fr

Calculation of Flory-Huggins Parameters.

Contrary to the conventional gas chromatography, in IGC, the material under study is packed into the column where injections of carefully selected probes with known physicochemical properties are made.[1–3] The probes can be injected onto the column either at infinite dilution or at finite concentration. In the first case, the injection of minor amounts of the tested solvent makes sure that the retention is governed by the stationary phase-probe interactions and the probe-probe interactions are avoided.[1] The key measurement in IGC experiments is the net retention volume of the probes, V_N. It is expressed as the volume of the carrier gas necessary to elute the solute from the column and is calculated by **Equation S1**.[4]

$$V_N = jF_M\left(t_R - t_M\right)\frac{T}{T_F}\left(1 - \frac{p_W}{P_O}\right) \qquad \textbf{(S1)}$$

where t_R, t_M are the probe's and marker's retention times, respectively, F_M is the carrier gas flow rate measured at the column outlet at ambient pressure, P_0 and at room temperature, T_F. Also, T is the column temperature, P_W is the vapour pressure of water at T_F and j is the James and Martin factor used to correct the gas carrier compressibility, defined by **Equation S2**.[4]

$$\mathrm{j} = \frac{3}{2}\cdot\left[\frac{\left(P_i/P_o\right)^2 - 1}{\left(P_i/P_o\right)^3 - 1}\right] \qquad \textbf{(S2)}$$

where P_i and P_0 are the column inlet and outlet pressures, respectively.

The specific retention volume, V_g^0 is necessary for the calculation of the thermodynamic properties and is given by **Equation S3**.[4]

$$V_g^0 = \frac{273V_N}{W_S T} \qquad \textbf{(S3)}$$

where W_S is the mass of the stationary phase.

The molar heat (enthalpy) of sorption, ΔH_1^s and the molar free energy of sorption, ΔG_1^s of the probe absorbed by the material under study were determined by **Equation S4** and **Equation S5**, respectively.[4]

$$\Delta H_1^s = -\frac{R\partial \ln V_g^0}{\partial\left(1/T\right)} \qquad \textbf{(S4)}$$

$$\Delta G_1^s = -RT\ln\left(\frac{M_1 V_g^0}{273.15\mathrm{R}}\right) \quad \textbf{(S5)}$$

where T is the column temperature, M_1 the molecular weight of the probe and R the gas constant.

The weight fraction activity coefficient, Ω_1^∞, the molar heat of mixing at infinite dilution, ΔH_1^∞ and the corresponding molar free energy of mixing, ΔG_1^∞ of each probe are calculated with the following relationships (**Eq. S6**, **S7**, and **S8**, respectively).[4]

$$\Omega_1^\infty = \frac{273.15R}{V_g^0 P_1^o M_1}\exp\left(\frac{-P_1^o\left(B_{11}-V_1\right)}{RT}\right) \quad \textbf{(S6)}$$

$$\Delta H_1^\infty = \frac{R\partial \ln \Omega_1^\infty}{\partial\left(1/T\right)} \quad \textbf{(S7)}$$

$$\Delta G_1^\infty = RT\ln\Omega_1^\infty \quad \textbf{(S8)}$$

where P_1^0 is the vapor pressure of the probe at temperature T, B_{11} is its second virial coefficient and V_1 is the probe's molar volume.

Apart from the weight fraction activity coefficient, the Flory-Huggins interaction parameter χ_{12}^∞ is used to describe the interaction between the material under study and the solute and is given by **equation S9**.[4]

$$\chi_{12}^\infty = \ln\left(\frac{273.15Rv_2}{V_g^0 P_1^o V_1}\right) - 1 - \frac{P_1^o\left(B_{11}-V_1\right)}{RT} \quad \textbf{(S9)}$$

where v_2 is the polymer's specific volume.

The values of probe retention time, t_R, specific retention volume, V_g^0 and interaction parameter χ_{P-S}^∞ for the FPES are given in **Table S1** (a, b) and for ps-PES in **Table S2** (a, b):

Table S1. Values of, t_r, V_g°, χ_{P-S}^{∞} between the hydrophobic oligomer FPES and the solvents (a) DMAc, DMSO, (b) DMF, DGDE.

(a)

solvent	DMAc			DMSO		
Température (°C)	$\bar{t}_R$ (sec)	Vg^0 (m^3/g)	χ_{P-S}^{∞}	$\bar{t}_R$ (sec)	Vg^0 (m^3/g)	χ_{P-S}^{∞}
220	39.6	1.01E-05	0.34	53.7	1.65E-05	0.66
230	35.1	8.32E-06	0.34	46.4	1.33E-05	0.65
240	31.6	6.88E-06	0.34	40.8	1.08E-05	0.64
250	29.6	5.87E-06	0.31	37.2	9.23E-06	0.60

(b)

solvent	DMF			DGDE		
Température (°C)	$\bar{t}_R$ (sec)	Vg^0(m^3/g)	χ_{P-S}^{∞}	$\bar{t}_R$ (sec)	Vg^0 (m^3/g)	χ_{P-S}^{∞}
220	33.2	7.26E-06	0.58	53.7	4.17E-06	0.65
230	30.5	6.17E-06	0.55	46.4	3.47E-06	0.63
240	28.7	5.43E-06	0.50	40.8	2.57E-06	0.73
250	27.0	4.70E-06	0.47	37.2	2.04E-06	0.77

Table S2. Values of, t_r, V_g°, χ_{P-S}^{∞} between the hydrophobic oligomer ps-PES and the solvents (a) DMAc, DMSO, (b) DMF, DGDE.

(a)

solvent	DMAc			DMSO		
Température (°C)	$\bar{t}_R$ (sec)	Vg^0 (m^3/g)	χ_{P-S}^{∞}	$\bar{t}_R$ (sec)	Vg^0 (m^3/g)	χ_{P-S}^{∞}
260	232.7	1.98E-04	-3.38	/	/	/
265	178.0	1.49E-04	-3.19	/	/	/
270	137.4	1.13E-04	-2.99	254.1	2.42E-04	-3.04
275	117.8	9.56E-05	-2.91	209.5	1.98E-04	-2.93

(b)

solvent	DMF			DGDE		
Température (°C)	$\bar{t}_R$ (sec)	Vg^0 (m^3/g)	χ_{P-S}^{∞}	$\bar{t}_R$ (sec)	Vg^0 (m^3/g)	χ_{P-S}^{∞}
260	82.9	6.07E-05	-2.26	45.8	2.08E-05	-1.72
265	71.8	5.17E-05	-2.18	41.2	1.78E-05	-1.66
270	64.5	4.57E-05	-2.14	38.1	1.57E-05	-1.63
275	58.3	4.07E-05	-2.10	35.4	1.36E-05	-1.60

REFERENCES

(1). Voelkel, A.; Strzemiecka, B.; Adamska, K.; Milczewska, K. Inverse Gas Chromatography as a Source of Physiochemical Data. *J. Chromatogr*. A **2009**, *1216*, 1551-1566.

(2). Kolodziejek, J.; Voelkel, A.; Heberger, K. Characterization of Hybrid Materials by Means of Inverse Gas Chromatography and Chemometrics. *J. Pharm. Sci.* **2013***, 102*, 1524-1531.

(3). Belgacem, M.N.; Czeremuszkin, G.; Sapieha, S.; Gandini, A. Surface Characterization of Cellulose Fibers by XPS and IGC. *Cellulose* **1995,** *2*, 145-157.

(4). Conder, J. R.; Young, C. L. *Physicochemical Measurement by Gas Chromatography*; Wiley: New York, **1979**, pp. 336–338.

Chapter 2B.

Controlling Microstructure–Transport Interplay in Highly Phase-Separated Perfluorosulfonated Aromatic Multiblock Ionomers via Molecular Architecture Design

Nguyen, H. D.; Assumma, L.; Judeinstein, P.; Mercier, R.; Porcar, L.; Jestin, J.; Iojoiu, C.; Lyonnard, S. *ACS Appl. Mater. Interfaces* **2017**, *9*, 1671-1683. DOI: 10.1021/acsami.6b12764

Controlling Microstructure–Transport Interplay in Highly Phase-Separated Perfluorosulfonated Aromatic Multiblock Ionomers via Molecular Architecture Design

Huu-Dat Nguyen,[†] Luca Assumma,[†] Patrick Judeinstein,[‡] Regis Mercier,[§] Lionel Porcar,[∥] Jacques Jestin,[‡] Cristina Iojoiu,[†] and Sandrine Lyonnard*[⊥]*

[†]LEPMI, Université Grenoble Alpes – CNRS, 38000 Grenoble, France

[‡]Laboratoire Léon Brillouin (LLB), CNRS-CEA, Université Paris-Saclay, CEA Saclay, 91191 Gif-sur-Yvette Cedex, France

[§]Ingénierie des Matériaux Polymères, Université de Lyon, 69622 Villeurbanne, France

[∥]Institut Laue Langevin (ILL), 38002 Grenoble, France

[⊥]INAC-SPrAM, Université Grenoble Alpes – CEA – CNRS, 38000 Grenoble, France

ABSTRACT. Proton-conducting multiblock polysulfones bearing perfluorosulfonic acid side chains were designed to encode nanoscale phase-separation, well-defined hydrophilic/hydrophobic interfaces and optimized transport properties. Herein we show that the superacid side chains yield highly ordered morphologies that can be tailored by best compromising ion-exchange capacity and block lengths. The obtained microstructures were extensively characterized by Small-Angle Neutron Scattering (SANS) over an extended range of hydration. Peculiar swelling behaviors were evidenced at two different scales and attributed to the dilution of locally flat polymer particles. We evidence the direct correlation between the quality of interfaces, the topology and connectivity of ionic nano-domains, the block superstructure long-range organization and the transport properties. In particular, we found that the proton conductivity linearly depends on the microscopic expansion of both ionic and block domains. These findings indicate that neat nanoscale phase-separation and block-induced long-range connectivity can be optimized by designing aromatic ionomers with controlled architectures to improve the performances of polymer electrolyte membranes.

KEYWORDS: Proton-exchange membranes, block copolymers, phase-separated structures, ionic/nonionic interfaces, PEMFCs

1. Introduction

Highly ion-conducting polymer electrolyte membranes are phase-separated materials composed of conducting (ionic) and non-conducting (non-ionic) domains. The ionic/non-ionic interfaces, the topology and connectivity of ionic nano-domains, and the long-range order play a key role in determining the local ion mobility and macroscopic transport properties. The design of molecular architectures tailored to yield highly nanostructured morphologies is an actual challenge in different fields as environmental science, nanotechnology, energy storage and conversion. In proton exchange membrane for fuel cells (PEMFCs), the polymer membranes must combine high ionic conductivity and proton transport efficiency, high chemical stability, good mechanical properties, and dimensional stability in hydrated state.[1,2] Currently the reference materials used in PEMFC are perfluorosulfonic acid (PFSA) ionomers, such as Nafion from DuPont, Aciplex from Asahi, Aquivion from Solvay or 3M membranes, due to their high performances (at temperatures below 90 °C) and high thermal-oxidative stability. PFSA ionomers consist of a hydrophobic perfluorinated backbone bearing hydrophilic perfluorosulfonic acid side chains.[3–5] Their high proton conductivities, even at low water content, are usually attributed to nanoscale phase-separated morphology as well as to the very high acidity of the perfluorosulfonic acid groups.[6–10] However, PFSA ionomers suffer from several drawbacks, including high production cost, a fairly questionable environmental compatibility, high gas permeability leading to the formation of aggressive radicals at the catalyst surface, as well as a decrease in conductivity and mechanical strengths above 80 °C.[11–13] As a consequence, much effort has been devoted over the last years to develop alternative sulfonated aromatic ionomers such as polysulfones, polyetherketones, polyimides, etc.[14–16] As aromatic ionomers possess high glass transition temperature, low gas permeability, low fabrication cost, they are believed to be very promising for overcoming the actual drawbacks of benchmarked PFSA membranes.[17] However, the performances of aromatic PEM at high temperature and low relative humidity (RH) were reported to be poorer than those of PFSA. This was mainly attributed to (i) the morphological differences between the two kinds of ionomer membranes and (ii) the lower acidity of aryl sulfonic acid as compared to that of PFSA. Therefore, to achieve highly conductive materials, it is crucial to design aromatic ionomer structures with highly dissociated ionic functions capable of self-organizing into neat hydrophilic-hydrophobic phase-separated structures, forming well-defined and interconnected hydrophilic channels with low tortuosity.[18,19] To control PEM microstructure, a variety of ionomer structures were proposed and explored.[20–24] Among them, ionomers with a very well controlled location and distribution of the sulfonic acid groups

within the polymer structure, e.g., sulfonated multiblock copolymers,[25–27] graft polymers[28,29] and ionomers bearing perfluorosulfonic acids,[30–33] showed improved morphologies and significantly higher conductivities at low RH, as compared to statistically sulfonated ionomers. Generally, the TEM images of sulfonated multiblock copolymers evidenced a lamellar morphology with alternating hydrophilic (sulfonated blocks) and hydrophobic domains.[34]

Analysis of the block copolymers by Small Angle X-rays Scattering (SAXS) also revealed that the morphology is highly dependent on the block lengths.[35] Accordingly, it was reported that (i) the size of ionic clusters increases with increasing block lengths and (ii) the presence of ordered periodic microstructures domains (confirmed by a sharp Gaussian peak and a weak 2nd order peak apparent at $2Q_{max}$) was attained only for long blocks, e.g., 10000 g/mol, while only one broad maximum was observed for shorter block lengths.[36] Regarding ionomers bearing perfluorosulfonic acids, most studies were conducted on random polymers.[32,37,38] They pointed a poorer nano-structuration and hydrophilic-hydrophobic phase separation, as compared to the well-developed ionic channels structures of sulfonated multiblock copolymers. Therefore, one may conclude that the enhancement of proton conductivity within perfluorosulfonic random copolymers mainly originates from the super-acidity of PFSA side chains, which yields greater proton dissociation and weaker interactions with the surrounding water. It was also reported that the topology of sulfonated groups, e.g., the nature and lengths of side chains (linear *vs* branched) can drastically modify the conductivity of PEM.[37]

Recently, we have developed by "one-pot-two-step synthesis" new multiblock-copolymers based on partially fluorinated hydrophobic blocks and hydrophilic blocks bearing perfluorosulfonic acid functions. AFM characterization and preliminary SANS measurements performed on membranes immersed in water evidenced that the block-copolymers exhibit a highly structured morphology.[39,40] They show much better performances as compared to those of the random ones.[40]

Nevertheless, despite the clear interest in block copolymer-based PEM, a fundamental understanding of the relationship between chemical structures, block copolymer composition, water content and resultant morphology is still lacking. To the best of our knowledge, there is no comprehensive study reported on block-copolymers bearing perfluorosulfonic functions. Therefore, herein we report a detailed analysis of the structure-transport interplay in the new aromatic multi-block copolymers as a function of their chemical architecture and the water content. Five block ionomer membranes with different block size and Ion-Exchange Capacity

(IEC) were prepared and investigated at different water contents. The hydration was quantified by the hydration number, $\lambda = [H_2O]/[SO_3^-]$, which was varied in the range ~0 to ~110. The multi-scale morphologies and their evolutions along water uptake were determined by SANS. The structure of diluted ionomer solutions was also analyzed to measure the form factor of polymer particles and shed light on the self-assembling process during solution cast. The transport properties, *i.e.,* proton conductivities and water diffusion coefficients, were measured along hydration. The correlation between the chemical architecture, the microstructure and the proton/water mobility was rationalized using the mean size of ionic and block domains as the relevant variables. This allowed us to correlate the transport properties to the reorganization of the structure upon hydration, and to establish the benefits of combining highly phase-separated nano-domains and block-induced long-range connectivity. These are crucial hints to rationalize the design of high performance ionomers.

2. Materials and Methods

2.1. Materials

Aromatic block ionomers (labeled as InX/Y) and random ionomers (labeled as InR) were synthetized as described elsewhere.[39] The chemical formula of the hydrophilic ps-PES blocks (molar mass of PES backbone X kg/mol) and hydrophobic FPES blocks (molar mass Y kg/mol) of ionomers InX/Y are presented in **Figure 1**, together with a schematic representation of polymer chains. Ionomers with different IEC were prepared by varying the length of the hydrophilic backbone of ps-PES block (IEC-series including In2.5/5, In5/5 and In7.5/5). The lengths of both backbones (ps-PES and FPES) were also varied while keeping a fixed IEC (length-series, including In5/5, In10/10 and In15/15). The average block molecular weights of PES and FPES, molecular weights of PES-FPES and corresponding values of the IEC of InX/Y are summarized in **Table 1**. The ionomers In2.5/5, In5/5 and In7.5/5 were synthesized using dimethylsulfoxide (DMSO) as reaction solvent.[39] Due to the low solubility of longer FPES blocks in DMSO, In10/10 and In15/15 were synthesized in DMAc. In order to check the potential impact of solvent reaction on the ionomers microstructure and properties, In5/5 was synthetized in both solvents, DMSO (labeled In5/5-1) and DMAc (labeled In5/5-2), respectively.

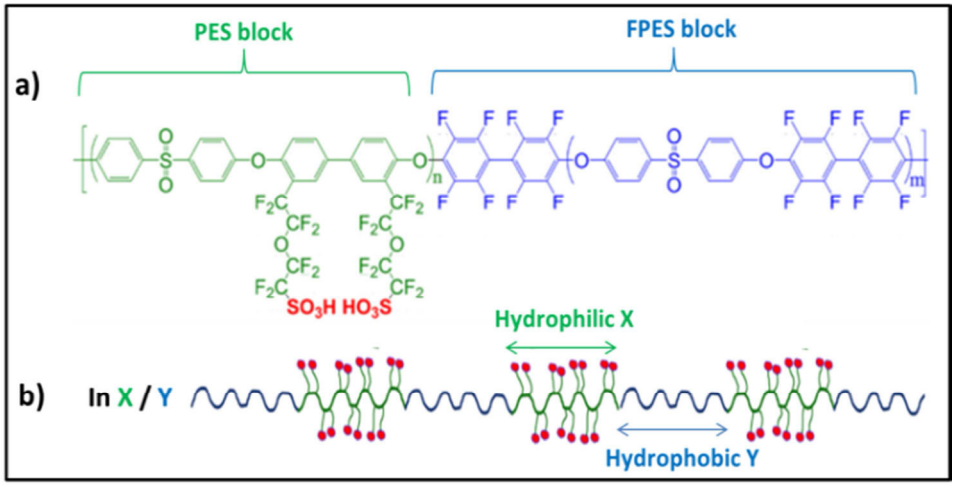

Figure 1. a) Chemical formula of ps-PES and FPES blocks. b) Schematic representation of InX/Y ionomers.

Table 1. Average Block Molecular Weights, PES-FPES Molecular Weights ($Mn_{PES\text{-}FPES}$, $Mw_{PES\text{-}FPES}$, Polydispersity (I_p), and IEC of Random Ionomer InR and Multi-Block Copolymers InX/Y

Code	Reaction Solvent	PES (g/mol)	FPES (g/mol)	$Mn_{PES\text{-}FPES}$[a] (kg/mol)	$Mw_{PES\text{-}FPES}$[a] (kg/mol)	I_p	IEC (meq H^+/g)
InR	DMSO	-	-	22	55	2.5	1.30 ± 0.04
In2.5/5	DMSO	2500	5000	90	260	2.9	0.96 ± 0.05
In5/5-1	DMSO	5000	5000	70	160	2.4	1.30 ± 0.05
In5/5-2	DMAc	5000	5000	108	330	3.1	1.30 ± 0.05
In7.5/5	DMSO	7500	5000	130	310	2.4	1.56 ± 0.10
In10/10	DMAc	10000	10000	113	278	2.5	1.35 ± 0.10
In15/15	DMAc	15000	15000	126	378	3.0	1.32 ± 0.10

[a]*SEC performed in THF, solution filtered with PP-based filter as described in ref.*[39]

2.2. Membrane Preparation

The ionomers in the lithium-salt form were dissolved in DMSO to obtain 7 wt % solutions, which were then stirred at 60 °C for 24h. After that, the solutions were centrifuged for 30 min at 5000 rpm to remove solid impurities, and degassed under vacuum for 30 min. The degassed solutions were cast onto a glass plate using a casting knife (Elcometer 4340 Automatic Film Applicator). The solvent was evaporated in an oven at 60 °C. Then the membranes were rinsed several times in distilled water over 24h to remove solvent residue.

The free solvent membranes were verified by ^{1}H-NMR. Finally, the membranes were acidified by immersing in 1M HCl solution for 24h at room temperature (RT), followed by washing with distilled water for at least 24h to remove acid trace.

The membranes were firstly dried under vacuum at 60 °C for 24h (dry membrane). Low hydration membranes ($\lambda < 10$) were prepared by exposing the dry membranes to different relative humidities (from 11% to 85%) for one week at 25 °C (**Table S1a**). High hydration membranes ($\lambda > 10$) were prepared by immersing the dry membranes for 24h in deionized water at different temperatures ranging from 20 to 90 °C. Then, the membranes were stored in water at room temperature before the SANS measurements (**Table S1b**). The method to determine the hydration number (λ) and polymer volume fraction (ϕp) is detailed in the **Supporting Information**, and all values are given in **Table S1**. The polymer density determined at 20 °C with the help of a Mettler-Toledo kit was found to be ~1.6 g/cm^3.[39,40]

2.3. Small Angle Neutron Scattering (SANS)

SANS measurements were performed on D22 spectrometer at Institut Laue-Langevin (ILL, Grenoble, France) and on PAXY spectrometer at Laboratoire Léon-Brillouin (LLB, Paris, France). The measurement protocol is similar to that described in references.[39,40] Two configurations were used to cover an extended Q-range, from 4×10^{-3} to 0.6 Å^{-1} and 7×10^{-3} to 0.6 Å^{-1} (ILL and LLB experiments, respectively), Q being the scattering vector defined as $Q = (4\pi/\lambda)\sin(\theta/2)$ where λ is the wavelength of the incident neutron beam, and θ the total scattering angle. The isotropic 2D patterns recorded in the two configurations were radially averaged to obtain the 1D scattered intensities I(Q), and further corrected using standard procedures (detector efficiency, background, and empty cell subtraction). As data taken in the two configurations perfectly overlap in the intermediate Q-region, the I(Q) plots were merged to obtain a single spectrum for each sample. The membranes prepared at low λ (**Table S1a**) were stored in air-tight mobile glove boxes containing saturated salt solutions. The membranes were inserted in round neutron cells inside the glove box to avoid contamination with the air. The cells were hermetically closed, taken out of the mobile glove box just before the SANS measurements (more details in the **Supporting Information**). The membranes prepared at high λ were taken out from the water and inserted in quartz Helma cells with some drops of water, and maintained at room temperature. Absolute intensities were obtained, although data are sometimes shifted for clarity and therefore plotted in arbitrary units.

2.4. Conductivity Measurements

The proton conductivity was measured at 25 °C via through-plane impedance technique[41] using a homemade measuring cell and a Material Mates 7260 frequency response analyzer. The impedance spectra were recorded between 10 MHz and 5 Hz. The ionomer membranes (~0.09–0.12 mm in thickness) were sandwiched between two stainless steel electrodes (blocking electrodes), the upper electrode is mobile, with the diameter of 2 mm, while the diameter of bottom electrode is 5 cm (**Figure S1**). The pressure of the upper electrode on the membrane was adjusted with a soft compression spring of 0.3 × 2.3 × 16.5 mm (in order to insure a good contact and to avoid an important thickness compressing, especially in the case of high water uptake membranes). To correlate the transport and morphological properties, the same sample preparation protocols were employed to condition the membranes for conductivity and SANS measurements. Thus, prior to conductivity measurement, the membranes with high λ were taken out from the water and placed quickly between the cell electrodes. The membranes with $\lambda < 10$ were placed between the electrodes and equilibrated at RH ranging between 11 % and 85 % in a climatic chamber (Vötsch VC 4018) at 25 °C temperature during 48h. The resistance of the membranes was taken at frequency intercept with the real axis in the Nyquist plot. Z view software was used to analyze and fit the data. The equivalent circuit used to fit the experimental data is presented in **Figure S2**. An example of the Nyquist plots and corresponding fitted curves is given in **Figure S3**. The impedance of the cell hardware was measured by shorting the electrodes and the value (0.2 Ω) of the resistance (R_{cable}) was introduced in the fit equation. The impedance of the ionomer membrane is composed of the the bulk resistance, R_b, in parallel with the bulk membrane capacitance, C_b. The behavior at electrode/membrane interfaces is merely capacitive[41] (represented in the circuit used to fit by CPE_{dl}) and appears at low frequency in the impedance spectra. An ideal capacitive behavior has to result in the vertical linear line in the Z' *vs.* Z" diagram. However, it is known that capacitance at solid electrodes deviates from ideal behavior,[41] and in our case seems to depend on the membrane hydration. Thus, higher deviation was observed in the case of membranes with high λ and this is, probably, due to the formation of thin water layer between the membrane and the electrode. The conductivity was calculated as follows:

$$\sigma = \frac{L}{R \times A}$$

where L is the thickness of the hydrated membrane, A is the electrode area, and R is R_b, the bulk membrane resistance.

2.5. Proton Diffusion Coefficients

The self-diffusion coefficients of water were measured by NMR pulsed field gradient methods (PFG-NMR) using a 9.4T Bruker 400 with a 5 mm diffusion probe and temperature control of ± 0.5 °C. Membranes were previously equilibrated in water for at least 24h, and then cut in bands with the following dimensions: 10 mm length, 3 mm width and thickness ranging between 0.09 and 0.12 mm. After removing from water, the membranes bands were wipe up quickly with absorbing paper and introduced in NMR sealed tube.

3. Results and Discussion

The microstructures of aromatic block ionomers and random ionomer were investigated by SANS over a wide range of hydration. In the following, first we establish the prominent structural features of the block copolymers morphology by qualitatively inspecting the SANS spectra obtained for the IEC- and length-series prepared under moderate swelling conditions. Next, the structural organization is discussed in more details by analyzing the impact of water content, the swelling laws, and the SANS of diluted solutions in DMSO solvent. A schematic representation of the self-assembling process during solution cast and final multi-scale structure of membranes is proposed. Last, we report on the characterization of transport properties and provide evidence of their correlation to the membrane structure.

3.1. Main Morphological Features of Block Copolymers

Hydrated Membranes. The SANS spectra of ionomer membranes prepared at λ ranging from 15 to 20 are reported on **Figure 2**. All InX/Y ionomers show long-range structural ordering at two characteristic length scales, as shown by the presence of two intense correlation peaks. In general, a well-defined scattering maximum indicates the existence of two phases characterized by two different neutron scattering length densities producing a significant contrast term. The position (Q_{max}) of the scattering maximum is related to the average mean separation distance $d = 2\pi/Q_{max}$ between scattering objects. Therefore, from **Figure 2** it can be concluded that all the multiblock ionomer membranes studied here are composed of correlated domains organized at two distinct length scales. For λ ranging between 15 and 20, the peaks are found at Q ≈ 0.15 and ~0.02 $Å^{-1}$, yielding typical mean separation distances of ~3–5 nm and ~20–50 nm, respectively. To establish the origin of these structural correlations, the SANS spectra of block copolymers are compared to those of the random polymer, which is solely constituted of ps-PES chains with perfluorosulfonated (ps) side-chains randomly distributed along the PES backbone, and to the Nafion reference (**Figure 2a**).

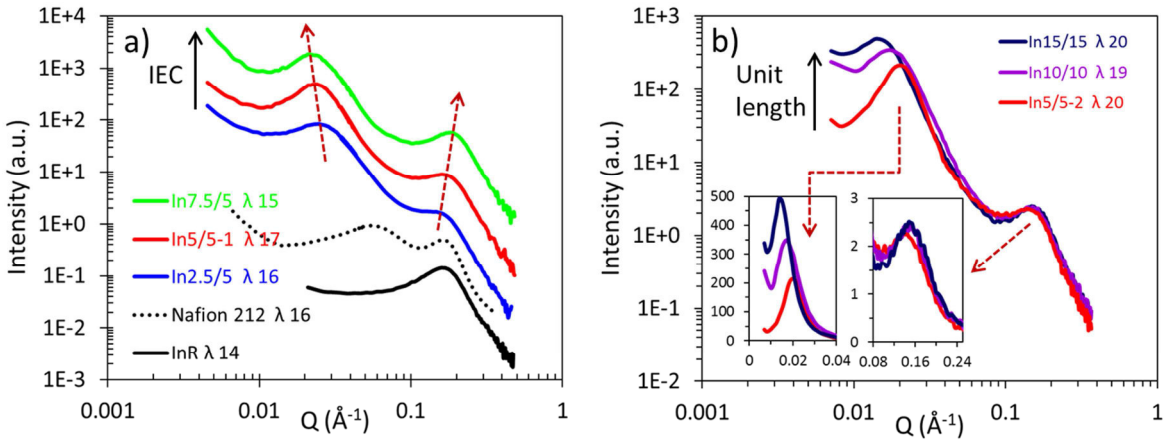

Figure 2. SANS spectra of hydrated aromatic block ionomers. (a) IEC-series and (b) Length-series. The spectra are shifted vertically for clarity, and compared to that of random ionomer (InR) and Nafion® 212 at similar λ. The SANS profile of Nafion® 212 membrane was taken from ref.[39]

We notice that the high-Q peak is present in the SANS profile of the random ionomer, and its position is found to be similar to that of the Nafion ionomer peak related to nano-phase separation between the hydrated perfluorosulfonic acid groups and the backbone. These findings support the existence of nanoscale phase separation in the multiblock copolymers, due to the adsorption of water in ionic domains containing the sulfonic acid head groups. On the other hand, the absence of the low-Q peak in the random ionomer indicates that the large scale correlations originate from the presence of hydrophobic blocks (FPES). Therefore, the intense and well-defined low-Q peak is likely to be related to the regular self-assembled arrangement of hydrophilic (ps-PES) and hydrophobic (FPES) blocks. Previous work focused on multiblock copolymers based on sulfonated hydrophilic block reported the presence of a characteristic peak in the same Q range (at a typical length scales of ~30 nm).[35,42,43] It was generally interpreted as the signature of phase separation between hydrophilic and hydrophobic blocks. Yet, in most studies, it was found that the ionomer peak is poorly defined and usually located at higher Q values as compared to that of Nafion. The presence of the high-Q correlation peak in our ionomers proves that the perfluorosulfonic side chains are able to organize and form well defined ionic clusters, contrarily to the aryl sulfonic ones.

In the following, the positions of the (high) low-Q peak are labeled as (high) low-Q_0. The mean correlation distances associated to multiblock ordering and to the distribution of ionic domains are defined as $d_{block} = 2\pi/\text{low-}Q_0$, and $d_{ionic} = 2\pi/\text{high-}Q_0$, respectively. On focusing on the IEC-series (**Figure 2a**), we notice that the positions of both low-Q and high-Q peaks are IEC-dependent, showing that the relative length of the hydrophilic blocks with respect to

the hydrophobic ones impacts both the ionic phase and the multi-block structuration, although in a different fashion. In fact, the low-Q peak position shifts to smaller Q-values upon increasing the IEC, while the high-Q peak position behaves opposite and shifts towards higher Q values. Hence, the shorter the hydrophilic block (In2.5/5), the shorter the correlation distance associated to multiblock ordering, d_{block}, and the larger the correlation distance associated to the distribution of ionic domains, d_{ionic}.

Indeed, it is observed that, with increasing the length of both backbone blocks (while keeping the same IEC), the high-Q peak showed no significant variations in shape, position and intensity, while the low-Q_0 values decreased (inserts in **Figure 2b**). The values of d_{block} are found to increase from 31 to 48 nm at a mean hydration λ close to 20, and this is directly correlated to the increase in the PES-FPES block lengths.

Dried Membranes. The microstructure of dried membranes was analyzed to bring additional insights into the polymer organization. The SANS spectra of dried ionomers are shown on **Figure 3a**. Well-defined scattering maxima are observed in the low-Q region, as in the hydrated samples (yet at lower Q values, from 0.02 to 0.03 $Å^{-1}$), while an extended flat profile is measured for Q > 0.1 $Å^{-1}$, with no coherent contribution arising from a two-phase contrast at the nanoscale. The low-Q peak position shifts toward small angles on increasing PES-FPES block length, as already observed on hydrated samples. The characteristic distances extracted from the low-Q peak position of dried membranes, labeled d_{dry}, are plotted on **Figure 3b** as a function of PES-FPES length. They are found in the range of ~240 Å (In2.5/5) to ~365 Å (In15/15). It is clearly observed that d_{dry} is linearly correlated to the total size of the hydrophilic-hydrophobic blocks.

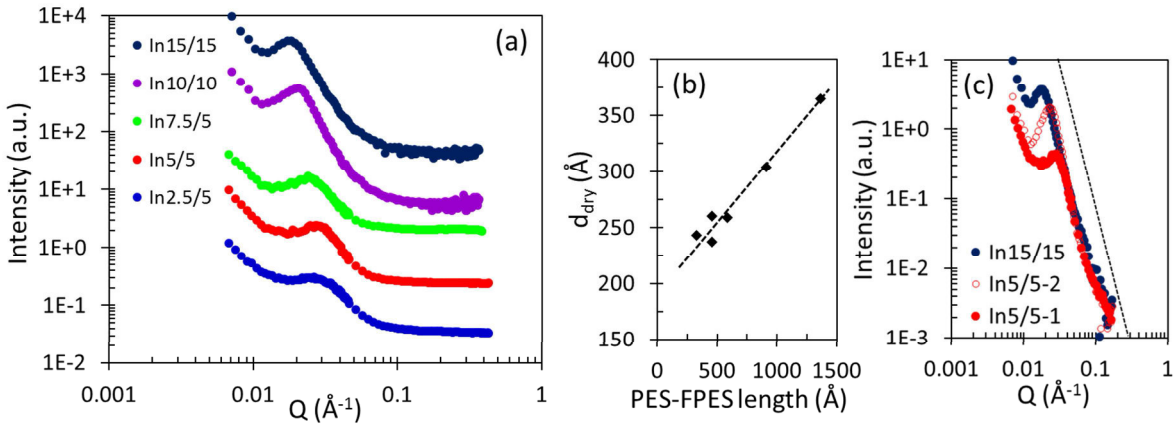

Figure 3. a) SANS spectra of dried aromatic block ionomers. The spectra were shifted vertically for clarity. b) Characteristic block distance d_{dry} obtained from the position of the

low-Q peak, as function of the total PES-FPES length. c) Incoherent-background subtracted spectra showing the Q^{-4} dependence of the intensity at high Q.

Proton-depleted and proton-rich domains usually produce a significant contrast term in neutron scattering, because the scattering cross section of hydrogen atoms is huge with respect to any other atomic species, i.e., C, F, O, and S. Hence, as for any hydrogenated system, the scattering intensity is dominated by the contribution of hydrogen atoms.[44,45] There are 8 hydrogen atoms per repeating unit in the hydrophobic FPES block, against $16 + 2\lambda$ hydrogen atoms per repeat unit in the hydrophilic block composed of PES main chain (14 structural protons), two perfluorosulfonic acid side-chains (two H^+) and 2λ hydration protons. As a consequence, a significant contrast is expected between the block domains whatever the hydration, which is presumably associated to the presence of the low-Q peak. Also, in the fully dried state, a significant contrast between PES blocks aggregates (14 protons) and perfluorinated side-chains (two H^+) is expected. Yet, at a mean hydration level of $\lambda \approx 3$, the neutron scattering length densities of the aromatic PES backbone and the hydrated pendent chains are found to be equal (zero contrast condition). Therefore, the extinction of high-Q peaks in dried ionomers (**Figure 3a**) can be explained by the fact that, despite drying under vacuum and preparation of SANS cells in the glove box, the membranes still contain water. The spectra of membranes equilibrated at RH ranging from 11% to 85% were further analyzed to clarify these assumptions. The ionomer peak was found to appear at $\lambda \geq 4$. Accordingly, it can be deduced that when the membranes are completely dried or contain few water molecules per ionic group ($\lambda < 4$), the PES blocks and perfluorosulfonic side-chains appear as a homogenous phase. On increasing water content, the well-defined ionic peak is recovered, as the organization of ionic clusters and the neutron contrast between PES chains and hydrated perfluorosulfonic aggregates ($\lambda > 4$, there are more than 10 protons per repeat unit in these aggregates, against 14 in PES) are enhanced.

The nature of the hydrophobic/hydrophilic interface of dried membranes can be analyzed by subtracting the high-Q SANS background arising from the incoherent scattering of hydrogen atoms. As shown in **Figure 3c**, the intensities nicely scale at Q^{-4} according to the Porod's law, which is typical of a sharp interface and reveals the neat separation between hydrophilic and hydrophobic block regions.[46]

Swelling Laws and Domain Expansion. To evaluate the evolution of the microstructure upon hydration, block copolymers were prepared over an extended range of hydration numbers, from $\lambda = 2$ to $\lambda = 111$. The hydration-dependent structure of the random ionomer

was also measured for comparison. The incoherent background-subtracted SANS spectra of the In10/10 membrane are displayed in **Figure 4**. Data of all InX/Y swollen membranes in water are shown in **Figure S4** and **Table S1**.

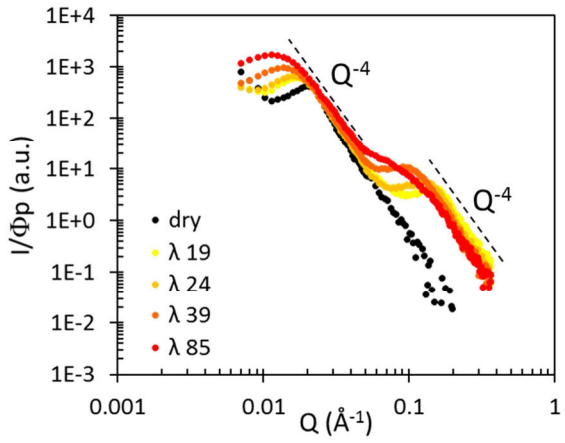

Figure 4. Evolution of normalized SANS spectra for In10/10 aromatic ionomer upon water content.

The evolution of SANS spectra upon hydration unambiguously evidences the continuous swelling of the microstructure at the two characteristic length scales. Both low-Q and high-Q correlation peaks shift towards smaller Q values as the hydration is increased, therefore showing the continuous increase of both d_{ionic} and d_{block} correlation distances. Note that d_{ionic} similarly increases in the random ionomer InR (**Figure S4g**). The incorporation of water molecules within the hydrophilic phase significantly increases the volume of the hydrophilic domains while enhancing the SANS contrasts between PES segment aggregates and ionic phase on one hand, and between the swollen hydrophilic domains (PES + ionic phase) and the hydrophobic domains on the other hand. This is accompanied by a more disordered organization of the inter-connected ionic domains, as evidenced by the broadening of the high-Q peak upon water loading. In addition, a noticeable feature of all spectra is the asymptotic behavior in the high-Q region, which is due to the formation of a new interfacial region created by water loading.

To further determine the size and shape of the segregated domains, as well as the nature of the FPES/PES and PES/ionic interfacial regions, we proceed to a quantitative analysis of the effect of water uptake by extracting the so-called swelling laws, i.e., the variations upon hydration of d_{ionic} and d_{block}.

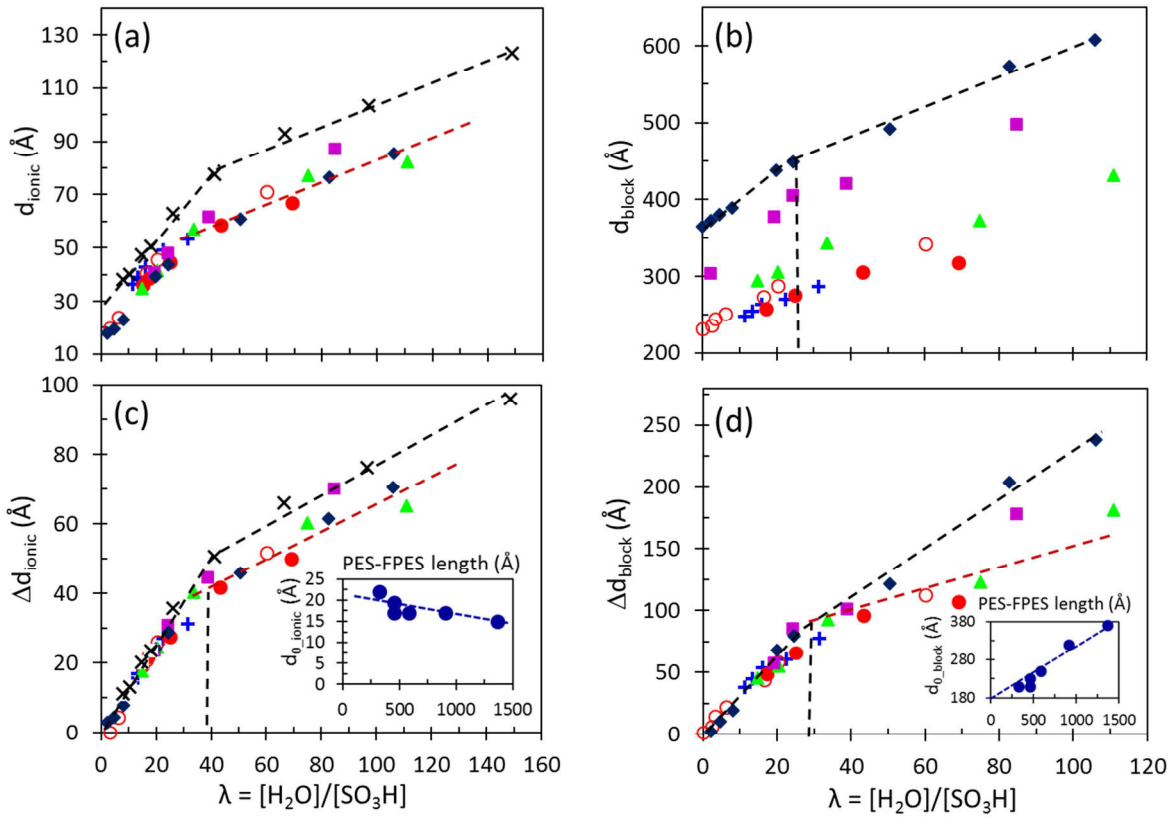

Figure 5. Variations of the mean separation distances of (a) ionic domains and (b) block structures as a function of the hydration number. Expansion of (c) ionic domains and (d) large scale structure. Inserts: variation of d_0 as a function of the PES-FPES length. The d_0_ionic values are extrapolated at λ = 0. Nafion 212 (black ×), In2.5/5 (blue +), In5/5-1 (red ●), In5/5-2 (red ○), In7.5/5 (green ▲), In10/10 (purple ■), In15/15 (dark blue ◆), Nafion values were taken from the ref.[47]

On **Figure 5a** and **5b** we report the variations of d_{ionic} and d_{block} as a function of λ. The d_{ionic} mean correlation distance varies typically from 2 to 8 nm, and d_{block} from 22 to 62 nm. Similar trends are evidenced for the five aromatic ionomer membranes: a steep linear increase of both ionic and block separation distances is observed until a mean threshold value of λ ≈ 30, followed by a more moderate swelling regime at higher water content. Note that In5/5-1 and In5/5-2 behave similarly, thus there is no major impact of reaction solvent on the ionomer swelling behavior. Values of the correlation distance d_{ionic} can be compared to those found in the benchmark PFSA Nafion membrane, extracted from the ionomer peak position variations in the same hydration range. Both, Nafion and aromatic polymers, are characterized by an affine behavior at low water contents (λ < 30) with a slope equal to ~1, while at larger swelling degrees, a linear trend is also observed with a slope close to ~0.5. The low hydration affine behavior is consistent with the dilution of a locally flat structure such as the "lamellar"

Nafion structure suggested initially by Litt et al.[9] and revisited by Kreuer et al.[8], the "sandwich-like" structure proposed by Haubold et al.[10] or the flat "ribbons" model proposed by Gebel et al.[6,7] The high hydration regime could be in turn associated to the dilution of elongated polymer aggregates (cylindrical or ribbon-like aggregates).

The transition between a 1D to 2D dilution regime has recently been rationalized by Kreuer and Portale[8] on the basis of electrostatic considerations. The flat structure was postulated to be energetically more favorable as long as separated charges are not completely screened by the high dielectric solvent (e.g., water). In flat structures, positively charged ionic defects may stabilize between negatively charged sulfonate counter ions located on different polymer objects, and there is more freedom to avoid disadvantageous accumulation of positive charges than in cylindrical structures. Only at very high water content, a progressive buckling is expected. Swelling laws of ionic surfactants used as models for Nafion side-chains were recently measured by SAXS[47] and reported by Molecular Dynamics simulations.[48] Both works highlight the similarities between PFSA and self-assembled ionic-nanostructure swelling behaviors. It was shown that transitions from lamellar to cylindrical structures are driven by the gradual increase in interfacial curvature needed to accommodate water loading. Berrod et al.[47] demonstrated that the hydration of Nafion results in the continuous dilution of polymer particles that are invariant in size, e.g., aggregates formed by packing of few polymer chains expelling the side-chains in the outer ionic phase. The d_{ionic} value extrapolated from the dilution law at zero water content, labeled as d_{0_ionic}, was introduced.[47] In the simplified picture of a lamellar ordering, d_{0_ionic} would be the average thickness of the surfactant bilayers, while in the framework of the ribbon-like Nafion model, d_{0_ionic} represents the mean thickness of the ribbon polymer aggregates embedded in the continuous ionic phase (d_{0_Nafion} ~27 Å). Additional insights on the expansion of the ionic phase were provided by extracting the mean expansion of ionic domains, and showed excellent agreement with the simulated mean size of ionic channels.[48]

In the present case, we can expect that a locally flat structure is also favored as the side-chains of the aromatic ionomers are similar to those of Nafion. Moreover, we expect strong electrostatic interactions in the segmented architectures, as the ionic functions are concentrated only on the PES blocks. The local IEC is about two times higher than that of Nafion (the equivalent weight for all ionomers is about 500 g of ps-PES/mol H^+ against 1100 g/mol H^+ in Nafion). We can extract d_{0_ionic} values for the aromatic ionomers (insert in **Figure 5c**) and tentatively ascribe them to the average thickness of flat aggregates formed by hydrophilic blocks. The d_{0_ionic} values obtained for the aromatic ionomers range from 23 to 15

Å (**Table S2**), therefore slightly lower than those obtained for Nafion. This can be related to the shorter length of their perfluorosulfonic acid side chains.[49] We also notice that d_{0_ionic} decreases when the total (or hydrophilic) block lengths is increased. Increasing the length of PES block (at same IEC or higher IEC) results in a reduced dimension of the aggregates, possibly due to a better packing of the ps-PES hydrophilic segments due to the increase of ionic interactions and the decrease of disordered zones ("dead zones") between hydrophilic and hydrophobic blocks.

If we assume that the shape and the size of the flat ps-PES aggregates are unchanged upon hydration, the quantity $\Delta d_{ionic} = d_{ionic} - d_{0\_ionic}$ represents the mean width of the ionic domains (inter-lamellae or inter-ribbon spacings) and therefore can be usefully reported as a function of λ to quantify the expansion of the ionic phase (**Figure 5c**). We find that the aromatic ionomers exhibit a behavior strikingly similar to that of the Nafion membrane, despite the profound difference in chemical structure of the polymer backbone and the ionic side chain distribution (local IEC). Moreover, the ionic domain expansion at low water contents ($\lambda < 30$) for all aromatic ionomers studied here displays the same affine increment, yielding typical values of the mean ionic width of 1 nm at $\lambda = 10$. These observations suggest that the organization of ionic domains is controlled by the sulfonic acid perfluorinated chain, which imposes the local topology and swelling behavior independently of the nature of the polymer backbone. At high hydration, we note that the ionic domains are less expanded in aromatic ionomers than in Nafion (80 Å against 110 Å in Nafion at $\lambda = 110$), and rather independent from the aromatic ionomer architecture.

Polymer swelling is controlled by a balance between driving forces and limiting factors. The ionic domains expansion is mainly driven by osmotic pressure (higher in the aromatic polymers due to the higher local density of charges), while the polymer backbone stiffness (higher in aromatic compounds) might restrict the ability of the chains to accommodate large volume expansions, therefore limiting the swelling with respect to the thermoplastic Nafion backbone. This is expected to be particularly true in the high hydration regime. Moreover, one can hypothesize that the peculiar block organization at large scales have some impact on the microscopic behavior of the polymer under increasing water uptake. This point is now further evaluated in more details by using the same approach, *i.e.,* we introduce d_{0_block} as the zero-water content limit of d_{block}, and define Δd_{block} as the expansion of the large scale structure. Values of d_{0_block} are represented in the insert on **Figure 5d**. As previously observed in the dried systems (**Figure 3b**), there is a direct correlation between the total length of the polymer

unit PES-PFES and d_{0_block}. As for d_{0_ionic}, d_{0_block} can be considered as the size of the large-scale repeating unit in the absence of water. It is found to vary between 210 and 370 Å (**Table S2**). For each polymer, this mean size is smaller than the total length of PES and/or FPES segments, therefore showing that the main chains have to be folded in the dry state. The expansion of the large scale structure is plotted on **Figure 5d** and shows interesting features. We observe that all aromatic ionomers display the same linear behavior at low water content, independently of IEC and block length. At the $\lambda = 30$ threshold, the structure has been expanded by 80 Å. At higher hydrations, the longer the blocks, the greater the expansion. It has also to be stressed that the swelling of the block superstructure is, on average, 2.5 times higher than that of the ionic domains (**Figure S5**). This block-to-ionic swelling ratio appears to be rather independent of ionomer design and invariant along hydration, except at very high hydration values ($\lambda > 60$). We can conclude that the incorporation of water molecules yields an important reorganization of the initially contracted PES segments into fully expanded chains. In the early stage of hydration, this effect is not limited by the total sequence length.

Diluted Solutions. As the membranes are manufactured by casting, the phase behaviour of block copolymers is controlled by the interactions among the solvent and the two component blocks. We have previously reported that DMSO is a selective solvent able to dissolve the InX/Y ionomers, although it is a good solvent only for ps-PES block.[40] In order to evaluate the organization of the aromatic ionomers in solution, diluted solutions of InX/Y were prepared in DMSO and subsequently analyzed by SANS. The scattering profiles indicate the presence of aggregates of elongated shape, e.g., cylinders of infinite size (**Figure S6**). As DMSO is not a good solvent for FPES segments, we can hypothesize that the internal core of the cylindrical particles is formed by hydrophobic FPES, with PES chains covering the surface to minimize FPES-DMSO contacts. Such hypothesis is sustained by the values of the mean diameter of the ionomer particles, which were determined after treating the SANS data using the Guinier representation (**Figure S6b**).[46,50]

Self-Assembly, Multi-Scale Morphology. The set of SANS results obtained on solutions and membranes can now be integrated to obtain the key features of the block copolymer microstructure. The block copolymer morphology results from a non-trivial interplay between energetically-driven need for phase-separating polar and non-polar groups (interaction between the two component blocks) while accommodating the block sequencing. The SANS analysis of IEC- and length-series on dried and hydrated membranes supports the regular and multi-scale organization of a complex three-phase structure, as schematically depicted on **Figure 6**.

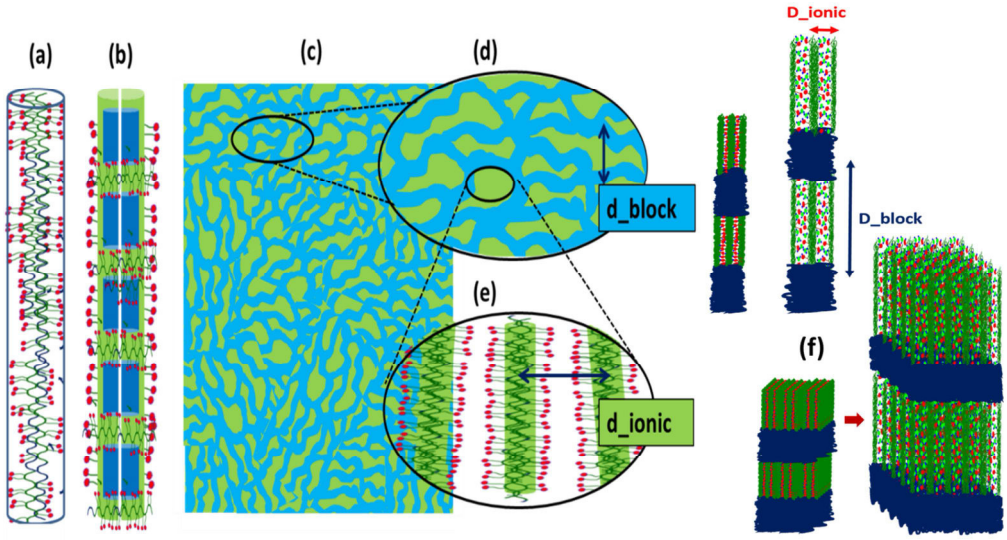

Figure 6. Schematic illustration of the block copolymer structure. a) Rod-like particle formed in DMSO by the packing of several PES-FPES chains. b) Aggregation of particles during solvent evaporation, leading to the formation of hydrophobic (FPES, blue) and hydrophilic (ps-PES, green) domains. c) Large scale random grain organization, with regular ordering of polar and non-polar domains. d) Mean separation distance between FPES regions ($d_{\_block}$). e) Nanoscale phase-separated morphology inside hydrophilic domains, showing the regular distribution of ionic channels containing side-chains, ions and water. f) Expansion of the structure upon hydration. The extension of the PES chain produces the block structure swelling (vertical) while water incorporation induces the ionic domain swelling (horizontal).

This structure originates from the packing of self-assembled rod-like elongated particles of polymer (which were found to form in the diluted solutions). Each polymer particle is possibly composed of few polymer chains (**Figure 6a**). During the casting process, the solvent evaporation drives the aggregation of the elementary polymer particles, leading to the formation of segregated polar/non-polar regions (**Figure 6b**). This process is triggered by i) the ability of polar and hydrophilic (perfluorosulfonic) side chains to aggregate and ii) their incompatibility with PES backbone. The alternated sequence of non-miscible hydrophobic and hydrophilic blocks within one polymer chain induces the regular arrangement of well-separated hydrophilic and hydrophobic domains, composed by ps-PES and FPES segments, respectively (**Fig. 6c**, **6d**). The sharp ps-PES/FPES interfaces are indicated by the presence of a Porod's behavior (slope of Q^{-4}) in the SANS spectra.[46] Long-range ordering of the intercalated hydrophilic/hydrophobic domains gives rise to the low-Q interaction peak. The domains are regularly distributed within large grains of random orientation (**Figure 6c**), leading to a powder-like isotropic neutron pattern. In the hydrophilic regions, which contain

block copolymer PES chains, perfluorosulfonic side-chains (ps), protons and water (**Figure 6e**), the PES polymer chains are locally aggregated, with the side-chains rejected into the surrounding ionic medium. The regular distribution of these aggregates within each ionic domain produces an internal structure, yielding the high-Q peak. In dried conditions, the hydrophilic aggregates adopt a locally flat (ribbon-like) morphology, as in Nafion.

The multi-phase, multi-scale organization, with the neat hydrophobic-hydrophilic interfacial regions as pictured in **Figure 6,** is kept along hydration, even at very large water uptakes. When water molecules penetrate the structure and solvate the sulfonic acid functions, an interconnected network of ionic channels forms and swells, yielding a significant expansion of both the ionic and block structures, as schematized on **Figure 6f**. The PES aggregated chains are forced to move apart to accommodate water molecules (ionic swelling). The ionic expansion is reminiscent of the well-established mechanism of lamellar-to-cylinder phase transitions in self-assembled surfactants,[48] and similar to that postulated in PFSA materials.[47] When a large amount of water is incorporated, the water channels network is more disordered in size and shape (broadening of ionic peak) and presumably more connected (loss of ionic specific surface). The shape of the PES particles is relaxed (ribbon-like to cylindrical, **Figure 6f**, bottom) due to the increase in interfacial curvature needed for up-taking more water molecules. Simultaneously, the PES chains extend under the effect of osmotic pressure, inducing a major expansion of the block structure along the direction of the PES polymer backbone (vertical direction on **Figure 6f**, top). In fact, on average, the block structure is expanded 2.5 times more than the ionic structure (**Figure S5**). This behavior relates to the peculiar organization and respective orientations of the ionic aggregates and self-assembled hydrophobic domains. Indeed, because of the high stiffness and high hydrophobicity of FPES blocks (Tg ≈ 200 °C)[39,40] the hydrophobic domains could act as rigid "nodes". Their mean thickness is roughly the FPES block length, and is not significantly affected by the increase of water content. As each ps-PES segment is bonded at its ends to two FPES segments, the two neighboring "nodes" and the interaction between the ps side chains retain a too large lateral volume change (horizontal direction in **Figure. 6e**, **6f**), while easily absorbing variations in the chain direction via chain unfolding.

3.2. Transport Properties

The efficiency of proton transfer across the membrane is usually dependent on the chemical architecture and controlled by a number of competing and/or intricate phenomena that rely on water content, interactions between charged species, backbone rigidity/flexibility,

chain dynamics, nanoscale confinement, tortuosity, connectivity, etc. In this section, we report the impact of block structures on the transport properties quantified by the through-plane proton conductivity, σ_i, and the self-diffusion coefficient of water molecules, Ds, measured by PFG-NMR. To correlate the morphology with the transport properties the membranes for all the measurements were prepared in similar conditions. The proton conductivity (σ_i) is defined as follows:

$$\sigma_i = \sum_{i=0}^{n} F Z_i C_i \mu_i$$

where F is the Faraday constant (~96485 C mol^{-1}), C_i is the ion concentration that contributes to the conductivity, Z_i is their charge (equal to unit for protons) and μ_i is the ion mobility. The variations of σ_i and D_s as a function of the hydration number are displayed on **Figure 7** for all aromatic ionomers. Values of D_s in Nafion (taken from ref.[47]) are also plotted for comparison.

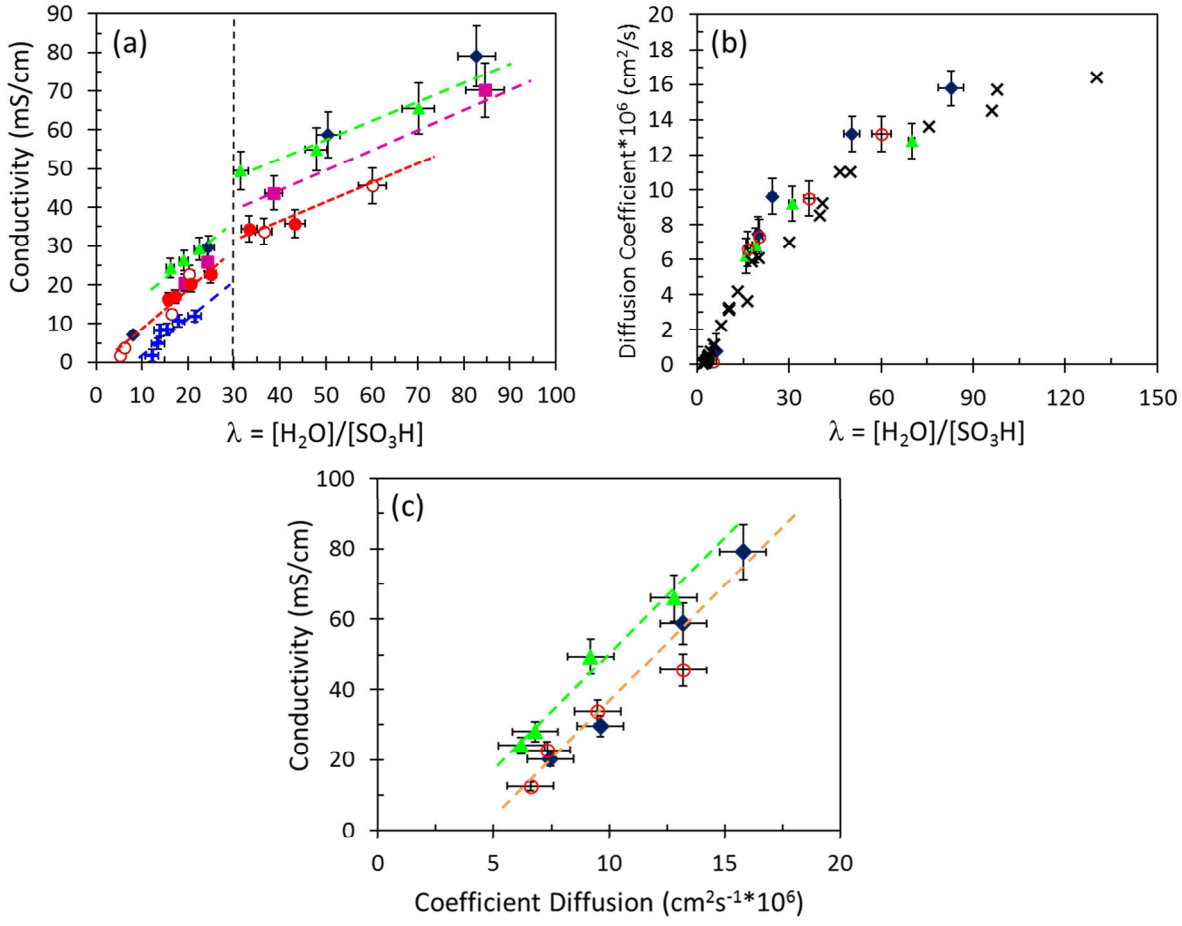

Figure 7. (a) Proton conductivity σ_i, (b) water self-diffusion coefficient D_s *vs* hydration number, and (c) their correlation. The values of Nafion are also reported for comparison.[47] Nafion 117 (black ×), In2.5/5 (blue +), In5/5-1 (red ●), In5/5-2 (red ○), In7.5/5 (green ▲), In10/10 (purple ■), In15/15 (dark blue ◆).

The enhancement of proton and water mobility is obviously deduced from σ_i and D_s increase upon increasing water content. However, as seen on **Figure 7,** the values of σ_i and D_s are highly dependent on the ionomer architecture. If we compare membranes with the same hydration level, we clearly observe that the higher the IEC, the higher the proton conductivity (**Figure 7a**). Similarly, the conductivity values are increased, at the same λ, when the block length is increased. Best performances are obtained for In7.5/5 and In15/15 which have the highest IEC and the longest hydrophilic/hydrophobic segments, respectively. As the mean size of ionic domains was found to be similar for all InX/Y ionomers at the same λ (**Figure 5**), the conductivity differences must be explained by differences in ionic-domain percolation and tortuosity induced by the ionomer architecture. As seen on **Figure 7**, there is a neat discontinuity in proton conductivity variations, with a slope change at $\lambda \approx 30$. This is a common feature to all studied ionomers. It could be correlated to the morphological transition from a locally flat structure to elongated aggregates which was observed at the same mean hydration threshold value in all InX/Y materials.

The impact of such morphological transition is also evidenced on the water dynamics, quantified on the micrometer scale (between 1−10 μm) by the water self-diffusion coefficient D_s (**Fig. 7b**). The values of D_s at $\lambda < 30$ are found to be close to those of Nafion and show a steep increase in this hydration range. Above the threshold, water molecules diffuse slightly faster in aromatic compounds, particularly in the membranes with long blocks sequences. Yet, it has to be recalled that λ depends on IEC, and the same λ value corresponds to higher water volume fractions in polymers of higher IECs.

On **Figure 7c** we have represented the proton conductivity *vs* the water diffusion coefficient. The two quantities are linearly correlated in the range of hydration of this study, showing that water dynamics have a direct impact on the final conductivity of our aromatic proton-conducting materials, as already observed in PFSA membranes.[51,52] It is well established that the mobility of protonic species is primarily affected by the dynamical behavior of the hydration water, which is in turn determined by the topology of the host matrix as well as the nature of the interfaces. In fact, we find that the relation between water dynamics (D_s) and proton mobility (σ_i) is independent of block length (In5/5 and In15/15) but impacted by the IEC. When the IEC is increased (In2.5/5 *vs* In7.5/5), the conductivity measured at the same water mobility is higher. These observations indicate that the transport of protons in the aromatic polymers is piloted by several factors, including the local concentration of charges within the hydrated phase, the volume fraction of hydrophilic

domains, and the mobility of water molecules. The latter is primarily determined, at a given hydration level, by morphological and topological constraints. Accordingly, we focus now on exploring the relations between the microstructure and the transport behavior.

3.3. Structure-to-Transport Correlations

To further discuss on the structure-to-transport interplay, the aromatic ionomers transport numbers σ_i and D_s are now expressed as a function of the microstructural parameters defined in the previous sections, e.g., the ionic (**Figure 8**) and block (**Figure 9**) expansions. With this representation, we evidence a direct correlation between the macroscopic transport number and the polymer multi-scale organization. Indeed, σ_i is linearly correlated to both Δd_{ionic} (**Figure 8a**, IEC-series; **Figure 8b**, length-series) and Δd_{block} (**Figure 9a**), for all ionomers over the whole hydration range. This appears to be a general property of our ionomers. For any given InX/Y ionomer, the efficiency of proton transport is proportional to both the degree of confinement (ionic domain size) of the hydrated phase (**Figure 8**) and to the block superstructure (**Figure 9a**).

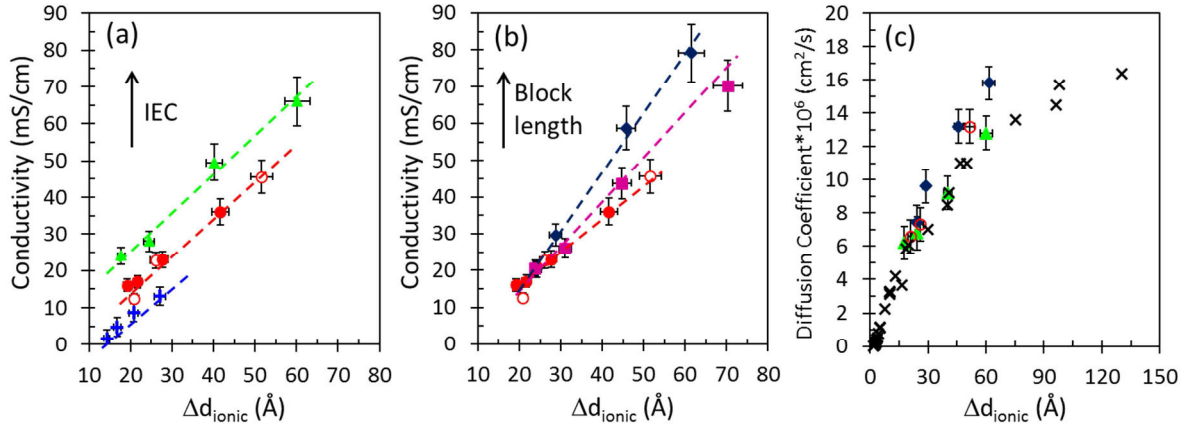

Figure 8. Variations of the proton conductivity σ_i (a: IEC-series, b: length-series) and (c) the water self-diffusion coefficient D_s as a function of the ionic expansion defined by Δd_{ionic}. Nafion 117 (black ×), In2.5/5 (blue +), In5/5-1 (red ●), In5/5-2 (red ○), In7.5/5 (green ▲), In10/10 (purple ■), In15/15 (dark blue ◆).

In general, decreasing the spatial nano-confinement obviously leads to a more bulk-like behavior of the fluid phase and subsequent enhancement of mobility. Importantly, it is seen that both the absolute values of σ_i, and the observed slopes are impacted by IEC and block length. At the same nanoscale confinement, i.e., similar mean size of ionic domains, the increasing of IEC induces a significant increase of the conductivity (**Figure 8a**) which is directly proportional to the IEC. It is clear that, when considering similar ionic nanoscale

morphologies, the simplest way to enhance proton mobility is to increase the local density of charge, as was already commented from **Figure 7c**. In addition to the effect of IEC and nanoscale confinement, we can postulate the importance of other factors from analyzing the impact of block length (**Figure 7b**). Indeed, the length of the block does not have a significant impact when the spatial confinement is severe. Typically, when the mean ionic domain size is below ~2 nm, the conductivity of ionomers prepared with the same IEC is found to be around 15 mS/cm, almost independent from the block lengths (**Figure 9a**). This can be understood because, under harsh confinement conditions, the mobility of a confined molecule is primarily determined by the constraints imposed by the local confining geometry and strong interactions with the charged walls.[53–56] Interestingly, we observe that the block length impacts the proton transport when the ionic nanoconfinement is reduced (i.e., at high hydrations, where large ion domains exceeding 3 nanometers are formed). The conductivity is significantly enhanced when PES and FPES block lengths are increased (at fixed IEC, **Figure 8b**).

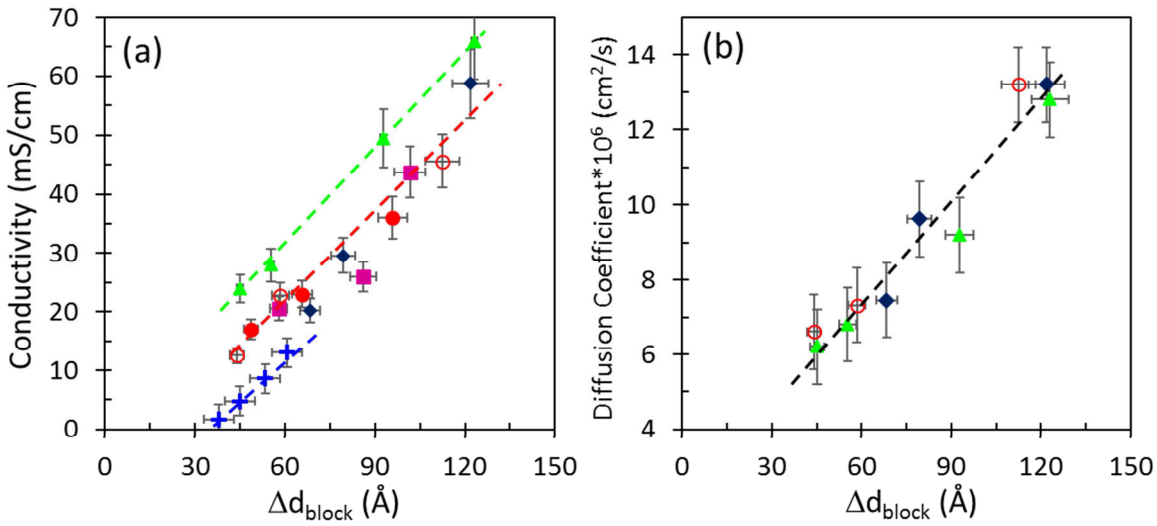

Figure 9. Variations of (a) the proton conductivity σ_i and (b) the water self-diffusion coefficient D_s as a function of the block structure expansion defined by Δd_{block}. In2.5/5 (blue +), In5/5-1 (red ●), In5/5-2 (red ○), In7.5/5 (green ▲), In10/10 (purple ■), In15/15 (dark blue ◆).

Therefore, within hydrated structures, local confinement is not any more the only key factor controlling ionic mobility, as evidenced also in PFSA materials.[47,57] Due to the large expansion of both ionic and block phases, it is reasonable to hypothesize that factors as tortuosity and long-range connectivity become the most prominent causes of restricted mobility. In fact, due to the complex (super) structure of our ionomers, it would be expected that long-range diffusion of ions (and water) require both inter-domains and intra-domains

connections. Intricate diffusion mechanisms acting at different length-scales could therefore yield scale-dependent and hydration-dependent dynamics. In this regard, we can hypothesize that the connectivity of ionic channels within each hydrophilic region (**Figure 6e**) and the availability of paths from one intercalated region to a neighboring one separated by hydrophobic nodes (**Figure 6d**) are crucial ingredients controlling the proton transport, in particular at high hydration. This assumption is in line with concepts of delocalization bodies as introduced by Di Noto and co-workers in PFSA, hybrid and diblock membranes.[58–60] Exchange mechanisms acting at different length scales and/or characterized by distinct time constants were established by combining molecular-level investigations, advanced techniques such as spectroscopy and broad band dielectric analysis. The coupling of intra- and inter-domains motions was also considered to analyze water dynamics in PFSA compounds by quasielastic neutron scattering.[47] In the present work, we are not focusing on unraveling the nature of motions at molecular, nano- and meso-scales, but we establish few general laws expressed using a limited number of structural variables to account for the intrinsic complexity of the transport and its dependence on hydration and chemical architecture. At this stage, inspecting again **Figure 8b**, we can suppose that proton conduction paths are less tortuous when longer (hydrophilic) chains are used, ion and water molecules mobility being facilitated by the enhanced hydrophilic segment flexibility.

As seen on the variations of the self-diffusion coefficient of water as a function of the width of ionic channels, the values of D_s are quite similar for all ionomers when the confinement is high (<2–3 nm), and comparable to those measured in Nafion in the same conditions. At lower confinement, the water diffusion is determined by the total amount of water and do not depend on the shape and size of the hydrophobic obstacles (**Figure S7**) where D_s is represented as a function of ϕp.

At this point, we can push our discussion further by analyzing the impact of the block structure on both the conductivity and the water diffusion coefficient (**Figure 9**). The superstructure organization is quantified by Δd_{block}, which characterizes the mean size of hydrophilic PES regions intercalated between hydrophobic FPES nodes. It has to be stressed that similar FPES region sizes obtained in different InX/Y ionomers correspond to distinct hydration states, hence distinct internal hydrophilic structures (different nano-domains confinement size). Therefore, **Figure 9** has to be cautiously interpreted because they reflect a combination of morphological effects which are differently balanced. First, we observe that for each ionomer the conductivity and the self-diffusion coefficient linearly increase with the expansion of the block superstructure. There are few main features to pinpoint: 1) given a

defined block structure expansion, σ_i is directly proportional to the IEC, 2) polymers prepared with different block lengths but the same IEC fall on a master (σ_i *vs* d_{block}) curve and 3) the value of the block structure expansion determines the self-diffusion coefficient of water molecules independently of chemical architecture. Therefore, as we did earlier, we can again separately highlight the impact of IEC (point 1) and water mobility (point 2) on proton conductivity. The D_s variations (point 3) express that long-range connectivity and tortuosity effects are integrated in the block structure parameter. With increasing Δd_{block}, the hydrophilic domains get better connected due to the continuous swelling that move the hydrophilic polymer units apart while extending them. Therefore, the same level of connectivity can be obtained in In5/5 with respect to In15/15, for instance, but this will require a much higher water uptake.

To summarize, we demonstrate that both ionic and block expansions are suited to compare and quantify the transport properties of our ionomers. Confinement and connectivity are differently balanced upon hydration depending on chain architecture and local ionic organization. Both can be optimized after compromising IEC and chain length to produce high performance membranes.

4. Conclusions

We reported, for the first time to the best of our knowledge, the direct correlation between proton transport efficiency and microstructure in aromatic block copolymers. We provided in-depth insights into the microstructure by extensive SANS characterizations performed on diluted polymer solutions and membranes prepared over an extended range of hydration. The relation between polymer architecture, morphology and transport properties was scrutinized by preparing materials at different IEC and different block lengths. It is evidenced that the ionomers are well-organized at two different length scales. The alternated sequence of hydrophobic and hydrophilic blocks within one polymer chain, and the need to phase-separate polar (side chains) and non-polar (PES backbone) groups belonging to different chains, lead to a complex arrangement within a multi-scale three-phase structure. This structure originates from the packing of rod-like elongated particles of polymer. Hydrophilic regions are composed of hydrophilic aggregates embedded in a continuous ionic medium are arranged within a regular network of hydrophobic nodes. The various domains are separated by sharp interfaces. The swelling behavior at various scales was fully rationalized in terms of dilution laws. The presence of perfluorinated ionic chains in the aromatic ionomers induces neat phase-separation and 1D-to-2D morphological evolution along hydration, similarly to the

benchmark PFSA materials. The block superstructure was found to accommodate the expansion of ionic domains due to water incorporation and provide flexibility to the system, yielding beneficial connectivity and efficient-conduction paths through the structure. The transport behavior within the family of aromatic block ionomer was quantitatively related to the microstructure at each hydration level. The proton conductivity and the self-diffusion coefficient of water were found to vary linearly with confinement (ionic domain expansion) and connectivity (block superstructure), although they have a differently balanced impact depending on the hydration regime (low *vs* high). With this work, we are now in the position to optimize the development of alternative hydrocarbon membranes by tailoring the materials in terms of IEC, side-chain and block design, towards the best architecture-structure-transport interplay for high PEMFC-oriented performances.

ASSOCIATED CONTENT

Supporting Information.

The Supporting Information is available free of charge on the ACS Publications website at DOI: 10.1021/acsami.6b12764.

Hydration number (λ) and polymer volume fraction (Φp) of all ionomers, schematic representation of conductivity cell, equivalent circuit model for data fitting, an example of Nyquist plot, evolution of SANS spectra of the swollen ionomer membranes upon water content (λ), extrapolated d_{0_ionic} and d_{0_block} of the ionomers, swelling ratio $\Delta d_{block}/\Delta d_{ionic}$); SANS intensities I(q) of ionomer solutions in DMSO (1.6% w/ w) as a function of the scattering vector q and their Guinier representation (ln(I)vs q2), and diffusion coefficient versus polymer volume fraction (Φp) (PDF).

AUTHOR INFORMATION

Corresponding Author

*Phone: +33 (0)476 82 65 61. Email: Cristina.Iojoiu@lepmi.grenoble-inp.fr

*Phone: +33 (0) 438 78 92 86. Email: Sandrine.Lyonnard@cea.fr

Notes

The authors declare no competing financial interest.

ACKNOWLEDGMENT

The authors would like to thank the FEDER-FUI France for providing financial support to this research work in the framework of the project "Nano-structurated High Performance Polymer". Laboratoire Léon Brillouin and Institut Laue Langevin is acknowledged for providing access to beam time. This work was performed within the framework of the Centre of Excellence of Multifunctional Architectured Materials "CEMAM" no. AN-10-LABX-44−01.

ABBREVIATIONS

DMSO = dimethyl sulfoxide

λ = hydration number (=[H2O]/[−SO3H]) PFSA = perfluorosulfonic acid

SANS = small-angle neutron scattering

AFM = atomic force microscopy

TEM = transmission electron microscopy

PEM = proton-exchange membrane

PEMFCs = proton-exchange membrane fuel cells

IEC = ion-exchange capacity

SAXS = small-angle X-ray scattering

PFG-NMR = pulse field gradient NMR

SEC = size-exclusion chromatography

REFERENCES

(1) Steele, B. C. H.; Heinzel, A. Materials for Fuel-Cell Technologies. *Nature* **2001**, *414*, 345−352.

(2) Kreuer, K.-D. Ion Conducting Membranes for Fuel Cells and other Electrochemical Devices. *Chem. Mater.* **2014**, *26*, 361−380.

(3) Mauritz, K. A.; Moore, R. B. State of Understanding of Nafion. *Chem. Rev.* **2004**, *104*, 4535−4585.

(4) Peron, J.; Mani, A.; Zhao, X.; Edwards, D.; Adachi, M.; Soboleva, T.; Shi, Z.; Xie, Z.; Navessin, T.; Holdcroft, S. Properties of Nafion® NR-211 Membranes for PEMFCs. *J. Membr. Sci.* **2010**, *356*, 44−51.

(5) Duan, Q.; Wang, H.; Benziger, J. Transport of Liquid Water through Nafion Membranes. *J. Membr. Sci.* **2012**, *392−393*, 88−94.

(6) Rubatat, L.; Rollet, A. L.; Gebel, G.; Diat, O. Evidence of Elongated Polymeric Aggregates in Nafion. *Macromolecules* **2002**, *35*, 4050−4055.

(7) Rubatat, L.; Gebel, G.; Diat, O. Fibrillar Structure of Nafion: Matching Fourier and Real Space Studies of Corresponding Films and Solutions. *Macromolecules* **2004**, *37*, 7772−7783.

(8) Kreuer, K.-D.; Portale, G. A Critical Revision of the Nano-Morphology of Proton Conducting Ionomers and Polyelectrolytes for Fuel Cell Applications. *Adv. Funct. Mater.* **2013**, *23*, 5390−5397.

(9) Litt, M. H. Reevaluation of Nafion Morphology. Am. Chem. Soc., *Polym. Prepr.* **1997**, *38*, 80−81.

(10) Haubold, H.-G.; Vad, T.; Jungbluth, H.; Hiller, P. Nano Structure of Nafion: A SAXS Study. *Electrochim. Acta* **2001**, *46*, 1559−1563.

(11) Collette, F. M.; Lorentz, C.; Gebel, G.; Thominette, F. Hygrothermal Aging of Nafion®. *J. Membr. Sci.* **2009**, *330*, 21−29.

(12) Collette, F. M.; Thominette, F.; Mendil-Jakani, H.; Gebel, G. Structure and Transport Properties of Solution-Cast Nafion® Membranes Subjected to Hygrothermal Aging. *J. Membr. Sci.* **2013**, *435*, 242−252.

(13) Naudy, S.; Collette, F.; Thominette, F.; Gebel, G.; Espuche, E. Influence of Hygrothermal Aging on the Gas and Water Transport Properties of Nafion® Membranes. *J. Membr. Sci.* **2014**, *451*, 293−304.

(14) Kerres, J. A. Development of Ionomer Membranes for Fuel Cells. *J. Membr. Sci.* **2001**, *185*, 3−27.

(15) Hickner, M. A.; Ghassemi, H.; Kim, Y. S.; Einsla, B. R.; McGrath, J. E. Alternative Polymer Systems for Proton Exchange Membranes (PEMs). *Chem. Rev.* **2004**, *104*, 4587−4612.

(16) Park, C. H.; Lee, C. H.; Guiver, M. D.; Lee, Y. M. Sulfonated Hydrocarbon Membranes for Medium-Temperature and Low- Humidity Proton Exchange Membrane Fuel Cells (PEMFCs). *Prog. Polym. Sci.* **2011**, *36*, 1443−1498.

(17) Rozière, J.; Jones, D. J. Non-Fluorinated Polymer Materials for Proton Exchange Membrane Fuel Cells. *Annu. Rev. Mater. Res.* **2003**, *33*, 503−555.

(18) Peckham, T. J.; Holdcroft, S. Structure-Morphology-Property Relationships of Non-Perfluorinated Proton-Conducting Membranes. *Adv. Mater.* **2010**, *22*, 4667−4690.

(19) Torquato, S. Optimal Design of Heterogeneous Materials. *Annu. Rev. Mater. Res.* **2010**, *40*, 101−129.

(20) Virgili, J. M.; Hoarfrost, M. L.; Segalman, R. A. Effect of an Ionic Liquid Solvent on the Phase Behavior of Block Copolymers. *Macromolecules* **2010**, *43*, 5417−5423.

(21) Weber, R. L.; Ye, Y.; Schmitt, A. L.; Banik, S. M.; Elabd, Y. A.; Mahanthappa, M. K. Effect of Nanoscale Morphology on the Conductivity of Polymerized Ionic Liquid Block Copolymers. *Macromolecules* **2011**, *44*, 5727−5735.

(22) Young, W.-S.; Epps, T. H. Ionic Conductivities of Block Copolymer Electrolytes with Various Conducting Pathways: Sample Preparation and Processing Considerations. *Macromolecules* **2012**, *45*, 4689−4697.

(23) Choi, J.-H.; Ye, Y.; Elabd, Y. A.; Winey, K. I. Network Structure and Strong Microphase Separation for High Ion Conductivity in Polymerized Ionic Liquid Block Copolymers. *Macromolecules* **2013**, *46*, 5290−5300.

(24) de Araujo, C. C.; Kreuer, K. D.; Schuster, M.; Portale, G.; Mendil-Jakani, H.; Gebel, G.; Maier, J. Poly(p-phenylene sulfone)s with High Ion Exchange Capacity: Ionomers with

Unique Micro- structural and Transport Features. *Phys. Chem. Chem. Phys.* **2009**, *11*, 3305−3312.

(25) Elabd, Y. A.; Hickner, M. A. Block Copolymers for Fuel Cells. *Macromolecules* **2011**, *44*, 1−11.

(26) Hoarfrost, M. L.; Segalman, R. A. Ionic Conductivity of Nanostructured Block Copolymer/Ionic Liquid Membranes. *Macromolecules* **2011**, *44*, 5281−5288.

(27) Choi, J.-H.; Willis, C. L.; Winey, K. I. Structure−Property Relationship in Sulfonated Pentablock Copolymers. *J. Membr. Sci.* **2012**, *394−395*, 169−174.

(28) Jannasch, P. Fuel Cell Membrane Materials by Chemical Grafting of Aromatic Main-Chain Polymers. *Fuel Cells* **2005**, *5*, 248−260.

(29) Wang, B.; Hong, L.; Li, Y.; Zhao, L.; Wei, Y.; Zhao, C.; Na, H. Considerations of the Effects of Naphthalene Moieties on the Design of Proton-Conductive Poly(arylene ether ketone) Membranes for Direct Methanol Fuel Cells. *ACS Appl. Mater. Interfaces* **2016**, *8*, 24079−24088.

(30) Chang, Y.; Brunello, G. F.; Fuller, J.; Disabb-Miller, M. L.; Hawley, M. E.; Kim, Y. S.; Hickner, M. A.; Jang, S. S.; Bae, C. Polymer Electrolyte Membranes Based on Poly(arylene ether sulfone) with Pendant Perfluorosulfonic Acid. *Polym. Chem.* **2013**, *4*, 272−281.

(31) Xu, K.; Oh, H.; Hickner, M. A.; Wang, Q. Highly Conductive Aromatic Ionomers with Perfluorosulfonic Acid Side Chains for Elevated Temperature Fuel Cells. *Macromolecules* **2011**, *44*, 4605−4609.

(32) Mikami, T.; Miyatake, K.; Watanabe, M. Poly(arylene ether)s Containing Superacid Groups as Proton Exchange Membranes. *ACS Appl. Mater. Interfaces* **2010**, *2*, 1714−1721.

(33) Danyliv, O.; Iojoiu, C.; Lyonnard, S.; Sergent, N.; Planes, E.; Sanchez, J.-Y. Highly Phase Separated Aromatic Ionomers Bearing Perfluorosulfonic Acids by Bottom-up Synthesis: Effect of Cation on Membrane Morphology and Functional Properties. *Macromolecules* **2016**, *49*, 4164−4177.

(34) Titvinidze, G.; Kreuer, K.-D.; Schuster, M.; de Araujo, C. C.; Melchior, J. P.; Meyer, W. H. Proton Conducting Phase-Separated Multiblock Copolymers with Sulfonated Poly(phenylene sulfone) Blocks for Electrochemical Applications: Preparation, Morphology, Hydration Behavior, and Transport. *Adv. Funct. Mater.* **2012**, *22*, 4456−4470.

(35) Lee, M.; Park, J. K.; Lee, H. S.; Lane, O.; Moore, R. B.; McGrath, J. E.; Baird, D. G. Effects of Block Length and Solution- Casting Conditions on the Final Morphology and Properties of Disulfonated Poly(arylene ether sulfone) Multiblock Copolymer Films for Proton Exchange Membranes. *Polymer* **2009**, *50*, 6129−6138.

(36) Chen, Y.; Rowlett, J. R.; Lee, C. H.; Lane, O. R.; VanHouten, D. J.;Zhang,M.; Moore, R. B.; McGrath,J. E. Synthesis and Characterization of Multiblock Partially Fluorinated Hydrophobic Poly(arylene ether sulfone)-Hydrophilic Disulfonated Poly(arylene ether sulfone) Copolymers for Proton Exchange Membranes. *J. Polym. Sci., Part A: Polym. Chem.* **2013**, *51*, 2301−2310.

(37) Chang, Y.; Mohanty, A. D.; Smedley, S. B.; Abu-Hakmeh, K.; Lee, Y. H.; Morgan, J. E.; Hickner, M. A.; Jang, S. S.; Ryu, C. Y.; Bae, C. Effect of Superacidic Side Chain Structures on High Conductivity Aromatic Polymer Fuel Cell Membranes. *Macromolecules* **2015**, *48*, 7117−7126.

(38) Yoshimura, K.; Iwasaki, K. Aromatic Polymer with Pendant Perfluoroalkyl Sulfonic Acid for Fuel Cell Applications. *Macromolecules* **2009**, *42*, 9302−9306.

(39) Assumma, L.; Iojoiu, C.; Mercier, R.; Lyonnard, S.; Nguyen, H. D.; Planes, E. Synthesis of Partially Fluorinated Poly(arylene ether sulfone) Multiblock Copolymers Bearing Perfluorosulfonic Functions. *J. Polym. Sci., Part A: Polym. Chem.* **2015**, *53*, 1941−1956.

(40) Assumma, L.; Nguyen, H.-D.; Iojoiu, C.; Lyonnard, S.; Mercier, R.; Espuche, E. Effects of Block Length and Membrane Processing Conditions on the Morphology and Properties of Perfluorosulfonated Poly(arylene ether sulfone) Multiblock Copolymer Membranes for PEMFC. *ACS Appl. Mater. Interfaces* **2015**, *7*, 13808−13820.

(41) Soboleva, T.; Xie, Z.; Shi, Z.; Tsang, E.; Navessin, T.; Holdcroft, S. Investigation of the Through-Plane Impedance Technique for Evaluation of Anisotropy of Proton Conducting Polymer Membranes. *J. Electroanal. Chem.* **2008**, *622*, 145−152.

(42) Nieh, M.; Guiver, M. D.; Kim, D. S.; Ding, J.; Norsten, T. Morphology of Comb-Shaped Proton Exchange Membrane Copolymers Based on a Neutron Scattering Study. *Macromolecules* **2008**, *41*, 6176−6182.

(43) Essafi, W.; Gebel, G.; Mercier, R. Sulfonated Polyimide Ionomers: A Structural Study. *Macromolecules* **2004**, *37*, 1431−1440.

(44) Chen, S. H. Small Angle Neutron Scattering Studies of the Structure and Interaction in Micellar and Microemulsion Systems. *Annu. Rev. Phys. Chem.* **1986**, *37*, 351−399.

(45) Chu, B.; Hsiao, B. S. Small-Angle X-Ray Scattering of Polymers. *Chem. Rev.* **2001**, *101*, 1727−1761.

(46) Beaucage, G. Approximations Leading to a Unified Exponential/Power-Law Approach to Small-Angle Scattering. *J. Appl. Crystallogr.* **1995**, *28*, 717−728.

(47) Berrod, Q.; Lyonnard, S.; Guillermo, A.; Ollivier, J.; Frick, B.; Manseri, A.; Améduri, B.; Gebel, G. Nanostructure and Transport Properties of Proton Conducting Self-Assembled Perfluorinated Surfactants: A Bottom-Up Approach toward PFSA Fuel Cell Membranes. *Macromolecules* **2015**, *48*, 6166−6176.

(48) Hanot, S.; Lyonnard, S.; Mossa, S. Water Confined in Self- Assembled Ionic Surfactant Nano-Structures. *Soft Matter* **2015**, *11*, 2469−2478.

(49) Paddison, S. Molecular Modeling of the Pendant Chain in Nafion®. *Solid State Ionics* **1998**, *113−115*, 333−340.

(50) Roche, E. J.; Stein, R. S.; MacKnight, W. J. Small-Angle X-Ray and Neutron Scattering Studies of the Morphology of Ionomers. *J. Polym. Sci., Polym. Phys. Ed*. **1980**, *18*, 1035−1045.

(51) Fumagalli, M.; Lyonnard, S.; Prajapati, G.; Berrod, Q.; Porcar, L.; Guillermo, A.; Gebel, G. Fast Water Diffusion and Long-Term Polymer Reorganization during Nafion Membrane Hydration Evidenced by Time-Resolved Small-Angle Neutron Scattering. *J. Phys. Chem. B* **2015**, *119*, 7068−7076.

(52) Gebel, G. Structural Evolution of Water Swollen Perfluor- osulfonated Ionomers from Dry Membrane to Solution. *Polymer* **2000**, *41*, 5829−5838.

(53) Alba-Simionesco, C.; Coasne, B.; Dosseh, G.; Dudziak, G.; Gubbins, K. E.; Radhakrishnan, R.; Sliwinska-Bartkowiak, M. Effects of Confinement on Freezing and Melting. *J. Phys.: Condens. Matter* **2006**, *18*, R15−R68.

(54) Ji, Q.; Lefort, R.; Busselez, Ŕ.; Morineau, D. Structure and Dynamics of a Gay-Berne Liquid Crystal Confined in Cylindrical Nanopores. *J. Chem. Phys.* **2009**, *130*, 234501.

(55) Chahine, G.; Kityk, A. V.; Démarest, N.; Jean, F.; Knorr, K.; Huber, P.; Lefort, R.; Zanotti, J. M.; Morineau, D. Collective Molecular Reorientation of a Calamitic Liquid Crystal (12CB) Confined in Alumina Nanochannels. *Phys. Rev. E - Stat. Nonlinear, Soft Matter Phys.* **2010**, *82*, 011706.

(56) Ghoufi, A.; Hureau, I.; Morineau, D.; Renou, R.; Szymczyk, A. Confinement of tert-Butanol Nanoclusters in Hydrophilic and Hydrophobic Silica Nanopores. *J. Phys. Chem. C* **2013**, *117*, 15203−15212.

(57) Kreuer, K.-D.; Paddison, S. J.; Spohr, E.; Schuster, M. Transport in Proton Conductors for Fuel-Cell Applications: Simulations, Elementary Reactions, and Phenomenology. *Chem. Rev.* **2004**, *104*, 4637−4678.

(58) Di Noto, V.; Piga, M.; Giffin, G. A.; Vezzù, K.; Zawodzinski, T. A. Interplay between Mechanical, Electrical, and Thermal Relaxations in Nanocomposite Proton Conducting Membranes based on Nafion and a [$(ZrO_2).(Ta_2O_5)_{0.119}$] Core-Shell Nanofiller. *J. Am. Chem. Soc.* **2012**, *134*, 19099−19107.

(59) Giffin, G. A.; Haugen, G. M.; Hamrock, S. J.; Di Noto, V. Interplay between Structure and Relaxations in Perfluorosulfonic Acid Proton Conducting Membranes. *J. Am. Chem. Soc.* **2013**, *135*, 822−834.

(60) Di Noto, V.; Giffin, G. A.; Vezzù, K.; Nawn, G.; Bertasi, F.; Tsai, T.; Maes, A. M.; Seifert, S.; Coughlinc, E. B.; Herring, A. M. Interplay between Solid State Transitions, Conductivity Mechanisms, and Electrical Relaxations in a [PVBTMA] [Br]-b-PMB Diblock Copolymer Membrane for Electrochemical Applications. *Phys. Chem. Chem. Phys.* **2015**, *17*, 31125−31139.

Supporting Information

Controlling Microstructure–Transport Interplay in Highly Phase-Separated Perfluorosulfonated Aromatic Multiblock Ionomers via Molecular Architecture Design

Huu-Dat Nguyen,[†] Luca Assumma,[†] Patrick Judeinstein,[‡] Regis Mercier,[§] Lionel Porcar,[∥] Jacques Jestin,[‡] Cristina Iojoiu,[†] and Sandrine Lyonnard*[⊥]*

[†]LEPMI, Université Grenoble Alpes – CNRS, 38000 Grenoble, France

[‡]Laboratoire Léon Brillouin (LLB), CNRS-CEA, Université Paris-Saclay, CEA Saclay, 91191 Gif-sur-Yvette Cedex, France

[§]Ingénierie des Matériaux Polymères, Université de Lyon, 69622 Villeurbanne, France

[∥]Institut Laue Langevin (ILL), 38002 Grenoble, France

[⊥]INAC-SPrAM, Université Grenoble Alpes – CEA – CNRS, 38000 Grenoble, France

Corresponding Author

* C. Iojoiu: Cristina.Iojoiu@lepmi.grenoble-inp.fr

* S. Lyonnard: Sandrine.Lyonnard@cea.fr

Table S1. Hydration Number (λ) and Polymer Volume Fraction (ϕp) of the Ionomers.

a) Membrane equilibrated at different relative humidities (RH, from 11 to 85%)

In5/5-2		In15/15	
λ	ϕp	λ	ϕp
2.4	0.92	2.2	0.92
3.3	0.89	3.2	0.89
4.3	0.86	4.6	0.85
5.2	0.84	6.2	0.81
6.2	0.81	8.0	0.77

b) Membrane Equilibrated in Water at Different Temperatures

In2.5/5		In5/5-1		In5/5-2		In7.5/5		In10/10		In15/15	
λ	ϕp	λ	ϕp	λ	ϕp	λ	ϕp	λ	ϕp	λ	ϕp
11	0.77	15	0.66	17	0.61	15	0.61	19	0.58	20	0.57
13	0.74	17	0.63	20	0.57	20	0.53	24	0.52	24	0.52
16	0.71	25	0.54	37	0.42	34	0.41	39	0.40	50	0.34
22	0.63	43	0.40	60	0.31	75	0.24	85	0.23	83	0.24

The hydration number (λ) and the polymer volume fraction (ϕp) were measured as follows:

i) The ionomer membranes in acidic form were firstly dried at 60 °C under vacuum for 48 h to obtain dry membranes. Then, two series of hydrated membranes were prepared, e.g., at low and high water content.

ii) Low-hydration membranes ($\lambda < 10$): the dry membranes were equilibrated at different RH using salt saturated aqueous solution to fix the vapor pressure, e.g., LiCl, $MgCl_2$, $Mg(NO_3)_2$, NaCl, and KCl for 11%, 32%, 52%, 75%, and 85%, respectively. They were exposed for one week at 25 °C in a mobile glove box.

iii) High-hydration membranes (λ > 10): the dry membranes were immersed in water at different temperatures (from 20 to 90 °C) for 24h.

The membrane water uptake (WU, wt %) was determined by **Equation S1**.

$$WU = \frac{W_h - W_d}{W_d} \times 100\% \quad (\mathbf{S1})$$

where W_h and W_d are the weights of hydrated and dry membranes, respectively. The membranes equilibrated at different RH were weighed in the glove box conditioned at a certain RH and then it was closed in neutron cell. The wet membranes equilibrated in water were quickly dried with paper to remove water on the surface before weighing.

The hydration number (λ), defined as the number of water molecules absorbed per each sulfonic acid unit, was determined from the water uptake and the IEC of the dry membrane, according to **Equation S2**.

$$\lambda = \frac{WU \times 10}{IEC \times MW_w} \quad (\mathbf{S2})$$

where MW_w is the molecular weight of water (~ 18.01 g/mol).

The polymer volume fraction (ϕp) was calculated by **Equation S3**.

$$\phi_p = \frac{1}{1 + 0.01 \times WU \times D} \quad (\boldsymbol{S3})$$

where WU is water uptake (wt%) as mentioned above and D is ionomer density (g/cm^3) measured via buoyancy method at 20 °C with the help of a Mettler-Toledo kit (D ~ 1.6 g/cm^3) and toluene was used as liquid phase.

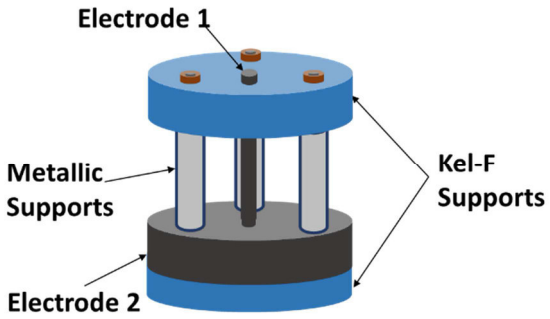

Figure S1. Schematic diagram of the conductivity cell.

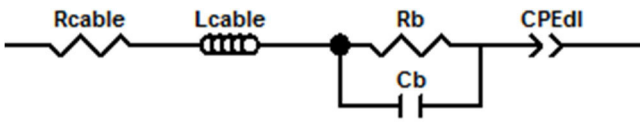

Figure S2. Simplified equivalent circuit for the proton-conducting membrane sandwiched between two electrodes. R_{cable} and L_{cable}, representing the impedance and inductance of cables and the empty cell, respectively, were measured by shorting the electrodes and fixed (~ 0.2 ohm and ~ 1×10^{-7} H, respectively) during data fitting; CPE_{dl} (constant phase element) represents the contribution of the membrane/electrode interfaces; R_b and C_b illustrate the bulk membrane resistance and capacitance, respectively.

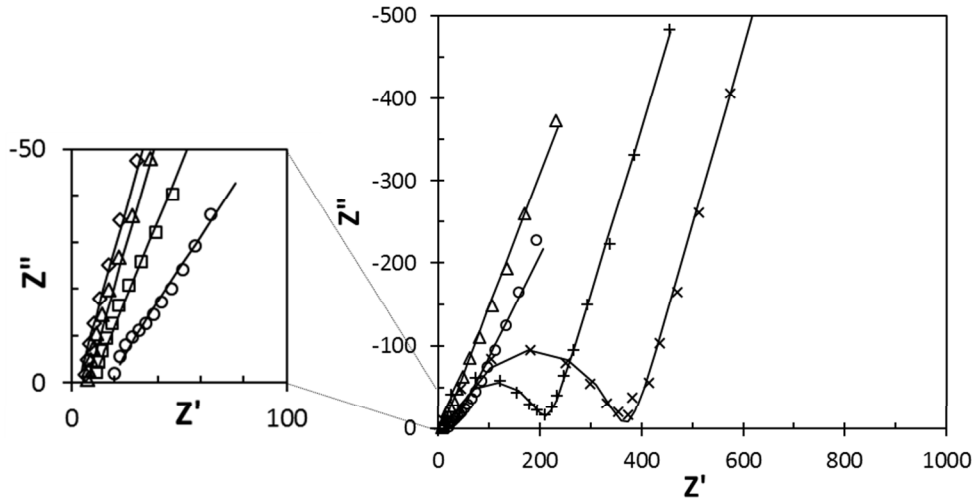

Figure S3. Nyquist plots of In5/5-2 at different hydration numbers (symbols) and corresponding fitted curves (lines). λ = 5 (×), λ = 6 (+), λ = 17 (○), λ = 20 (□), λ = 37 (△), λ = 60 (◇). Some overlapped curves were removed for clarity.

Table S2. Extrapolated d_{0_ionic} and d_{0_block} of the Ionomers

ionomer	d_{0_ionic} (Å)	d_{0_block} (Å)	PES length (Å)	FPES length (Å)	PES-FPES length
Nafion 117	27	/	/	/	/
InR	23	/	/	/	/
In2.5/5	22	210	131	193	324
In5/5-1	17	210	262	193	455
In5/5-2	19.5	230	262	193	455
In7.5/5	17	250	393	193	586
In10/10	17	320	524	386	910
In15/15	15	370	786	579	1365

d_{0_ionic} and d_{0_block} values were calculated from the dilution laws by extrapolation of d_{ionic} and d_{block} at zero water content ($\lambda = 0$). The length of PES and FPES blocks were calculated using bond distances.

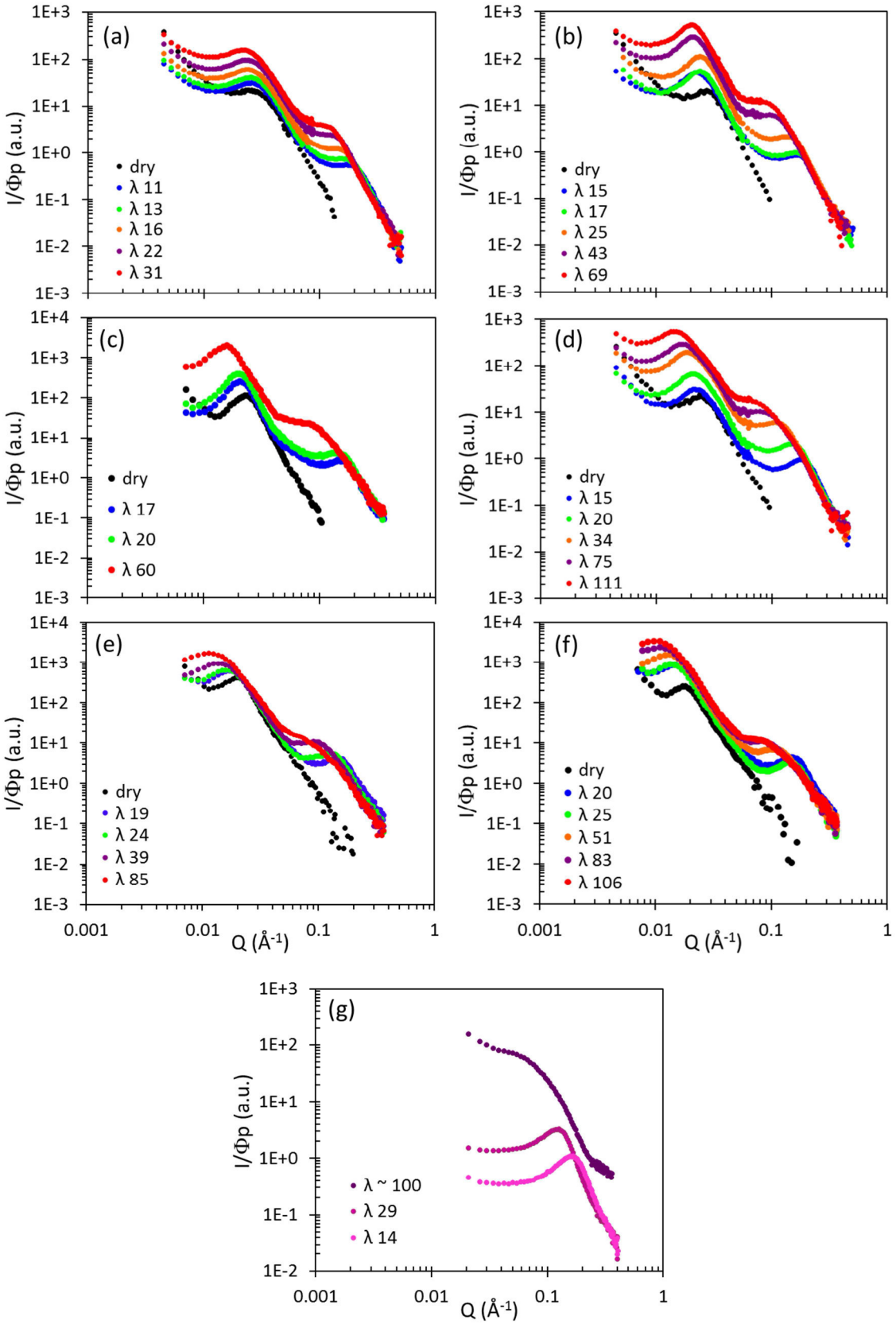

Figure S4. Evolution of SANS spectra of the swollen aromatic ionomers upon water content: (a) In2.5/5, (b) In5/5-1, (c) In5/5-2, (d) In7.5/5, (e) In10/10, (f) In15/15, (g) InR.

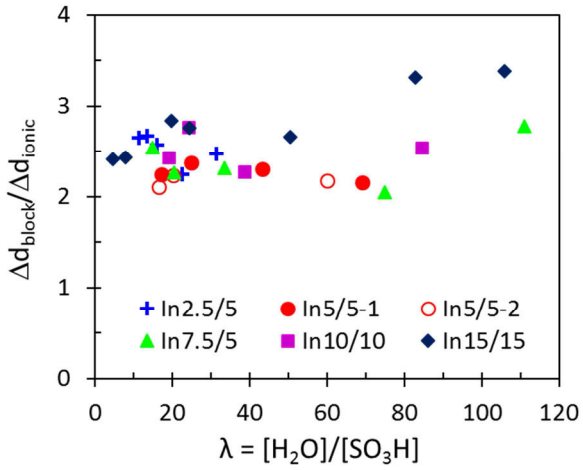

Figure S5. Swelling ratio $\Delta d_{block}/\Delta d_{ionic}$.

The expansion of the hydrophobic domains is, on average, 2.5 times higher than that of the ionic domains. The block/ionic swelling ratio appears to be rather independent of ionomer design and invariant along hydration up to $\lambda = 60$.

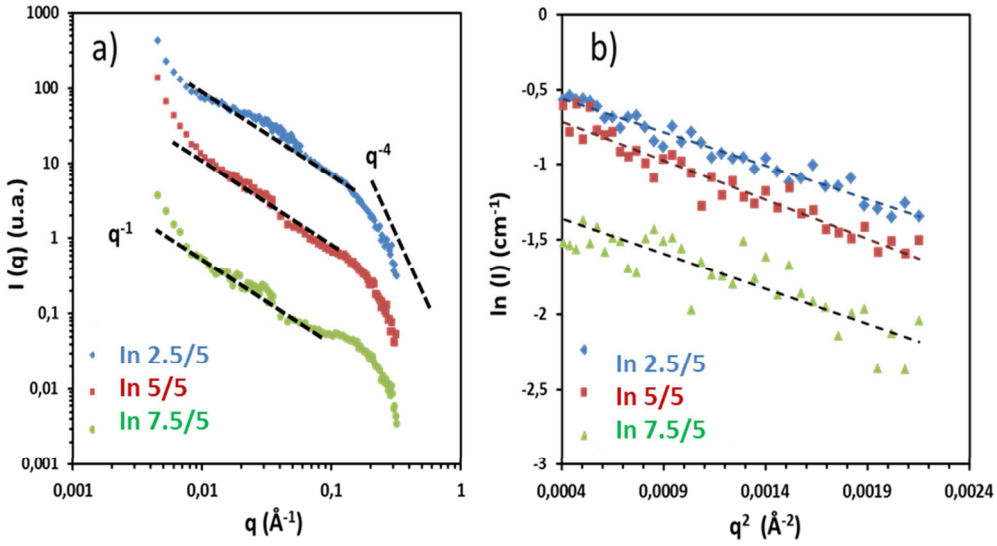

Figure S6. a) SANS intensities I(q) of ionomer solutions in DMSO (1,6 % w/w) as a function of the scattering vector Q. The I(Q) curves were shifted for clarity. b) Guinier representation (ln(I) vs Q^2).

The analysis of diluted solutions provides interesting insights into the average size and shape of polymeric aggregates that are likely to constitute the elementary brick of the polymer structure in the bulk state. The SANS study of Nafion solutions gave evidence of the presence of elongated cylindrical polymer particles in the highly diluted regime.[52] This result was a key finding in the search for rationalizing the PFSA polymer organization, leading to postulate

that ribbon-like hydrophobic aggregates are the basic constituents of Nafion membranes.[6,7] In the same spirit, we investigated the block ionomer solutions by SANS. The SANS technique is a valuable method to evaluate the average size and shape of particles.[44,45] Generally, in the case of binary mixtures, the scattered intensity I(Q) can be defined as in **Equation S4**:

$$I(q) = N(\Delta\bar{\rho}V)^2 P(q)S(q) \qquad \textbf{(S4)}$$

where N is the number of particles, V the sample volume and Δρ the so-called contrast between the two phases (typically, phase 1 is the solvent and phase 2 is the polymer). The form factor P(q) and the structure factor S(q) respectively characterize the shape and the size of the scattering objects and their distribution. If the system of scattering objects has no inter-particle correlation (e.g. it is a dilute solution), then S(Q) = 1 and it is possible to determine the form of the scattering objects.

In the SANS spectra of DMSO solutions of the aromatic block ionomers (**Fig. S6**), three different regimes can be identified: at high q values (> 0.1 $Å^{-1}$), the intensity decreases according to a q^{-4} power law, while a q^{-1} behavior typical of elongated particles is observed in the intermediate region (0.01 < q < 0.1 $Å^{-1}$). At low scattering wave vectors, a strong intensity upturn is visible, that could arise from the folding of very long cylindrical and flexibles colloids. In reason of the q^{-1} behavior, the scattering curves can be fitted with the form factor of cylindrical particles,[6] or using the Guinier approximation[46,50] for qRg < 1 (**Eq. S5**):

$$I(q) = \frac{(\Delta\rho)^2\pi^2R^2\phi}{q}\exp(-\frac{q^2R_g^2}{3}) \qquad \textbf{(S5)}$$

where R is the radius, ϕ is the polymer volume fraction and Rg is the radius of gyration defined as $Rg^2 = R^2/2$. As shown on **Figure S6**, a linear behavior is found in the Guinier representation of the SANS spectra. The extracted values of the radius of gyration are around 20 Å for the ionomers. On the basis of these SANS data, it can be deduced that the solutions in DMSO of the present aromatic ionomers are constituted of elongated polymer particles formed by the aggregation of few main polymer chains, as for Nafion.

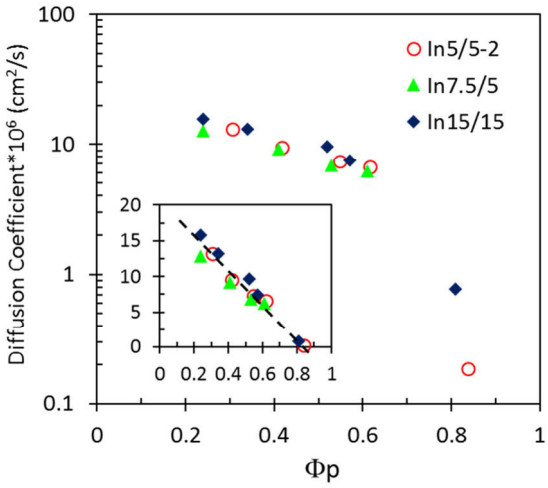

Figure S7. Water self-diffusion coefficient *vs* polymer volume fraction (ϕp)

The variations of the self-diffusion coefficient of water as a function of polymer volume fraction are quite similar for all ionomers. At low polymer fraction, the water diffusion is driven by the total amount of water and not sensitive to the details of the polymer aggregates, as already observed in PFSA compounds.[47]

Chapter 3.

Conductivity and Thermomechanical Stability of Fuel Cell Membranes Boosted by Blending Block Copolymers with Nafion

Nguyen, H.-D.; Jestin, J.; Porcar, L.; Lyonnard, S. Iojoiu, C. To be submitted to *Journal of Membrane Science*.

Preamble

The new molecular architecture of InX/Y ionomers, together with optimized membrane processing condition, leads to well nano-structured membranes with much improved performances as compared to the state of the arts. However, the proton conductivities of these ionomers are highly dependent on their block size and IEC, especially at low relative humidity. Increasing block length or IEC leads to membranes with equivalent proton conductivity to those of the benchmark ionomers, i.e., Nafion and other PFSAs, but significantly increases the membrane water uptake. In general, high water uptake within the fuel cell membrane is not desired because of water management and membrane durability issues. In fact, even if the PEMFC is operated at low RH, water is formed at the cathode, hence the membranes on the cathode side can swell much more than those on the anode side. Such highly heterogeneous swelling can induce enormous tension in the membranes, which could accelerate the degradation.

Therefore, we explored the possibility to blend the promising InX/Y ionomers with another well-chosen ionomer in order to mitigate the excessive swelling while keeping the excellent thermomechanical properties of the aromatic materials and maintaining high proton conductivities. It appeared that Nafion would be an excellent choice for this purpose, because of its outstanding transport properties at relatively limited swelling (typically ~12 water molecules per ionic group in liquid water, e.g., ~20 wt%). Hence, we produced InX/Y-Nafion blends with PFSA amount in the range 10–50 wt%. In the following, our methods and results are exposed in the form of a publication that we intend to submit to Journal of Membrane Science. We discuss the functional properties of the blends as a function of the composition (amount of Nafion, choice of block architecture) and the processing conditions (solvent and annealing). Extensive SANS characterization was conducted to obtain the correlation between the microstructure and the properties. In particular, we evidence the beneficial role of Nafion as an annealing agent in improving ionomer morphology, in particular during thermal annealing.

Conductivity and Thermomechanical Stability of Fuel Cell Membranes Boosted by Blending Block Copolymers with Nafion

Huu-Dat Nguyen,[1] Jacques Jestin,[2] Lionel Porcar,[3] Sandrine Lyonnard,[4] Cristina Iojoiu*[1]*

[1]LEPMI, Université Grenoble Alpes – CNRS, 38000 Grenoble, France

[2]Laboratoire Léon Brillouin (LLB), CEA Saclay, CEA – CNRS – Université Paris Saclay, 91191 Gif-sur-Yvette Cedex, France.

[3]Institut Laue Langevin (ILL), 38000 Grenoble, France

[4]INAC-SPrAM, CEA Grenoble, CEA – CNRS – Université Grenoble Alpes, 38000 Grenoble, France

Correspondence to: C. Iojoiu (E-mail: Cristina.Iojoiu@lepmi.grenoble-inp.fr) and S. Lyonnard (E-mail: sandrine.lyonnard@cea.fr)

ABSTRACT: Nafion was exploited for the first time as a reorganizing agent to enhance the performances of perfluorosulfonated copoly(arylene ether sulfone)s designed for PEMFC application. Despite the partial immiscibility of flexible random Nafion and rigid aromatic ionomers, the blend membranes give much improved conductivities and excellent mechanical strengths. Most blend membranes exhibited higher proton conductivities than those of corresponding pristine ionomers. Annealed membranes showed lower water uptake but higher proton conductivity, especially at low relative humidity, in comparison to those of cast membranes. The highest proton conductivities were obtained with the annealed membranes containing 20 wt% Nafion. The conductivity is three times higher than that of pristine Nafion cast in the same conditions. These findings were correlated to the microstructure of the blend membranes, which was investigated by small-angle neutron scattering in function of the blending ratio and the block architecture. The two ionomers are found to form phase-separated nanodomains, a morphology that is homogenized on uptaking large amounts of water. During thermal annealing, the Nafion molecules get incorporated into the ion conducting phase of the aromatic ionomer, where they serve to better connect ionic channels, therefore facilitating much more efficient long-range charge transfer.

KEYWORDS: polymer blend; aromatic ionomers; block copolymers; Nafion blend; poly(arylene ether sulfone); PEMFCS; proton exchange membranes; SANS

1. Introduction

Expected to be one of the key technologies of this century, polymer electrolyte membrane fuel cells (PEMFCs) are extremely attractive power-conversion devices thanks to the ability to directly transform chemical energy stored in hydrogen into electricity with high fuel efficiency and low pollutant emission. The key component of a PEM fuel cell is the proton-exchange membrane which serves as conductor for hydrated protons and barrier for fuel, oxidant and electron.[1,2] Although technological advances achieved in the past decades lead to significant cost reduction of PEMFCs, Nafion and similar perfluorosulfonic acid (PFSA) ionomers remain the benchmark PEM materials.[3] The excellent thermal-chemical stability and well-defined hydrophilic-hydrophobic phase separation, leading to high proton conductivity, of Nafion are derived from their chemical structure which composes of an extremely hydrophobic PTFE backbone and a perfluorinated pendant chain terminated with a superacidic group.[4–6] However, due to their high cost, large fuel crossover, reduced conductivity and mechanical properties above 90 °C, together with environmental issues related to the synthesis procedure, etc., Nafion and other PFSA membranes are not referred to as prosperous PEM materials, which prevent PEMFCs from worldwide commercialization.[3,7]

Much effort, therefore, has been dedicated to developing alternative PEM materials.[8] Aromatic ionomers are currently receiving more attention owing to their excellent thermomechanical properties, high thermal and oxidative stabilities, ease of synthesis/modification, and low cost, etc.[7,9–11] However, most sulfonated aromatic ionomers are inferior to Nafion with respect to PEM performance. In fact, high proton conductivities can be achieved using higher ion-exchange capacity (IEC), but this goes at the expense of the mechanical properties which severely suffer from excessive swelling at high hydrated condition. On the other hand, sulfonated aromatic ionomers with equivalent IEC to Nafion show lower proton conduction, especially at low RH. These drawbacks are originated from the chemical architecture of sulfonated aromatic ionomers, i.e., (i) the random distribution of proton-conducting groups on rigid polymer backbone leading to poor hydrophilic-hydrophobic phase separation, (ii) the proximity of sulfonic acid to the polymer main chain resulting in low structuration of ionic clusters, and (iii) the low acidity of aryl sulfonic acid (pKa ~ −2.5) as compared to that of perfluorosulfonic acid (pKa from −12 to −14).[12,13] With the aim of improving both morphology and acidity, we have recently developed a new aromatic ionomer with designed molecular architecture, e.g., the multi-block copoly(arylene ether sulfone)s bearing perfluorosulfonic acid pendant chain.[14,15] The new molecular architecture, together with optimized membrane processing condition, i.e., solvent selectivity

and thermal annealing, led to well-defined phase-separated morphologies and high performance of the ionomer membranes.[16] It was shown that the conductivity at low relative humidity and water uptake are highly dependent on the block lengths and IEC. Copolymers with longer blocks show similar or higher conductivities than Nafion, but the water uptake is much higher, which is not acceptable for a practical use in PEMFC due to water management and durability issues. On the other hand, the copolymers with shorter blocks show a moderate water uptake but the conductivities at low RH are lower than those of Nafion. Clearly, further optimization of the newly developed block copolymer membranes is difficult since two intrinsically antagonist properties need to be best compromised. One potentially interesting strategy at this stage is to blend the aromatic compound with a well-chosen ionomer in order to mitigate excessive swelling, while maintaining the excellent thermomechanical properties and the high conductivity. In this regard, PFSAs are appealing because of their unchallenged transport capability at relatively low water content (typically ~12 water molecules per ionic group in liquid water).

In fact, blending aromatic ionomers with Nafion has been referred to as a simple-but-plausible approach to obtain PEMs combining the excellent thermomechanical properties of aromatic ionomers and high performance of Nafion.[17–21] Most of Nafion/aromatic ionomer blend systems reported over the last decades were based on sulfonated poly(ether ether ketone)s (SPEEKs),[22] sulfonated poly(aryl ether ketone),[23] etc. However, poor performances were reported and ascribed to unfavorable morphologies with large isolated Nafion domains. Such two-phase-separated microstructures probably arise from the total immiscibility between the rigid sulfonated aromatic ionomer and Nafion. Recently, more flexible main chain structures were explored to improve the cross-organization of the two blending compounds at the nanoscale, e.g., blend membranes based on poly(vinyl alcohol),[24–26] sulfonated poly(propylene oxide),[21] poly(vinylphosphonic acid),[27] polyvinylidene fluoride,[17,28–30] etc. Yet, these attempts did not succeed in producing the desired combination of improved properties, mostly due, again, to polymer compatibility issues. In contrast with previously used aromatic polymers, the perfluorosulfonated multi-block copoly(arylene ether sulfone)s are believed to be much more compatible with Nafion because of similar perfluorosulfonic acid side chain structure.

Therefore, PEMs based on blends of perfluorosulfonated multi-block copoly(arylene ether sulfone)s and Nafion were prepared and characterized. The impact of blend membranes architecture, i.e., block length of the aromatic ionomer and the Nafion content in the range of 10–50 wt%, were investigated. The effect of thermal annealing on the structure reorganization

and functional properties was also studied. Herein we present the methods and results on series of blends characterized by DMA, sorption isotherms, conductivity measurements and small-angle neutron scattering.

2. Materials and Methods

2.1. Materials

Partially-fluorinated multiblock copoly(arylene ether sulfone)s bearing perfluorosulfonic acid functions (named as InX/Y, where X and Y are molar weight of the hydrophilic PES and hydrophobic FPES block of copolymer backbone in kg/mol, as seen on **Figure 1a**) were synthesized by regioselective bromination of partially fluorinated multiblock copoly(arylene ether sulfone)s (namely PES/FPES), followed by Ullman coupling reaction with lithium 1,1,2,2-tetrafluoro-2-(1,1,2,2-tetrafluoro-2-iodoethoxy)ethanesulfonate (I-psLi), as described elsewhere.[14] In this work, two block copolymers with two different block length, i.e., In5/5 and In10/10, were used to prepare blend membranes (**Table 1**).

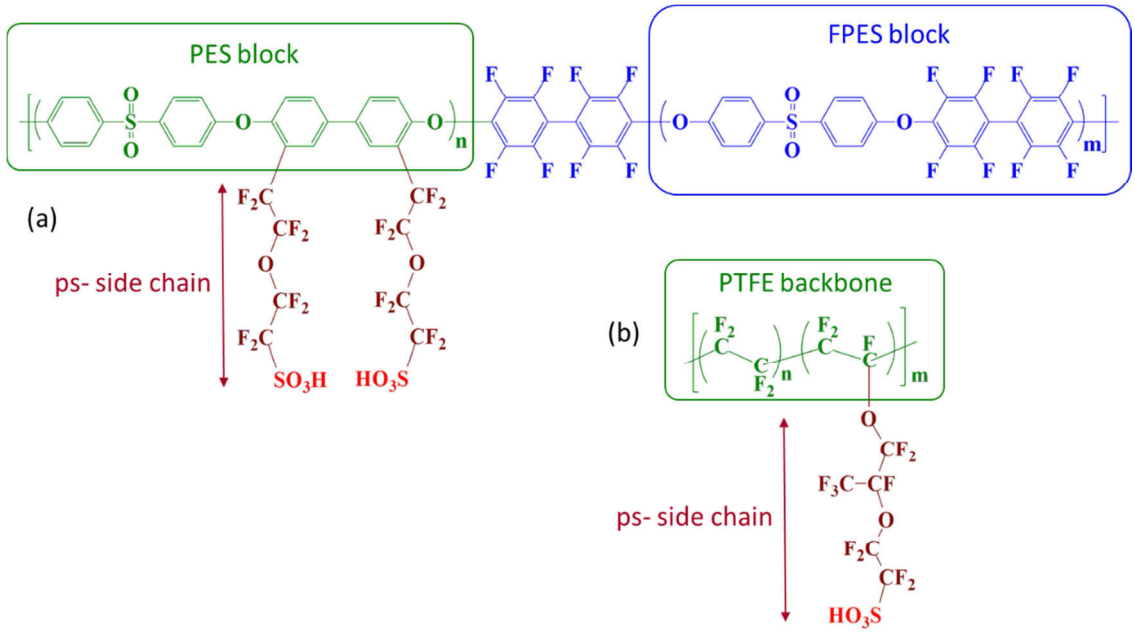

Figure 1. Chemical structure of (a) multi-block aromatic ionomer InX/Y and (b) Nafion.

Nafion® 117 membranes (**Figure 1b**), supplied by Alfa Aesar, were activated by boiling in 2M HNO_3 aqueous solution for 2h, followed by boiling in distilled water for 2h, and converted into lithium-salt form by cation exchange with 1M LiCl solution. Then, the lithium-salt Nafion membranes were dissolved in 50/50 v/v mixture of water/ethanol in an autoclave at 250 °C, 60 bar to obtain homogeneous polymer solution from which polymer powder was obtained by freeze drying.

Table 1. Composition and IEC of Ionomer and Blend Membranes

membrane code	PES-FPES (kg/mol)	wt % Nafion	IEC[a] (meq. H^+/g)	D[b] (g/cm^3)	IEC (meq. H^+/cm^3)
N117	/	100	0.91	2.04	1.86
In5/5	5-5	0	1.30 ± 0.05	1.60 ± 0.02	2.08
In5/5N10	5-5	10	1.26 ± 0.05	1.64 ± 0.02	2.08
In5/5N20	5-5	20	1.22 ± 0.05	1.67 ± 0.02	2.06
In5/5N50	5-5	50	1.10 ± 0.05	1.77 ± 0.02	1.95
In10/10	10-10	0	1.35 ± 0.05	1.63 ± 0.02	2.20
In10/10N10	10-10	10	1.30 ± 0.05	1.65 ± 0.02	2.14
In10/10N20	10-10	20	1.26 ± 0.05	1.67 ± 0.02	2.10
In10/10N50	10-10	50	1.13 ± 0.05	1.78 ± 0.02	2.01

[a]The IEC of InX/Y and Nafion was determined by NMR spectra and by acid-base titration in organic medium, following the protocol described previously.[31] The IEC of blend membranes was calculated from the wt% of both ionomers. [b]Measured via buoyant method using a Mettler-Toledo Density Kit at 20 °C with toluene as liquid phase.

2.2. Membrane Preparation

InX/Y and Blend Membranes. Dimethylsulfoxide (DMSO) was used to prepare membranes. 1.00 g of blend of InX/Y and Nafion (in different ratio), both ionomers in lithium-salt form, was introduced into 14 ml of DMSO and the mixture was stirred at 60 °C for 24h to obtain homogeneous solution. Then, the polymer solution was centrifuged at 5000 rpm for 15 minutes to remove solid impurities, re-stirred for 5 minutes, and left under vacuum to remove gas bubbles for 15 minutes. The homogeneous mixture was cast onto a clean glass substrate using Elcometer 4340 Automatic Film Applicator. The solvent was evaporated at 60 °C in an oven to obtain "as-cast membranes". Then the membrane was immersed and rinsed many times in distilled water for 24h to completely remove solvent residue. The solvent-free membranes, verified by ^{1}H NMR, were converted to their acidic form by stirring in 2M HCl solution for 24h, and then stirred in distilled water for 24h to remove acid trace. After drying the "cast membrane" (namely InX/YNz, where z is the wt% of Nafion) was obtained. Annealed membranes were prepared by following the protocol reported previously.[16] Briefly, "as-cast" membranes were submitted to an additional thermal treatment at 150 °C for 24h in a

closed vacuum chamber. The annealed membranes were then acidified by the same method applied for the cast membranes. For the nomenclature, a suffix "A" was added to the sample name to indicate the annealed membrane.

The annealing temperature was selected based on the transition temperature (Tg) of blend membrane after drying in the oven at 60 °C.[16] The thermal annealing temperature is much higher than the transition temperature of "as-cast" membranes, which shows one Tg ranging from 54 to 58 °C for the as-cast membranes (**Table S1**). After thermal annealing, the Tg of the membranes increase to around 102−105 °C for the annealed membranes. These values are much lower than two distinct transition temperatures of solvent-free membrane, which are around 145–155 °C for both Nafion and ps-PES bocks, and ≈ 220 °C for FPES hydrophobic block of InX/Y (**Figure S1**).

Nafion Membranes. For comparison, both activated Nafion® 117 and annealed DMSO-cast Nafion membranes were used as reference.

2.3. Water Uptake

The solvent-free acidified ionomer/blend membranes were firstly dried under vacuum at 60 °C for 48h. Then, dry membranes were immersed in water at different temperatures (from 20 to 90 °C) for 24h. The membrane water uptake (WU, %) was determined by **Equation 1**.

$$WU = \frac{W_h - W_d}{W_d} \times 100\% \qquad (\mathbf{1})$$

where W_h and W_d are the weights of hydrated and dry membranes, respectively. The wet membranes were taken out of water, quickly dried with paper to remove water on the surface before weighing. The hydration number (λ), the number of water molecules absorbed per each sulfonic acid function, was determined from the water uptake and the IEC of dry membranes via **Equation 2**.

$$\lambda = \frac{WU \times 10}{IEC \times MW_w} \qquad (\mathbf{2})$$

where MW_w is the molecular weight of water (~ 18.01 g/mol).

2.4. Differential Scanning Calorimetry (DSC)

The DSC measurements were performed using a DSC 1 STAR^e System from Mettler-Toledo under argon flow (50 ml/min) with a heating rate of 20 °C/min. The glass transition temperature (Tg) of "as-cast" and "annealed" membranes without removing of residue solvent were determined as the mid-point values of the first heating scan from 25 to 250 °C. For

solvent-free acidified membranes, the first scan was performed from 25 to 200 °C to remove water trace and the membrane Tg was determined as mid-points values of the second scan from 25 to 250 °C.

2.5. Dynamic Mechanical Analysis (DMA)

The DMA was performed on a DMA Q800 from TA Instruments in the temperature range from 25 to 200 °C with a heating rate of 2 °C/min. The dried membrane of average dimensions 20×6 mm^2 and ~100−130 μm in thickness is introduced to the film-tension clamp with the following measuring configurations: multifrequency-strain mode, frequency 1.0 Hz, preload force 0.1 N, force track 150%, and strain deformation was fixed at 0.1%.

2.6. Small-Angle Neutron Scattering (SANS)

SANS measurements were performed on D22 spectrometer at Institut Laue-Langevin (Grenoble, France) and on PAXY spectrometer at Laboratoire Léon-Brillouin (Paris, France). The measurement was conducted on solvent-free acidified membranes using the same protocol, as described elsewhere.[14–16] The hydrated membranes with different hydration number were taken out from the water and inserted in quartz Helma cells with some drops of water, and maintained at room temperature.

2.7. Proton Conductivity of Membranes

The proton conductivities were measured via through-plane impedance technique using a Material Mates 7260 frequency response analyzer and a homemade cell, as described elsewhere.[15] The ionomer films (≈ 0.10–0.12 mm in thickness) were sandwiched between two stainless steel electrodes (blocking electrodes). The membranes were equilibrated in water at room temperature for 24h before measuring. The measurements were firstly started at different temperatures (from 30 to 90 °C) at 95% RH in a climatic chamber (Vötsch VC4018) with a step of 10 °C. Then the temperature was stabilized at 80 °C and the relative humidity (RH) was decreased from 95 to 30% with the help of the climatic chamber. The membrane is stabilized at measuring condition for 5h before probing data.

The impedance spectra were recorded from 10 MHz to 5 Hz and Zview software was used to analyze and fit data. The equivalent circuit used to fit the experimental data and fitting parameters are depicted elsewhere.[15] The conductivity was calculated by **Equation 3**:

$$\sigma = \frac{L}{R \times S} \qquad (\mathbf{3})$$

where L is the thickness of polymer film, S is the upper electrode surface area, and R is the bulk membrane resistance.

3. Results and Discussion

The combination of aromatic ionomers bearing perfluorosulfonic acid side chains and Nafion was performed with the aim of obtaining a membrane with high mechanical strength, improved proton conductivity and optimal water uptake. As both ionomers are functionalized with perfluorosulfonic acid functions, a better miscibility can be expected as compared to the state of the art.[22,23] We reported previously that the conductivity and water uptake of InX/Y membranes increase with both IEC and block length.[14–16] Here, we selected two ionomers with the close IEC, i.e., In5/5 and In10/10. The focus is put on evaluating the impact of block length on the final properties of Nafion-based blends prepared with 10, 20 and 50 wt% Nafion. All membranes were cast at 60 °C or further thermal annealing at 150 °C, as improved conductivity of pristine aromatic ionomers can be achieved via annealing at this temperature.[16]

In the following, we will systematically discuss the impact of blend architecture and thermal annealing on the properties and the microstructure in function of the membrane hydration. First, we present the thermomechanical properties measured by DMA, the water sorption isotherms and the proton conductivities as a function of temperature and hydration. Second, we analyze the microstructure of the blends by SANS and discuss on the structure-property relationship. This allows us to draw some conclusions to guide the best rational design for optimized blends. The results are compared to those reported with commercial Nafion® 117. However, it is well established that industrial processing by extrusion improves the performance with respect to lab scale membranes. Hence, we are interested in quantifying the quality of our blends with respect to a PFSA material prepared and characterized using the same experimental protocols. Therefore, we prepared home-made Nafion membrane cast from solution at 60 °C and annealed at 150 °C, labeled “cast Nafion”. Note that the Nafion cast at 60 °C (without thermal treatment at 150 °C) showed poor mechanical properties and could not be manipulated, therefore only the annealed Nafion was obtained and was added in our discussion. The cast Nafion membrane in this work presents higher water uptake and lower conductivity than commercial Nafion 117, which can be explained by the absence of crystallinity leading to the poor-defined nanostructure. Solution-cast Nafion membranes were reported with a wide range of morphology,[32–36] water uptake[24,37] and proton conductivity[37,38] depending on the manufacturing process.

3.1. Thermomechanical Properties

Thermomechanical properties of blend membranes were investigated by DMA. The evolution of the storage modulus and tan δ with temperature allow evaluating the thermomechanical and relaxation properties of the blended material and bring some insight on the miscibility of the two polymers. In **Figure 2**, the results obtained on IN5/5 blend series before and after annealing are presented. The Nafion® 117 is added for comparison. As seen from **Figure 2a**, the storage modulus decreases with increasing the amount of Nafion, but it remains extremely high with respect to pristine Nafion. The poorest blend in terms of thermomechanical behavior, e.g., In5/5N50 membrane, has a storage modulus of ~1200 MPa at 30 °C, three times higher than that of Nafion® 117, and 1.4 times lower than that of In5/5. Therefore, Nafion blending up to 50 wt% does not degrade too much the mechanical strength of ionomer membranes. In addition, we observe that thermal annealing produces higher storage modulus and drops at higher temperature (**Figure 2b**). Such increase of storage modulus and creeping temperature, after annealing, was previously reported[16] and was associated to a better ionic blocks organization and stronger ionic interactions. Interestingly, the tan δ variations show that all blend membranes cast at 60 °C show two relaxation temperatures. By comparing the DMA results to bare Nafion and InX/Y, it can be noticed that the small low-temperature peak (~80 °C) is close to that of Nafion 117, while the second high-temperature (~150−160 °C) peak is close to that of ionic block of In5/5 (ps-PES block).[14] The presence of two relaxation temperatures could indicate that the two ionomers form separated microstructures inside the blend membranes, Nafion being not completely miscible with InX/Y. It is seen that the high temperature relaxation peak is much larger in the blends than in pure In5/5 (**Figure 2c**). Moreover, it is shifted towards higher temperature on increasing the Nafion content. Such large peak could originate from a more complex inter-chain interactions of ps-PES blocks due, probably, to a more inhomogeneous ps-PES domain organization and to the interactions of ps-PES and Nafion.

By submitting the membranes to a thermal treatment at 150 °C, we observe interesting modifications of the tan δ, e.g., the disappearance of the peak corresponding to pure Nafion phase and moderate thinning of the second peak at 150−160 °C (**Figure 2d**). As compared to In5/5 annealed membrane (In5/5-A), the width of the tan δ peak of blends remains, however, larger.

To conclude, the DMA analysis shows that (i) the blends possess excellent thermomechanical properties, mostly dictated by the aromatic polymer behavior, ii)

microphase separation between Nafion and InX/Y is probably observed, and disappears after thermal annealing and (ii) the relaxation of ionic blocks, ps-PES, in blend membranes take place in a larger temperature range due probably to additional interactions as compared to pure InX/Y.

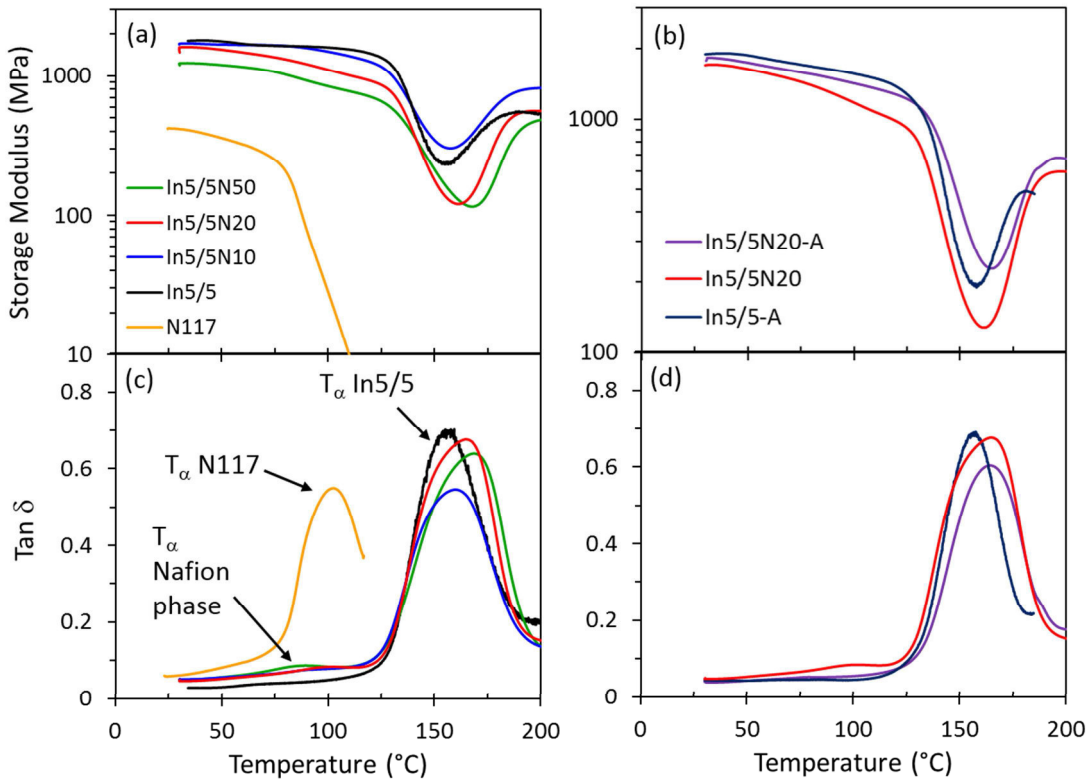

Figure 2. (a) Storage modulus and (c) tan δ of blend membranes containing different Nafion content, in comparison with those of Nafion® 117 and pristine In5/5 membranes. (b) Storage modulus and (d) tan δ of In5/5N20 and In5/5N20-A membranes. (* the increase of storage modulus after 160 °C is due to the membrane dehydration and was discussed elsewhere.[14,16])

3.2. Water Uptake

Water uptake is considered as a key property for PEM because of its tremendous impact on both functional properties and morphology. It is primarily controlled by the membrane IEC, the morphology, including the topology of ionic domains and their connectivity, the quality of the interfaces and the mechanical strengths. The capacity of In5/5 blend membranes before and after thermal annealing to uptake water, expressed as $\lambda = [H_2O]/[SO_3H]$, are plotted on **Figure 3**. Nafion® 117 and cast Nafion were included for comparison.

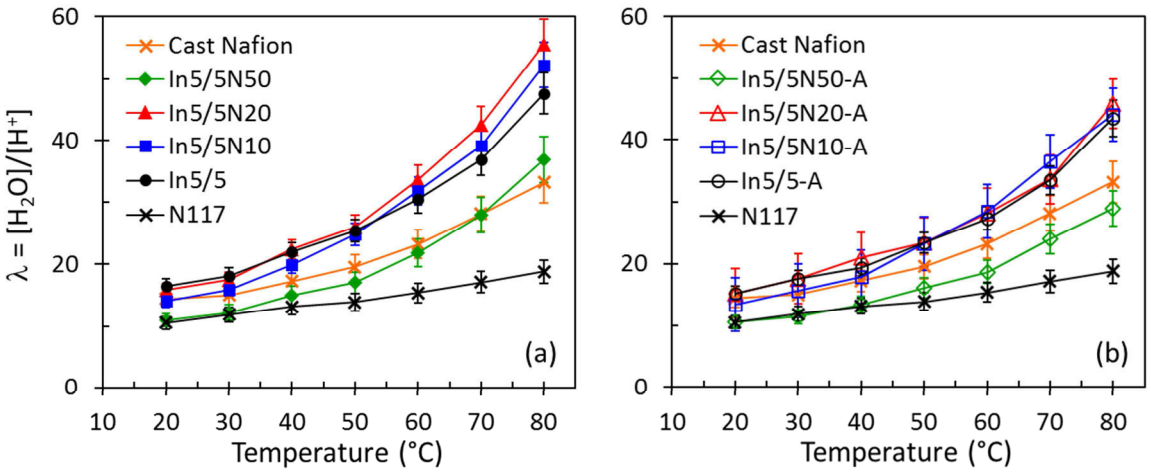

Figure 3. Water uptake of (a) as-cast and (b) annealed membranes expressed as the number of water molecules per ionic group, λ, as a function of the temperature.

Low Nafion content blends (10 and 20 wt%) behave very similarly to the pristine aromatic ionomer. Yet, they uptake more water molecules at temperatures higher than 50 °C. In turn, the high Nafion content material (50/50) exhibits an intermediate behavior between bare Nafion and aromatic ionomer. Thermal annealing at 150 °C produces an appreciable reduction of water uptake for all blend membranes at all temperature, in particular for the low Nafion content blends which now behave the same as annealed InX/Y ionomer. In contrast, the water uptake profile of In5/5N50-A is very close to that of cast Nafion, in between cast Nafion and Nafion 117. The decrease of water uptake after annealing can be correlated with the improvement of the membrane mechanical strengths. A similar behavior was previously reported for aromatic multi-block copolymers.[16] Based on these results, it can be hypothesized that in low Nafion content (10 or 20 wt%) membranes, the morphology, connectivity and mechanical properties are controlled by the In5/5 component, while in In5/5N50 the Nafion plays a preponderant role.

3.3. Proton Conductivity

Along with water uptake, proton conductivity (σ) plays a vital role in performance of PEMs. The water uptake and the transport properties of ionomer membranes are highly interrelated. One of the challenge in PEMFCs is to propose PEMs able to perform high conductivity at low RH[39,40] along with high mechanical properties. The conductivities of all blend membranes, before and after annealing, were measured at 95% RH from 30 to 90 °C, and at 80 °C in the range 30–95% RH. These data are shown on **Figure S2** and **S3**, respectively. On **Figure 4**, we adopt a synthetic representation to compile the obtained results and highlight the respective importance of blend composition and annealing. The conductivity

measured at 80 °C is plotted against the ratio of Nafion, which is equal to 0 for pure InX/Y, 100 for pure Nafion (commercial and cast), 10, 20 and 50 for the blends. Three hydration regimes are represented, namely high (80% RH), medium (50% RH) and low (30% RH) hydration. The water uptake at 80 °C is also reported using the same x-axis for comparison, even if it is obtained in liquid water and not at the selected RH values.

A number of interesting features are visible on **Figure 4**. First of all, we observe that all blends perform in general better than the pure ionomer. Also, blends made with smaller blocks (In5/5) are in general less conductive than those using longer blocks (In10/10), independently from the Nafion content. One striking observation is that a non-monotonous profile is obtained along the x-axis, with a maximum conductivity recorded for membranes containing 20 wt% of Nafion, whatever the aromatic block length and process treatment. This is also obvious from **Figure S2** and **S3**. The conductivities of In5/5N20 at 95% RH are ~1.5−1.7 times higher than those of In5/5, and ~1.2−1.3 times higher than Nafion 117 over the whole temperature range. We can remark that blends made with lower (10 wt%) or higher (50 wt%) content of Nafion perform in general quite similarly, although the water uptake and IEC are significantly lower for the 50 wt% membranes. Therefore, the distinct and remarkable behavior of the InX/YN20 blends cannot be ascribed to a pure water content effect, as water uptake in InX/Y, InX/YN10 and InX/YN20 materials are in the same range (**Figure 4d**). Hence, the blends membrane behavior, including the peculiarity of the N20 ones, must be dictated by true differences in morphology and/or transport mechanisms.

Another remarkable behavior illustrated in **Figure 4** is the effect of annealing (red curves), which improves the transport properties whatever the Nafion content and the ionomer block length. The enhancement of conductivity after thermal treatment is more pronounced at lower relative humidity. For instance, after thermal annealing the conductivity at 30% RH of In5/5N20 and In10/10N20 increases from 0.0011 and 0.0016 S/cm to 0.0025 and 0.0030 S/cm, respectively, therefore multiplied by a factor ~2.5. In addition, these values are three times higher than those obtained in the same conditions for the cast Nafion. In general, the blends show better conductivity than that of cast Nafion at all RH, and conductivities after thermal annealing are found on the order of, or higher than, commercial Nafion 117. Moreover, it is important to underline that annealing improves the conductivity while reducing the water uptake, which indicates internal rearrangement of the polymers yielding more efficient ion conduction.

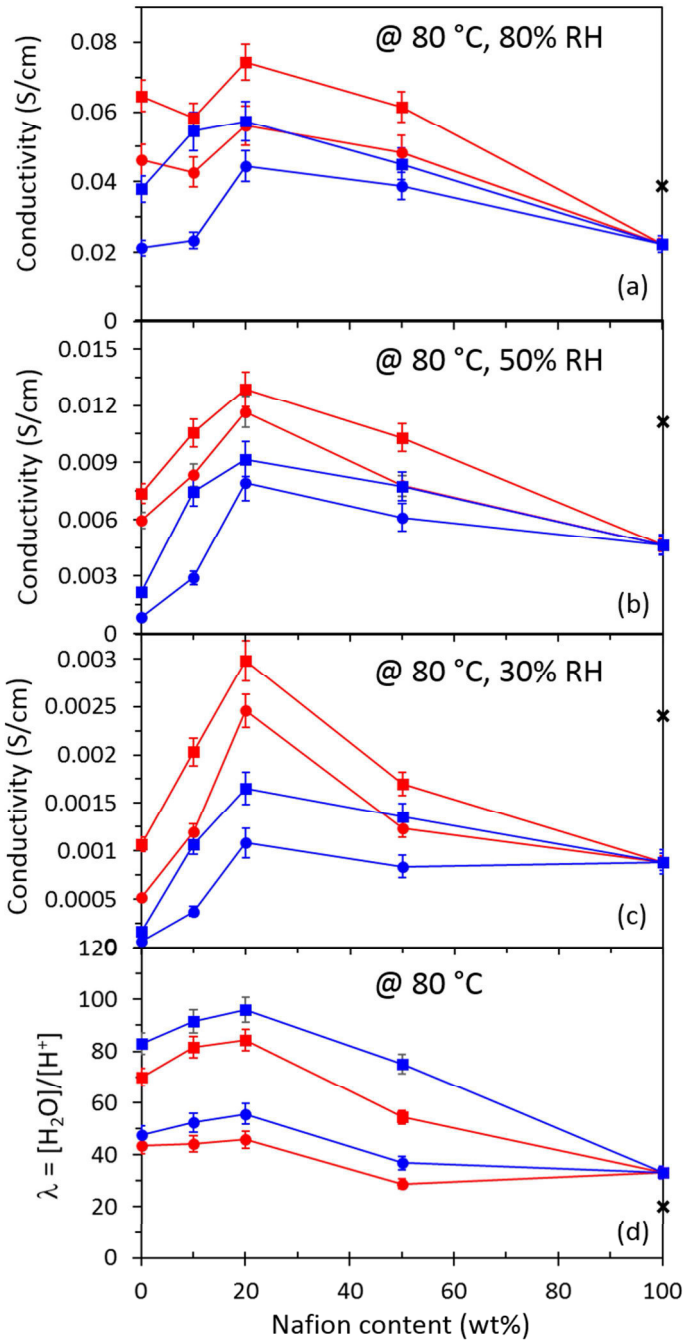

Figure 4. Proton conductivity at (a) 80% RH, (b) 50% RH, (c) 30% RH and (d) water uptake as a function of Nafion content in comparison with Nafion 117 (×) and cast Nafion. The pure InX/Y ionomer corresponds to 0 and pure Nafion to 100 on the x-axis. All the measurements were performed at 80 °C. In5/5N (blue ●), In5/5N-A (red ●), In10/10N (blue ■), In10/10N-A (red ■).

We can conclude that the blending process combined with subsequent annealing at 150 °C is extremely efficient to boost the conductivity of aromatic ionomers. The best blend (N20-A) corresponds to a gain factor of 3 and 5 at 30% RH with respect to annealed In10/10 and In5/5, respectively. The gain with respect to bare ionomer is more limited at high RH (gain factor

~1.2 at 80% RH), yet the blend membranes conductivity is almost 2 times higher than commercial Nafion and 4 times higher than cast Nafion at 80% RH. Overall, we report here on improvements that constitute a significant step towards real application in fuel cells, considering also the neat benefit in terms of mechanical strength. Our results establish the impact of Nafion in improving the PEM performance of the aromatic ionomer, in particular at reduced humidity, which is of potential great interest.

At this stage, however, further understanding on the blends structure is needed to elucidate the origin of their distinct functional behavior. We can hypothesize that the conductivity depends on the IEC, the water uptake, as well as the ionic domains connectivity and tortuosity. By increasing the amount of Nafion up to 20%, the IEC slightly decreases (**Table 1**) while the water uptake remains almost constant (**Figure 3** and **4**). Hence, to explain the increase of conductivities with Nafion content, we hypothesize that Nafion plays the role of structuring agent capable of facilitating the connectivity and structuration of ionic domains. It was reported that thermal annealing induces better percolation of ionic domains in the InX/Y,[16] and this is likely to occur also in the blends in combination with the effect of Nafion molecules. Moreover, we can note that the temperature dependence of the conductivity for all blends follows the same trend as the InX/Y ionomers (**Figure S2**). This supports that the blend properties are mostly aromatic-driven, even at quite large Nafion content, with similar proton conduction mechanism operating in both the pure and blend materials.

3.4. Morphology of Hydrated Blend PEMs

The morphology of cast and annealed hydrated blends was investigated by SANS, a well-established technique which was widely employed to characterize the microstructure in both PFSA[5,6,41] and aromatic ionomers.[15,42–44] Typically, the hydrophobic/hydrophilic phase-separation due to the amphiphilic character of ionomers produces a well-defined scattering maximum called the ionomer peak, located in the Q range of 0.1–0.2 $Å^{-1}$. Usually, the position of this peak (Q_{ion}) is shifted upon hydration due to microscopic swelling, e.g., the mean separation distance between polymer aggregates ($d_{ion} = 2\pi/Q_{ion}$) increases and the ionic nanodomains are expanded. In addition to the nanoscale structure, ionomers might also exhibit long range organization at larger scales. For instance, the SANS profiles of InX/Y block copolymers contain a second correlation peak located at much lower-Q values. This low-Q peak was associated with the block superstructure, e.g., the alternated sequence of hydrophilic ps-PES and hydrophobic FPES blocks[15,45–47] with mean correlation distances d_{block} in the range ~30–50 nm. In Nafion and other PFSAs, a rather ill-defined low angle peak

called the matrix knee was frequently found and tentatively correlated to the semi-crystalline nature of the polymer.[6,8]

The series of InX/Y-Nafion blends are characterized by the presence of several peaks revealing a multi-phase material organized at different length scales. The position, shape and intensity of these peaks are differently impacted by the blend composition, on one hand, and by the thermal annealing treatment, on the other hand. This is exemplified on **Figure 5**, where the SANS profiles of as-cast (**Figure 5a**) and annealed (**Figure 5b**) blend membranes prepared using In5/5 and immersed in liquid water ($\lambda \approx 15-16$) are shown, together with cast Nafion and In5/5 membranes for comparison. Note that the matrix knee is not found in the cast Nafion due to low crystallinity, which also supports the above assumption about the higher water uptake, but lower proton conductivity of cast Nafion membrane as compared to those of commercial Nafion 117. We observe that the SANS profiles of cast blend membranes (**Figure 5a**) are characterized by a low-Q peak (peak 1) located at typically $Q \approx 0.02$ Å^{-1} and two partially overlapping peaks in the ionomer region (peaks 2 and 3). A well-chosen weighted sum of Nafion and In5/5 spectra would produce resulting I(Q)s similar to the cast blend spectra. This would suggest that i) the presence of Nafion do not impede the organization, e.g., the block superstructure and the ionic domains of the InX/Y ionomers and ii) the ionic domains of pristine Nafion are formed and must coexist next to those of the InX/Y phase. To further evaluate these assumptions, the base-line subtracted spectra in the high-Q region were fitted using two Gaussian components. The fitted curves and the contribution of each Gaussian component are shown on **Figure 5c** for cast blends containing 10, 20, and 50 wt% Nafion, values of the positions and widths are reported in **Table 2**. The double ionomer peak of the blends spectra is well reproduced using this method, supporting the assumption of two distinct ionic domains. Interestingly, we observe that the positions of the two ionomer peaks are unaffected by the Nafion content. Peak 3 is found at $Q \approx 0.11$ Å^{-1}, a value close to that of cast Nafion measured at the same λ, in agreement with reported values of Nafion.[48–51] Peak 2 is found at $Q \approx 0.15–0.17$ Å^{-1}, close to that of In5/5 ionomer peak at the same hydration.[14,15] The associated mean separation distances are 5.6±0.1 nm and 3.85±0.15 nm, respectively (**Table 2**). The widths of these peaks are not significantly modified on increasing Nafion content, which indicates a similar degree of disorder in the ionic structures. In contrast to the positions and widths, however, the peaks intensities are very sensitive to the Nafion content. The peak area ratio (In5/5 over Nafion, labeled R_i) decreases from 6.4 to 0.7 (**Table 2**), in qualitative accordance with the decreasing amount of In5/5.

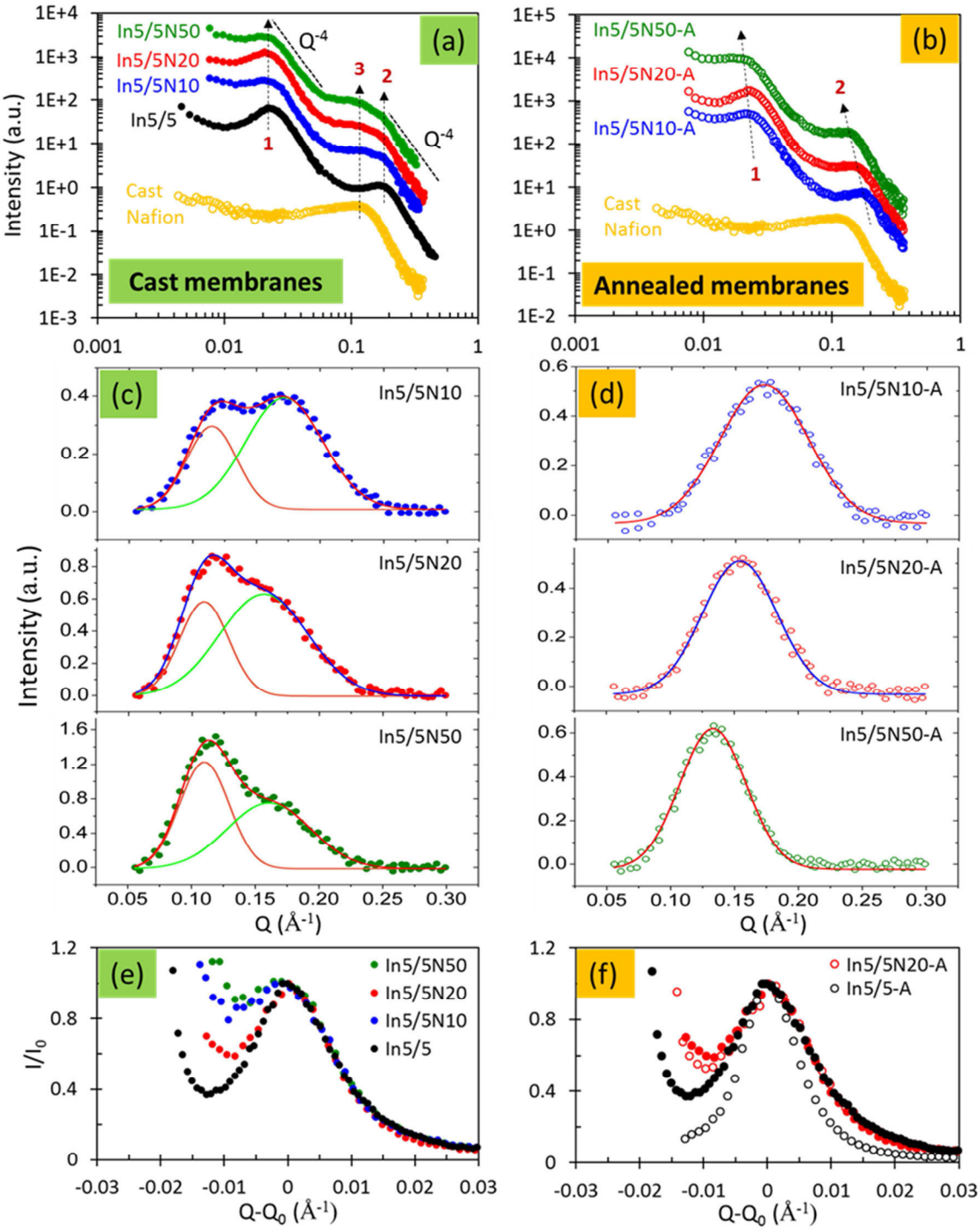

Figure 5. Incoherent background-subtracted SANS profiles of (a) cast and (b) annealed In5/5-based blend membranes prepared at similar hydration number ($\lambda \approx 15-16$) in comparison with pristine In5/5 and cast Nafion. The spectra are shifted vertically for clarity. The dashed lines represent the Q^{-4} Porod behavior, indicating the presence of sharp interfaces at nanoscopic scale.[52] Fits of the baseline subtracted high-Q data using (c) two Gaussian peaks for cast membranes and (d) one Gaussian peak for annealed membranes. Normalized representation of the low-Q peak (I/I_0 vs $Q-Q_0$, I_0 being the maximum intensity of the low-Q peak and Q_0 is its position), for as-cast (e) and annealed (f) membranes.

Table 2. Full Width at Half-Maximum/Q_0 (FWHM/Q_0) and d_{ionic} of Different Membranes

Sample	as-cast					annealed	
	Nafion peak		In5 peak		R_i[a]	FWHM/Q_0	d_{ionic} (Å)
	FWHM/Q_0	d_{ionic} (Å)	FWHM/Q_0	d_{ionic} (Å)			
Cast Nafion	0.65	57	-	-	-	-	-
In5/5	-	-	0.35	37	-	0.34	37
In5/5N10	0.34	55	0.36	37	6.4	0.40	36
In5/5N20	0.35	57	0.44	40	2.8	0.38	41
In5/5N50	0.35	57	0.41	39	0.7	0.39	47

[a]*The volume fraction of ps-PES block of InX/Y over Nafion.*

Regarding the low-Q peak, we can observe that its position is not affected by Nafion content (**Figure 5a**), at least within present experimental accuracy. Variations of the peak shape can be noticed, as highlighted in the normalized representation adopted in **Figure 5e**. In particular, the superstructure peak is broadened in the N10 and N50 blends, while not altered in the highly conductive N20 material with respect to bare In5/5. Moreover, an excess scattering intensity is found at $Q < 0.013$ Å^{-1}. Such small angle upturn could be related to the organization of the polymer into large grains and/or bundles of typical size exceeding 50 nm. These results could suggest that blending with Nafion degrades the long range order of the block superstructure when the Nafion-to-aromatic ratio is not optimum.

Thermal annealing has almost no effect on the block superstructure. The correlation distances among block structures (d_{block}) are found in the range 30±2 nm, similarly to values in pure InX/Y. The shape of the low-Q peak is mostly unchanged after thermal treatment (**Figure 5f** and **Figure S4**), contrarily to the effect of thermal annealing on pristine In5/5 membrane. In the pristine InX/Y, the low-Q superstructure peak becomes thinner due to the better packing of ps-PES and FPES polymer chains, resulting in a more compact and regular organization of both hydrophobic nodes and PES aggregates.[15] In the blend, thermal treatment above the Tg does not favor a better packing of hydrophobic domains. We can suppose that this is due to additional constraints introduced by the presence of long flexible Nafion chains and the need to accommodate them into or nearby the structured InX/Y grains. Beside, we

notice that the Porod's behaviors found in pristine InX/Y are maintained in the blends with no particular modifications of the sharp PES/FPES and PES/ionic phase interfaces after annealing.

In contrast, a prominent impact is evidenced on the nanoscale, as observed on **Figures 5b** and **5d**. In fact, the double peak shape of cast blend membranes is replaced by a single ionomer peak perfectly fitted using one Gaussian component (**Figure 5d**). With increasing the Nafion content from 10 to 50 wt%, the ionomer peak shifts toward lower-Q indicating a continuous increase of mean separation distance between polymer aggregates from 3.6 to 4.7 nm, while the peak widths are practically identical (**Table 2**). Hence, it is clear that thermal treatment induces rearrangements leading to a more homogeneous nanoscale structure. We can hypothesize that the ionic domain reorganization is driven by the favorable ionic interaction between the side chains of both ionomers and their high flexibility, enhanced by the presence of residual solvent which interact preferentially with ionic functions (**Table S1**).[16] Accordingly, Nafion and aromatic molecules must intimately self-organize during the annealing process, forming a final structure similar to bare Nafion and InX/Y, e.g., elongated polymer aggregates embedded into a well-connected ionic phase containing sulfonic acid headgroups pertaining to both polymers, protonic species and water molecules. The nature of the aggregates is certainly unclear at this stage, e.g., whether Nafion and aromatic particles coexist down to the nanoscale, or whether individual chains aggregate within mixed Nafion-aromatic particles or mixed hydrophobic nodes. Further insights can be gained by analysing the hydration dependence of the blend morphology.

3.5. Dilution Laws

The swelling behavior of the blend membranes can be obtained by analyzing the variations of the low-Q peak (peak 1, Q_{block}) and high-Q peak (peaks 2 and peak 3, Q_{ionic}) positions in function of hydration number. The dilution laws express the dependence on hydration of the various d-spacings, and the expansion of the block superstructure and the ionic domains, respectively. In our previous works on PFSAs and InX/Y, we have reported that these polymers exhibit very similar ionic dilution laws,[15,53] despite the obvious differences in chemical architectures. We showed that the swelling is dictated by few topological and structural constraints realized in both systems because they have similar side-chains, (i) the hydrophobic aggregates reject their side-chains outwards and present well-defined locally flat interfaces with the hydrated phase, (ii) variations in block architecture and/or PFSA side-chain length affect the mean size of the aggregates, which can be

determined from the asympotitc value of d_{ionic} at zero λ (d_{0_ionic}), (iii) the inter-lamellar ionic domains size ($\Delta d_{ionic} = d_{ionic} - d_{0\_ionic}$) increases linearly in function of λ up to a threshold value of ~ 30 and (iv) above this threshold, the swelling obeys the dilution law of elongated particles (1D-to-2D morphological transition, d_{ionic} follows a slope ~1/2). At high water content, the proton diffusion is determined by the overall water volume fraction and mostly limited by the presence of obstacles, e.g., polymer particles. At low hydration, the spatial confinement controls the water and proton mobility. In all cases, the interplay between local interactions (IEC-dependent), nanoscale confinement, tortuosity and connectivity critically controls the final conductivity of the materials.

We proceed to the blend data analysis following the method used in previous works on PFSA and InX/Y. The In5N10 blend SANS spectra obtained at various water contents are shown on **Figure 6**. All blends present the same typical behavior, e.g., shift of the peaks towards low angles on increasing λ. Yet, we observe that the doublet present in the high Q-region merges into a single broad ionomer peak. This is found to occur at λ~30 in all blends, independently of Nafion content and block length. On **Figure 7a–b**, the d_{ionic} variations, obtained by fitting the SANS profiles of cast In5/5-based blend membranes with 2 ionomer peaks at low hydration (<30) and 1 ionomer peak at high hydration (>30), are presented. The dilution laws from cast Nafion, commercial Nafion and In5/5 are added as references. In general, two swelling regimes are found in the blends, with a change in slope at λ~30 as in pristine materials. **Figure 7b** zooms into the low hydration region to further highlight the peculiar two-phase behavior of the blends. Indeed, it is found that the two ionomer peaks present in the blends yield d_{ionic} values very close to those found in cast Nafion (peak 3) and pristine InX/Y (peak 2) at the same mean hydration number. In other terms, the dilution laws of peak 3 and peak 2 nicely superimpose to that of InX/Y and Nafion, respectively. This finding strongly supports the segregation of Nafion and InX/Y domains which swell as the corresponding pristine material. The IEC of the two polymers being different, PFSA and aromatic phases uptake different amounts of water. But, locally, the structures accommodate the same number of water molecules per ionic site, because of fast exchange and equilibrium adsorption fixed by osmotic pressure and water activity. Above the λ ~30 threshold, the volume fraction of water is superior to that of the polymer phase, hence the degree of freedom of the hydrophobic objects is significantly released. Enhanced chains and particle mobility are likely to favor the extended connection of ionic domains as well as the re-organization of ionic domains. Ultimately, the medium appears as a continuous, connected network of large water pools embedding Nafion and ps-PES aggregates. The separation distance between

scattering objects is averaged with little impact of aggregates sizes (Nafion is typically 27 Å in diameter against 15-17 Å for ps-PES) and their respective number.

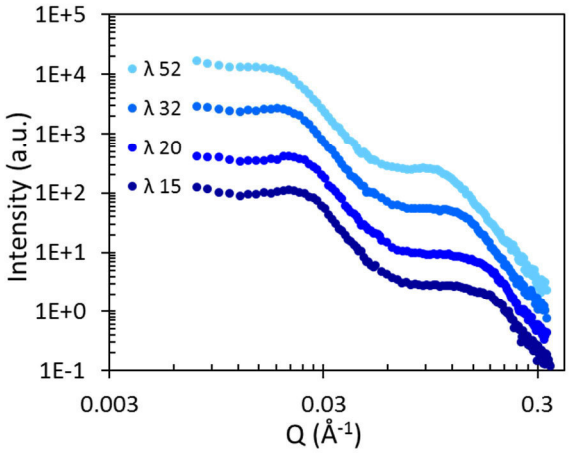

Figure 6. Incoherent background-subtracted SANS spectra of In5N10 membranes upon hydration degree. The spectra are shifted vertically for clarity.

On **Figure 7c** we represent the dilution laws of blends in the low hydration regime after annealing. Here, as reported in the previous section, there is only one ionomer peak and, consequently, one dilution law per blend. We obtain d-spacing values regularly intercalated in between the extreme InX/Y and Nafion behaviors. On increasing the Nafion content, the absolute distances, as well as the zero-hydration limit, are increased accordingly. The average size of polymer aggregates is found to be 16, 19, 24, 30 Å in In5/5-A, In5/5N10-A, In5/5N20-A and In5/5N50-A, respectively. Note that in the high content Nafion-blend, we obtain similar sizes of aggregates and similar separation distances as in pure Nafion, showing that, at the ionic domain scale, the behavior of this blend is primarily impacted by the PFSA material. As we know that the conductivity of the InX/YN50-A blend is higher than that of cast Nafion, we can conclude that large-scale effects, including domains connectivity, must play a decisive role in promoting the transport in the blend. In fact, let us now consider the dilution laws from the low-Q superstructure peak (**Figure 7d–e**).

A raw inspection of **Figure 7d** leads to the following conclusions: blending with Nafion does not significantly change the swelling behavior at this scale. The zero-λ extrapolated values are more or less in the range of pristine InX/Y ionomers (e.g., 23 and 30 nm for 5/5 and 10/10, respectively), with small deviations in function of the Nafion content. The resolution of these datasets is too poor to provide a more detailed view of the morphology. Still, we can suppose that Nafion is not adsorbed inside the ionic phase of the InX/Y, at least not completely. Indeed, this would exert a significant extra-pressure onto the hydrophobic

FPES nodes and lead to much higher d_{block}. Hence, it is more likely that Nafion molecules locate at the interfaces of InX/Y domains. The situation after annealing is not greatly modified, apart from one noticeable exception. In fact, we can see on **Figure 7e** that the low hydration sloped-regime do not nicely scale according to Nafion content, as was found at the ionic scale (**Figure 7c**). More precisely, we find that N20 blend is structured as native In5/5, while the block size (d_{0_block}) is increased in both 10 and 50 wt% blends. We have already commented the fact that the superstructure peak of the N20 blend is as narrow as the aromatic ionomer itself, while the two others are broader. Hence, we can postulate that N20 correspond to the amount of Nafion needed to best improve the overall connectivity and percolation paths.

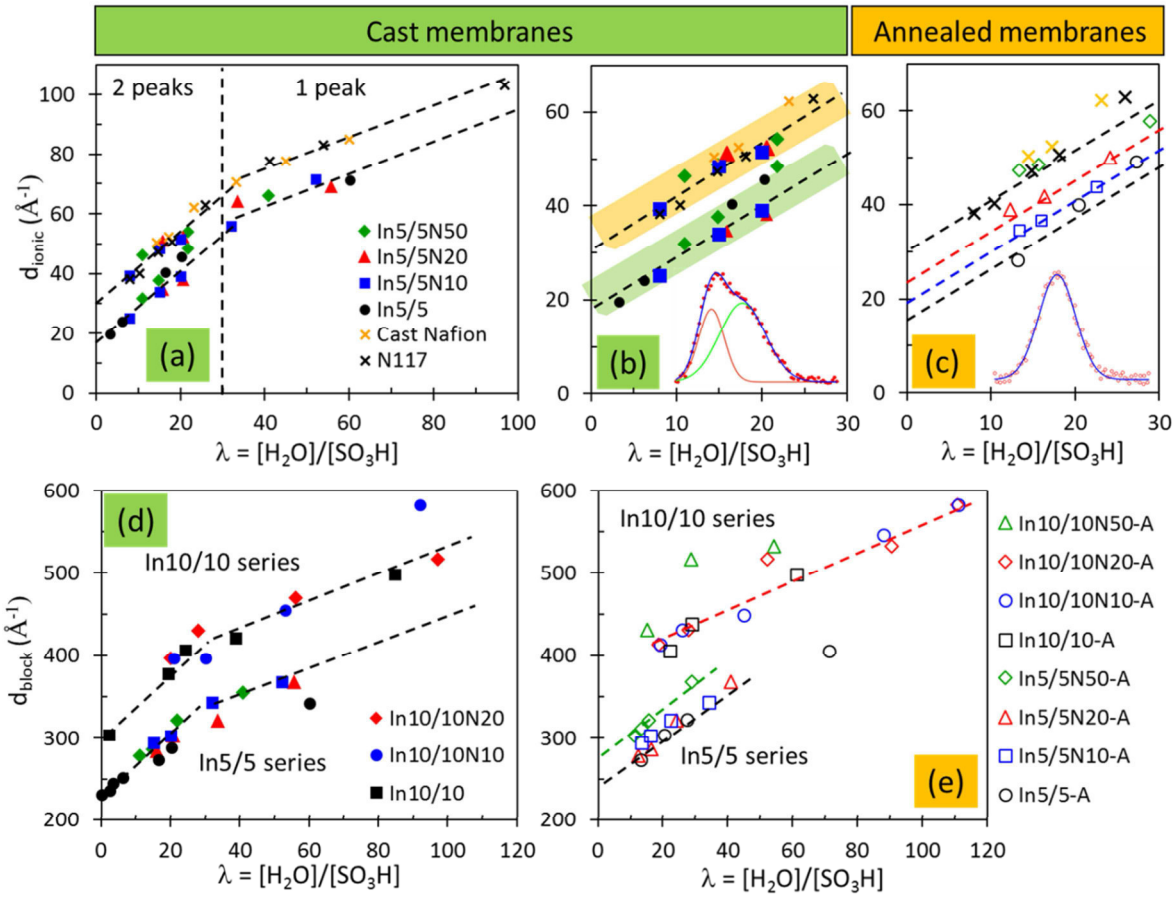

Figure 7. Variations of the ionic (top) and block (bottom) correlation distances of cast (a, b, d) and annealed (c, e) membranes upon λ. The cast Nafion, commercial Nafion and InX/Y ionomer ionic domain dilution laws are plotted for comparison.

3.6. Morphological Model of Blend Membranes

The SANS investigation has provided clues to decipher the principal mechanisms, in particular the beneficial impact of annealing on conductivity is clearly associated to the facilitated mixing of Nafion and InX/Y producing a single ionomer peak and homogeneous ionic phase. More generally, we can pinpoint the importance and the distinct behavior of the structural organization at two relevant scales in the blends, as in pure InX/Y membranes. The morphology is largely imposed by the nature of the aromatic block copolymers, e.g., large scale ordering resulting from the alternated block structure, and the phase-separation between ionic domains and polymer aggregates of nanoscopic dimensions. We have shown that blended membranes are originally constituted of a mix of InX/Y and Nafion domains. Their enhanced conductivities probably arise from a combination of factors. In fact, better transport property in the Nafion domains with respect to pristine InX/Y could explain the improved conductivity in In5/5N10 and in5/5N50, for instance, as their final conductivity could simply be the weighted sum of each component. However, such basic additivity of independent properties cannot explain that all InX/YN20 membranes, and some InX/YN50 blends, present a higher conductivity than both pure Nafion and pure InX/Y. This result means that mixing the two polymers is a relevant strategy creating synergistic interactions between the two ionomers. In particular, the efficiency of transport mechanism is improved in the blend structures, e.g., better connectivity and/or mitigation of detrimental effects as dead-zones, entangled channels, local defects of ineffective boundaries, are achieved. This must be triggered by the morphological evolution of ionomer blends during solvent-cast process and the morphological re-arrangement after thermal treatment, as schematically depicted on **Figure 8**.

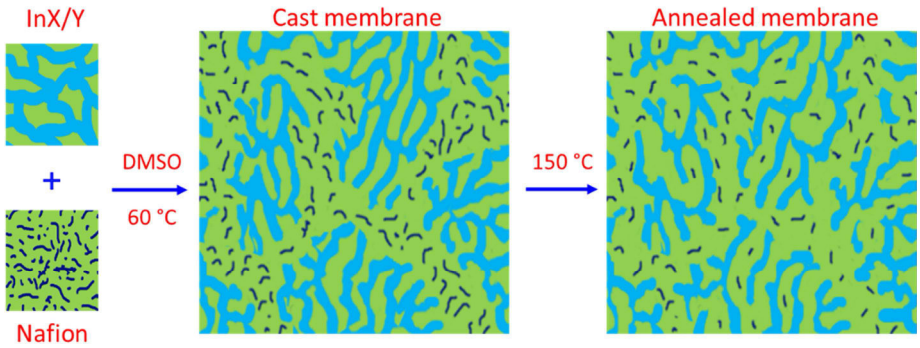

Figure 8. Schematic illustration of the morphological evolution of blend membranes during solvent-cast process and after thermal annealing.

Due to the different nature of main chain structure, Nafion (bearing flexible PTFE backbone) and InX/Y ionomer (bearing rigid poly(arylene ether sulfone) backbone) are partially immiscible. Yet, Nafion is more compatible with the hydrophilic ps-PES block than the hydrophobic FPES block of InX/Y due to similar side chain structure. During the drying process, we can expect the molecules of InX/Y aggregate and self-assemble as described in pure InX/Y.[15] The hydrophobic FPES blocks form hydrophobic domains, and the hydrophilic ps-PES blocks form hydrophilic domains, intercalated at large scales (≈ 20–40 nm) depending on block size. Inside the hydrophilic domains, the ionic groups aggregate to form ionic clusters at smaller scales (≈ 2 nm) due to the nanophase separation between ionic side chains (ps-) and PES polymer main chains. Simultaneously, the phase separation procedure takes place in Nafion leading to the formation of randomly distributed ionic clusters (≈ 3–5 nm). Note that the statistic structure of Nafion does not allow the formation of hydrophobic domains at large scale. The microstructure of Nafion and InX/Y are formed separately in blend membranes, although it cannot be excluded that a moderate amount of Nafion molecules penetrates the aromatic polymer ionic phase. Importantly, the flexibility of Nafion chain and compatibility of side-chains probably allows to have soft interfacial regions. When immersed in water at different temperatures, both the ionic domains accommodate water. At high hydration degree, two ionic domains become connected to form interconnected water channels. When submitted to the thermal annealing at temperature higher than their transition temperature, the molecules of both ionomers re-arrange which results in the morphology change. Thanks to the rigid polymer backbone, the microstructure of InX/Y was maintained while that of Nafion is mostly destructed, evidenced by the disappearance of Nafion-ionomer peak after thermal treatment. At this point, Nafion with higher molecular mobility derived from flexible PTFE backbone plays the role of plasticizer and accelerates the reorganization of InX/Y ionic domains. The movement of Nafion molecules into the hydrophilic domains of InX/Y is driven by the aggregation of the ionic groups of both ionomers. As Nafion is only compatible with the ps-side chain of the hydrophilic block of InX/Y ionomer, it can partially enter into the InX/Y ionic domains and locate at the grain interfaces. When a small amount of Nafion is incorporated, it does match the available specific surface and unsufficiently covers the InX/Y domains. On the other hand, too much Nafion is not beneficial because the PFSA chains can penetrate into the InX/Y structure. Moreover the final functional properties are mostly Nafion-induced (lower water uptake, lower conductivity, lower mechanical strength). The optimum therefore corresponds to Nafion serving as connecting and wetting agent. The benefits of the Nafion coverage is really important at low relative humidity because it helps in

reducing dead-zones and uneffective ionic regions. At high hydration, the structure is largely expanded, and water molecules plasticize the polymer aggregates, substituting to the Nafion. Thus, the performance of blends at high water uptake are not spectacularly improved with respect to pristine InX/Y.

4. Conclusions

For the first time, Nafion as structuring agent, in combination with solvent-aided thermal annealing, was used to improve morphology and properties of perfluorosulfonated copoly(arylene ether sulfone)s for PEM application in fuel cells. The blend membranes showed much higher thermomechanical properties than those of Nafion. Moreover, the presence of a moderate quantity of Nafion inside the aromatic ionomers did not destroy the distinct multiphase-separated morphology of InX/Y. Adding Nafion to aromatic ionomer, in combination with thermal treatment, leads to a significant improvement in proton conductivity. We found that the optimized Nafion content for preparing blend membranes with InX/Y ionomers is 20 wt%. The In5/5N20 membrane is the most promising material for fuel cell application because it best compromises excellent proton conductivity, in particular at low humidity (three times higher than cast Nafion), excellent thermos-mechanical properties (storage modulus 4 times higher than Nafion) and acceptable water uptake (not exceeding 60% in volume at 80 °C in water).

ACKNOWLEDGMENTS

The authors acknowledge the Institut Laue-Langevin (ILL) and Laboratoire Léon Brillouin (LLB), both in France, for providing the neutron facilities used in this work (proposal numbers 9-11-1709 and 11968, respectively). We are grateful to Dr. L. Porcar (ILL) and Dr. J. Jestin (LLB) for beamline alignment and helpful discussion during the neutron scattering experiments.

This work was performed within the framework of the Centre of Excellence of Multifunctional Architectured Materials “CEMAM” no. AN-10-LABX-44–01.

REFERENCES

(1) Carrette, L.; Friedrich, K. A.; Stimming, U. *Fuel Cells* **2001**, *1*, 5–39.

(2) Steele, B. C. H.; Heinzel, A. *Nature* **2001**, *414*, 345–352.

(3) Zhang, H.; Shen, P. K. *Chem. Soc. Rev.* **2012**, *41*, 2382–2394.

(4) Mauritz, K. A.; Moore, R. B. *Chem. Rev.* **2004**, *104*, 4535–4585.

(5) Kreuer, K.-D.; Portale, G. *Adv. Funct. Mater.* **2013**, *23*, 5390–5397.

(6) Kusoglu, A.; Weber, A. Z. *Chem. Rev.* **2017**, *117*, 987–1104.

(7) Hickner, M. A.; Ghassemi, H.; Kim, Y. S.; Einsla, B. R.; McGrath, J. E. *Chem. Rev.* **2004**, *104*, 4587–4612.

(8) Kreuer, K.-D. *Chem. Mater.* **2014**, *26*, 361–380.

(9) Rozière, J.; Jones, D. J. *Annu. Rev. Mater. Res.* **2003**, *33*, 503–555.

(10) Zhang, H.; Shen, P. K. *Chem. Rev.* **2012**, *112*, 2780–2832.

(11) Park, C. H.; Lee, C. H.; Guiver, M. D.; Lee, Y. M. *Prog. Polym. Sci.* **2011**, *36*, 1443–1498.

(12) Chang, Y.; Brunello, G. F.; Fuller, J.; Hawley, M.; Kim, Y. S.; Disabb-Miller, M.; Hickner, M. A.; Jang, S. S.; Bae, C. *Macromolecules* **2011**, *44*, 8458–8469.

(13) Mikami, T.; Miyatake, K.; Watanabe, M. *ACS Appl. Mater. Interfaces* **2010**, *2*, 1714–1721.

(14) Assumma, L.; Iojoiu, C.; Mercier, R.; Lyonnard, S.; Nguyen, H. D.; Planes, E. *J. Polym. Sci. Part A Polym. Chem.* **2015**, *53*, 1941–1956.

(15) Nguyen, H. D.; Assumma, L.; Judeinstein, P.; Mercier, R.; Porcar, L.; Jestin, J.; Iojoiu, C.; Lyonnard, S. *ACS Appl. Mater. Interfaces* **2017**, *9*, 1671–1683.

(16) Assumma, L.; Nguyen, H.-D.; Iojoiu, C.; Lyonnard, S.; Mercier, R.; Espuche, E. *ACS Appl. Mater. Interfaces* **2015**, *7*, 13808–13820.

(17) Cho, K. Y.; Eom, J. Y.; Jung, H. Y.; Choi, N. S.; Lee, Y. M.; Park, J. K.; Choi, J. H.; Park, K. W.; Sung, Y. E. *Electrochim. Acta* **2004**, *50*, 583–588.

(18) Kumar, P.; Dutta, K.; Das, S.; Kundu, P. P. *Appl. Energy* **2014**, *123*, 66–74.

(19) Hu, J.; Baglio, V.; Tricoli, V.; Arico, A. S.; Antonucci, V. *J. Appl. Electrochem.* **2008**, *38*, 543–550.

(20) Costamagna, P.; Srinivasan, S. *J. Power Sources* **2001**, *102*, 242–252.

(21) Lin, Y. F.; Hsiao, Y. H.; Yen, C. Y.; Chiang, C. L.; Lee, C. H.; Huang, C. C.; Ma, C. C. M. *J. Power Sources* **2007**, *172*, 570–577.

(22) Tsai, J. C.; Cheng, H. P.; Kuo, J. F.; Huang, Y. H.; Chen, C. Y. *J. Power Sources* **2009**, *189*, 958–965.

(23) Kim, I. T.; Choi, J.; Kim, S. C. *J. Memb. Sci.* **2007**, *300*, 28–35.

(24) DeLuca, N. W.; Elabd, Y. A. *J. Memb. Sci.* **2006**, *282*, 217–224.

(25) DeLuca, N. W.; Elabd, Y. A. *J. Power Sources* **2006**, *163*, 386–391.

(26) Lin, H.-L.; Wang, S.-H. *J. Memb. Sci.* **2014**, *452*, 253–262.

(27) Sen, U.; Acar, O.; Celik, S. U.; Bozkurt, A.; Ata, A.; Tokumasu, T.; Miyamoto, A. *J.*

Polym. Res. **2013**, *20*.

(28) Mai, Z.; Zhang, H.; Li, X.; Xiao, S.; Zhang, H. *J. Power Sources* **2011**, *196*, 5737–5741.

(29) Kumar, P.; Jagwani, S. K.; Kundu, P. P. *Mater. Today Commun.* **2015**, *2*, e1–e8.

(30) Cho, K.-Y.; Park, J.-K.; Jung, H.-Y. *Chem. Eng. Commun.* **2015**, *202*, 593–599.

(31) Iojoiu, C.; Genova-Dimitrova, P.; Maréchal, M.; Sanchez, J.-Y. *Electrochim. Acta* **2006**, *51*, 4789–4801.

(32) Kusoglu, A.; Kushner, D.; Paul, D. K.; Karan, K.; Hickner, M. A.; Weber, A. Z. *Adv. Funct. Mater.* **2014**, *24*, 4763–4774.

(33) Page, K. A.; Landis, F. A.; Phillips, A. K.; Moore, R. B. *Macromolecules* **2006**, *39*, 3939–3946.

(34) Fernandes, A. C.; Ticianelli, E. A. *J. Power Sources* **2009**, *193*, 547–554.

(35) Lin, H. L.; Yu, T. L.; Huang, C. H.; Lin, T. L. *J. Polym. Sci. Part B Polym. Phys.* **2005**, *43*, 3044–3057.

(36) Saccà, A.; Carbone, A.; Pedicini, R.; Portale, G.; D'Ilario, L.; Longo, A.; Martorana, A.; Passalacqua, E. *J. Memb. Sci.* **2006**, *278*, 105–113.

(37) Silva, R. F.; Passerini, S.; Pozio, A. *Electrochim. Acta* **2005**, *50*, 2639–2645.

(38) Silva, R. F.; De Francesco, M.; Pozio, A. *Electrochim. Acta* **2004**, *49*, 3211–3219.

(39) Kerres, J. A. *Polym. Rev.* **2015**, *55*, 273–306.

(40) Alberti, G.; Casciola, M. *Annu. Rev. Mater. Res.* **2003**, *33*, 129–154.

(41) Gebel, G.; Lambard, J. *Macromolecules* **1997**, *30*, 7914–7920.

(42) Gebel, G. *Macromolecules* **2013**, *46*, 6057–6066.

(43) Danyliv, O.; Iojoiu, C.; Lyonnard, S.; Sergent, N.; Planes, E.; Sanchez, J.-Y. *Macromolecules* **2016**, *49*, 4164–4177.

(44) Danyliv, O.; Gueneau, C.; Iojoiu, C.; Cointeaux, L.; Thiam, A.; Lyonnard, S.; Sanchez, J.-Y. *Electrochim. Acta* **2016**, *214*, 182–191.

(45) Chen, Y.; Rowlett, J. R.; Lee, C. H.; Lane, O. R.; VanHouten, D. J.; Zhang, M.; Moore, R. B.; McGrath, J. E. *J. Polym. Sci. Part A Polym. Chem.* **2013**, *51*, 2301–2310.

(46) Lee, M.; Park, J. K.; Lee, H. S.; Lane, O.; Moore, R. B.; McGrath, J. E.; Baird, D. G. *Polymer (Guildf).* **2009**, *50*, 6129–6138.

(47) Essafi, W.; Gebel, G.; Mercier, R. *Macromolecules* **2004**, *37*, 1431–1440.

(48) Rollet, A.-L.; Diat, O.; Gebel, G. *J. Phys. Chem. B* **2002**, *106*, 3033–3036.

(49) Rubatat, L.; Gebel, G.; Diat, O. *Macromolecules* **2004**, *37*, 7772–7783.

(50) Rubatat, L.; Rollet, A. L.; Gebel, G.; Diat, O. *Macromolecules* **2002**, *35*, 4050–4055.

(51) Gebel, G. *Polymer (Guildf).* **2000**, *41*, 5829–5838.

(52) Beaucage, G. *J. Appl. Crystallogr.* **1995**, *28*, 717–728.

(53) Berrod, Q.; Lyonnard, S.; Guillermo, A.; Ollivier, J.; Frick, B.; Manseri, A.; Améduri, B.; Gebel, G. *Macromolecules* **2015**, *48*, 6166–6176.

Supporting Information

Conductivity and Thermomechanical Stability of Fuel Cell Membranes Boosted by Blending Block Copolymers with Nafion

Huu-Dat Nguyen,[1] Jacques Jestin,[2] Lionel Porcar,[3] Sandrine Lyonnard,[4] Cristina Iojoiu*[1]*

[1]LEPMI, Université Grenoble Alpes – CNRS, 38000 Grenoble, France

[2]Laboratoire Léon Brillouin (LLB), CEA Saclay, CEA – CNRS – Université Paris Saclay, 91191 Gif-sur-Yvette Cedex, France.

[3]Institut Laue Langevin (ILL), 38000 Grenoble, France

[4]INAC-SPrAM, CEA Grenoble, CEA – CNRS – Université Grenoble Alpes, 38000 Grenoble, France

Corresponding author:

C. Iojoiu (E-mail: Cristina.Iojoiu@lepmi.grenoble-inp.fr) and S. Lyonnard (E-mail: sandrine.lyonnard@cea.fr)

Table S1. Glass Transition Temperature of As-Cast and Annealed Blend Membranes

Membrane	Tg^a (°C)	
	as-cast	annealed
In5/5N10	58	104
In5/5N20	54	102
In5/5N50	56	105

[a]*The temperature variation is ±2 °C.*

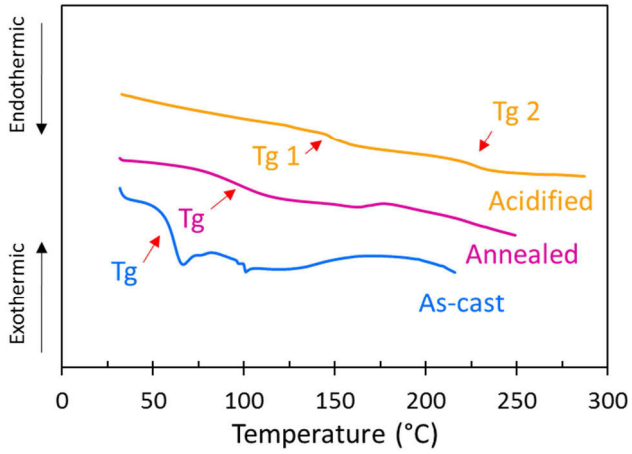

Figure S1. DSC diagrams of as-cast, annealed, and acidified In5/5N20 membranes (as cast: membranes membranes in Li form obtaned after the casting: it still contains solvent residue therefore the Tg is so low. Annealed: membranes in Li form resulted after thermal treatement it still contain solvent traces. Acidified: membrane in acidic form obtained after washing with water to completely remove solvent trace and acidifciation).

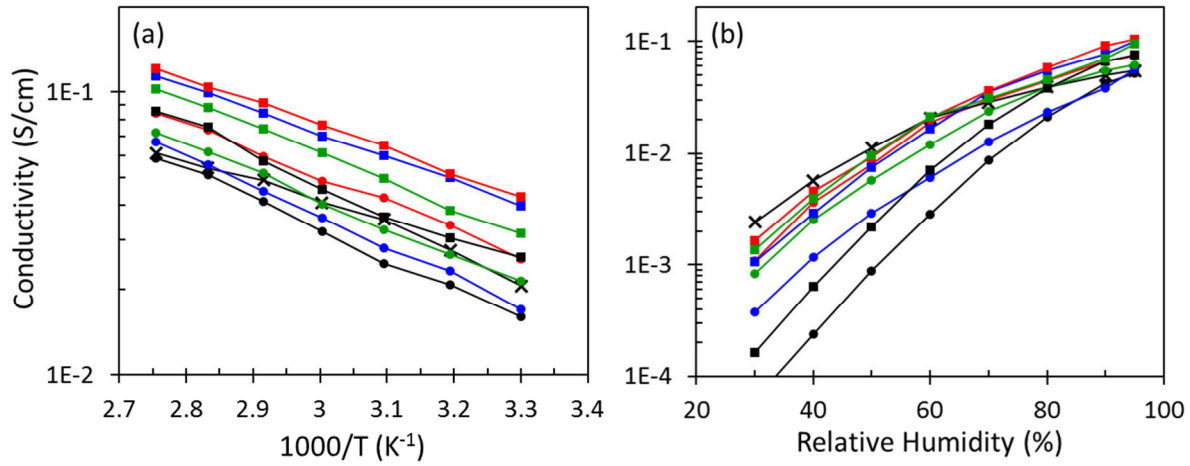

Figure S2. Proton conductivity (a) at 95 % RH as a function of 1000/T and (b) at 80 °C as a function of relative humidity of cast membrane as following: In5/5 (black ●), In5/5N10 (blue ●), In5/5N20 (red ●), In5/5N50 (green ●), In10/10 (black ■), In10/10N10 (blue ■), In10/10N20 (red ■), In10/10N50 (green ■), in comparison with Nafion 117 (×).

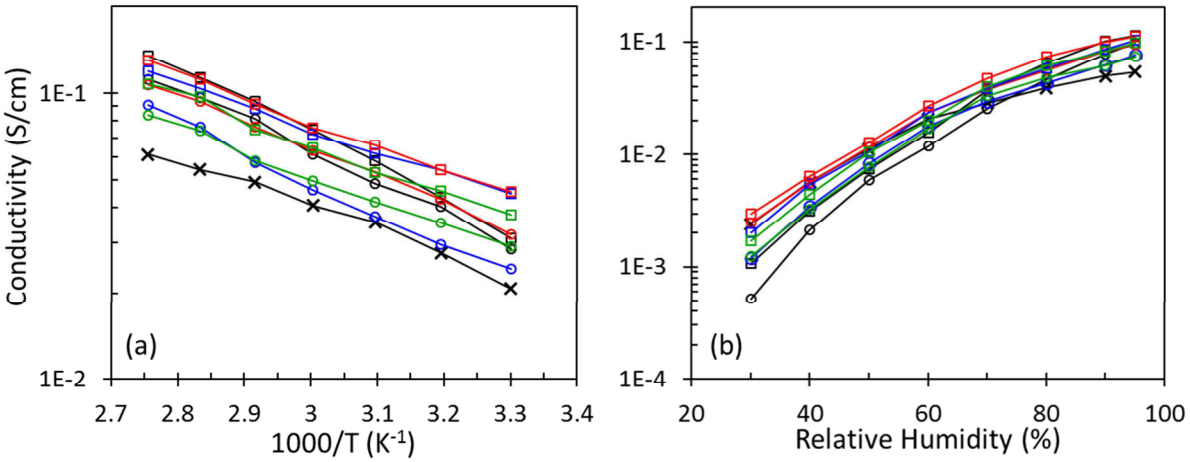

Figure S3. Proton conductivity (a) at 95 % RH as a function of 1000/T and (b) at 80 °C as a function of RH of annealed membrane as following: In5/5-A (black ○), In5/5N10-A (blue ○), In5/5N20-A (red ○), In5/5N50-A (green ○), In10/10-A (black □), In10/10N10-A (blue □), In10/10N20-A (red □), In10/10N50-A (green □), in comparison with Nafion 117 (×).

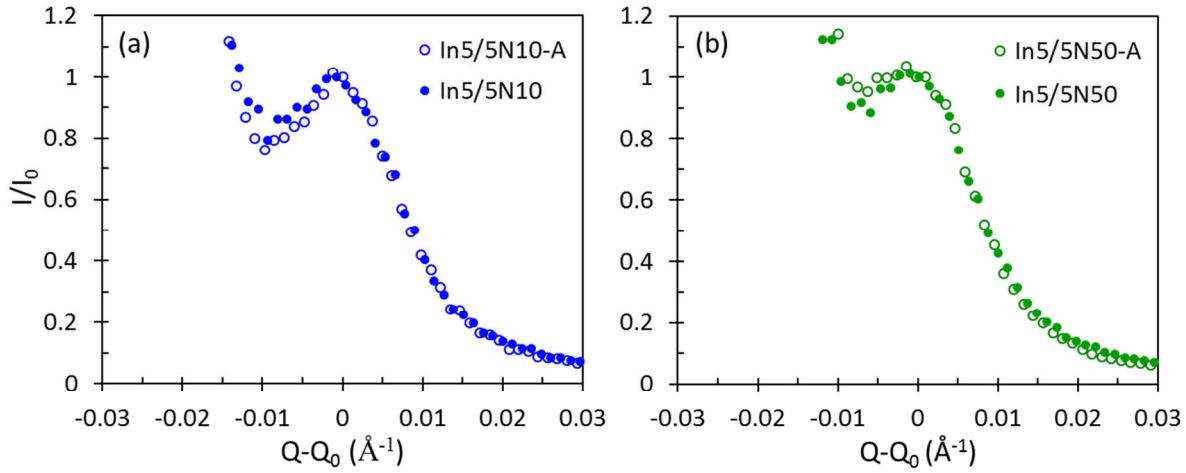

Figure S4. Normalized SANS profiles at low-Q region of (a) In5-based membranes and (b) In5/5N20 and In5/5N20-A membranes at similar hydration number in comparison with In5/5 and In5/5-A membranes. I_0 is the maximum intensity of the low-Q peak and Q_0 is its position.

Chapter 4.

Aromatic Multi-Block Ionomers with Extensively-Delocalized Negative Charge for PEMFC Application

Huu-Dat Nguyen, Emilie Planes, Priscillia Soudant, Lionel Porcar, Sandrine Lyonnard, Cristina Iojoiu. To be submitted to *Journal of Physical Chemistry.*

Preamble

This chapter is focused on the design and characterization of new nanostructured ionomers with the aim of exploring the influence of the delocalization of anion charge on the conductivity, water uptake, and morphology.

It was demonstrated that InX/Y exhibited a more phase-separated morphology and higher proton conductivity than those of the poly(arylene ether)s bearing sulfonic acid groups. This much higher conductivity was explained by two factors, i.e., the higher acidity of perfluorosulfonic acids as compared to aryl sulfonic acids, and the development of highly phase-separated and organized microstructure due to both the high acidity of ionic function and block structure.

The perfluorosulfonyl imide acid was reported to possess stronger gas-phase acidity and improved thermal stability than those of perfluorosulfonic acid. The high ion dissociation induced by the extensively-delocalized negative charge in the perfluorosulfonimide function is expected to significantly improve the PEM conductivity, especially at low RH.

Therefore, in this chapter we explore a new class of ionomers, i.e., multiblock co-poly(arylene ether sulfone)s bearing perfluorosulfone imide functions. The perfluorosulfoimide is grafted on PES-FPES multi-block copolymers with similar block lengths to InX/Y.

In the following, our methods and results are exposed in the form of a publication that we intend to submit to Journal of Physical Chemistry. The thermomechanical properties, water uptake and proton conductivity, are presented and compared with those of InX/Y.

Aromatic Multi-Block Ionomers with Extensively-Delocalized Negative Charge for PEMFC Application

Huu-Dat Nguyen,[1] Emilie Planes,[1] Priscillia Soudant,[1] Lionel Porcar,[2] Sandrine Lyonnard,[3] Cristina Iojoiu,[1]*

[1]LEPMI, Université Grenoble Alpes – CNRS, 38000 Grenoble, France

[2]Institut Laue Langevin (ILL), 38002 Grenoble, France

[3]INAC-SPrAM, Université Grenoble Alpes – CEA – CNRS, 38000 Grenoble, France

Correspondence to: C. Iojoiu (E-mail: Cristina.Iojoiu@lepmi.grenoble-inp.fr)

ABSTRACT: This publication deals with the synthesis and characterization of new ionomers based on polysulfone multi-block copolymer bearing highly delocalized anion, i.e., perfluorosulfonimide (SiX/Y). The influence of ionomer structure, i.e., block lengths and ion-exchange capacity on membrane microstructure, thermo-mechanical and transport properties was extensively discussed. The tri-phases microstructure, evidenced on the humidified membranes, by small-angle neutron scattering, is directly correlated with ionomer structure. As compared with their homologues, multiblock copolymers bearing perfluorosulfonic acid side chains (InX/Y), the proton conductivity of SiX/Y ionomers was found to be more dependent on the relative humidity (RH). At similar IEC and water uptake, the conductivity of SiX/Y is two times higher at 30 °C and 95% RH, but ten times lower at 80 °C and 30% RH as compared to those of InX/Y.

KEYWORDS: Aromatic block copolymer, ionomer, poly(arylene ether sulfone); perfluorosulfonimide; sulfonimide, PEMFC; proton exchange membrane, polymer synthesis, SANS

1. Introduction

Polymer electrolyte membrane fuel cells (PEMFCs) are considered as one of the promising energy technology alternative to fossil fuel owing to their high-energy conversion and environment compatibility. Considered as a central component of a PEM fuel cell, proton-exchange membranes (PEMs) play a critical role in transporting hydrated protons from anode to cathode where they combine with oxygen to form water. Due to harsh operating condition as well as commercialization requirement, a novel PEM material for fuel cell must possess combined properties such as high proton conductivity, especially at low relative humidity, good mechanical properties, high thermal and chemical stability, low fuel and oxidant permeability, and low cost, etc.[1–3]

Currently standard PEM materials are still perfluorosulfonic acid (PFSA) membranes such as Nafion®, a commercial product from DuPont introduced in the 1960s. The high proton conductivity and superior chemical-electrochemical stabilities of Nafion are originated from (i) the highly microphase separation between hydrophobic polymer backbone and hydrophilic ionic domains, promoted by its chemical structure composing of an extremely hydrophobic flexible PTFE backbone coupled with a pendant perfluorosulfonic acid side chain, and (ii) the super-acidity of perfluorosulfonic acid groups.[4–7] However, Nafion® and other PFSA membranes have some drawbacks such as reduced proton conductivity and mechanical properties above 80 °C, and high cost. Considerable effort, therefore, has been dedicated to developing alternative ionomers with improved morphology and properties.[8–11] Among numerous investigated ionomers,[12,13] aromatic ionomers such as poly(phenylene)s,[14] poly(arylene ether sulfone)s,[15–17] poly(ether ether ketone)s,[18,19] polyimides,[20,21] and polybenzimidazoles[22,23] are attractive for the next-generation PEM materials because of the their low cost, excellent thermal and thermomechanical properties and good oxidative stability, etc. The aromatic ionomers bearing perfluoroalkyl sulfonic acid groups, recently developed, have brought significant interest owing to their improved conductivity as compared to directly sulfonated ionomers, especially at lower RH.[17,24–27] This improved conductivity is due to the higher acidity of the acidic side chain and its ability to dissociate in the limited presence of water (pKa ~ −6 in perfluorosulfonic acid and pKa ~−1 in aryl sulfonic acid).[28] The perfluorosulfonyl imide acid is known to possess stronger gas-phase acidity[29] and improved thermal stability[30] relative to those of perfluorosulfonic acid. In this anion the negative charge is extensively delocalized resulting in weak cation-anion interaction.[31,32] The dissociation depends on the extent of negative-charge delocalization induced by electron-withdrawing groups through inductive and resonance effects. This is

optimized in bis(trifluoromethanesulfonyl)imide (TFSI) anion by two CF_3SO_2 nitrogen substituents, by both inductive (CF_3) and resonance (SO_2) effects.[33] Accordingly, the aromatic ionomers bearing perfluorosulfonimide side chains could constitute a new promising materials for high performance PEMFC, the perfluorosulfonimide anion, perfectly replicating the TFSI anion, should benefit from the same delocalization of the negative charge and thus dissociation of ion pairs.

To the best of our knowledges, only some examples of ionomers bearing perfluorosulfonimide acid were reported and most of them concern alkyl perfluorinated polymer backbone, similar to that of Nafion. These ionomers were developed by DesMarteau et al.[34–39] and a wide range of monomers and ionomers was reported. Savett et al.[40] reported that the fuel cell performance with a thin membrane of polytetrafluoroethylene bearing perfluorosulfonimide side chains (psi) was notably better than that of fuel cells based on a commercially available Nafion. This suggests that the sulfonimide ionomers are more favorable for proton conduction.

This work deals with the synthesis and characterization of aromatic ionomers bearing perfluorosulfonimide functions (SiX/Y) with different IEC and block lengths. The grafting of perfluorosulfonimide side chains was performed by Ullmann coupling reaction. In order to evaluate the impact of the anion on the transport properties, the water uptake, proton conductivity and water diffusion coefficient of SiX/Y membrane were compared with those of partially-fluorinated poly(arylene ether sulfone) multiblock copolymers bearing pendant perfluorosulfonic acid side chains (InX/Y).

2. Experimental Section

2.1. Materials

Dimethylsulfoxide (DMSO), Dimethylacetamide (DMAc), Copper (Cu) powder for organic synthesis, purchased from Sigma Aldrich, Potassium Carbonate (K_2CO_3), Bromine (Br_2), Toluene, ethyl acetate, purchased from Acros Organics, 5-iodooctafluoro-3-oxapentanesulfonyl fluoride ($ICF_2CF_2OCF_2CF_2SO_2F$), purchased from Interchim, Trifluoromethanesulfonamide ($CF_3SO_2NH_2$), purchased from FluoroChem, Lithium Hydroxide (LiOH), Diethylene Glycol Methyl Ether (DEGME), purchased from Alfa Aesar, were used as received. Acetonitrile (ACN), Dichloromethane (DCM), Trimethylamine (TEA), purchased from Sigma Aldrich, were distilled from Calcium Hydride (CaH_2) before use. Acetic Acid purchased from Sigma Aldrich was distilled under vacuum before use. 4,4'-Difluorodiphenyl Sulfone (DFDPS), 4,4'-Biphenol (BP), and 4,4'-Dihydroxydiphenyl

Sulfone (DHDPS), purchased from Alfa Aesar, were recrystallized from isopropanol before use. Decaflurobiphenyl (DFBP), purchased from FluoroChem, was sublimated before use.

2.2. Synthesis of Ionomers

2.2.1. Synthesis of Perfluorosulfonimide Ionic Compound (I-psiLi)

The synthesis of N-(trifluoromethanesulfonyl)-1,1,2,2-tetrafluoro-2-(1,1,2,2-tetrafluoro-2-iodoethoxy)ethanesulfonamide lithium ($ICF_2CF_2OCF_2CF_2SO_2N^-(Li^+)SO_2CF_3$ or I-psiLi) was displayed in **Scheme 1**. In a typical procedure, 8.400 g (0.0563 mol) of $CF_3SO_2NH_2$ was introduced into a 100-mL two-necked round bottom flask charged with an air condenser, a magnetic stirrer. Then, 10.452 g (0.103 mol) of TEA and 20 mL of ACN, both freshly distilled from CaH_2, were added. The mixture was stirred to dissolve $CF_3SO_2NH_2$ and 20.000 g (0.0469 mol) of $ICF_2CF_2OCF_2CF_2SO_2F$ was added. The mixture was heated to 40 °C and the reaction was carried out ~36−40h. The conversion of reaction was monitored by ^{19}F NMR, when the peak corresponding to SO_2F (44.77 ppm) was disappeared the reaction was stopped. The resulting red mixture was concentrated on the rotary evaporator at 40 °C. The residue was dissolved in (200−250 ml) dichloromethane, washed with 1000 mL of distilled water, and dried over magnesium sulfate. After solvent evaporation at 40 °C, the red oil was obtained.

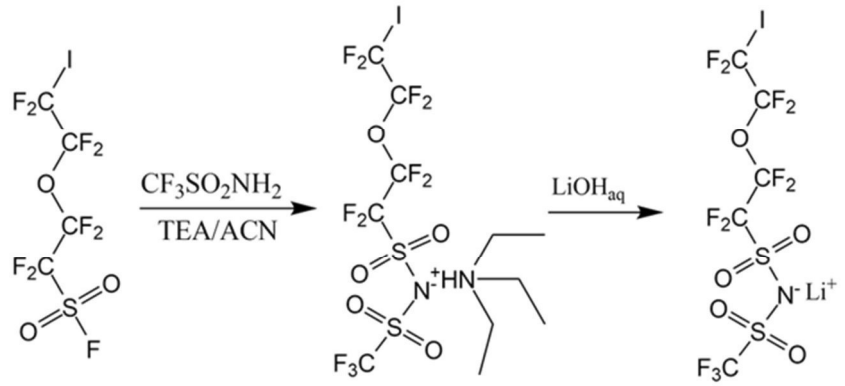

Scheme 1. Synthesis of I-psiLi compound.

^{19}F-NMR (Acetone-d6) δ (ppm): -69.36 (t, ICF_2), -82.06 (t, CF_2O), -86.37 (t, OCF_2), -117.18 (m, CF_2SO_2), -79.87 (s, CF_3).

This salt was dissolved in 0.5 M LiOH aqueous solution (excess 5 % molar of LiOH).[41] After stirring for 15 minutes, water was removed by freeze-drying. The resulting viscous oil was dissolved in ethyl acetate, dried over magnesium sulfate, and concentrated on the rotary evaporator. The residue was dried under vacuum for at 40 °C 24h to obtain the light yellow solid. The final yield of the I-psiLi synthesis is ~65−70 %.

2.2.2. Synthesis of PES-FPES Block Copolymers, BrPES-FPES, and Si Ionomers

The synthesis of multi-block copolymers PES-FPES and BrPES-FPES were described elsewhere (**Scheme 2**).[17] The nomenclature for block copolymer backbones, brominated block copolymer backbones, and ionomers are PES-FPES X/Y, BrPES-FPES X/Y, SiX/Y, respectively, where X and Y are the molar weight of the hydrophilic PES block backbone and the hydrophobic FPES block (both in kg/mol). As an example, Si15/10 refers to an ionomer with the length of PES segment = 15 000 g/mol and of FPES = 10 000 g/mol.

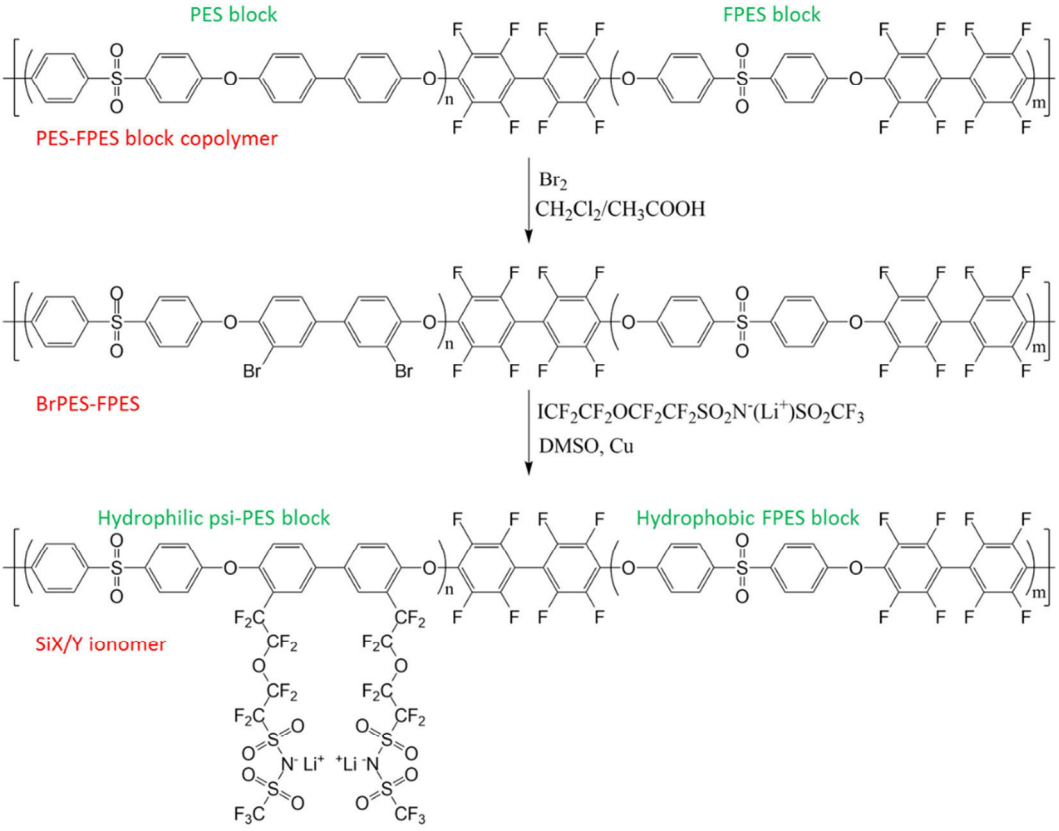

Scheme 2. Synthesis of SiX/Y ionomers.

Synthesis of PES-FPES Block Copolymer Backbones. The multiblock copolymer backbones are synthesized via one-pot-two-reaction synthesis, which was discussed elsewhere.[17] However, due to the low solubility of FPES block in DMSO,[42] all block copolymer backbones in this work were synthesized in DMAc. At first, the PES oligomers terminated by hydroxyl biphenyl units were synthesized. The lengths of PES blocks are modulated by controlling the molar ratio between BP and DHDPS monomers using Carothers' equation. Secondly, the block copolymer PES-FPES is formed by adding to the reaction mixture the two monomers composing the FPES blocks, i.e., DHDPS and DFBP. The ratio (R) between the number of repeating units of PES and those of FPES was calculated by using the ratio between the integration of biphenylsulfone from both blocks. In this study, five

block copolymers with different lengths of blocks were synthesized (**Table 1**). The obtained values appear to be very close to the expected ones. Molecular weight as well as polydispersity index of the PES-FPES block copolymer were summarized in **Table 2**.

^{1}H-NMR: ($CDCl_3$): δ (ppm) 7.91–7.89 (d, 4H), 7.83–7.81 (d, 4H), 7.52–7.50 (d, 4H), 7.09–6.98 (m, 12H).

^{19}F-NMR: ($CDCl_3$): δ (ppm) -137.81 (s, Ar–F), -138.20 (m, Ar–F), -153.28 (s, Ar–F), -153.68 (m, Ar–F).

Table 1. Theoretical Mn of PES, Experimental Mn of FPES, the Ratio, R, between the Repeating Units of PES Block, and Those of FPES Blocks

polymer code	Mn_{PES_theo} [a] (g/mol)	Mn_{FPES_exp} [b] (g/mol)	R_{theo} [a]	R_{exp} [c]
PES-FPES 5/5	5000	4900 ± 200	1.40	1.45 ± 0.03
PES-FPES 10/10	10000	10600 ± 400	1.38	1.41 ± 0.04
PES-FPES 15/15	15000	16100 ± 1400	1.37	1.35 ± 0.03
PES-FPES 15/10	15000	10800 ± 350	2.08	2.16 ± 0.02
PES-FPES 15/05	15000	5200 ± 200	4.32	4.26 ± 0.08

[a]theoretical value, [b]determined by ^{19}F NMR, [c]determined by ^{1}H NMR.[17]

Bromination of PES/FPES. The bromination reaction was performed under inert atmosphere (Argon) using bromine as reactant in the presence of acetic acid. The bromination degree, calculated from ^{1}H-NMR,[17] is from 95 to 98 %.

Synthesis of SiX/Y Ionomers. The perfluorosulfonimide-based ionomers were synthesized via Ullman coupling reaction of BrPES-FPES with lithium 1,1,2,2-tetra- fluoro-2-(1,1,2,2-tetrafluoro-2-iodoethoxy)ethanesulfonimide (I-psiLi, **Scheme 2**) (cross coupling reaction). In a typical procedure, 4.000 g (3.599 mmol of BP units) BrPES-FPES 5/5, 3.43 g (54.0 mmol) of copper powder and 30 ml of DMSO were added into a 100-mL three neck round bottom flask, equipped with a mechanical stirrer, a condenser, an argon inlet-outlet and an addition funnel. The mixture was stirred at 60 °C until the polymer was completely dissolved. Then, the bath temperature was increased to 120 °C under strong stirring for 2h. After that, 8.076 g (14.40 mmol) of I-psiLi compound dissolved in DMSO (30% m/v) was added drop-by-drop into the reaction mixture and the bath temperature was increased to 140 °C. The reaction was allowed to proceed at that temperature for 24h. After the residue of

copper powder was removed by centrifugation at 5000 rpm for 15 minutes and the ionomer was precipitated into 1000 mL 1M HCl aqueous solution and kept with strong agitation for 24h. Finally, the polymer was filtered and washed with distilled water until neutral pH. The ionomer was dried at 60 °C under vacuum for 24h.

^{1}H-NMR: (DMSO.d6): δ (ppm) 8.09–7.82 (m), 7.45 (s), 7.35–7.32 (m), 7.27–7.05 (m).

^{19}F-NMR: (DMSO.d6): δ (ppm) -78.77 (d, CF_3SO_2), -81.16 (s, $-CF_2O$), -86.11 (s, $-OCF_2$), -110.70 (d, $Ar-CF_2$), -116.54 (s, CF_2SO_2), -137.81 (s, Ar–F), -138.20 (m, Ar–F), -153.28 (s, Ar–F), -153.68 (m, Ar–F).

Table 2. Molecular Weights of PES/FPES Copolymers and SiX/Y Ionomers

polymer code	Mn (kDa)[a]	Mw (kDa)[a]	Mw/Mn[a]	polymer code	Mn (kDa)[b]	Mw (kDa)[b]	Mw/Mn[b]
PES-FPES 5/5	108	330	3.07	Si5/5	150	396	2.64
PES-FPES 10/10	113	278	2.46	Si10/10	167	379	3.74
PES-FPES 15/15	126	378	3.00	Si15/15	264	724	2.74
PES-FPES 15/10	92	258	2.79	Si15/10	186	570	3.06
PES-FPES 15/05	90	262	2.91	Si15/05	126	408	3.24

[a]SEC performed in THF, solution filtered with PP-based filter. [b]SEC performed in 1M $NaNO_3$ in DMF, solution filtered with PTFE-based filter.

2.3. Membrane Preparation

2.3.1. SiX/Y Membranes

The 7 wt % solution of ionomers in lithium-salt form dissolved in DMSO was stirred for 24h at 60 °C. After removing air bubbles by leaving under vacuum for 30 mins, the solution was centrifuged for 15 min at 5000 rpm to remove solid impurities. The homogeneous mixture was cast onto a clean glass substrate using a casting knife (Elcometer 4340 Automatic Film Applicator). The membrane thickness was controlled by adjusting the distance between the knife and the plate. The solvent was evaporated in an oven at 60 °C for 24h and then submitted to additional thermal annealing at 150 °C for 24h in a closed vacuum chamber. Then the membrane was immersed and rinsed many times with distilled water for 24h to remove solvent residue. The solvent-free membranes, verified by ^{1}H NMR, were converted into their acidic form by stirring in 2M HCl solution for 24h, and then stirred in distilled water for 24h to remove acid residue. Membranes with a thickness of 90–120 μm were obtained.

2.3.2. Nafion Membranes

Nafion® 117 membranes (thickness ~180 mm) were activated by boiling in 1M HNO_3 aqueous solution for 2h, followed by boiling in distilled water for 2h. Then the membranes were washed in deionized water for 48h to eliminate residual acid trace.

2.4. Characterization

2.4.1. NMR Spectroscopy

Chemical structure and constituent of the monomers, oligomers, block copolymers and ionomers were confirmed by ^{1}H, ^{19}F NMR using a Bruker Ascend™ 400 spectrometer. All spectra were obtained from 5 mg of sample dissolved in 0.5 ml solvent of monomers in acetone.d6 (C_3D_6O), oligomers and block copolymers in chloroform.d6 ($CDCl_3$), ionomers in dimethylsulfoxide.d6 (C_2D_6SO).

2.4.2. Ion-Exchange Capacity (IEC)

The IEC (meq. H^+/g) have been calculated by NMR and acid-base titration in DEGME solution and Methyl orange as indicator by following the protocol described elsewhere.[43]

2.4.3. SEC-MALLS

SEC analyses were performed at ambient temperature using a Waters 590 GPC equipped with a Waters 410 differential refractometer and a Waters 745 Data Module. THF and 1M $NaNO_3$ in DMF was used as solvents in the case of PES-FPES X/Y and SiX/Y, respectively (**Table 2**), with flow rate of 1 mL/min through three ultrastyragel columns of 5×10^2, 10^3, and 10^4 Å. The 1 wt% solutions of polymer were filtered through a 0.45 mm Millipore filter based on PP and PTFE, respectively. The calibration was performed using polystyrene standards. Each measurement is repeated twice and the values are calculated if the elution volumes of the two chromatograms are identical.

2.4.4. Water Uptake

The ionomer membranes in acidic form were dried (for 48h at 60 °C under vacuum), weighed, measured the thickness, length, width, and immersed in deionized water at different temperature (between 30 to 90 °C) for 24h. Then the membrane was removed from water, the surface membrane is quickly dried with absorbent paper. The water uptake (WU, wt %) was determined at different temperatures ranging from 30 to 90 °C by **Equation 1**.

$$WU = \frac{W_w - W_d}{W_d} \times 100\% \quad (\mathbf{1})$$

where W_w and W_d are the weight of the wet and dry membranes, respectively.

The hydration number (λ), defined as the number of water molecules absorbed per each sulfonic acid unit, was determined from the water uptake and the IEC, via **Equation 2**.

$$\lambda = \frac{WU \times 10}{IEC \times MW_w} \quad (\mathbf{2})$$

where MW_w is the molecular weight of water.

2.4.5. Density Measurement

The density (D, g/cm^3) of the membranes was measured by Mettler-Toledo's density kits (using the buoyancy technique) at 20 °C with toluene (0.87 g/mL) as liquid phase.

2.4.6. Differential Scanning Calorimetry (DSC)

The DSC measurements were performed using a DSC 1 STAR^e System from Mettler-Toledo. The measurements were carried out under argon flux of 50 mL/min with a heating rate of 20 °C/min from 25 to 200 °C for the first scan. The second scan was performed from 25 to 300 °C for the acid forms. The glass transition temperatures were determined as the mid-point Tg values of the second scan.

2.4.7. Thermal Gravimetrical Analysis (TGA)

The TGA measurements were performed on a TGA 1 STAR^e System supplied by Mettler-Toledo under air flow 20 ml/min (a mixture of 80 % N_2 and 20 % O_2) and a temperature ramp of 10 °C/min from 50 °C to 750 °C. To remove water, the samples were dried at 110 °C under vacuum for 24h before measuring.

2.4.8. Dynamic Mechanical Analysis (DMA)

The DMA was performed with DMA Q800 supplied by TA Instruments in the temperature range from 20 to 350 °C using a temperature ramp of 2 °C/min. The dried membranes, of average dimensions 20×6 mm^2 and thickness of 100−120 μm are mounted to the film-tension clamp in multifrequency-strain mode. The measurement condition was set as follows: frequency 1.0 Hz, preload force 0.1 N, force track 150 %, and strain deformation was fixed at 0.1%.

2.4.9. Water Sorption

The dynamic vapor sorption of ionomer membranes was determined using a DVS Advantage (Surface Measurement Systems Ltd, London, UK). The partial pressure of vapor was controlled by mixing dry and saturated nitrogen using electronic mass flow control. The measurements were carried out at 80 °C and the initial weight of the samples was ≈ 50 mg. The samples were previously dried in the instrument by exposure to dry nitrogen. The sample was considered as equilibrated when the mass change in time (dm/dt) was less than 0.0002 for five consecutive minutes. The relative humidity was increased to 90% by steps of 10%. The measurement error was estimated to be less than 7%.

2.4.10. Proton Conductivity

The conductivity was measured via through-plane impedance technique using a Material Mates 7260 frequency response analyzer and a homemade measuring cell, as described elsewhere.[44] The ionomer membranes equilibrated in water at room temperature for 24h (~0.09−0.12 mm in thickness) were sandwiched between two stainless steel electrodes to form blocking electrodes. The measurements were firstly started at different temperatures (from 30 to 90 °C with a step of 10 °C) at 95% relative humidity (RH), and then at different RH (decreased from 95 to 30% with a step of 10%) at 80 °C. The membrane is stabilized in a climatic chamber (Vötsch VC4018) at measuring condition for 5h before probing data. Zview software was used to analyze and fit data. Equivalent circuit and fitting parameters was described elsewhere.[45] The conductivity was calculated by **Equation 3**.

$$\sigma = \frac{L}{R \times A} \qquad (\mathbf{3})$$

where L is the thickness of the hydrated membrane, A is the electrode area, and R is the bulk membrane resistance.

2.4.11. Small-Angle Neutron Scattering (SANS)

SANS measurements were performed on PAXY spectrometer at Laboratoire Léon-Brillouin (Paris, France) and D22 spectrometer at Institut Laue-Langevin (Grenoble, France). The solvent-free acidified membranes were measured using the same protocol described elsewhere.[17,42,45] The membranes with different hydration degree were taken out from water, inserted in quartz Helma cells, and maintained at room temperature before the measurement.

2.4.12. Proton Diffusion Coefficients

The self-diffusion coefficients of water were measured by pulsed field gradient NMR methods (PFG-NMR) using a 9.4T Bruker 400 with a 5-mm diffusion probe and temperature control of ±0.5 °C. The ionomer membranes in acidic form were firstly dried at 60 °C under vacuum for 48h and two series of hydrated membranes were prepared as follows:

i) Low-hydration membranes ($\lambda < 10$): the dry membranes were cut in band of 10×3 mm^2 (the thickness ranging between 0.09 and 0.12 mm) and introduced into NMR tubes. The NMR tubes were equilibrated at different RH for one week at 80 °C in a mobile glove box and quickly sealed before the measurement. Salt saturated aqueous solutions were used to fix the vapor pressure, e.g., LiCl, $MgCl_2$, $Mg(NO_3)_2$, and KCl for 11%, 32%, 52%, and 85%, respectively.[46]

iii) High-hydration membranes ($\lambda > 10$): the dry membranes were immersed in water at different temperatures (from 20 to 90 °C) for 24h, and then cut in bands with the following dimensions: 10 mm length, 3 mm width, and thickness ranging between 0.10 and 0.15 mm. After removing from water, the membranes bands were wiped up quickly with absorbing paper and introduced in an NMR sealed tube.

3. Results and Discussion

3.1. Synthesis of SiX/Y Ionomers

Five multi-block copolymers bearing perfluorosulfonimide side chains (**Table 1**) were synthesized via cross-coupling reaction between BrPES-FPES and I-psiLi precursor (**Scheme 2**) by following a protocol previously reported for the ionomers functionalized with perfluorosulfonic acids (InX/Y).[17] However, it has to be mentioned, despite the same spacer between the iodide and ionic function (i.e., sulfonated I-psLi[17] or sulfonimide I-psiLi) the synthesis of SiX/Y occurs with lower yield. As an example, by using an excess of 1.5 I-psiLi per Br (from Br-PES-FPES) (**Scheme 2**) a chemical yield of 60% was obtained for SiX/Y instead of 85% in the case of InX/Y. Moreover, even in presence of higher excess of precursor

(I-psiLi/Br ratio ~3), the chemical yield of cross-coupling reaction was 85–90% (against 100% in the case of InX/Y ionomer) (**Table S1**). It seems the side reaction, consisting in the homocoupling reaction between I-psiLi, is promoted by the sulfonimide function. Also, we suppose the bulkiness of sulfonimide makes more difficult the second substitution on polymer structural unit.

The grafting degree of perfluoroalkyl sulfonimide groups as well as the IEC of SiX/Y was determined by ^{19}F NMR spectroscopy (**Figure 1**) and by acid base titration. Based on the ^{19}F NMR, the IECs are calculated with a good accuracy (**Table 3**), using the **Equation 4** and **Equation 5**.

$$IEC_{NMR} = N_{NMR} \times IEC_{theo} = \frac{N_{NMR} \times \chi n_{PES}}{\left(Mn_{ps-PES} + Mn_{FPES}\right)} \times 1000 \qquad (\mathbf{4})$$

$$N_{NMR} = \frac{2 \times I_1}{\left[(I_6) \times R_{exp}\right]} \qquad (\mathbf{5})$$

where N_{NMR} is the number of ionic function per PES repeating unit, I_1 is peak integral of F_1 (-110.70 ppm), I_6 is peak integral of fluorine atoms of the FPES block [F_6 (-153.28 ppm) or F_7 (-137.81 ppm)] + peak integral of fluorine atoms at the end of the FPES block ($F_{6'}$ or $F_{7'}$, respectively). χn_{PES} is average repeating unit number in PES blocks, Mn_{FPES} is molar mass of FPES block. $Mn_{psi\text{-}PES}$ is molar mass of psi-PES block = $(M_{PES} + N \times M_{psi}) \times \chi n_{PES}$ (where M_{PES} is molar mass of structural unit of PES and M_{psi} is molar mass of psi side chain).

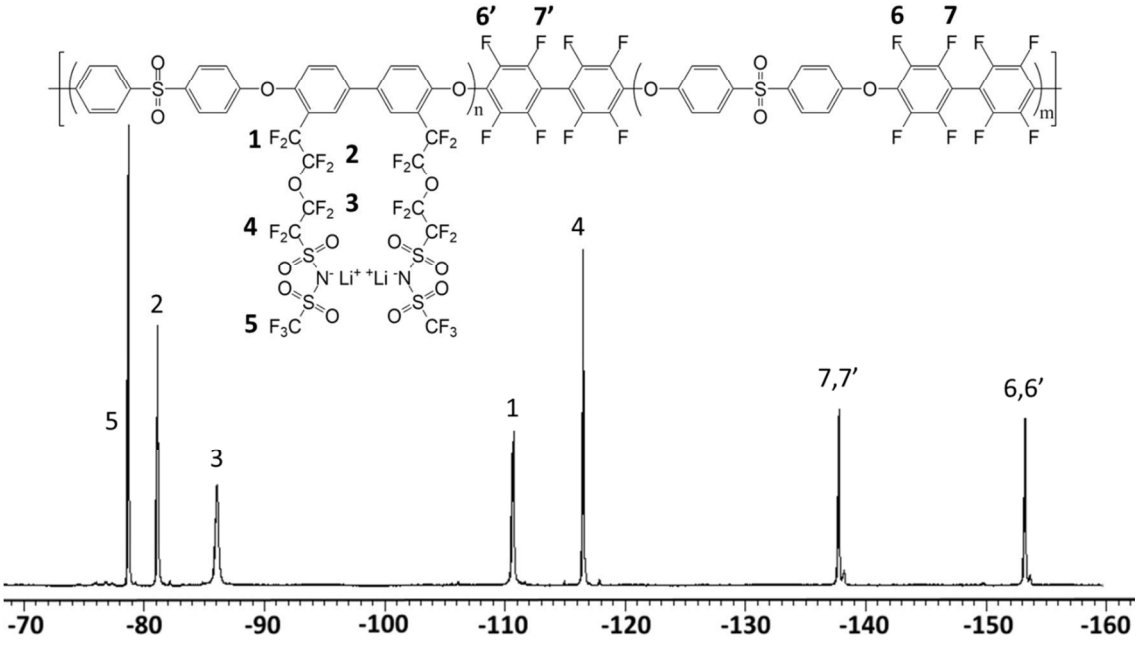

Figure 1. ^{19}F NMR spectra of ionomer Si5/5 (Solvent: DMSO.d6).

Two ionomer series are proposed for this study: the first series concerns the ionomers with same IEC (~1.0 meq. H^+/g), the lengths of the backbone of both blocks varying between 5000 and 15000 g/mol (the block-series − Si5/5, Si10/10, Si15/15) and the second series consisting of ionomers with different IEC (the IEC-series). In the latter, the length of block PES is maintaining constant (15000 g/mol) while the FPES block is varied from 15000 g/mol to 5000 g/mol, e.g., Si15/15, Si15/10, Si15/5.

Table 3. IEC of SiX/Y Ionomers and Nafion® 117 Determined from NMR Spectra and by Titration

ionomers	IEC_{theo} [a] (meq H^+/g)	IEC_{NMR} (meq H^+/g)	$IEC_{Titration}$ (meq H^+/g)	IEC_{mean} (meq H^+/g)	d (g/cm^3)	IEC_v (meq H^+/cm^3)
N117	0.90	-	0.91	0.91	2.04	1.84
Si5/5	1.23	1.03 ± 0.03	0.99 ± 0.03	1.01 ± 0.03	1.61 ± 0.02	1.63 ± 0.03
Si10/10	1.22	1.02 ± 0.03	0.98 ± 0.04	1.00 ± 0.04	1.60 ± 0.02	1.60 ± 0.03
Si15/15	1.22	1.04 ± 0.04	1.03 ± 0.04	1.04 ± 0.04	1.61 ± 0.02	1.67 ± 0.04
Si15/10	1.32	1.15 ± 0.05	1.10 ± 0.05	1.13 ± 0.05	1.63 ± 0.03	1.84 ± 0.05
Si15/5	1.45	1.28 ± 0.05	1.21 ± 0.05	1.25 ± 0.05	1.63 ± 0.03	2.03 ± 0.05
In10/15[c]	1.27	1.23 ± 0.05	1.11 ± 0.05	1.17 ± 0.05	1.61 ± 0.03	1.9 ± 0.1
In15/15[c]	1.45	1.37 ± 0.05	1.28 ± 0.10	1.32 ± 0.10	1.63 ± 0.03	2.2 ± 0.1

[a]Calculated considering two ionic function/repeat unit of PES block. [b]In10/15 and In15/15 were added for comparison.[42]

The density of SiX/Y ionomers was found to be close to 1.6 g/cm^3. The volumic IEC (IECv) of SiX/Y ionomers are lower (Si5/5, Si10/10 Si15/15), similar (Si15/10) or higher (Si15/5) than that of Nafion® 117. The perfluorosulfonimide groups have larger molar mass (212.1 g/mol of $-SO_2NHSO_2CF_3$ as compared to 81.1 g/mol of $-SO_3H$) contributing to the whole ionomer molar mass. It means that more ionic groups need to be added to raise to a certain value of IEC, leading to a longer hydrophilic block, as compared to InX/Y.

3.2. Thermal and Thermomechanical Properties

The degradation temperature (T_d) and glass transition temperature (T_g) of ionomers were determined by TGA and DSC, respectively. In **Figure 2** the TGA curves of copolymer backbone, PES-FPES 5/5, and ionomer Si5/5 are represented. The grafting of the perfluoroalkyl sulfonimide side chain leads to an important decrease in polymer thermal stability; the degradation onset is around 260 °C which is approximatively 150 °C lower than that of PES/FPES 5/5. The T_d seems to be independent from IEC and the lengths of blocks (**Table S2**).

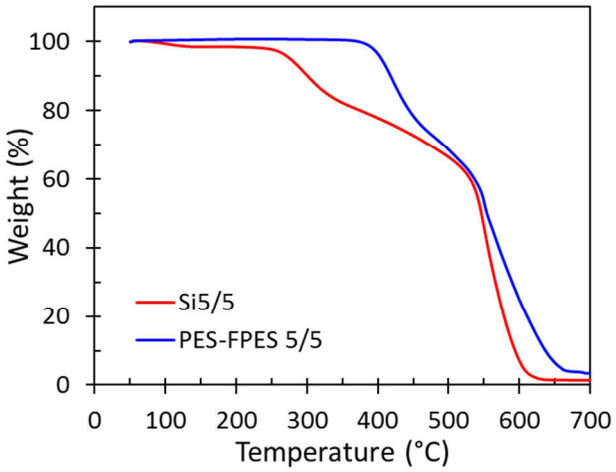

Figure 2. TGA curves of PES/FPE 5/5 (blue) and Si5/5 (red).

The degradation temperature values of SiX/Y are much lower than that of Nafion bearing perfluorosulfonimide side chains, for the latter, a T_d of 400 °C was reported.[30] It seems that the perfluorosulfonimide moieties are less thermally stable when attached to an aromatic polymer backbone than to a perfluorinated polymer backbone. A similar behavior was observed by Chang et al.[24] in the case of perfluorosulfonic acid moieties.

However, by comparing with their homologue, poly(arylene ether sulfone)s bearing perfluorosulfonic acid (InX/Y), the thermal stability of ionomer SiX/Y is improved with more than 40 °C.[17,24] The first degradation step on poly(arylene ether sulfone)s bearing perfluorosulfonic acid, due to the dehydration process of perfluorosulfonic functions at ≈ 220 °C, does not take place in the case of SiX/Y ionomers. Moreover, the introduction of a perfluorinated spacer between poly(arylene ether sulfone) backbone and the acidic functions induces an important increase of T_d due to the greater stability of perfluosulfonimide groups as compared to aryl sulfonimide one.[47,48]

The DSC thermograms of PES-FPES block copolymers show one Tg at ~225 ± 2 °C that is close to that of PES block (**Table S2** and **Figure 3**).[17] Two transition temperatures were observed for all multi-block ionomer samples (**Table 4**), indicating a micro-phase separation. In the case of the block series both Tg values increase with the lengths of block copolymers. The upper Tg values are close to that of polymer backbone (~220 ± 2 °C) while the lower Tg is ~142±2 °C for the shorter block lengths (Si5/5) and its value slightly increases with the block molar mass. Taking into account the multi-block copolymers structures and the DSC data of PES-FPES (**Table S2**) it can be supposed that the upper values corresponds to FPES blocks while the lower values corresponds to the glass transition of psi-PES chains.

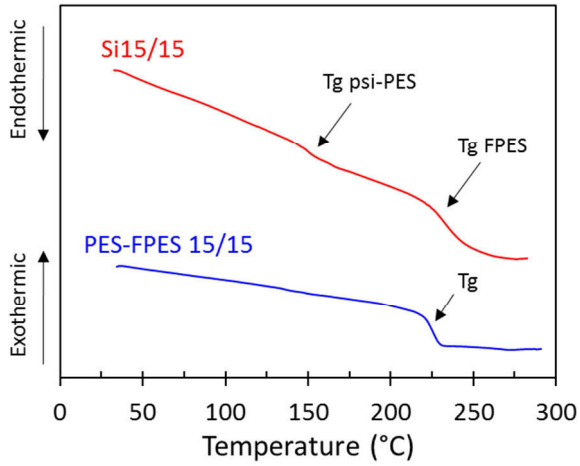

Figure 3. DSC curves of PES-FPES 15/15 and Si15/15 membranes.

Yet, analyzing the series with different IEC, the decrease of the length of FPES block induces a peculiar behavior on both Tgs. First it can be noticed, despite the same molecular weight, the Tg of psi-PES decreases significantly with the length of FPES blocks. Thus the Tg of psi-PES of Si15/15 is close to 152 °C, which is with 16 °C higher than that of Si15/5. The increase of FPES length might lead to larger, more rigid and more percolated hydrophobic domains, which could have an influence on the Tg of psi-PES chains. The FPES domains constraint probably the psi-PES domains, in the case of longer FPES chain more energy is needed to allow psi-PES chain moving. As concerning the Tg of FPES, the decrease of the block molecular weight from 15 kg/mol to 5 kg/mole induces a decrease of its Tg with more than 50 °C (while in the case of "block length series" only a decrease of 8 °C is observed). This surprising behavior suggests a poorer FPES phase separation for copolymers with shorter FPES blocks.

More insights on the phase separations and thermal behavior can be obtained from the DMA. In **Figure 4a** and **4c** the evolutions of storage modulus and tan δ, respectively, of the ionomer block series versus temperature are represented.

Table 4. Glass Transition Temperature (Tg), Degradation Temperature (Td), Alpha Relaxation (Tα) and Storage Modulus of Ionomers

ionomers	$Tg_{mid\text{-}point}$ (°C)	Td_{onset} (°C)	Tα[a] (°C)	E'[b] (MPa)
Si5/5	142 ± 2, 218 ± 2	265 ± 2	144 ± 2	~1410
Si10/10	148 ± 2, 221 ± 2	265 ± 2	151 ± 2	~1450
Si15/15	152 ± 2, 226 ± 2	267 ± 2	160 ± 2	~1450
Si15/10	150 ± 2, 190 ± 2	265 ± 2	142 ± 2	~1390
Si15/05	136 ± 2, 171 ± 2	269 ± 2	134 ± 2	~1360

[a]The value of Tα was taken as temperature at peak of Tan δ. [b]at 80°C °C in dry state.

The relaxation temperatures of ps-PES are increased with the lengths of block in accordance with the DSC results (**Table 4**). The second transition, corresponding to the α relaxation of the FPES block, cannot be clearly observed, in both, the storage modulus and tan δ plots. This is related to the dramatically decrease of storage modulus after psi-PES relaxation. This huge modulus decrease is attributed to the high-volume fraction of psi-PES, i.e., more than 70 wt% (**Table S3**). However, it can be noticed the mechanical behavior, after the psi-PES transition, is dependent on the block lengths. Thus for the ionomers with longer blocks (Si15/15), a storage modulus of approximately 5 MPa is maintain up to 220 °C and a shoulder appears, on tan δ, at around 200 °C. In the case of shorter block (Si5/5), after psi-PES relaxation the storage modulus of membrane is completely dropped. All the three copolymers contain roughly the same fraction of FPES, the different mechanical behavior could be attributed to the percolation and chain entanglements in FPES domains. As concerning the IEC series, by decreasing the volume fraction of FPES, IEC-series, (**Figure 4b** and **4d**), the α relaxation of psi-PES block decrease significantly in accordance with DSC results.

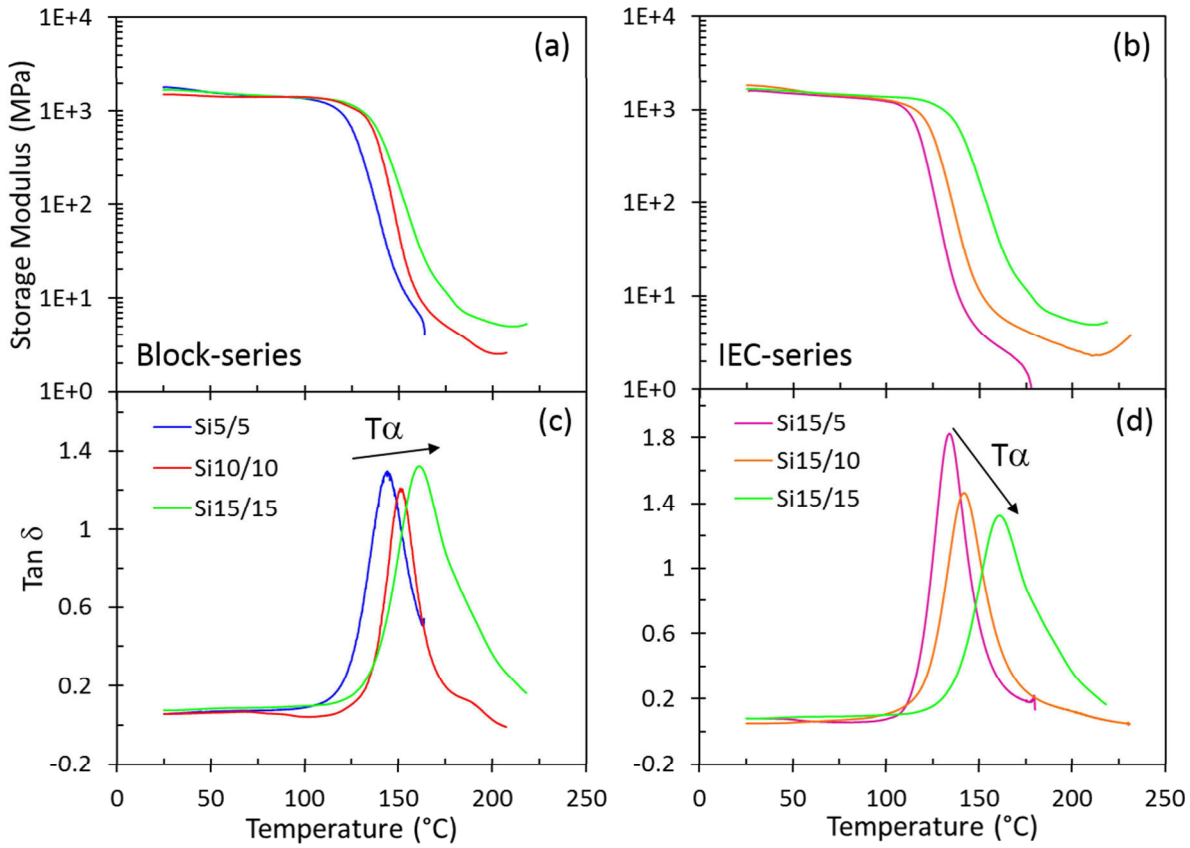

Figure 4. Storage modulus (E') and Tan δ vs temperature of block-series (a and c) and IEC-series (b and d).

3.3. Morphology

The microstructure of the aromatic block ionomers were investigated by SANS. In general, a well-defined scattering maximum indicates the existence of two separated phases characterized by two different neutron-scattering length densities producing a significant contrast term. The position (Q_{max}) of the scattering maximum is related to the average mean separation distance $d = 2\pi/Q_{max}$ between scattering objects.[49] In the following, we firstly establish the structural features of the dried membranes, then analyze the structural organization of hydrated membranes, and finally give details on the impact of water content on the swelling law.

The SANS profiles of all the dried membranes (**Figure 5**) show one peak, indeed the position of scattering maxima, the shape, the width and the intensity of peak depending profoundly on ionomer structure (block length, IEC). The scattering maxima are observed at Q values, from ~0.02–0.03 $Å^{-1}$ and for $Q > 0.1$ $Å^{-1}$ an extended flat profile is found (**Figure 5a**). Based on DSC and DMA results, in combination with the previous reported data,[42,45] the Q peak can be related to the self-assembled arrangement of hydrophilic psi-PES and hydrophobic FPES

blocks. However, with the decrease of the block lengths the mean separation distance is lower and the structure regularity (intensity/width of peak) is poorer. The nature of the hydrophobic/hydrophilic interface of dried membranes can be analyzed by subtracting the high-Q SANS background. As shown in **Figure 5b**, the intensities of the peak follow the Porod's law (nicely scale as Q^{-4}), which proves a sharp interface and a neat separation between hydrophilic and hydrophobic block domains.[50]

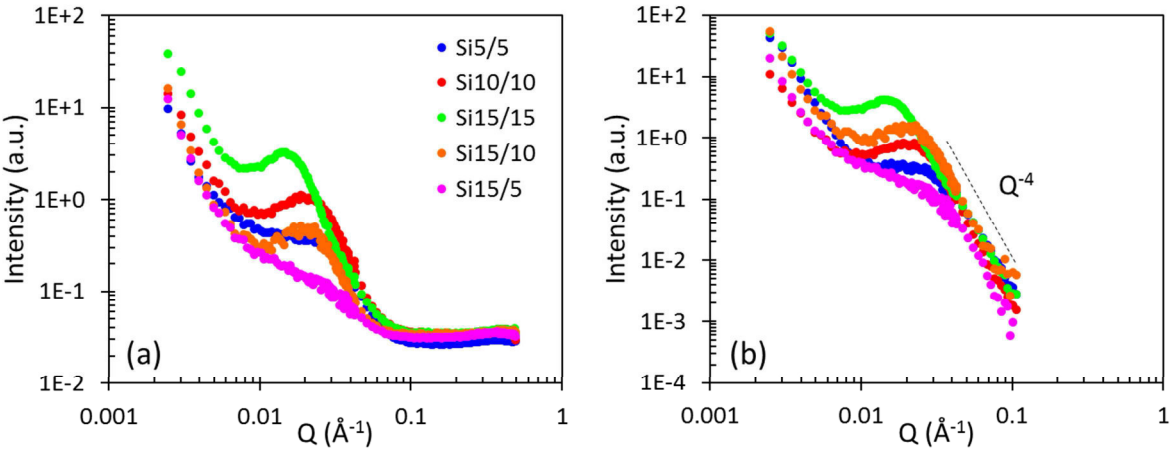

Figure 5. SANS profiles of dried SiX/Y ionomers (a) before and (b) background subtraction.

By hydrating the membranes a new peak appears at higher-Q values which are in the Q-range values corresponding to the ionic peak of Nafion[6,51] and of ionomers bearing perfluorosulfonic acids.[17] This peak can be attributed to the aggregation of perfluorosulfonimide functions and phase separation between the ionic functions and PES backbone. From the Q position, characteristic distance has been interpreted as the mean separation distance between inter-connected ionic domains[8,7] or elongated hydrophobic aggregates embedded in a continuous hydrophobic phase.[10,52,53]

Thus, it can be supposed the SiX/Y in hydrated state has three-phase microstructure: (i) phase 1 composing of FPES blocks (8 structural protons per unit), phase 2 composing of PES blocks (14 structural protons per unit) and phase 3 including side-chains, perfluorosulfonimide groups, protons and water (2λ hydration protons + 2 protons per unit). This organization feature was already proposed for their homologues bearing perfluorosulfonic acids.[45]

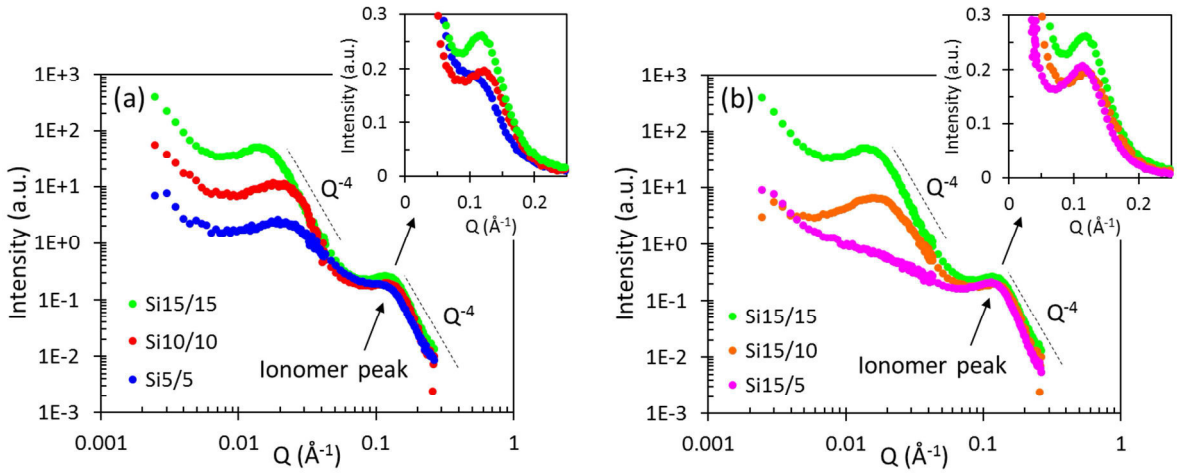

Figure 6. Normalized SANS profiles of hydrated SiX/Y membrane at close hydration number (λ ~20–25): (a) Block-series and (b) IEC-series.

By analyzing the SANS profiles, at the close value of hydration number and as function of ionomer structure, it can be concluded that for the block series with the increase of block lengths from 5000 g/mol to 15000 g/mol (**Figure 6a**), the ionomer peak slightly shifts toward higher Q, signifying the mean separation distance between inter-connected ionic domains decrease slightly. It could indicate a better organization (more aligned, less dead zone) of longer ionic blocks than shorter ones. The hydrophobic peak (at low-Q region) significantly shifts toward lower Q, signifying the correlation distance increase notably with the size of both blocks.

On the other hand, for the IEC series, when the block size of psi-PES was conserved at 15000 g/mol and the block size of FPES was decreased from 15000 g/mol to 5000 g/mol (**Figure 6b**), the ionomer peak appears exactly at the same Q value while the hydrophobic peak shifts to higher Q and drastically decreases in intensity. Moreover, it becomes larger and almost flat in the case of Si15/5. The observed behavior reveals the role of FPES block length in maintaining the organized structure at this scale range. Based on SANS results (on both dried and hydrated membranes), along with DSC and DMA it can be concluded with the decrease of the FPES length and thus of FPES volume fraction the size and the distribution of FPES domains are very inhomogeneous. When the hydration number (λ) is increased, both ionomer peak and hydrophobic peak shift toward lower Q indicating the increase of correlation distance of both domain (d_{ionic} and d_{block}) (**Figure S1**).

The correlation distances as function of λ are represented in **Figure 7a–b**. By extrapolation at λ = 0 the d_{0_ionic} and d_{0_block} were obtained. The d_{0_ionic} is 2.5 ± 0.2 nm and it is good correlation with the length of side chains (~2×1.3 nm) (**Table S4**).

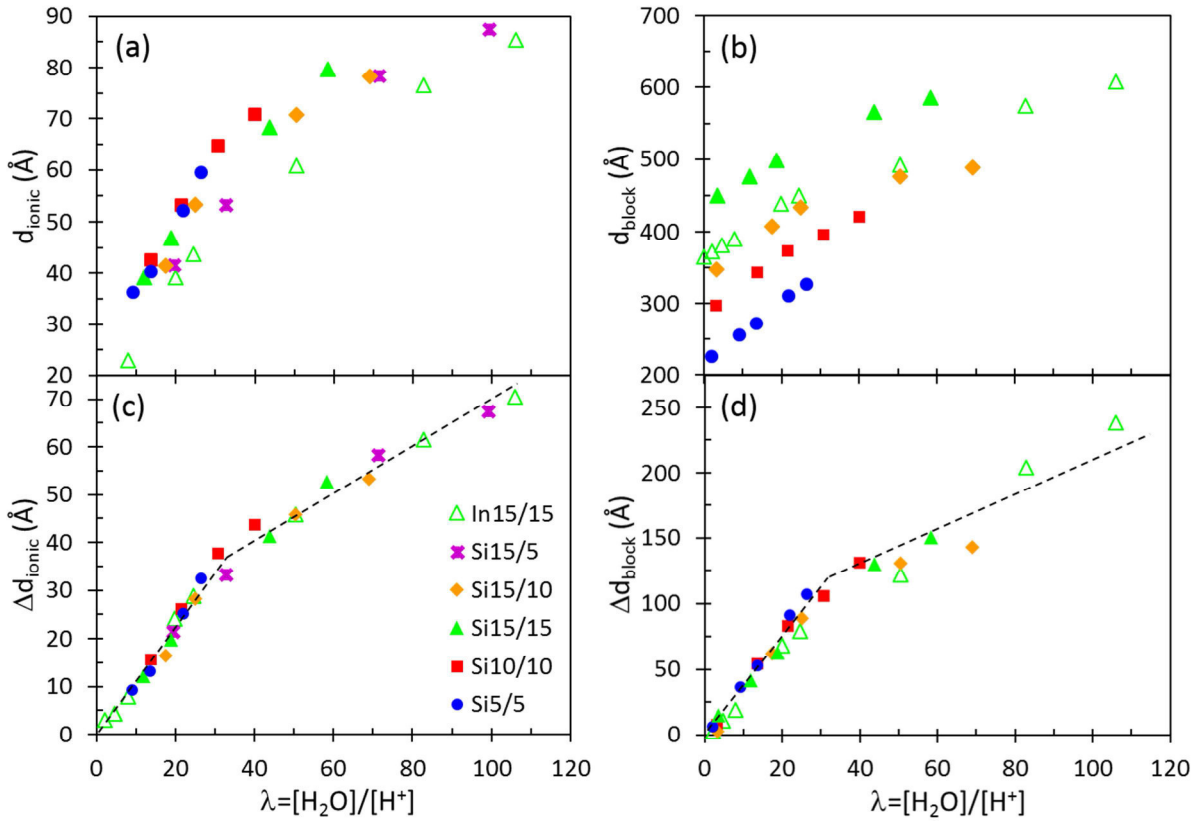

Figure 7. Variations of mean separation distances of (a) ionic domains (d_{ionic}), (b) block structures (d_{block}) as a function of λ and their expansions: (c) Δd_{ionic} and (d) Δd_{block}.

On **Figure 7c** and **7d** we report the variations of ionic and block domains, i.e., $\Delta d_{ionic} = d_{ionic} - d_{0\_ionic}$ and $\Delta d_{block} = d_{block} - d_{0\_block}$, respectively, as a function of λ. If we assume that the shape and the size of the flat ps-PES aggregates is unchanged upon hydration, the quantity Δd_{ionic} represents the mean width of the ionic domains (inter-lamellae or inter-ribbon spacings), and therefore can be usefully reported as a function of λ to quantify the expansion of the ionic phase (**Figure 7c**). We found that the aromatic ionomers exhibit a behavior which is strikingly similar to that of the aromatic ionomers bearing perfluorosulfonate, these observations suggest that the organization of ionic domains, the local topology and swelling behavior of both kind of ionomers are rather similar.

3.4. Water Uptake and Proton Conductivity

Referred to as an important property of proton exchange membranes, water uptake (WU) is determined by membrane's chemical composition, IEC, morphology and mechanical properties, etc. The WU has vital effects on proton conductivity, mechanical properties as well as morphology change, as discussed above. In **Figure 8,** the water uptake of SiX/Y ionomers were shown as hydration number (λ) obtained by immersing dry membranes in

water at different temperature. The results were compared with those of InX/Y with similar bock structure and IEC as well as with that of Nafion® 117.

The water uptake of SiX/Y block lengths series are very close to Nafion at low temperature but significantly enlarge above 50 °C, indicating the water uptake of the aromatic ionomers is more dependent on temperature (**Figure 8a**). Moreover, the water uptake increases significantly with the IEC and block lengths. A similar behavior was reported with perfluorosulfonated aromatic ionomer and was explain by better percolation of hydrophilic channels.[42,54]

Yet, by comparing the SiX/Y and InX/Y at the same IEC, higher water uptake would be anticipated for the former due to the longer hydrophilic domains. However, Si15/10 membrane absorbs similar amount of water as In10/15, probably, due to the less hydrophilic nature of sulfonimide groups (**Figure 8b**). On the other hand, Si15/5 and In15/15 show similar water uptake despite lower IEC of the former (IEC ~1.25 and ~1.32 mequiv. H^+/g, respectively) due probably to the poor percolation of FPES domains and lower elastic counter pressure emerging from the deformation of hydrophobic domain.

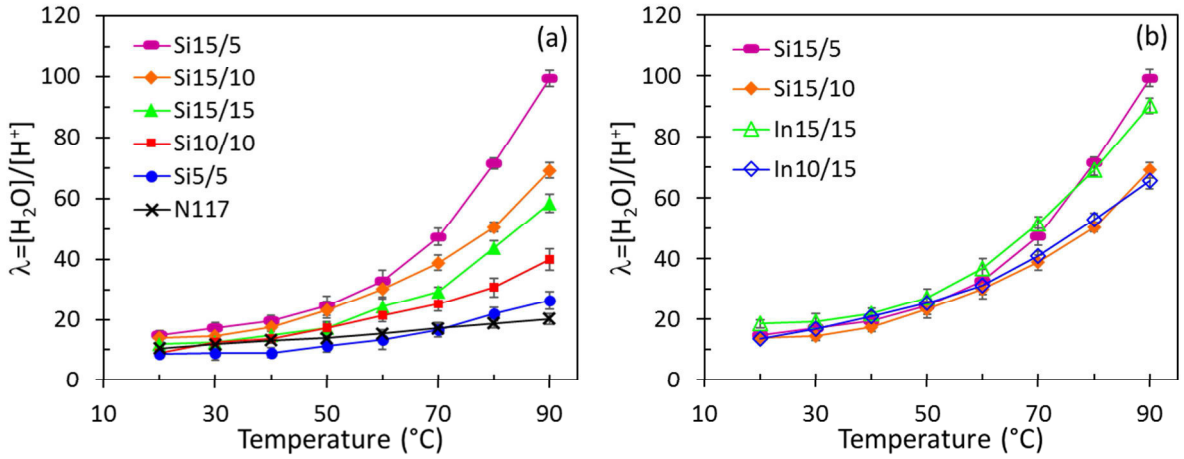

Figure 8. a) Water uptake of SiX/Y ionomers in comparison with Nafion® 117, and b) Water uptake of SiX/Y ionomers in comparison with InX/Y.

In addition to water uptake, proton conductivity (σ) is a key property of PEMs. The proton conductivity is directly controlled by the connectivity of hydrophilic domains and the efficiency of proton conduction mechanism. The evolution of conductivity with 1000/T of three ionomers Si5/5, Si10/10 and Si15/15 follow the same trend as that of Nafion (**Figure 9a**), and seems to be less thermal activated as compared with their homologues InX/Y (**Figure 9b**).[17,42] The conductivity generally rises with hydration degree as a consequence of (i) the reduction of confinement effect at nanoscale, (ii) the increase of connectivity, and (iii)

the development of structural diffusion.[17] In the case of block lengths series, the conductivity significantly increases with block length, Si15/15 > Si10/10 > Si5/5 (**Figure 9a**), presumably due to enhanced percolation and improved connectivity of hydrophilic channels. As a consequence, the conductivity of Si15/15 is superior to Nafion despite lower IECv. With increasing IEC the conductivities increase due to the higher concentration of protons and efficiency of charge carriers.

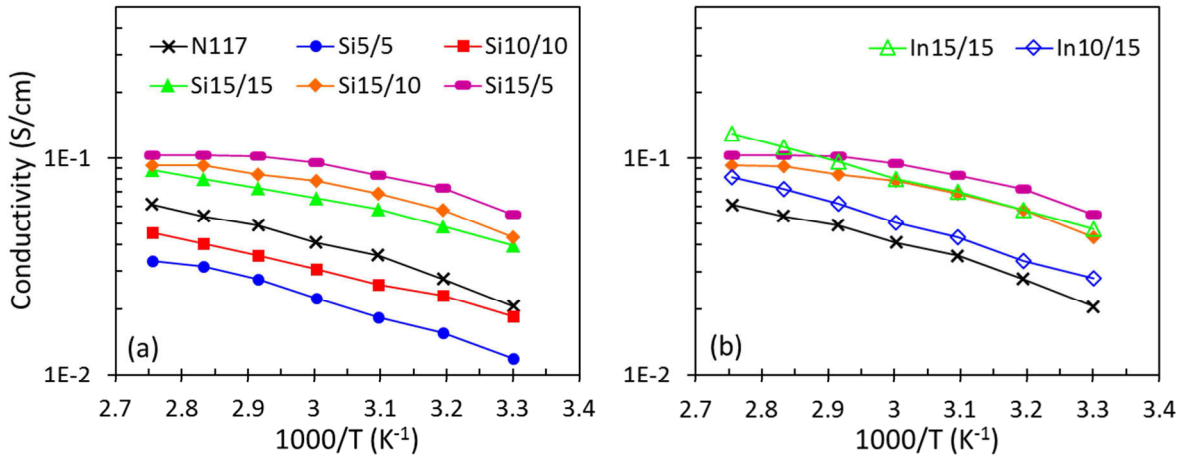

Figure 9. Proton conductivity of SiX/Y ionomers at 95 % RH as function of 1000/T; a) in comparison with Nafion® 117 and b) in comparison with InX/Y with similar IEC and water uptake, and Nafion® 117.

To compare the conductivity of SiX/Y and InX/Y we selected ionomers with close IEC and water uptake, i.e., Si15/10 vs In10/15 and Si15/5 vs In15/15. The Arrhenius plots of the four aromatic ionomers in comparison with Nafion 117 are represented in **Figure 9b.** At lower temperature, the Si15/10 gives conductivities almost two time higher than In10/15. By increase the temperature, and consequently of the water uptake, the gap in conductivity between two ionomers became smaller. Similar results were obtained for the ionomers with higher IEC, i.e., Si15/5 vs In15/15, however, but with lower conductivity difference are lower.

By taking into account the similar water uptake, microstructure, and water confinement, it can be concluded that the proton conduction of SiX/Y ionomer membranes, at 95% RH is more efficient, especially at lower temperature. This is probably due to (i) the better dissociation of acidic function in SiX/Y, and (ii) the higher flexibility of psi anion as compare to that of ps anion.[55–61] The flexibility of anion could influence the local viscosity in the ionic channels that can impact the water diffusion rate. To confirm our assumption on the water diffusion rate, we measured the water diffusion coefficient by PFG-NMR and it was observed

at the same λ the values of water diffusion coefficient of SiX/Y are only slightly higher than those of InX/Y (**Figure 10**).

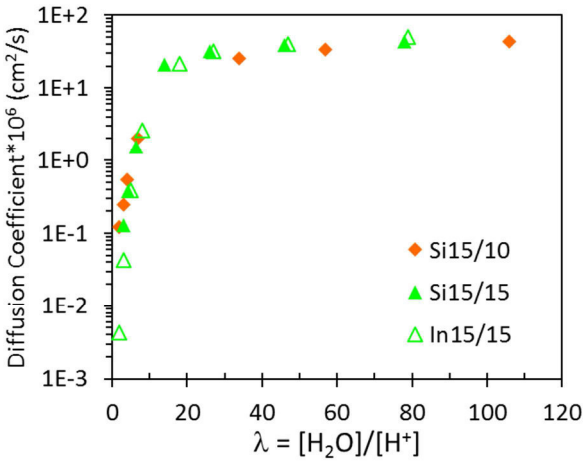

Figure 10. Diffusion coefficient as a function of λ of SiX/Y ionomers in comparison to InX/Y ionomer.

Yet, by analyzing the conductivities at 80 °C at different RH, it was very surprising to note all the membranes SiX/Y give lower conductivity values than those of Nafion® 117 (**Figure 11a**) and InX/Y (**Figure 11b**), with similar IEC, below 80% RH. At 30 % RH, for example, the highest conductivity for SiX/Y was ~3.8×10^{-4} S/cm while for Nafion was ~2.4×10^{-3} S/cm. The water sorption measurements performed at 80 °C, however, showed similar behavior for both ionomers, in the whole range of RH (**Figure 11c**), and their values are superior to those of Nafion. It can be pointed out the increase of conductivities for all the SiX/Y ionomers is much more activated by the RH as compared to that of Nafion® 117 and InX/Y, that means the conduction mechanisms are different in these membranes. At above 80 % RH, the conductivities of Si15/15, Si15/10 and Si15/5 are higher than those of Nafion® 117.

To explain the lower conductivity of SiX/Y membranes two hypotheses can be emitted: (i) the hydrophilic domains are less connected at low RH, or (ii) the structural proton-diffusion network of proton is not well developed. The diffusion coefficient of water in SiX/Y at low hydration number, i.e., up to 6 are higher than in InX/Y membranes (**Figure 12a**), hence, the first hypothesis is not sustained by the experimental results. By representing the conductivity as function of diffusion coefficient (**Figure 12b**) it can be observed at low λ (up to 6) at same value of water self-diffusion coefficient the proton conductivity is much lower for the SiX/Y as compared to InX/Y. These results should be interpreted by a local organization of anions and/or interaction of anion and proton which impede the proton diffusion.

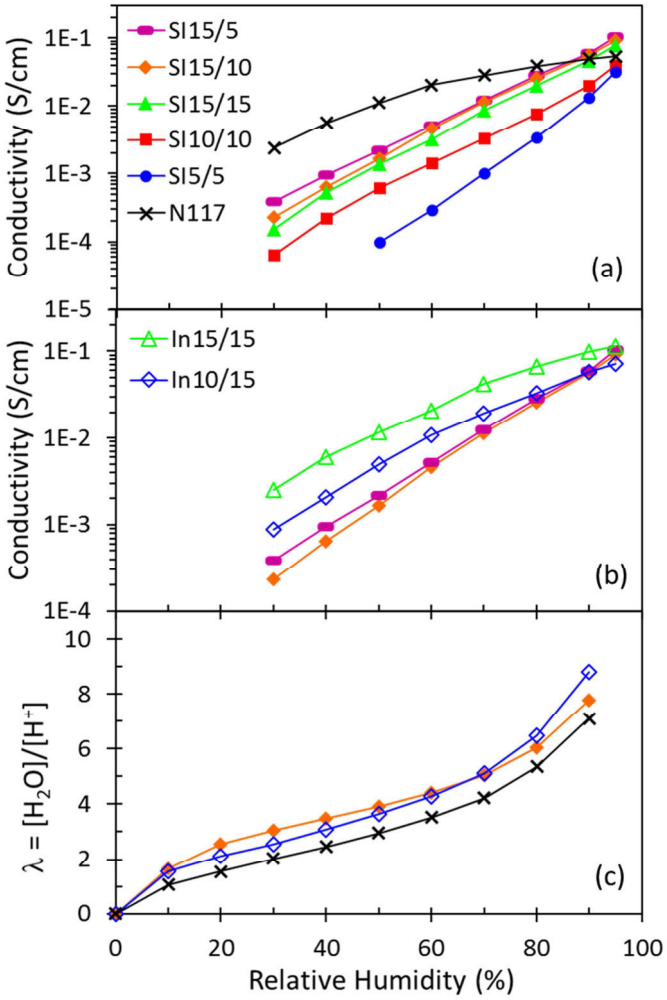

Figure 11. Proton conductivity as a function of relative humidity of SiX/Y ionomers in comparison with (a) Nafion® 117, and (b) InX/Y ionomers. (c) Water uptake as a function of relative humidity of SiX/Y ionomers in comparison with InX/Y ionomers.

It is known the TFSI anion can adopt two different conformations (cis or trans) energetically inequivalent. It was reported for the blends of ionic liquids based on butylmethylimidazole TFSI and HTFSI (or LiTFSI) that higher conductivity were obtained when the anion is cis-conformer.[55–61] In SiX/Y, the perfluorosulfoimide side chain can, probably, also adopt two conformations, which could explains the strong dependence of the conductivity with the RH. Thus it can be supposed the isomerization from one conformation to another can take place with the increase of the water content. Another explanation of low conductivity could be related to the inability of perfluorosulfoimide acid to protonate the water at low RH. It was reported, in a nonpolar solutions the HTFSI is not able to protonate the water.[62] In the case of our ionomers the polymer backbone could be considered as a non-polar solvent.

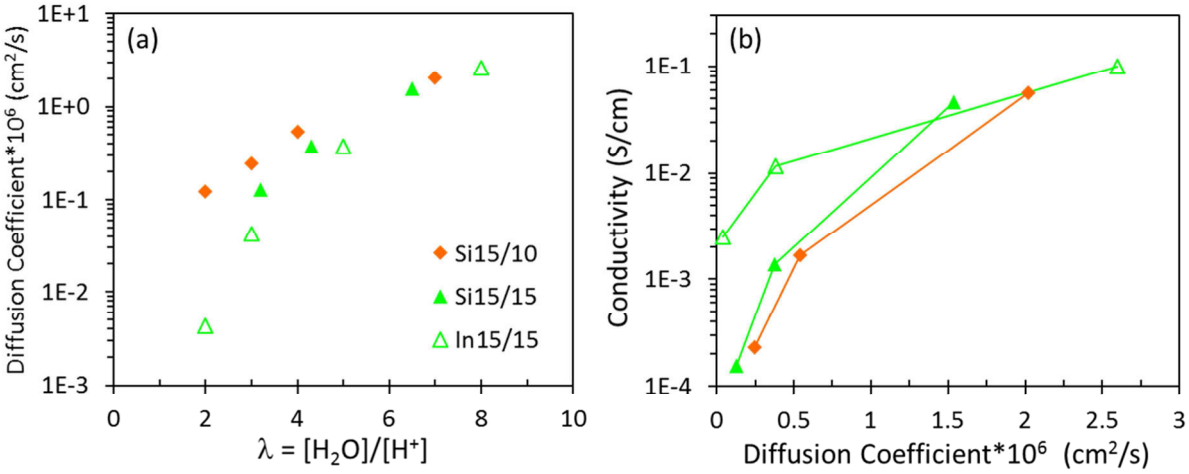

Figure 12. (a) Diffusion coefficient at low hydration number and (b) proton conductivity as a function of diffusion coefficient of SiX/Y ionomers in comparison to InX/Y ionomer.

4. Conclusions

Aromatic ionomers bearing pendant perfluorosulfonimide side chains with different block lengths and IEC were successfully synthesized. A two-phase system observed for dried membranes (DSC, DMA, and SANS) strongly supports the formation of PES/FPES multiblock copolymers as well as hydrophilic/hydrophobic separation. In hydrated membranes, a multi-phase separation with sharp interfaces evidenced by two peaks of SANS spectra reveals the structural organization at two different scales and the characteristic distances are in correlation with the expected block size and side-chain length of ionomers. Copolymers with an increase of both block size (psi-PES and FPES) showed gradually higher proton conductivity and water uptake (Si15/15 > Si10/10 > Si5/5), presumably due to better connectivity among the ionic domains. The conductivities of SiX/Y with longer block chain and higher IEC is much higher those of Nafion 117 at 95% RH. However, at 80 °C at low RH the conductivity of SiX/Y is much lower than both, Nafion 117 and InX/Y. To understand better this peculiar behavior additional study are needed. Thus, the interactions between the anion, proton and water, at different RH will be further investigated by IR and Raman.

ACKNOWLEDGMENTS

The authors acknowledge the Institut Laue-Langevin (ILL) for providing the neutron facilities used in this work (proposal numbers 9-11-1709). We are grateful to Dr. L. Porcar (ILL) for beamline alignment and helpful discussion during the neutron scattering experiments. This work was performed within the framework of the Centre of Excellence of Multifunctional Architectured Materials “CEMAM” no. AN-10-LABX-44–01.

REFERENCES

(1) Carrette, L.; Friedrich, K. A.; Stimming, U. *ChemPhysChem* **2000**, *1*, 162–193.

(2) Hickner, M. A.; Ghassemi, H.; Kim, Y. S.; Einsla, B. R.; McGrath, J. E. *Chem. Rev.* **2004**, *104*, 4587–4612.

(3) Zhang, H.; Shen, P. K. *Chem. Rev.* **2012**, *112*, 2780–2832.

(4) Mauritz, K. A.; Moore, R. B. *Chem. Rev.* **2004**, *104*, 4535–4585.

(5) Peron, J.; Mani, A.; Zhao, X.; Edwards, D.; Adachi, M.; Soboleva, T.; Shi, Z.; Xie, Z.; Navessin, T.; Holdcroft, S. *J. Memb. Sci.* **2010**, *356*, 44–51.

(6) Kusoglu, A.; Weber, A. Z. *Chem. Rev.* **2017**, *117*, 987–1104.

(7) Kreuer, K.-D.; Portale, G. *Adv. Funct. Mater.* **2013**, *23*, 5390–5397.

(8) Schmidt-Rohr, K.; Chen, Q. *Nat. Mater.* **2008**, *7*, 75–83.

(9) Haubold, H.-G.; Vad, T.; Jungbluth, H.; Hiller, P. *Electrochim. Acta* **2001**, *46*, 1559–1563.

(10) Rubatat, L.; Rollet, A. L.; Gebel, G.; Diat, O. *Macromolecules* **2002**, *35*, 4050–4055.

(11) Rollet, A.-L.; Diat, O.; Gebel, G. *J. Phys. Chem. B* **2002**, *106*, 3033–3036.

(12) Park, C. H.; Lee, C. H.; Guiver, M. D.; Lee, Y. M. *Prog. Polym. Sci.* **2011**, *36*, 1443–1498.

(13) Zhang, H.; Shen, P. K. *Chem. Soc. Rev.* **2012**, *41*, 2382–2394.

(14) Skalski, T. J. G.; Britton, B.; Peckham, T. J.; Holdcroft, S. *J. Am. Chem. Soc.* **2015**, *137*, 12223–12226.

(15) Harrison, W. L.; Hickner, M. A.; Kim, Y. S.; McGrath, J. E. *Fuel Cells* **2005**, *5*, 201–212.

(16) Lee, H.-S.; Roy, A.; Lane, O.; Dunn, S.; McGrath, J. E. *Polymer (Guildf).* **2008**, *49*, 715–723.

(17) Assumma, L.; Iojoiu, C.; Mercier, R.; Lyonnard, S.; Nguyen, H. D.; Planes, E. *J. Polym. Sci. Part A Polym. Chem.* **2015**, *53*, 1941–1956.

(18) Paddison, S. J.; Paul, R.; Kreuer, K.-D. *Phys. Chem. Chem. Phys.* **2002**, *4*, 1151–1157.

(19) Gebel, G. *Macromolecules* **2013**, *46*, 6057–6066.

(20) Genies, C.; Mercier, R.; Sillion, B.; Cornet, N.; Gebel, G.; Pineri, M. *Polymer (Guildf).* **2001**, *42*, 359–373.

(21) Asano, N.; Aoki, M.; Suzuki, S.; Miyatake, K.; Uchida, H.; Watanabe, M. *J. Am. Chem. Soc.* **2006**, *128*, 1762–1769.

(22) Maity, S.; Jana, T. *ACS Appl. Mater. Interfaces* **2014**, *6*, 6851–6864.

(23) Kulkarni, M. P.; Peckham, T. J.; Thomas, O. D.; Holdcroft, S. *MRS Proc.* **2014**, *1677*, mrss14-1677-m04-01.

(24) Chang, Y.; Brunello, G. F.; Fuller, J.; Disabb-Miller, M. L.; Hawley, M. E.; Kim, Y. S.; Hickner, M. A.; Jang, S. S.; Bae, C. *Polym. Chem.* **2013**, *4*, 272–281.

(25) Miyatake, K.; Shimura, T.; Mikami, T.; Watanabe, M. *Chem. Commun. (Camb).* **2009**, 6403–6405.

(26) Mikami, T.; Miyatake, K.; Watanabe, M. *J. Polym. Sci. Part A Polym. Chem.* **2011**, *49*, 452–464.

(27) Ghassemi, H.; Schiraldi, D. A.; Zawodzinski, T. A.; Hamrock, S. *Macromol. Chem. Phys.* **2011**, *212*, 673–678.

(28) Kreuer, K.-D.; Paddison, S. J.; Spohr, E.; Schuster, M. *Chem. Rev.* **2004**, *104*, 4637–4678.

(29) Koppel, I. A.; Taft, R. W.; Anvia, F.; Zhu, S.-Z.; Hu, L.-Q.; Sung, K.-S.; DesMarteau, D. D.; Yagupolskii, L. M.; Yagupolskii, Y. L.; Ignat'ev, N. V.; Kondratenko, N. V.; Volkonskii, A. Y.; Vlasov, V. M.; Notario, R.; Maria, P.-C. *J. Am. Chem. Soc.* **1994**, *116*, 3047–3057.

(30) Thomas, B. H.; Shafer, G.; Ma, J. J.; Tu, M.-H.; DesMarteau, D. D. *J. Fluor. Chem.* **2004**, *125*, 1231–1240.

(31) Johansson, P.; Tegenfeldt, J.; Lindgren, J. *J. Phys. Chem. A* **2000**, *104*, 954–961.

(32) Rey, I.; Johansson, P.; Lindgren, J.; Lasse, J. C. *J. Phys. Chem. A* **1998**, *102*, 3249–3258.

(33) Arnaud, R.; Benrabah, D.; Sanchez, J. Y. *J. Phys. Chem.* **1996**, *100*, 10882–10891.

(34) Desmarteau, D.; Hunter, L. *J. Fluor. Chem.* **1991**, *52*, 7–12.

(35) Zhu, S.-Z.; Jin, G.-F.; DesMarteau, D. D. *Chinese J. Chem.* **2002**, *20*, 1268–1273.

(36) Creager, S. E.; Sumner, J. J.; Bailey, R. D.; Ma, J. J.; Pennington, W. T.; Desmarteau, D. D. *Electrochem. Solid-State Lett.* **1999**, *2*, 434–436.

(37) Zhang, J.; Desmarteau, D. D.; Zuberi, S.; Ma, J.; Xue, L.; Gillette, S. M.; Blau, H.; Gerhardt, R. *J. Fluor. Chem.* **2002**, *116*, 45–48.

(38) Atkins, J. R.; Sides, C. R.; Creager, S. E.; Harris, J. L.; Pennington, W. T.; Thomas, B. H.; Desmarteau, D. D. *J. New Mater. Electrochem. Syst.* **2003**, *6*, 9–15.

(39) Ford, L. A.; DesMarteau, D. D.; Smith, D. W. *J. Fluor. Chem.* **2005**, *126*, 651–658.

(40) Savett, S. C.; Atkins, J. R.; Sides, C. R.; Harris, J. L.; Thomas, B. H.; Creager, S. E.; Pennington, W. T.; Desmarteau, D. D. *J. Electrochem. Soc.* **2002**, *149*, A1527–A1532.

(41) Feiring, A. E.; Wonchoba, E. R. *J. Fluor. Chem.* **2000**, *105*, 129–135.

(42) Assumma, L.; Nguyen, H.-D.; Iojoiu, C.; Lyonnard, S.; Mercier, R.; Espuche, E. *ACS Appl. Mater. Interfaces* **2015**, *7*, 13808–13820.

(43) Iojoiu, C.; Genova-Dimitrova, P.; Maréchal, M.; Sanchez, J.-Y. *Electrochim. Acta* **2006**, *51*, 4789–4801.

(44) Nguyen, H. D.; Assumma, L.; Judeinstein, P.; Mercier, R.; Porcar, L.; Jestin, J.; Iojoiu, C.; Lyonnard, S. *ACS Appl. Mater. Interfaces* **2017**, *9*, 1671–1683.

(45) Nguyen, H. D.; Assumma, L.; Judeinstein, P.; Mercier, R.; Porcar, L.; Jestin, J.; Iojoiu, C.; Lyonnard, S. *ACS Appl. Mater. Interfaces* **2017**, *9*, 1671–1683.

(46) Perrin, J.-C.; Lyonnard, S.; Volino, F. *J. Phys. Chem. C* **2007**, *111*, 3393–3404.

(47) Assumma, L.; Iojoiu, C.; Albayrak Ari, G.; Cointeaux, L.; Sanchez, J.-Y. *Int. J. Hydrogen Energy* **2014**, *39*, 2740–2750.

(48) Cho, C. G.; Kim, Y. S.; Yu, X.; Hill, M.; McGrath, J. E. *J. Polym. Sci. Part A Polym. Chem.* **2006**, *44*, 6007–6014.

(49) Gebel, G.; Lambard, J. *Macromolecules* **1997**, *30*, 7914–7920.

(50) Beaucage, G. *J. Appl. Crystallogr.* **1995**, *28*, 717–728.

(51) Gebel, G.; Diat, O. *Fuel Cells* **2005**, *5*, 261–276.

(52) Rubatat, L.; Gebel, G.; Diat, O. *Macromolecules* **2004**, *37*, 7772–7783.

(53) Kreuer, K. D.; Schuster, M.; Obliers, B.; Diat, O.; Traub, U.; Fuchs, A.; Klock, U.; Paddison, S. J.; Maier, J. *J. Power Sources* **2008**, *178*, 499–509.

(54) Nakabayashi, K.; Higashihara, T.; Ueda, M. *Macromolecules* **2011**, *44*, 1603–1609.

(55) Gejji, S. P.; Suresh, C. H.; Babu, K.; Gadre, S. R. *J. Phys. Chem. A* **1999**, *103*, 7474–7480.

(56) Saito, Y.; Umecky, T.; Niwa, J.; Sakai, T.; Maeda, S. *J. Phys. Chem. B* **2007**, *111*, 11794–11802.

(57) Valencia, H.; Kohyama, M.; Tanaka, S.; Matsumoto, H. *J. Phys. Chem. C* **2012**, *116*, 8493–8509.

(58) Umecky, T.; Saito, Y.; Okumura, Y.; Maeda, S.; Sakai, T. *J. Phys. Chem. B* **2008**, *112*, 3357–3364.

(59) Andriola, A.; Singh, K.; Lewis, J.; Yu, L. *J. Phys. Chem. B* **2010**, *114*, 11709–11714.

(60) Monti, D.; Jónsson, E.; Palacín, M. R.; Johansson, P. *J. Power Sources* **2014**, *245*, 630–636.

(61) Menne, S.; Vogl, T.; Balducci, A. *Phys. Chem. Chem. Phys.* **2014**, *16*, 5485.

(62) Stoyanov, E. S.; Kim, K.; Reed, C. A. *J. Phys. Chem. A* **2004**, *108*, 9310–9315.

Supporting Information

Aromatic Multi-Block Ionomers with Extensively-Delocalized Negative Charge for PEMFC Application

Huu-Dat Nguyen,[1] Emilie Planes,[1] Priscillia Soudant,[1] Lionel Porcar,[2] Sandrine Lyonnard,[3] Cristina Iojoiu,[1]*

[1]LEPMI, Université Grenoble Alpes – CNRS, 38000 Grenoble, France

[2]Institut Laue Langevin (ILL), 38002 Grenoble, France

[3]INAC-SPrAM, Université Grenoble Alpes – CEA – CNRS, 38000 Grenoble, France

Correspondence to: C. Iojoiu (E-mail: Cristina.Iojoiu@lepmi.grenoble-inp.fr)

Table S1. Chemical Yield of Coupling Reaction vs Precursor/Br Molar Ration

Precursor/Br[a]	SiX/Y conversion (%)	InX/Y conversion (%)
1.5	60 ± 3	85 ± 3
2.0	85 ± 3	100 ± 3
2.5	85 ± 3	100 ± 3
3.0	87 ± 3	100 ± 3

[a]*The molar ratio of precursor, e.g., I-psiLi for SiX/Y synthesis or I-psLi for InX/Y synthesis, per bromine function of brominated block copolymer backbone.*

Table S2. Glass Transition Temperature (Tg), Alpha Relaxation (Tα) and Degradation Temperature (Td) of Copolymers

polymer code	$T_{g\_midpoint}$ (°C)	T_{d_onset} (°C)	Tα[a] (°C)	E'[b] (MPa)
FPES	211 ± 2	435 ± 3	208 ± 2	≈ 1900
PES	224 ± 2	530 ± 3	222 ± 2	≈ 2000
PES-FPES 5/5	225 ± 2	419 ± 2	218 ± 2	≈ 2000
PES-FPES 10/10	224 ± 2	424 ± 2	221 ± 2	≈ 2100
PES-FPES 15/15	226 ± 2	422 ± 2	219 ± 2	≈ 2100
PES-FPES 15/10	225 ± 2	418 ± 2	220 ± 2	≈ 2000
PES-FPES 15/5	226 ± 2	425 ± 2	222 ± 2	≈ 1900

[a]*Temperature at peak of Tan δ.* [b]*At 80 °C in dry state.*

Table S3. Percentage of Ionomer Components (wt%)

ionomers	psi-PES[a]	FPES[b]
Si5/5	76.0	24.0
Si10/10	76.0	24.0
Si15/15	76.0	24.0
Si15/10	82.6	17.4
Si15/5	90.5	9.5

[a]*Calculated based on IEC.* [b]*Theoretical values.*

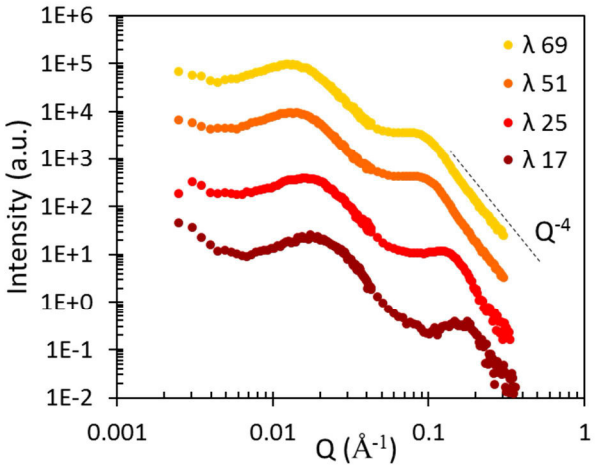

Figure S1. SANS profiles of ionomer Si15/10 with increasing hydration number (λ). The spectra are shifted vertically for clarity.

Table S4. Extrapolated d_{0_ionic} and d_{0_block} of the Ionomers (Å).

ionomer	d_{0_ionic}[a]	d_{0_block}[a]
Si5/5	27	220
Si10/10	27	290
Si15/15	27	435
Si15/10	25	345
Si15/5	20	-

[a]*Estimated from the dilution laws by extrapolation of d_{ionic} and d_{block} at zero water content ($\lambda = 0$).*

[b]*The theoretical length of PES and FPES blocks were calculated using bond distances.*

Overall Conclusions and Perspectives

1. Conclusions

The literature review on the structure-morphology-property interplay of membranes based on aromatic ionomers highlights the limitations of sulfonated aromatic ionomers are originated from (i) the random distribution of sulfonic acid groups on the rigid polymer backbone, (ii) the proximity of proton-conducting functions to the polymer backbone, and (iii) the low acidity of the aryl sulfonic acid (**Chapter 1**). To overcome these drawbacks, we designed and developed aromatic ionomers possessing:

- A multi-block structure with the aim of enhancing the hydrophilic-hydrophobic phase separation,
- Ionic functions separated from polymer backbone by a flexible and hydrophobic spacer to improve the structuration of ionic clusters,
- Super-acidic functions (perfluorosulfonic acid) or highly delocalized anion such as perfluorosulfonimide to boost the proton conductivity, especially at reduced RH.

In the following, we present a brief overview of the most important research results and conclusions we have reached during this project.

We deeply investigated the effects of block lengths and membrane-manufacturing conditions, i.e., solvent selectivity and thermal annealing, on the morphologies and the properties of ionomer membranes (**Chapter 2A**) of the partially-fluorinated multi-block copoly(arylene ether sulfone)s bearing perfluorosulfonic acid functions (InX/Y).

- We proved the solvent nature has a strong impact on the membrane morphology and functional properties. For the study, two solvents were selected based on Flory−Huggins interaction parameters measured by IGC, i.e., DMAc (good solvent for both FPES and ps-PES block) and DMSO (good solvent for only ps-PES block as selective solvent). The membranes cast from DMSO exhibit much better ps-PES/FPES phase separation with more interconnected ionic clusters yielding higher conductivities and water uptake as compared to those of the DMAc-cast ones.
- We showed that the membrane morphology and properties are also highly impacted by the solvent-aided thermal treatment. Thus we obtained, after annealing the

membranes at 150 °C, a 10-fold increase in proton conductivity with respect to untreated polymers.

- The ionomers with longer block lengths, i.e., 15 kg/mol, show equivalent conductivities to those of Nafion at reduced RH (< 50%), and higher above. At 95% RH all the annealed membranes show higher conductivities than the Nafion 117 especially above 60 °C. However, the hydration number of membranes based on aromatic ionomers with longer block lengths, above this temperature, become more than 2 times higher than those of Nafion 117.

The structure-morphology-property interplay of the InX/Y ionomers was elucidated by systematically investigating a wide variety of InX/Y ionomers possessing different block lengths and IEC (**Chapter 2B**). Among the most important results we can point out the following:

- In hydrated states, a multi-phase separation with sharp interfaces was evidenced by two well-defined peaks in SANS profiles, which implies the structural organization at two different length scales. The alternated segmentation of hydrophobic FPES and hydrophilic ps-PES blocks, along with the high phase separation between polar perfluorosulfonated side chains (ps-) and non-polar PES main chain, lead to acomplex multi-scale three-phase structure, evidenced by two SANS scattering maxima. This structure derives from packing rod-like elongated polymer particles in solution during solvent evaporation. The ionic domains have a similar organization and follow the same dilution as Nafion.
- A microstructure model was proposed to explain the self-organization of the ionomer molecules during solvent-cast process and the membrane's morphological behavior during water sorption/desorption. The presence of perfluorinated ionic side chains induces neat phase-separation and 1D-to-2D morphological evolution along λ.
- We clarified the relation between their chemical architecture, microstructure and proton-transport efficiency. The proton conductivity and the self-diffusion coefficient of water were found to vary linearly with confinement (Δd_{ionic}) and connectivity (block superstructure), although they have a differently balanced impact depending on the hydration regime.

- The main conclusion of this work is that the InX/Y properties can be tailored at the microscopic level by the choice of the chemical architecture and processing conditions. This might be of interest for selecting the best compromised conditions towards a given application.

Then, we explored Nafion as percolating agent of ionic domains of InX/Y (**Chapter 3**). This study was performed on a series of InX/Y-Nafion blends containing from 10 to 50 wt% Nafion. The blend was cast from DMSO at 60 °C to obtain membranes. The influence of thermal treatment was also investigated. As main findings it can be noted:

- Most of blend membranes exhibit higher proton conductivities than those of corresponding pristine ionomer membranes and the highest proton conductivity was obtained with membranes containing 20 wt% Nafion.
- The incorporation of Nafion into aromatic ionomer, in combination with thermal annealing, leads to a significant improvement in morphologies, notably in the connectivity of ionic domains, and functional properties.
- By analyzing the SANS and DMA profiles, we found that the two ionomers are not completely miscible after casting while after annealing both ionomers seem to mix and form only one phase.
- Annealed membranes showed lower water uptake as compared to that of cast ones, but higher proton conductivity, especially at low RH. Particularly, a 3-fold increase in proton conductivity was achieved after thermal treatment.

  The blending approach therefore yielded very promising results which could be further developed by optimizing the process.

Last, new ionomers with highly delocalized anions, i.e., multiblock co-poly(arylene ether sulfone)s bearing perfluorosulfonyl imide functions (SiX/Y), were successfully synthesized with different block lengths and IEC (**Chapter 4**).

- These ionomers show a similar morphology at the nanoscale as their InX/Y counterparts but higher thermal stability.
- At 95% RH, SiX/Y exhibits much higher conductivities than InX/Y and Nafion 117, but they drastically decrease with the reduction of RH.

2. Perspectives

The present work opens a number of paths for the future developments, including applications beyond the fuel cells. Herein, we propose to highlight the following issues and perspectives:

2.1. Understanding the proton-conducting mechanisms in SiX/Y as a function of hydration number

We suspect that the conduction mechanism in SiX/Y is highly different as compared to that in InX/Y. In fact, SiX/Y membranes with similar IEC and water uptake as InX/Y show more efficient proton conduction at 95% RH, but much lower below 80% RH. To gain more insight into this peculiar behavior it would be interesting to (i) perform IR and Raman analysis on membranes exposed at different RH, (ii) study the interaction of NH group with water molecules, the ionization of water, and (iii) correlate them with the proton conductivity and water diffusion. Also by Raman and IR, the conformation of the side chain, i.e., cis or trans conformations, could be followed and the relationship between conformation−water content and transport properties could be established.

2.2. Crosslink the polymer main chain to reduce water uptake, but maintain high proton conductivity

Although the new aromatic ionomers show promising properties for PEMFC application, i.e., high proton conductivity, high thermomechanical properties, etc., their excessive swelling in water at high temperature would limit their potential utilization to a limited range of temperatures and RH. To overcome these limitations a very plausible approach is to crosslink the polymer main chain. However, to avoid a dramatic decrease of the conductivity we propose to crosslink the hydrophobic domains. Considering the synthesis procedure and membrane-manufacturing condition, the crosslink step can be done via adding crosslinking agents into polymer solution before casting membrane or during the thermal annealing process of the "as-cast" membranes while the polymer molecules are moving and re-organizing. The crosslinking agents have to be selected to react only with the hydrophobic chains.

2.3. Explore the effects of counter cations on morphology and properties of acidic ionomer membranes

In addition to solvent selectivity and thermal annealing, another factor that should be considered in membrane-elaborating process is the counter cation of in-put ionomers. Conventionally, ionomers in lithium-salt form are used to prepare the membrane in order to avoid the degradation of perfluorosulfonic acid functions during thermal annealing. However, it would be interesting to investigate what happens if the lithium cation is replaced by other cations with different diameter and valence. In this direction, we have already performed preliminary experiments. Four annealed membranes cast from DMAc were prepared from ionomers in salt form with four different counter cations, i.e., Li^+, K^+, Ca^{2+}, Cs^+. The SANS first results revealed that the counter cation has a strong effect on membrane morphology (**Figure P1**). A deep study on the influence of counter cation on PEM performance and morphology is needed.

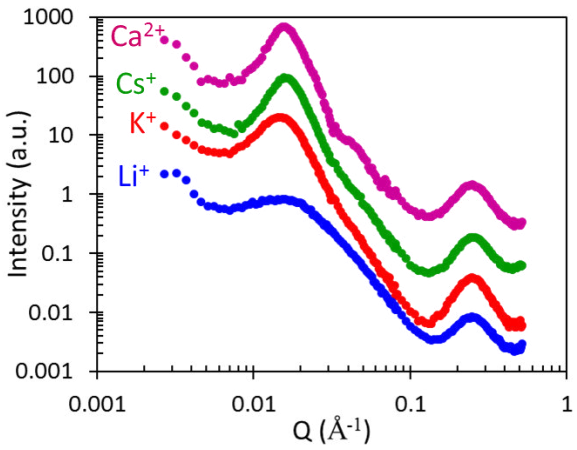

Figure P1. SANS profiles of acidified-annealed DMAc-cast In10/10 membranes cast from ionomers in different salt forms. There is a clear impact of the cation on the block superstructure organization (low Q peak).

2.4. Using the aromatic ionomers as binders for catalyst layers

To optimize the fuel cell cost, durability and power density, a re-built membrane-electrode assembly (MEA) is required. One major issue is the nature of the ionomer present in both proton exchange membrane (PEM) and catalyst layer (CL). Usually the membranes are prefabricated and catalyst layers are spray-coated on both sides from a colloidal ink of carbon/Pt and ionomer, which subsequently solidify into a phase-segregated composite possessing interpenetrating, percolating phases that supports the transport of electrons (C phase), protons (ionomer phase) and gases (porosity) (**Figure P2**).

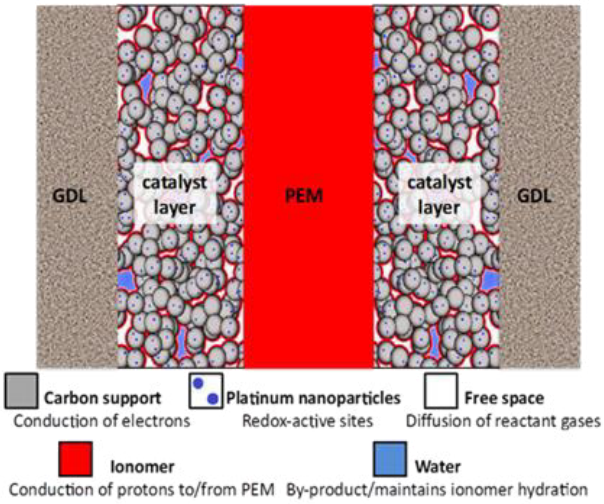

Figure P2. Schematic representation of the fuel cell layered structure.

Currently, the catalyst layer consists of perfluorosulfonic ionomers such as Nafion. Reports in literature regarding the employment of hydrocarbon ionomers in the catalyst layer are rather limited. This limitation is related to the inability of aromatic ionomers to form porous nano-structured layers, in order to allow the diffusion of gases and water. However, a study by the Lindbergh group (KTH) on sulfonated polysulfone (sPSU) ionomers[1] provided evidence of the benefits of reducing interfacial resistance between the PEM and CL. This clearly highlights the gap to be filled towards an all-HC integrated fuel cell and the potential for innovation in this field. It would be interesting to develop catalyst layers based on the new aromatic ionomers and then produce durable, efficient fully hydrocarbon-based fuel cells. The advantages of our ionomers consist in their nanostructured morphology (similar to that of Nafion), which makes them very promising to succeed in the formulation of CL.

Reference

(1) von Kraemer, S.; Puchner, M.; Jannasch, P.; Lundblad, A.; Lindbergh, G. *J. Electrochem. Soc.* **2006**, *153*, A2077–A2084.

Annexes

Annexe 1. Synthesis and Characterization of Partially-Fluorinated Multi-Block Copoly(Ether Sulfone)s Bearing Perfluorosulfonic Acid Functions (InX/Y Ionomer).

1. Experimental Section

1.1. Materials

Dimethylsulfoxide (DMSO), Dimethylacetamide (DMAc), Tetrahydrofuran (THF), Dimethylformamide (DMF), Copper (Cu) powder for organic synthesis, purchased from Sigma Aldrich, Potassium Carbonate (K_2CO_3), Bromine (Br_2), Toluene, purchased from Acros Organics, 1,1,2,2,-Tetrafluoro-2-(1,1,2,2,-tetrafluoro-2-iodoethoxy)ethane sulfonyl fluoride ($ICF_2CF_2OCF_2CF_2SO_2F$), purchased from Interchim, Lithium Hydroxide (LiOH), Sodium Hydroxide (NaOH), Diethylene Glycol Dimethyl Ether (Diglyme), purchased from Alfa Aesar, were used as received. Dichloromethane (DCM) and Acetonitrile (ACN), purchased from Sigma Aldrich, were distilled from Calcium Hydride (CaH_2) before use. Acetic Acid purchased from Sigma Aldrich was distilled under vacuum before use. 4,4'-Difluorodiphenyl Sulfone (DFDPS), 4,4'-Biphenol (BP), and 4,4'-Dihydroxydiphenyl Sulfone (DHDPS), purchased from Alfa Aesar, were recrystallized from isopropanol before use. Decafluorobiphenyl (DFBP), purchased from FluoroChem, was sublimated before use.

1.2. Synthesis of PES-FPES Multiblock Copolymers

In a typical protocol for the synthesis of block copolymer PES-FPES 5/5 (see **Table A1**), a 100-mL three-neck round bottom flask, equipped with a mechanical stirrer, a condenser, an argon inlet-outlet and a Dean-Stark trap, was charged with DFDPS (4.000 g, 15.733 mmol), BP (3.184 g, 17.098 mmol). DMAc (30 mL) was added to provided ≈ 25 % (w/v) solid concentration. As the mixture was completely dissolved, K_2CO_3 (7.089 g, 0.0513 mol) and 15 mL of toluene, an azeotroping agent, was added. The ratio of DMAc to toluene (v/v) was 2:1. The reaction bath was heated to 150 °C and kept at this temperature for 4h to dehydrate the system. Then, the bath temperature was slowly raised to 160 °C by the controlled removal of toluene. Then, the temperature of the reaction bath is decreased to 120 °C and the polymerization was allowed to proceed at this temperature for 24h. Then, the reaction bath was cooled down to 70 °C and K_2CO_3 (4.569 g, 0.0331 mol) was introduced, and the solution containing 2.758 g of DHDPS (11.021 mmol) in 7 mL of DMAc (≈ 40 % m/v) was dripped

drop-by-drop. After that, the solution containing DFBP (4.139 g, 12.387 mmol) (≈ 40 % m/v) and 20 mL of DMAc were added. When the viscosity of the reaction bath was sufficiently high (generally after 120 minutes), the reaction mixture was precipitated into 1000 mL of 1 M HCl solution with magnetic agitation for 8 h and then filtered and rinsed with distilled water until neutral pH. The final product was dried in vacuum at 100 °C for 12h (**Scheme A1**). The procedure was adopted for the synthesis of other block copolymer with different block lengths (**Table A1**).

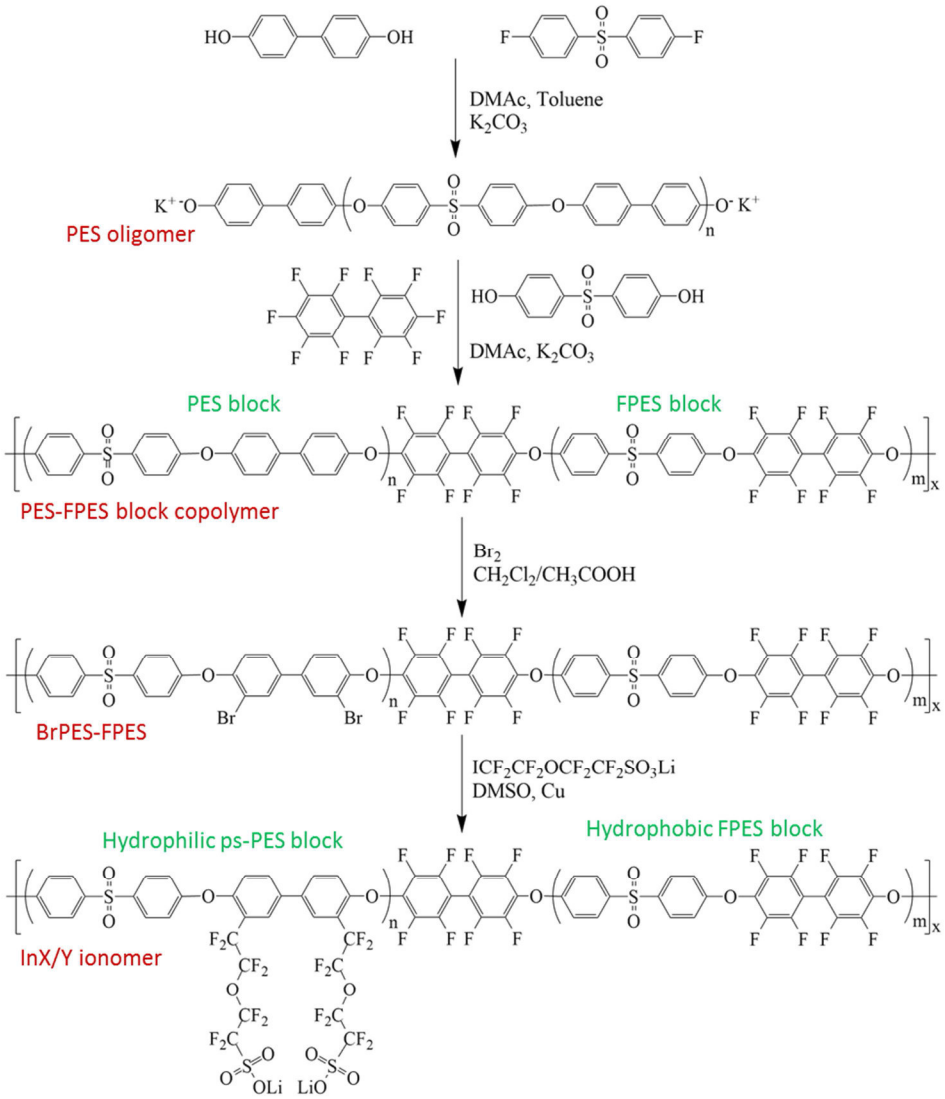

Scheme A1. The synthesis procedure of ionomer InX/Y.

^{1}H-NMR ($CDCl_3$): δ (ppm) 7.91–7.89 (d, 4H), 7.83–7.81 (d, 4H), 7.52–7.50 (d, 4H), 7.09–6.98 (m, 12H).

^{19}F-NMR ($CDCl_3$): δ (ppm) -137.81 (s, Ar–F), -138.20 (m, Ar–F), -153.28 (s, Ar–F), -153.68 (m, Ar–F).

Table A1. Quantity of Monomers Used for the Synthesis of Block Copolymer

block copolymer	PES-FPES (g/mol)	BP (g)	DFDPS (g)	DHDPS (g)	DFBP (g)
PES-FPES 5/5	5000-5000	3.184	4.000	2.758	4.139
PES-FPES 10/10	10000-10000	3.052	4.000	2.830	3.997
PES-FPES 10/15	10000-15000	3.052	4000	4.337	6.008
PES-FPES 15/15	15000-15000	3.010	4.000	2.853	3.953

1.3. Synthesis of BrPES-FPES Intermediate

The bromination of PES-FPES was carried out in a mixture of distilled dichloromethane and acetic acid (10% v/v) by addition of a large excess of bromine (Br_2) at room temperature. In a typical procedure, 10 g of PES-FPES 5/5 (12.572 mmol of BP unit) was introduced in a 500-mL three-necked flask equipped with an argon inlet, a condenser, and a mechanical stirrer. Then 180 mL of dichloromethane (CH_2Cl_2) distilled from CaH_2 and 18 mL of distilled acetic acid were added. After the polymer is dissolved completely, 9.712 mL (0.189 mol) Br_2 was drop-by-drop introduced to the reaction mixture through the addition funnel. After 24h of reaction, the reaction mixture was poured into methanol and kept agitation for 24h. After that, the polymer was filtered and rinsed carefully with methanol until no trace of the residual bromine and acid was reached. The obtained polymer powder was dried in vacuum at 60 °C in vacuum for 24h (**Scheme A1**).

^{1}H-NMR ($CDCl_3$): δ (ppm) 7.91–7.89 (d, 4H), 7.85–7.82 (d, 4H), 7.77 (s, 2H), 7.45–7.43 (d, 2H), 7.08–7.06 (d, 6H), 6.96–6.94 (d, 4H)

^{19}F-NMR ($CDCl_3$): δ (ppm) -137.81 (s, Ar–F), -138.20 (m, Ar–F), -153.28 (s, Ar–F), -153.68 (m, Ar–F).

1.4. Synthesis of $ICF_2CF_2OCF_2CF_2SO_3Li$ Ionic Function (I-psLi)

The ionic function 1,1,2,2-tetrafluoro-2-(1,1,2,2-tetrafluoro-2-iodoethoxy)ethanesulfonate lithium ($ICF_2CF_2OCF_2CF_2SO_3Li$) was synthesized as follows: 10.00 g (23.48 mmol) of $ICF_2CF_2OCF_2CF_2SO_2F$, 1.181 g (49.298 mmol) of LiOH and 40 mL of THF was introduced into a 100-mL three-necked round bottom flask charged with a magnetic stirrer. After 24 h of reaction at room temperature, the reaction mixture was centrifuged to remove solid phase including excess LiOH and LiF. After evaporation of THF, a white solid was obtained. This

solid was dissolved in distilled acetonitrile and centrifuged to completely remove solid phase. Finally, acetonitrile was evaporated to obtained white powder responsible to the final product, which was dried under vacuum at 40 °C for 24 h before doing reaction.

^{19}F-NMR (Acetone d6): δ (ppm) -69.82 (t, ICF_2), -82.87 (t, CF_2O), -86.44 (t, OCF_2), -118.54 (m, CF_2SO_3Li).

1.5. Synthesis of InX/Y Ionomer

The ionomer InX/Y was synthesized via Ullmann coupling reaction in anhydrous condition. In a typical procedure to obtain In5/5, 4.000 g (4.195 mmol of diphenyl units) of bromated block copolymer BrPES-FPES 5/5, 5.332 g (83.906 mmol, 20 eq of diphenyl units) of copper powder and 32 ml of DMSO were added into a 100-mL three neck round bottom flask, equipped with a mechanical stirrer, a condenser, an argon inlet and an addition funnel. The mixture was stirred at 60 °C until the polymer was completely dissolved. Then, the bath temperature was increased to 120 °C followed by strong stirring for 2 h. After that, 7.215g (16.781 mmol, 4 eq of diphenyl units) of $ICF_2CF_2OCF_2CF_2SO_3Li$ dissolved in DMSO (30% m/v) was slowly added drop-by-drop into the reaction mixture and the bath temperature was increased to 140 °C. The reaction was allowed to proceed at that temperature for 24 h. After verifying the product by ^{19}F NMR, residue of copper powder was removed by centrifugation at 5000 rpm for 15 minutes and the ionomer was precipitated into 1000 mL HCl 1M and kept with strong agitation until the ionomer particles become transparent. Finally, the polymer was filtered and washed with distilled water until neutral pH was reached. The ionomer was dried at 100 °C under vacuum for 24 h (**Scheme A1**).

^{1}H-NMR (DMSO.d6): δ (ppm) 8.09–7.82 (m), 7.45 (s), 7.35–7.32 (m), 7.27-7.05 (m).

^{19}F-NMR (DMSO.d6): δ (ppm) -82.11 (s, –CF_2O), -86.17 (s, –OCF_2), -110.55 (s, Ar–CF_2), -117.85 (s, $CF_2SO_3^-Li^+$), -137.81 (s, Ar–F), -138.20 (m, Ar–F), -153.28 (s, Ar–F), -153.68 (m, Ar–F).

1.6. Membrane Preparation

The ionomers in lithium-salt form were dissolved in DMSO to obtain 7 wt % solutions, which were then stirred at 60 °C for 24h. After that, the solutions were centrifuged for 30 min at 5000 rpm to remove solid impurities, and degassed under vacuum for 30 min. The homogeneous solutions were cast onto a glass plate using a casting knife (Elcometer 4340 Automatic Film Applicator). The solvent was evaporated in an oven at 60 °C for 48h. Then the membranes were rinsed several times in distilled water over 24h to remove solvent

residue. The solvent-free membranes were verified by ^{1}H NMR. Finally, the membranes were acidified by stirring in 1M HCl solution for 24h at room temperature (RT), followed by immersing in distilled water for at least 24h to remove acid trace.

2. Characterization

2.1. NMR Spectroscopy

Chemical structures and constituents of the monomers, oligomers, block copolymers and ionomers were confirmed by ^{1}H and ^{19}F NMR using a Bruker Ascend™ 400 spectrometers. All spectra were obtained from a 10% w/v solution of monomers in acetone.d6 (C_3D_6O), oligomers and block copolymers in chloroform.d6 ($CDCl_3$), ionomers in dimethylsulfoxide.d6 (C_2D_6SO).

2.2. Ion-Exchange Capacity (IEC)

The IEC, expressed by the milliequivalent of proton per gram of polymer (meq. H^+/g), has been calculated by ^{19}F NMR based on the integral of side chain peaks and main chain peaks which will be discussed later and by acid-base titration in organic solution.[3] In the latter, NaOH solution was prepared by dissolving 0.0500 g of anhydrous NaOH in 100 ml of diethylene glycol dimethyl ether (Diglyme) and ionomer solution was prepared by dissolving 0.1 g of ionomer in acid form, previously dried at 60 °C under vacuum for 72 h, in 5.00 ml of Diglyme. Methyl orange was used as pH indicator.

2.3. Density Measurement

The density of the membranes was measured using Mettler-Toledo density kits (the buoyancy technique) at 20 °C with toluene (0.87 g/mL) as the liquid phase.

2.4. Size-Exclusion Chromatography (SEC-MALLS)

SEC analyses were performed at ambient temperature using a Waters 590 GPC equipped with a Waters 410 differential refractometer and a Waters 745 Data Module. THF and 1 M $NaNO_3$ in DMF were used as eluent in the case of block copolymers and ionomers, respectively, with flow rate of 1 mL/min through three ultrastyragel columns of 500, 103, and 104 Å. The 1 % m/v solutions of block copolymer in THF and ionomer in 1 M $NaNO_3$ in DMF were filtered through a 0.45 mm Millipore filter based on PP and PTFE, respectively. The calibration was performed using polystyrene standards. The values of Mw and Mn depend on the elution volume and are markedly affected by possible fluctuations, for instance by the presence of bubbles. Each sample is analyzed twice and the values are calculated if the elution volumes of the two chromatograms are identical.

2.5. Thermal Gravimetric Analysis (TGA)

The measurements were performed on a TGA 1 STAR^e System supplied by Mettler Toledo under air flow of 20 ml/min (a mixture of 80% Ar and 20% O_2) with a temperature ramp of 10 °C/min from 50 to 750 °C.

2.6. Differential Scanning Calorimetry (DSC)

The DSC measurements were performed using a DSC 1 STAR^e System from Mettler Toledo under an argon flux of 50 mL/min with a heating rate of 20 °C/min from 25 to 200 °C for the first scan to completely remove water. The second scan was performed from 25 to 300 °C for the acid forms and from 25 to 320 °C for the lithiated forms. The glass transition temperatures of solvent-free membranes were determined as the mid-point values of the second scan.

2.7. Dynamic Mechanical Analysis (DMA)

The DMA was performed with a DMA Q800 supplied by TA Instruments using a temperature ramp of 2 °C/min in the temperature range from 25 to 270 °C for acidified membranes and from 25 to 350 °C for lithium-salt membranes. Data treatment was performed with TA Universal Analysis software. The dried membranes, in lithium form or acidic form, of average dimensions 20 × 6 mm^2 and thickness of 100−150 μm are attached to the film-tension clamp in multifrequency-strain mode. The measurement condition was set as follows: frequency 1.0 Hz, preload force 0.1 N, force track 150 %, and strain deformation was fixed at 0.1%.

3. Results and Discussion

3.1. NMR Analysis

3.1.1. Synthesis of PES-FPES Block Copolymer Backbone

The PES-FPES multiblock copolymers were prepared via one-pot-two-step synthesis. In the first reaction, the PES oligomers terminated with hydroxyl biphenyl units were performed. The molecular weight of PES blocks was controlled through the BP/DHDPS molar ratio using Carothers' equation (**Table A1**). In the next step, the block copolymer was formed by introducing two monomers composing the FPES blocks, e.g., DHDPS and DFBP, to the same reaction pot, without PES oligomer purification. The PES/FPES molar ratio is equal to 1.

The second reaction was allowed to proceed at lower temperature (70 °C) due to the high reactivity of DFBP toward the nucleophilic aromatic substitution. In the reaction mixture

during the second reaction, moreover, two nucleophile phenolates derived from (i) DHDPS, and (ii) hydroxyl biphenyl-ended PES oligomers are present at the same time. Thus, the fluorine atoms in para positions of DFBP monomers with higher reactivity than those in ortho and meta positions can be substituted (i) either by two PES oligomers (ii) or by two DHDPS monomers (to form FPES oligomers) or (iii) by both nucleophiles (to form PES-FPES block copolymers). However, due to the concentration, the reactivity, and the mobility of DHDPS-based phenolates are much higher, it is expected that the FPES oligomers are formed with a certain polydispersity and then the FPES oligomers are linked to the PES oligomers. Actually, ^{1}H NMR spectrum of PES-FPES 5/5 (**Figure A1a**) shows the characteristic peaks of both PES and FPES oligomers,[1] indicating, at least qualitatively, the formation, during the second synthesis reaction, of FPES sequences and no influence of reaction solvent (DMSO or DMAc).

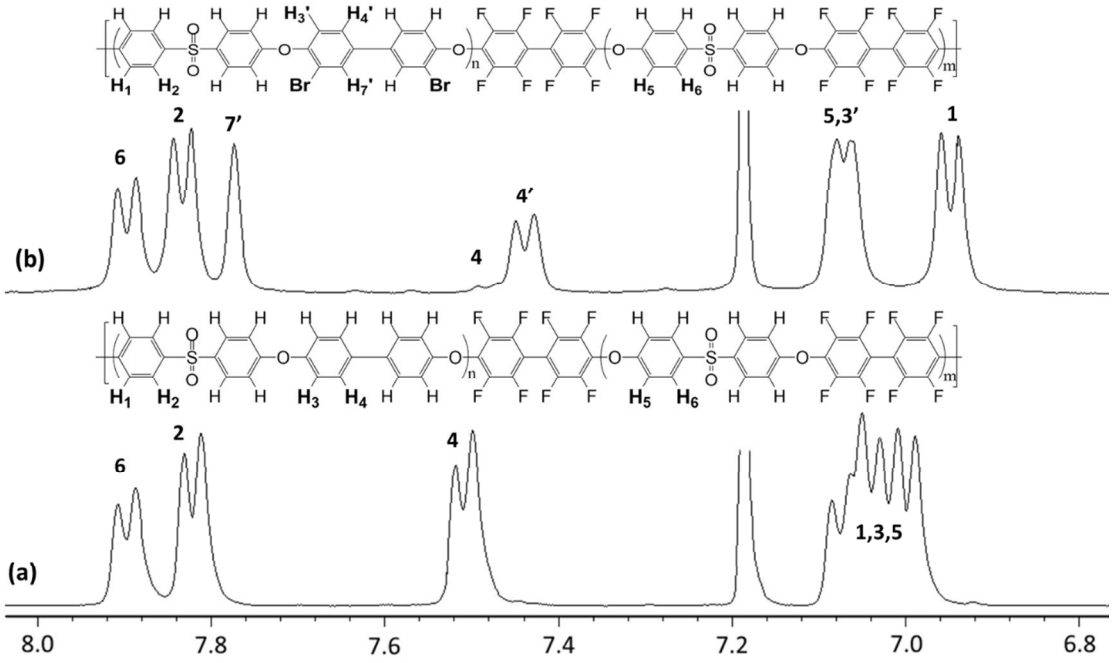

Figure A1. ^{1}H NMR spectra of (a) PES-FPES 5/5 and (b) BrPES-FPES 5/5.

As the diphenyl sulfone moiety appears in the repeating units of both PES and FPES blocks, the ratio, R, between the repeating unit of both blocks was calculated via the ratio between the integration of biphenyl sulfone peaks from both blocks. The obtained R values and the molecular weight of FPES blocks calculated from ^{19}F NMR of PES-FPES block copolymers are close to the expected ones (**Table A2**).

Table A2. Characteristic Properties of PES-FPES Block Copolymer Backbone

block copolymer	Mn_{PES}[a] (g/mol)	Mn_{FPES}[b] (g/mol)	R_{th}[a,c]	R_{exp}[b,c]
PES-FPES 5/5	5000	4900 ± 200	1.40	1.45 ± 0.03
PES-FPES 10/10	10000	10600 ± 400	1.38	1.41 ± 0.04
PES-FPES 10/15	10000	11200 ± 500	0.96	0.94 ± 0.03
PES-FPES 15/15	15000	16100 ± 1400	1.37	1.35 ± 0.03

[a]*Theoretical value.* [b]*Determined by* ^{19}F *NMR.* [c]*The ratio between the number of repeating units of PES. block, and that of FPES block.*

The formation of FPES segments with preformed PES oligomers to form multiblock copolymers was evidenced by sharp increase in viscosity of reaction mixture after 120 minutes and by the high molecular weight (Mw > 250 kg/mol, **Table A3**) with moderated polydispersity.

Table A3. PES-FPES Molecular Weights (Mn, Mw) and Polydispersity (I_p)

ionomer	Mn[a] (kg/mol)	Mw[a] (kg/mol)	I_p
PES-FPES 5/5	108	330	3.1
PES-FPES 10/10	113	278	2.5
PES-FPES 10/15	86	261	3.0
PES-FPES 15/15	126	378	3.0

[a]*SEC performed in THF, solution filtered with PP-based filter.*

3.1.2. Bromination of PES-FPES

The bromination reaction was performed under inert atmosphere using bromine as reactant in the presence of acetic acid (10% v/v). The bromination degree, determined from ^1H NMR (**Figure A1b**) indicates the chemical yield from 95–98 %. No evidence of chain cleavage was observed from NMR spectra of brominated block copolymers.

The degree of bromination was calculated from ^1H NMR spectra based on **Equation A1**:

$$\% Br = \frac{Y}{X+Y} \times 100 \qquad (\boldsymbol{A1})$$

where X is the number of structural units un-brominated and Y is the number of structural units brominated, which were extracted by **Equation 2** and **Equation 3**:

$$I_1 = \left(4 + \left(\frac{4}{R}\right)\right)X + \left(4 + \left(\frac{4}{R}\right) + 2\right)Y \qquad (\boldsymbol{A2})$$

$$I_2 = 4X + 2Y \qquad (\boldsymbol{A3})$$

where I_1 is the integral of the region 7.72–7.96 ppm corresponding to proton in the ortho position of the SO_2 group (4 proton in block PES and 4 proton in block FPES) and proton in the ortho position of atom Br; R is the ratio between the number of repeating units of PES and those of FPES blocks ($R = \chi n_{PES}/\chi n_{FPES}$); I_2 is the integral of the region 7.4–7.6 ppm corresponding to proton in the para position of atom Br (2 protons per structural unit brominated and 4 protons per structural units un-brominated).

3.1.3. Synthesis of $ICF_2CF_2OCF_2CF_2SO_3Li$ Ionic Function

The ionic function was synthesized in THF at room temperature. ^{19}F NMR spectra of $ICF_2CF_2OCF_2CF_2SO_2F$ precursor and $ICF_2CF_2OCF_2CF_2SO_3Li$ ionic function are presented in **Figure A2**.

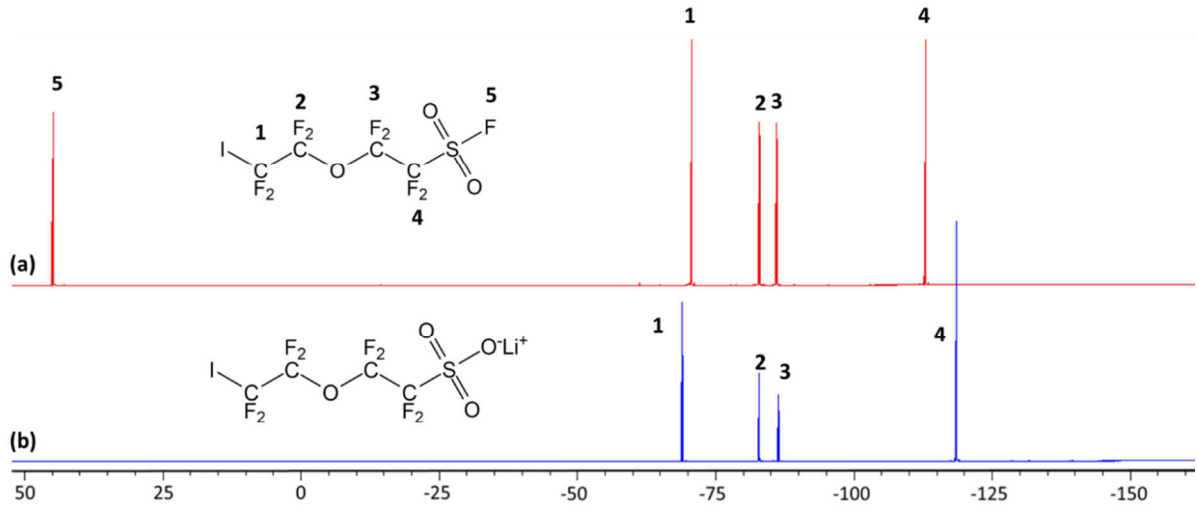

Figure A2. ^{19}F NMR spectra of (a) $ICF_2CF_2OCF_2CF_2SO_2F$ and (b) $ICF_2CF_2OCF_2CF_2SO_3Li$.

3.1.4. Synthesized of InX/Y Ionomer

The grafting of perfluorosulfonic acid groups onto BrPES-FPES backbones was performed via copper-mediated coupling reaction (Ullmann reaction).[4–6] No gelation was observed which means that the coupling reaction between two PES chains did not take place, probably due to the excess amount of ionic functions (≈ 2 eq of Br), the hindrance effect caused by rigid polymer backbones, and their low mobility. However, the coupling reaction between two ionic functions is unavoidable, which was alleviated by slow reactant introduction and compensated by the excess amount of ionic functions (I-psLi). The grafting degree of perfluorosulfonated groups expressed as the IEC of InX/Y was determined by ^{19}F

NMR spectroscopy (**Figure A3**) with high accuracy and by acid base titration (**Table A4**). Based on the ^{19}F NMR, the IECs are calculated with a good accuracy, using the **Equation A4** and **A5**.

$$IEC_{NMR} = N_{NMR} \times IEC_{theo} = \frac{N_{NMR} \times \chi n_{PES}}{\left(Mn_{ps-PES} + Mn_{FPES}\right)} \times 1000 \qquad (\boldsymbol{A4})$$

$$N_{NMR} = \frac{2 \times I_1}{\left[(I_5) \times R_{exp}\right]} \qquad (\boldsymbol{A5})$$

where N_{NMR} is the number of ionic function per PES repeating unit, I_1 is peak integral of F_1 (-110.55 ppm), I_5 is peak integral of fluorine atoms of the FPES block [F_5 (-153.28 ppm) or F_6 (-137.81 ppm)] + peak integral of fluorine atoms at the end of the FPES block ($F_{5'}$ or $F_{6'}$, respectively). χn_{PES} is average repeating unit number in PES blocks, Mn_{FPES} is molar mass of FPES block. $Mn_{ps\text{-}PES}$ is molar mass of psi-PES block = (M_{PES} + N × M_{ps}) × χn_{PES} (where M_{PES} is molar mass of structural unit of PES and M_{ps} is molar mass of ps side chain).

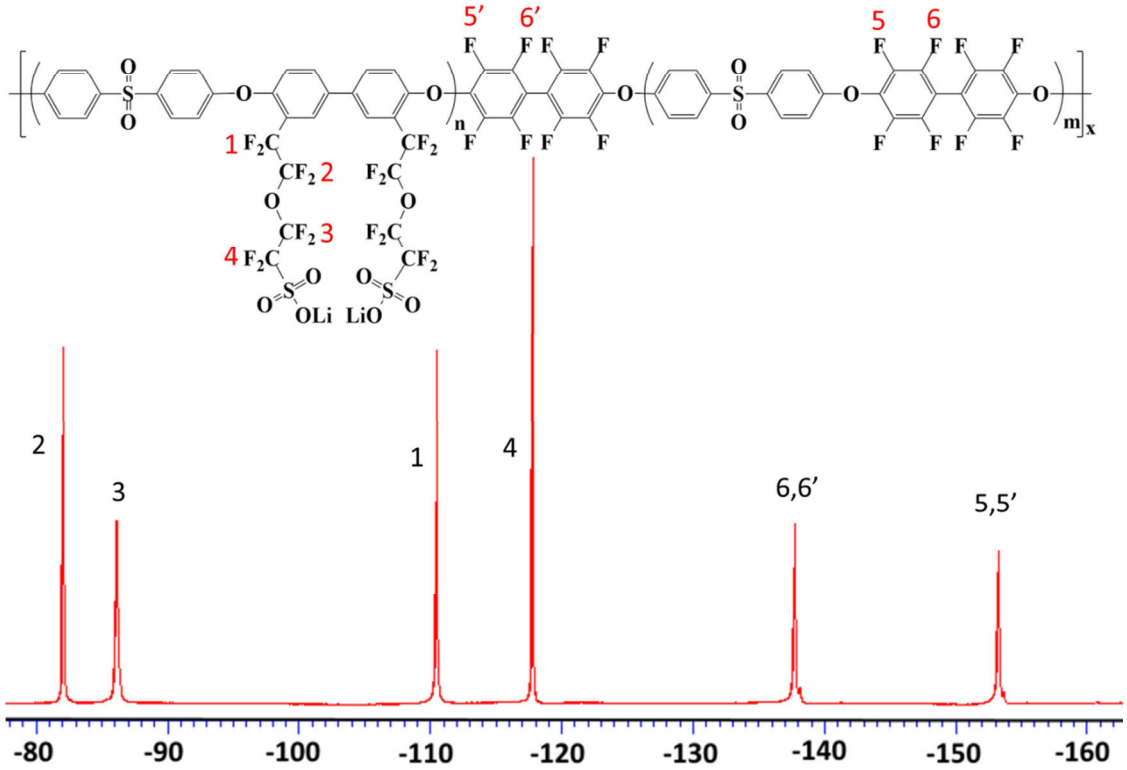

Figure A3. ^{19}F NMR of In5/5 ionomer.

Table A4. IEC Values of InX/Y Ionomers

ionomer	IEC_{theo} (meq H^+/g)	IEC_{NMR} (meq H^+/g)	IEC_{titr} (meq H^+/g)	IEC_{mean} (meq H^+/g)	D (g/cm^3)	IEC_v (meq H^+/cm^3)
In5/5	1.47	1.33 ± 0.05	1.28 ± 0.10	1.30 ± 0.10	1.61 ± 0.03	2.1 ± 0.1
In10/10	1.45	1.40 ± 0.05	1.30 ± 0.10	1.35 ± 0.10	1.63 ± 0.03	2.2 ± 0.1
In10/15	1.27	1.23 ± 0.05	1.11 ± 0.05	1.17 ± 0.05	1.61 ± 0.03	1.9 ± 0.1
In15/15	1.45	1.37 ± 0.05	1.28 ± 0.10	1.32 ± 0.10	1.63 ± 0.03	2.2 ± 0.1

3.2. Thermal and Thermomechanical Properties

3.2.1. PES-FPES Block Copolymer

The glass transition temperature (Tg) and degradation temperature (Td) of block copolymers are presented in **Table A5**. DSC curves of all block copolymer show single glass transition due to the proximity of glass transitions two individual blocks. Thus, PES and FPES homo-polymers corresponding to the PES and FPES blocks of PES-FPES copolymer show Tg of 224 ± 2 and 211 ± 2 °C, respectively. Moreover, DMA curves of all block copolymers also exhibit one relaxation (**Figure A4**).

Table A5. Thermal and Thermomechanical Properties of PES-FPES Block Copolymers

block copolymer	Tg[a] (°C) DSC	Td_{onset} (°C) TGA	Tα[b] (°C) DMA	E'[c] (MPa) DMA
FPES	211 ± 2	435 ± 3	208 ± 2	≈ 1900
PES	224 ± 2	530 ± 3	222 ± 2	≈ 2000
PES-FPES 5/5	225 ± 2	419 ± 2	218 ± 2	≈ 2000
PES-FPES 10/10	224 ± 2	424 ± 2	221 ± 2	≈ 2100
PES-FPES 10/15	220 ± 2	426 ± 2	220 ± 2	≈ 2000
PES-FPES 15/15	226 ± 2	422 ± 2	219 ± 2	≈ 2100

[a]mid-point values. [b]temperature at peak of Tan δ. [c]at 80 °C in dry state.

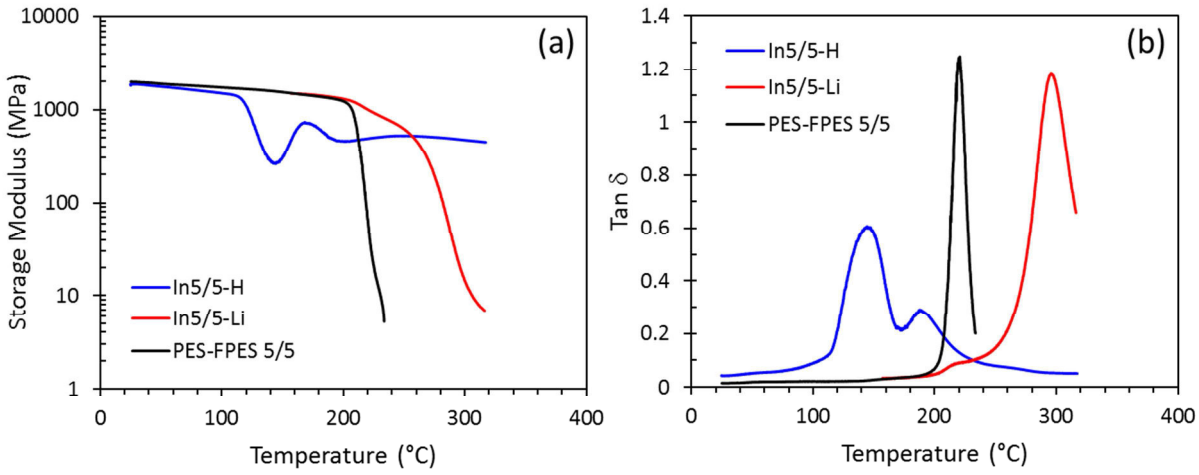

Figure A4. (a) Storage modulus and (b) Tan δ of PES-FPES 5/5, lithiated In5/5, and acidified In5/5.

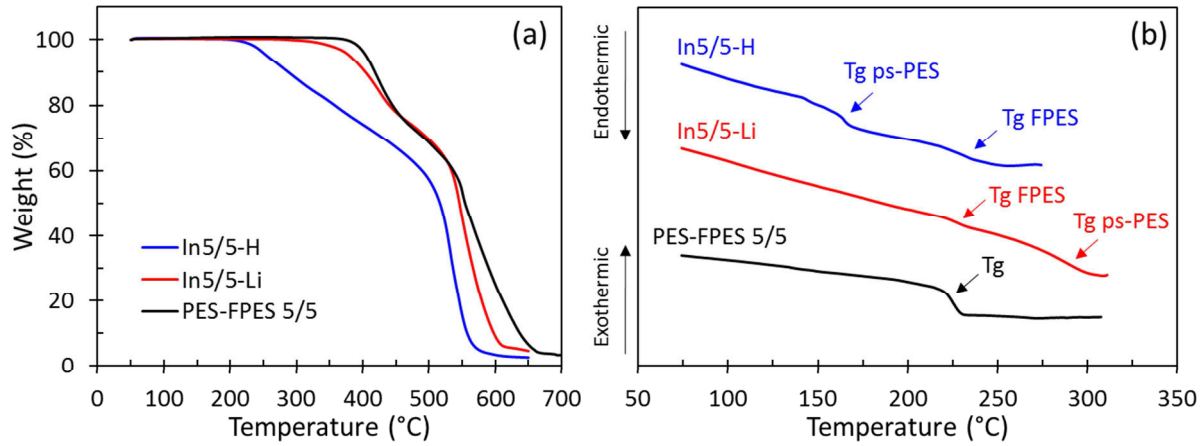

Figure A5. (a) DSC and (b) TGA curves of PES-FPES 5/5, In5/5-Li, and In5/5-H.

3.2.2. InX/Y Ionomers

The grafting of the ionic function onto the aromatic backbone induces a significant decrease in thermal stability (**Table A6**) as compared with PES-FPES copolymers (**Figure A5a**). DSC curves of block copolymer backbone PES-FPES 5/5, ionomer In5/5 in lithium-salt and acidic forms are given in **Figure A5b**.

Table A6. Thermal and Thermomechanical Properties of InX/Y Ionomers

Ionomer	Acidic form			Lithium-salt form		
	Tg (°C)	T_d (°C)	T_α[a] (°C)	Tg (°C)	T_d (°C)	T_α[a] (°C)
In5/5	142, 224	217	148, 194	221, 275	367	220, 298
In10/10	144, 224	221	148, 196	223, 276	360	215, 306
In10/15	149, 222	220	154, 195	220, 282	365	209, 286
In15/15	160, 225	219	150, 204	225, 271	369	205, 311

[a]*temperature at peak of Tan δ. Variation ±2 °C.*

4. Conclusions

This annexe presents the synthesis of aromatic ionomers based on partially fluorinated copoly(arylene ether sulfone)s bearing perfluorosulfonic acid functions. Five ionomers with different block length and IEC were successfully synthesized by following the protocol developed in our lab. The ionic functions were grafted onto PES-FPES block copolymer backbone via two steps, e.g., bromination followed by Ullmann coupling reaction, the yields of both reactions being higher than 90%. Chemical structure of the polymers was confirmed by ^{1}H and ^{19}F NMR spectroscopy. The presence of high separation between the hydrophobic and hydrophilic blocks was observed by DSC and DMA. The results confirmed that there is no effect of reaction solvent on chemical structure of obtained ionomers.

Annexes 2. Effect of Thermal Annealing on Morphology of InX/Y Ionomer Membranes

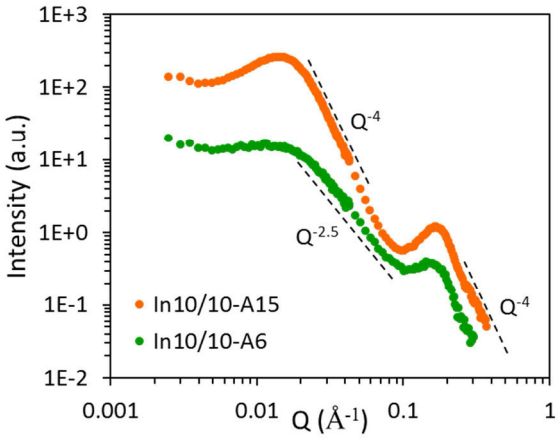

Figure A6. SANS profile of In10/10-A6 and In10/10-A15 membranes at similar λ (~ 22). The spectra have been shifted vertically for clarity.

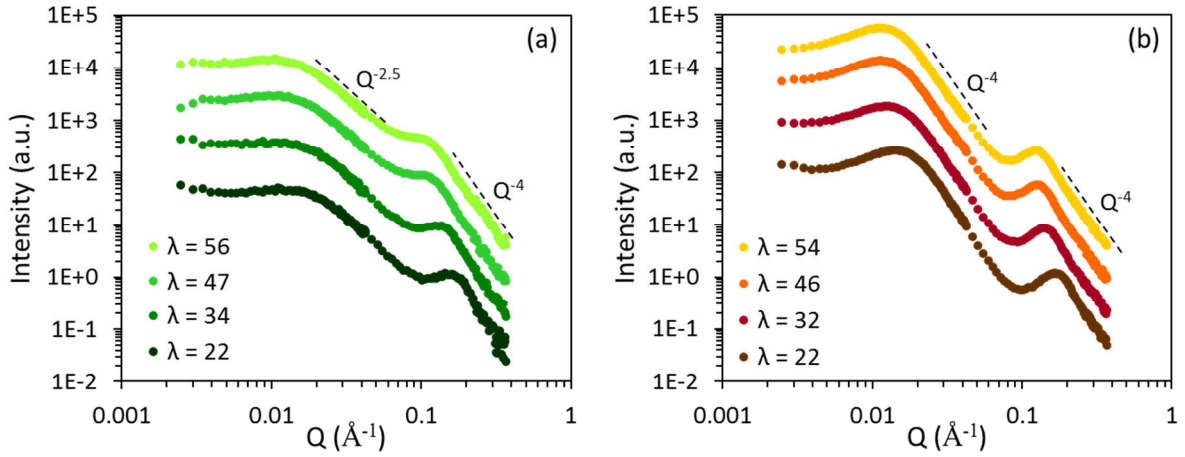

Figure A7. SANS profile of (a) In10/10-A6 and (b) In10/10-A15 membranes with increasing λ. The spectra have been shifted vertically for clarity.

Résumé de thèse en français

La conversion de l'énergie à partir de ressources renouvelables et respectueuses de l'environnement, telles que l'énergie solaire, la biomasse, l'hydrogène, etc., et son stockage sont vitaux pour notre société. Les piles à combustible à membrane échangeuse de protons (PEMFCs) sont l'une des technologies les plus prometteuses pour la conversion de l'énergie. Ces systèmes convertissent, avec un rendement énergétique élevé et une faible émission de polluants, l'énergie chimique stockée par l'hydrogène en énergie électrique. L'un des composants clé d'un PEMFC est la membrane échangeuse de protons (MEPs), qui joue le rôle de : séparateur entre les électrodes, conducteur des protons hydratés, barrière aux carburants et aux électrons. Actuellement, les membranes de référence, comme le Nafion, l'Aquivion, les membranes Gore, 3M, etc., sont à base d'acide perfluorosulfonique (PFSA). Grâce à leur structure chimique – un squelette polymère perfluoré portant des chaînes latérales d'acide perfluorosulfonique, leur nano-structuration et la séparation des phases hydrophile-hydrophobe, la superacidité de l'acide perfluorosulfonique, ces membranes présentent une excellente stabilité thermique/oxydante et de très bonnes conductivités jusqu'à 80 °C.

Cependant, ces membranes présentent aussi des inconvénients : (i) la synthèse des ionomères n'est pas respectueuse de l'environnement, (ii) le coût de production est élevé, (iii) une forte perméabilité à l'oxygène, ce qui entraîne une formation de peroxyde menant à la dégradation de l'assemble membrane-électrode (MEA), (iv) la chute de conductivité et de la tenue thermomécanique après 90 °C. Par conséquent, beaucoup d'efforts ont été dédiés à l'élaboration d'une membrane alternative au Nafion et plus généralement aux PFSAs.

Parmi les nombreux ionomères alternatifs développés au cours des dernières décennies, les ionomères aromatiques ont attiré l'attention en raison de leurs excellentes propriétés thermomécaniques, de leurs bonnes stabilités thermique/oxydative, de leur facilité de synthèse/mise en forme et de leur faible coût, etc. Malheureusement, la plupart des ionomères aromatiques sulfonés ne peuvent pas rivaliser avec le Nafion en termes de performance. Les ionomères aromatiques sulfonés possédant une capacité d'échange ionique (CEI) supérieure au Nafion possèdent une conductivité protonique supérieure à celle de Nafion® à haute humidité relative (HR), mais ils perdent leurs propriétés mécaniques en raison d'un gonflement excessif. D'autre part, les ionomères aromatiques avec une CEI équivalente au Nafion ont une conductivité protonique beaucoup plus faible, en particulier à faible HR.

Dans le but de développer des membranes échangeuses de protons efficaces pour une PEMFC haute performance, cette thèse a porté sur le design, la synthèse et la caractérisation d'une nouvelle famille de ionomères aromatiques nano-structurés. De plus, une étude approfondie a été menée sur l'impact des conditions de mise en forme (solvant, température, etc.) sur la morphologie et les propriétés de la membrane. Afin, d'optimiser la percolation des domaines ioniques, des membranes composites à base de mélange de ionomères aromatiques et de Nafion ont été développées et étudiées.

Le manuscrit de thèse est divisé en quatre chapitres :

Le **chapitre 1** présente brièvement le principe et l'état actuel des PEMFC, ainsi que les défis à surmonter pour répondre aux besoins du marché. Ensuite, une discussion scientifique sur les propriétés et la morphologie des membranes de type Nafion®, ainsi que leurs avantages et inconvénients, est présentée. Les ionomères aromatiques sont décrits comme une alternative prometteuse pour la prochaine génération de MEP, et dans ce manuscrit une attention particulière a été accordée à l'élucidation des interactions structure-morphologie-propriétés, notamment à l'impact de la structure de la chaîne latérale et de la nature de l'acide, sur la morphologie et les propriétés fonctionnelles.

Ce chapitre bibliographique a mis en évidence que les limites des ionomères aromatiques sulfonés proviennent de (i) la répartition aléatoire des fonctions d'acide sulfonique sur le squelette polymère rigide, (ii) la proximité de la fonction sulfonique du squelette polymère, et (iii) la faible acidité de l'acide aryl sulfonique. Pour surmonter ces inconvénients, nous avons développé des copoly(arylène éther sulfone) multi-blocs partiellement-fluorés portant des acides perfluorosulfoniques (InX/Y) ou perfluorosulfonimide (SI X/Y). Les nouveaux ionomères aromatiques possèdent :

- Une structure à blocs multiples dans le but d'améliorer la séparation de phase hydrophile-hydrophobe,
- Des fonctions ioniques séparées du squelette du polymère par un espaceur hydrophobe et flexible pour améliorer la structuration des fonctions ioniques,
- Des fonctions superacides (acide perfluorosulfonique) ou un anion hautement délocalisé tel que le perfluorosulfonimide pour augmenter la conductivité du proton, en particulier à une faible humidité relative (HR).

Une série d'ionomères InX/Y avec différentes longueurs de blocs et différentes CEI a été synthétisée à partir d'un protocole préalablement établi par Assumma et al.[1] et Danyliv et al.[2-4] dans notre laboratoire. Les ionomères ont été synthétisés par la bromation d'un copoly(arylène

éther sulfone) multi-blocs partiellement fluorés, suivie d'une perfluoro-sulfonation par une réaction d'Ullmann. Le squelette du copolymère multi-bloc (à savoir PES-FPES) a été synthétisé par "une synthèse en deux étapes". La structure chimique des produits intermédiaires et des produits finaux a été suivie par la spectroscopie de résonance magnétique nucléaire du proton ou du fluor (RMN ^{1}H et ^{19}F). Les propriétés thermiques et thermomécaniques des ionomères ont été caractérisées par calorimétrie à compensation de puissance (DSC), analyse thermogravimétrique (TGA) et analyse dynamo-mécanique (DMA). La procédure de synthèse et la caractérisation des ionomères sont brièvement présentées dans l'**Annexe** 1.

Le **chapitre 2** se concentre sur l'optimisation des conditions de mise en forme de la membrane et l'élucidation de la relation structure-morphologie-propriétés fonctionnelles des ionomères InX/Y. Ce chapitre est divisé en deux parties : le **chapitre 2A** met l'accent sur les effets de la longueur de l'architecture moléculaire (longueurs du bloc, CEI), de la température de mise en forme de la membrane (traitement thermique), de la nature du solvant (sélectif ou pas), sur la morphologie et les propriétés des membranes ionomères[5] et le **chapitre 2B** se concentre sur la corrélation entre la structure/morphologie de l'ionomère et le transport ionique.[6]

Dans le **chapitre 2A** nous avons prouvé que la nature du solvant a un impact important sur la morphologie. Pour cette étude, deux solvants ont été choisis, un solvant sélectif (bon solvant pour un seul bloc) et un solvant non sélectif (bon solvant pour les deux blocs). Pour déterminer les paramètres d'interaction de Flory-Huggins, nous avons utilisé la chromatographie gazeuse en phase inverse (CGI). Suite à cette étude nous avons choisi le diméthyle acétamide (DMAc) comme solvant non-sélectif et diméthysulfoxide (DMSO) comme solvant sélectif (bon solvant pour le bloc ionique-PES). L'étude a montré que les membranes obtenues à partir d'une solution d'ionomère en DMSO présentent une meilleure nano-structuration avec des domaines ioniques mieux interconnectés. Ces différences morphologiques conduisent à des conductivités et absorptions d'eau plus élevées dans le cas des membranes obtenues à partir DMSO que dans le cas de celles obtenues à partir d'une solution d'ionomère en DMAc.

La morphologie et les propriétés de la membrane sont également fortement influencées par le recuit thermique. Ainsi, nous avons obtenu, après recuit les membranes à 150 °C, une augmentation de la conductivité du proton d'un facteur 10 par rapport aux membranes non traitées thermiquement. Les ionomères ayant des blocs plus longs, c'est-à-dire 15 kg/mol, présentent des conductivités équivalentes à celles du Nafion à HR réduite (<50%) et bien plus élevées au-delà 70% de HR. A 95% RH toutes les membranes recuites présentent des

conductivités plus élevées que le Nafion® 117, notamment au-dessus de 60 °C. Cependant, le nombre d'hydratation (nombre de molécules d'eau/fonction ionique) pour les membranes à base d'ionomères aromatiques à plus longs blocs est 2 fois supérieur à celui du Nafion® 117.

Bien que tous les copolymères à blocs présentent des propriétés thermomécaniques similaires, leurs propriétés fonctionnelles, c'est-à-dire l'absorption d'eau et la conductivité du proton, dépendent fortement de l'architecture moléculaire des ionomères. Par conséquent, la corrélation structure-morphologie-propriétés fonctionnelles pour les membranes obtenues à partir de l'ionomère InX/Y a largement été étudiée et discutée dans le **chapitre 2B**. L'étude a été systématiquement menée avec des ionomères sous différentes formes, c'est-à-dire sous forme de films polymères secs ou hydratés et sous forme d'une solution de polymère diluée dans DMSO ou DMAc. L'étude morphologique a été principalement menée par diffusion des neutrons aux petits angles (SANS).

- Dans les profils SANS des membranes hydratées, deux pics bien définis apparaissent à différentes valeurs du transfert de moment Q, ce qui indique une organisation structurale à deux échelles (d_{ionic}, d_{block}). De plus l'intensité suit une loi de Porod à grands Q, ce qui indique la présence d'une séparation très nette entre les différentes phases (interface parfaitement définie, non rugueuse). Nous avons attribué le pic à plus grand Q à la nano-structuration des fonctions ioniques et du squelette polymère (PES), et déterminé la distance de corrélation moyenne associée à cette phase (d_{ionic}) ainsi que la taille moyenne des domaines ioniques. Le pic à plus grand Q correspond à la l'organisation à plus grande échelle de la structure à blocs, e.g., à la séparation régulière des domaines de ps-PES et de FPES (d_{block}).
  Un modèle de microstructure a été proposé pour expliquer l'auto-organisation des molécules d'ionomère pendant le processus de mise en forme de la membrane par coulée-évaporation. L'évolution de la morphologie lors de la sorption/désorption de l'eau a été étudiée.
- Les lois de gonflement, à savoir l'expansion des domaines ioniques (Δd_{ionic}) et de la superstructure (Δd_{block}), ont été obtenues en analysant l'évolution des spectres SANS en fonction du nombre d'hydratation (λ). Les domaines ioniques suivent la même loi de dilution que le Nafion, avec une transition morphologique entre une structuration de type lamellaire (1D, dilution d'objects plats de type rubans) à basse hydratation et cylindrique (2D, dilution d'objets allongés) au-delà d'un seuil autour de $\lambda \sim 30$. Par conséquent, nous avons conclu que la présence des chaînes latérales ioniques

perfluorées induit une séparation de phase très marquée et impose localement une morphologie et une topologie similaires à celle du Nafion.

- Les propriétés du transport ont ensuite été analysées en utilisant les tailles structurelles microscopiques (d, Δd) comme variables pertinentes. Nous avons clarifié la relation entre l'architecture chimique, la microstructure et l'efficacité du transport de protons. La conductivité du proton et le coefficient d'autodiffusion de l'eau se sont révélé varier linéairement avec l'expansion du domaine ionique (Δd_{ionic}) et de la superstructure du bloc (Δd_{block}).

La conclusion principale de ce travail est que la microstructure et les propriétés des membranes à base de InX/Y peuvent être adaptées par l'architecture chimique de l'ionomère ainsi que les conditions de mise en forme de la membrane.

En optimisant tant la structure chimique de InX/Y que la mise en forme nous avons obtenu des membranes nano-structurées avec des performances nettement améliorées par rapport à l'état de l'art. Cependant, les conductivités ioniques et la sorption de l'eau de ces membranes dépendent fortement de la taille des blocs et de la CEI, plus particulièrement à faible RH. Les ionomères avec des blocs plus longs conduisent à des membranes plus conductrices mais la quantité d'eau absorbée est plus élevée, ce qui affecte les propriétés mécaniques.

Afin de diminuer la prise d'eau nous avons développé des membranes à base d'un mélange d'un ionomères InX/Y avec des blocs plus courts (faible prise en eau) et le Nafion. (**chapitre 3**).[7] Par conséquent, nous avons produit des mélanges InX/Y-Nafion avec une quantité de Nafion comprise entre 10 et 50% en poids.

Nous avons réalisé une étude très approfondie sur l'impact de la composition de la membrane (quantité de Nafion, choix de l'architecture des blocs) sur les propriétés fonctionnelles et la microstructure (SANS). Par cette étude nous avons démontré que le Nafion a un rôle important sur la percolation des domaines ioniques, notamment après que les membranes ont été traitées à 150°C. Comme principaux résultats, on peut noter :

- La plupart des membranes composites Nafion-InX/Y présentent des conductivités protoniques plus élevées que celles des membranes ionomères correspondantes. La conductivité protonique la plus élevée a été obtenue avec des membranes contenant 20% en poids de Nafion.
- L'incorporation de Nafion dans l'ionomère aromatique, en combinaison avec un recuit thermique, conduit à une amélioration significative des morphologies, notamment la connectivité des domaines ioniques, et des propriétés fonctionnelles.

- En analysant les profils de SANS et DMA, nous avons constaté que les deux ionomères ne sont pas complètement miscibles après la coulée. Après recuit, les deux ionomères semblent se mélanger et ne former qu'une seule phase homogène.
- Les membranes recuites ont montré une absorption d'eau plus faible et une conductivité protonique plus élevée, en particulier à faible HR. On note une augmentation d'un factor 3 de la conductivité protonique après le traitement thermique.
- L'approche composite a donc donné des résultats très prometteurs qui pourraient être encore améliorés en optimisant le procédé de fabrication de la membrane.

Il a été démontré que les membranes ionomères InX/Y présentaient une meilleure nano-structuration et une conductivité protonique supérieure à celle des poly(éther d'arylène) directement sulfonés.

Dans le **chapitre 4**, nous avons donc exploré une nouvelle classe d'ionomère aromatique (SiX/Y) à base de co-poly(arylène éthersulfone)s multi-blocs portant un acide perfluorosulfonimidique. L'acide bis(trifluoromethane sulfoimidique) est connu comme un acide qui possède une acidité plus élevée en phase gazeuse et une stabilité thermique améliorée par rapport à celles de l'acide perfluorosulfonique. On s'attend à ce que la forte dissociation ionique induite par la charge négative largement délocalisée sur l'anion perfluorosulfonimide améliore significativement la conductivité, en particulier à faible HR. Les fonctions perfluorosulfonimidures de lithium ont été greffées sur des copolymères multi-blocs PES-FPES avec des longueurs de bloc similaires à InX/Y. Une gamme d'ionomères SiX/Y avec des masses molaires de blocs et CEI différentes a été obtenue par réaction de couplage Ullmann entre le squelette du copolymère séquencé bromé et les fonctions perfluorosulfonimidures. Leurs propriétés thermomécaniques, leurs morphologies et leurs propriétés de transport ont été systématiquement étudiées.[8]

- Ces ionomères présentent une morphologie similaire au InX/Y à l'échelle nanométrique mais une plus grande stabilité thermique.
- À 95% de HR, SiX/Y présente des conductivités plus élevées que InX/Y et le Nafion® 117, mais elles diminuent drastiquement avec la réduction de la HR.

Ce travail sur les ionomères aromatiques à blocs ouvre des perspectives de développement, notamment pour des applications au-delà des membranes pour piles à combustible, par exemple :

- Utilisation des ionomères aromatiques comme liants pour les couches de catalyseur de piles.
- Développement des électrolytes polymères multi-bloc mono-ion pour les batteries au lithium-ion à base de copoly(arylène éthersulfone) à blocs multiples portant des fonctions perfluorosulfonylimide.

Références

(1) Assumma, L.; Iojoiu, C.; Mercier, R.; Lyonnard, S.; Nguyen, H. D.; Planes, E. Synthesis of Partially Fluorinated Poly(Arylene Ether Sulfone) Multiblock Copolymers Bearing Perfluorosulfonic Functions. *J. Polym. Sci. Part A Polym. Chem.* **2015**, *53* (16), 1941–1956.

(2) Danyliv, O.; Gueneau, C.; Iojoiu, C.; Cointeaux, L.; Thiam, A.; Lyonnard, S.; Sanchez, J.-Y. Polyaromatic Ionomers with a Highly Hydrophobic Backbone and Perfluorosulfonic Acids for PEMFC. *Electrochim. Acta* **2016**, *214*, 182–191.

(3) Danyliv, O.; Iojoiu, C.; Barbier, V.; Martin, V.; Sanchez, J.-Y. Aromatic Ionic Monomer Bearing Perfluorosulfonate Moiety and Its Polycondensation toward High Performance Superacid Ionomers. *J. Fluor. Chem.* **2016**, *189*, 43–50.

(4) Danyliv, O.; Iojoiu, C.; Lyonnard, S.; Sergent, N.; Planes, E.; Sanchez, J.-Y. Highly Phase Separated Aromatic Ionomers Bearing Perfluorosulfonic Acids by Bottom-up Synthesis: Effect of Cation on Membrane Morphology and Functional Properties. *Macromolecules* **2016**, *49* (11), 4164–4177.

(5) Assumma, L.; Nguyen, H.-D.; Iojoiu, C.; Lyonnard, S.; Mercier, R.; Espuche, E. Effects of Block Length and Membrane Processing Conditions on the Morphology and Properties of Perfluorosulfonated Poly(arylene Ether Sulfone) Multiblock Copolymer Membranes for PEMFC. *ACS Appl. Mater. Interfaces* **2015**, *7* (25), 13808–13820.

(6) Nguyen, H. D.; Assumma, L.; Judeinstein, P.; Mercier, R.; Porcar, L.; Jestin, J.; Iojoiu, C.; Lyonnard, S. Controlling Microstructure-Transport Interplay in Highly Phase-Separated Perfluorosulfonated Aromatic Multiblock Ionomers via Molecular Architecture Design. *ACS Appl. Mater. Interfaces* **2017**, *9* (2), 1671–1683.

(7) Nguyen, H.-D.; Jestin, J.; Porcar, L.; Lyonnard, S. Iojoiu, C. Conductivity and Thermomechanical Stability of Fuel Cell Membranes Boosted by Blending Block Copolymers with Nafion. To be submitted to *Journal of Membrane Science*.

(8) Nguyen, H.-D.; Planes, E.; Soudant, P.; Porcar, L.; Lyonnard, S.; Iojoiu, C. Aromatic Multi-Block Ionomers with Extensively-Delocalized Negative Charge for PEMFC Application. To be submitted to *Journal of Physical Chemistry.*

Abstract

Aromatic ionomers are considered as a promising alternative to Nafion due to their good oxidative stability, excellent thermomechanical properties, and low cost, etc. Most sulfonated aromatic ionomers reported over the past decades, however, show lower performance than that of Nafion. With similar ion-exchange capacity (IEC), on one hand, aromatic ionomers are much less conductive than Nafion, notably at low relative humidity. Aromatic ionomers with sufficient IEC to give equivalent conduction to that of Nafion, on the other hand, exhibit excessively swelling behavior in water. The shortcomings of sulfonated aromatic ionomers derive from (i) the random distribution of acidic groups on rigid polymer backbone leading to poor hydrophilic-hydrophobic separation, (ii) the proximity of proton-conducting moieties to the polymer main chain resulting in low nanostructure of ionic clusters, and (iii) the low acidity of aryl sulfonic acid. With the aim of overcoming these drawbacks, my PhD work focuses on developing new aromatic ionomers with improved morphology and properties via molecular architecture design, in combination with optimized membrane processing condition. Based on this objective, two series of aromatic ionomers based on partially-fluorinated multi-block copoly(arylene ether sulfone)s bearing pendant perfluorosulfonic acid (InX/Y series) or perfluorosulfonimide (SiX/Y series) side chains have been developed and characterized. Moreover, PEMs based on Nafion/InX/Y blend have also been investigated. Much attention has been paid to optimizing the membrane processing conditions and elucidating the structure-morphology-property relation in these materials.

Résumé

Les ionomères aromatiques sont considérés comme une alternative prometteuse au Nafion en raison de leur bonne stabilité à l'oxydation, excellentes propriétés thermomécaniques et faible coût, etc. Cependant, la plupart des ionomères aromatiques sulfonés, rapportés au cours des dernières décennies, présentent des performances inférieures à celles de Nafion. A une capacité d'échange ionique (CEI) similaire, les ionomères aromatiques sont beaucoup moins conducteurs que le Nafion, notamment à faible humidité relative. Les ionomères aromatiques ayant une CEI suffisante et une conductivité équivalente à celle de Nafion, gonflement excessivement dans l'eau. Les inconvénients des ionomères aromatiques sulfonés proviennent de (i) la répartition aléatoire de groupes acides sur le squelette polymère rigide conduisant à une faible séparation entre les phases hydrophile-hydrophobe, (ii) la proximité de fonctions conductrices de protons du squelette polymère conduisant à une faible agregation des domaines ioniques, et (iii) la faible acidité de l'acide arylsulfonique. Dans le but de surmonter ces inconvénients, mon travail de doctorat a eu comme objectif de développer de nouveaux ionomères aromatiques, avec differentes architecture moléculaire, afin d'ammelirer la morphologie et les propriétés fonctionnels des membranes. Pour atteindre cet objectif, deux séries d'ionomères aromatiques à base de copoly (arylène éther sulfone) partiellement fluoré, portant des chaînes latérales pendantes d'acide perfluorosulfonique (séries InX/Y) ou perfluorosulfonimide (SiX/Y) ont été développées et caractérisées. De plus, les PEM à base de mélanges Nafion/InX/Y ont également été investigués. Une grande attention a été portée à l'optimisation de la mise en forme des membranes et à l'élucidation de la relation structure-morphologie-propriété des matériaux.